

# Nonsteady operation of trickle-bed reactors : hydrodynamics, mass and heat transfer

**Citation for published version (APA):**

Boelhouwer, J. G. (2001). *Nonsteady operation of trickle-bed reactors : hydrodynamics, mass and heat transfer*. [Phd Thesis 1 (Research TU/e / Graduation TU/e), Chemical Engineering and Chemistry]. Technische Universiteit Eindhoven. <https://doi.org/10.6100/IR549731>

**DOI:**

[10.6100/IR549731](https://doi.org/10.6100/IR549731)

**Document status and date:**

Published: 01/01/2001

**Document Version:**

Publisher's PDF, also known as Version of Record (includes final page, issue and volume numbers)

**Please check the document version of this publication:**

- A submitted manuscript is the version of the article upon submission and before peer-review. There can be important differences between the submitted version and the official published version of record. People interested in the research are advised to contact the author for the final version of the publication, or visit the DOI to the publisher's website.
- The final author version and the galley proof are versions of the publication after peer review.
- The final published version features the final layout of the paper including the volume, issue and page numbers.

[Link to publication](#)

**General rights**

Copyright and moral rights for the publications made accessible in the public portal are retained by the authors and/or other copyright owners and it is a condition of accessing publications that users recognise and abide by the legal requirements associated with these rights.

- Users may download and print one copy of any publication from the public portal for the purpose of private study or research.
- You may not further distribute the material or use it for any profit-making activity or commercial gain
- You may freely distribute the URL identifying the publication in the public portal.

If the publication is distributed under the terms of Article 25fa of the Dutch Copyright Act, indicated by the "Taverne" license above, please follow below link for the End User Agreement:

[www.tue.nl/taverne](http://www.tue.nl/taverne)

**Take down policy**

If you believe that this document breaches copyright please contact us at:

[openaccess@tue.nl](mailto:openaccess@tue.nl)

providing details and we will investigate your claim.

# **Nonsteady operation of trickle-bed reactors**

Hydrodynamics, mass and heat transfer

PROEFSCHRIFT

ter verkrijging van de graad van doctor aan de  
Technische Universiteit Eindhoven, op gezag van de  
Rector Magnificus, prof. dr. R.A. van Santen, voor een  
commissie aangewezen door het College voor  
Promoties in het openbaar te verdedigen  
op woensdag 28 november 2001 om 16.00 uur

door

Jacobus Gerrit Boelhouwer

geboren te Linschoten

Dit proefschrift is goedgekeurd door de promotoren:

Prof. Dr. ir. A.A.H. Drinkenburg  
en  
Prof. Dr. G. Wild

Sponsor: Nederlandse Organisatie voor Wetenschappelijk Onderzoek (NWO)

Druk: Universiteitsdrukkerij, Technische Universiteit Eindhoven

CIP-DATA LIBRARY TECHNISCHE UNIVERSITEIT EINDHOVEN

Boelhouwer, Jaco G.

Nonsteady operation of trickle-bed reactors : hydrodynamics, mass and heat transfer / by  
Jaco G. Boelhouwer. – Eindhoven : Technische Universiteit Eindhoven, 2001.

Proefschrift. – ISBN 90-386-2553-7

NUGI 813

Trefwoorden: chemische reactoren / trickle-bed reactoren; periodieke bedrijfsvoering /  
hydrodynamica / gepulseerde stroming / warmte- en stofoverdracht

Subject headings: chemical reactors / trickle-bed reactors; periodic operation /  
hydrodynamics / pulsing flow / heat and mass transfer

Marjolein  
Mijn ouders



---

## Summary

---

### Introduction

A trickle-bed reactor is a type of three-phase reactors in which a gas and a liquid phase cocurrently flow downward over a packed bed of catalyst particles. Most commercial trickle-bed reactors operate adiabatically at high temperatures and high pressures and generally involve hydrogenations, oxidations and desulfurizations.

Trickle-bed reactors may be operated in several flow regimes. At present, steady state operation in the trickle flow regime is common in industrial applications. Liquid maldistribution, formation of hot spots and decreased selectivity are serious problems experienced during trickle flow operation. An intriguing flow regime, termed pulsing flow, prevails at higher gas and liquid flow rates compared to trickle flow. Pulsing flow is a kind of self-organization through which the bed is periodically run through with waves of liquid followed by relatively quiet periods of gas and liquid continuous flow. The pulses are characterized by high particle-liquid mass and heat transfer rates, large gas-liquid interfacial areas, complete catalyst wetting, mobilization of stagnant liquid and diminished axial dispersion.

Almost all reaction systems can be classified as being liquid reactant or gas reactant limited. For liquid-limited reactions, the highest possible wetting efficiency and particle-liquid mass transfer rates result in the fastest transport of the liquid phase reactant to the catalyst. For gas-limited reactions, it is advantageous to reduce the mass transfer resistance added by the liquid phase, without the danger of gross liquid maldistribution and hot spot formation.

### Objective

The objective of the present study is essentially process intensification of a trickle-bed reactor by forced nonsteady operation. For process intensification it is required to improve the mass transfer characteristics of the limiting reactant. Simultaneously, flow maldistribution and the formation of hot spots must be prevented or at least controlled. The present study aims at controlling the wetting efficiency as a function of time and utilizing the advantages associated with pulsing flow in order to meet the demands for process intensification. This is achieved by square-wave cycling of the liquid feed. The possibility of a forced induction of pulses is examined. Particle-liquid heat and mass transfer rates are determined. The effect of periodic operation on reactor performance is examined by a dynamic modeling study.

---

### **Natural pulsing flow**

Experimental results on pulse properties reveal that liquid holdup, velocity and duration are invariant to the liquid flow rate at a constant gas flow rate. The only effect of increasing the liquid flow rate is then an increase in the pulse frequency. These experimental results provide a means to determine the relative contribution of the pulses, and the parts of the bed in between pulses, to an average measured property. By implementation of this concept it is shown that the linear liquid velocity inside the pulses is very high and is responsible for the enhanced mass and heat transfer rates.

The liquid holdup in the parts of the bed in between pulses equals the liquid holdup at the transition to pulsing flow at all gas flow rates. The same trend holds for the linear liquid velocity in between pulses. Pulsing flow then is a hybrid of two transition states. The pulses reside at the transition to bubble flow, while the bases reside at the transition to trickle flow.

### **Liquid feed cycling**

Cycling the liquid feed results in the formation of continuity shock waves. The shock waves decay by leaving liquid behind their tail. This process of decay limits the frequency of the cycled liquid feed to rather low values since at relatively high frequencies, total collapse of the shock waves occurs.

By the induction of natural pulses inside the shock waves, the mass and heat transfer rates during the liquid flush are improved. Shorter flushes can therefore be applied and the usual encountered periodic operation using shock waves is optimized. Especially the danger of hot spot formation is prevented. This first feed strategy is termed the slow mode of liquid-induced pulsing flow.

The second feed strategy, termed the fast mode of liquid-induced pulsing flow, may be viewed as an extension of natural pulsing flow. Individual natural pulses are induced at an externally set pulse frequency less than 1 Hz. The characteristics of the induced pulses equal the pulse characteristics of natural pulsing flow at equivalent gas flow rates. A critical liquid holdup in between pulses is necessary for the induced pulses to remain stable. This feed strategy appears to be the only fast mode of periodic operation possible.

### **Particle-liquid mass and heat transfer**

Local time-averaged particle-liquid heat and mass transfer rates in both trickle and pulsing flow are determined. In the trickle flow regime, local mass and heat transfer coefficients increase with both increasing liquid and gas flow rate.

---

The transition to pulsing flow is accompanied by a substantial increase in mass and heat transfer rates. Particle-liquid mass and heat transfer coefficients inside pulses are 2 to 3 times higher than in between pulses. Particle-liquid mass and heat transfer rates in between pulses are constant due to the constant linear liquid velocity in between pulses. The linear liquid velocity is identified as the main parameter that governs mass and heat transfer rates in both flow regimes.

Even in the pulsing flow regime, large differences in local mass and heat transfer coefficients exist. This is attributed to non-uniformities in the local voidage distribution and the effect of stagnant liquid holdup held at the contact points between particles. Pulses are macroscopically uniform but on the particle scale pulses are characterized by substantial non-uniformities.

The penetration theory is useful in calculating both particle-liquid heat and mass transfer coefficients during pulsing flow. Additionally, the analogy between heat and mass transfer rates proposed by penetration theory outperforms the Chilton-Colburn analogy based on boundary layer theory.

#### **Dynamic modeling**

A dynamic model is developed to study the effect of periodic operation on trickle-bed reactor performance for both liquid-limited and gas-limited reactions. Internal diffusion is incorporated in the model since the rate of internal diffusion largely determines the optimal cycle periods. The effect of periodic operation on conversion, selectivity and production capacity is investigated.

Periodic operation results in significant increases in production capacity and conversion compared to steady state operation for gas-limited reactions. For liquid-limited reactions, however, steady state operation is superior to periodic operation. The optimal durations of the high and low liquid feed are strongly interdependent. For fast reactions, a shorter period of low liquid feed and a higher ratio of the period of high liquid feed to the period of low liquid feed are preferred compared to slow reactions.

A fast cycling of the liquid feed is most effective in terms of production capacity, conversion and selectivity. With increasing cycled liquid feed frequency, the time average concentration of the liquid phase reactant inside the catalyst increases and the time-average concentration of the product decreases. High concentrations of liquid phase reactant result in high reaction rates for the desired reaction. Low concentration levels of the product lead to low reaction rates for the undesired reaction.



---

**Concluding remarks**

For both liquid-limited and gas-limited reactions, different nonsteady operation modes exist that increase the mass transfer of the rate-limiting reactant. For liquid-limited reactions, the operation of a trickle-bed reactor in the natural pulsing flow regime seems most appropriate since complete catalyst wetting and high particle-liquid mass transfer rates are achieved. Additionally, the fast mode of liquid-induced pulsing flow at high frequencies may be applied to increase the residence time of the liquid phase. For gas-limited reactions, controlled partial wetting without flow maldistribution can be achieved by liquid feed cycling. The mass transfer rate of the limiting gaseous reactant is periodically increased during the low wetting period. Especially, the slow mode of liquid-induced pulsing flow prevents the danger of hot spot formation. The fast mode of liquid-induced pulsing flow may be used in case a relatively fast cycling of the liquid flow rate in the trickle-bed reactor is needed, as for example for selectivity reasons. More generally speaking, flow maldistribution and hot spot formation, the main problems experienced during steady state trickle flow operation, are diminished by periodic operation of a trickle-bed reactor.

Since the periodic operation rests upon the manipulation of an external variable, existing trickle-bed reactors may relatively simply be modified to meet the demands of performance improvement. For trickle-bed reactors to be developed, a decrease in investment cost is expected, since liquid redistributors and inter-bed heat exchangers may be eliminated. Moreover, smaller reactors and reduced operating pressures may be achieved. These considerations suggest that periodic operation is a general method and should find wide application.

The findings of this Ph.D. thesis have been largely instrumental in the setting up of the EU-project CYCLOP (Cyclic operation of trickle-bed reactors) to develop design and operation rules for cyclic operated trickle-bed reactors.

---

# Samenvatting

---

## Inleiding

Een trickle-bed reactor is een met katalysatordeeltjes gepakte kolom waarin een gas en een vloeistof in meestroom neerwaarts stromen. De meeste industriële trickle-bed reactoren worden adiabatisch bedreven bij hoge temperaturen en drukken. Deze reactoren worden veelvuldig toegepast voor hydrogeneringen, oxidaties en ontzwavelingsreacties.

Trickle-bed reactoren kunnen in verschillende stromingstoestanden worden bedreven. Momenteel worden industriële trickle-bed reactoren stationair bedreven in het trickle flow regime. Een niet-uniforme vloeistofverdeling, vorming van hot spots en verminderde selectiviteit zijn serieuze problemen die optreden tijdens bedrijfsvoering in het trickle flow regime. Bij hogere gas- en vloeistofsnelheden bevindt de trickle-bed reactor zich in een veel interessantere stromingstoestand, genaamd pulsing flow. Deze stromingstoestand kenmerkt zich door de afwisselende passage van vloeistofrijke golven en rustige periodes van continue gas- en vloeistofstroming. De pulsen worden gekarakteriseerd door hoge stof- en warmteoverdrachtscoëfficiënten, een groot gas-vloeistof contactoppervlak, complete katalysatorbenutting, mobilisatie van stagnante vloeistof-holdup en verminderde axiale dispersie.

In praktisch alle reagerende systemen is het overall stoftransport van de gasfase reactant danwel de vloeistoffase reactant limiterend. Voor de zogenaamde vloeistofgelimiteerde reacties leiden een hoge stofoverdracht tussen de vloeistof en de katalysator en de grootst mogelijke katalysatorbenutting tot het meest effectieve stoftransport van de vloeistoffase reactant naar de katalysator. Voor reacties die door het overall stoftransport van de gasfase reactant gelimiteerd worden, is het gunstig de stofoverdrachtsweerstand, ten gevolge van de vloeistoffilm, te verminderen, zonder daarbij het gevaar te lopen op een niet-uniforme vloeistofverdeling en de vorming van hot spots.

## Doelstelling

De doelstelling van het hier gepresenteerde onderzoek is de intensivering van processen uitgevoerd in trickle-bed reactoren door geforceerde, niet-stationaire bedrijfsvoering. Essentieel hierbij is het vergroten van de stofoverdrachtssnelheid van de limiterende reactant. Tegelijkertijd dient een niet-uniforme vloeistofverdeling en de vorming van hot spots te worden voorkomen of in ieder geval te kunnen worden beheerst.

---

Het onderzoek richt zich op een combinatie van het instellen van de katalysatorbenutting als functie van de tijd en het benutten van de voordelen van pulsing flow. Dit leidt tot een aantal niet-stationaire methodes van bedrijfsvoering, die berusten op het toevoeren van een in de tijd variërend vloeistofdebiet aan de trickle-bed reactor. De mogelijkheid van het gecontroleerd opwekken van pulsen is onderzocht. Daarnaast zijn de stof- en warmteoverdracht tussen de vloeistof en de pakking bepaald. Het effect van een periodieke bedrijfsvoering op de prestatie van trickle-bed reactoren is onderzocht met behulp van een dynamisch model.

#### **Natuurlijke pulsing flow**

Pulseigenschappen zoals vloeistof-holdup, pulssnelheid en pulsduur zijn onafhankelijk van de superficiële vloeistofsnelheid bij een constante gassnelheid. De pulsfrequentie daarentegen neemt toe met toenemende superficiële vloeistofsnelheid. Deze resultaten bieden de mogelijkheid om de relatieve bijdrage van de pulsen en de gedeeltes van het bed tussen de pulsen aan een gemiddelde grootte te berekenen. Bij de implementatie van dit concept is vastgesteld dat de lineaire vloeistofsnelheid in de pulsen erg hoog is en verantwoordelijk is voor de hoge stof- en warmteoverdracht.

De vloeistof-holdup tussen de pulsen is gelijk aan de vloeistof-holdup op de overgang naar pulsing flow bij constante gassnelheid. Hetzelfde fenomeen geldt voor de lineaire vloeistofsnelheid tussen de pulsen. De pulsen bevinden zich op de overgang naar bubble flow en de gedeeltes van het bed tussen de pulsen bevinden zich op de overgang naar trickle flow.

#### **Cyclisch vloeistofdebiet**

Door een cyclisch vloeistofdebiet aan de kolom toe te voeren ontstaan er schokgolven in de kolom. Deze schokgolven raken in verval doordat ze aan de achterkant vloeistof achterlaten. Dit proces limiteert de frequentie van het cyclisch vloeistofdebiet tot relatief lage waarden. Bij een relatief hoge frequentie van het vloeistofdebiet verdwijnen de schokgolven uiteindelijk volkomen.

Door het induceren van natuurlijke pulsen in de schokgolven worden de stof- en warmteoverdracht in de schokgolf sterk verbeterd. Hierdoor kan met kortere schokgolven worden volstaan en kan de periodieke bedrijfsvoering dus verder worden geoptimaliseerd. Deze voedingsstrategie wordt de 'slow mode of liquid-induced pulsing flow' genoemd. Met name de vorming van hot spots wordt door deze methode van bedrijfsvoering voorkomen.

---

De tweede ontwikkelde voedingsstrategie, de zogenaamde 'fast mode of liquid-induced pulsing flow', kan worden opgevat als een uitbreiding van natuurlijke pulsing flow. Deze voedingsstrategie bestaat uit het induceren van individuele natuurlijke pulsen waarvan de frequentie kan worden vastgesteld op alle waarden minder dan 1 Hz. De eigenschappen van deze geïnduceerde pulsen zijn gelijk aan de eigenschappen van natuurlijke pulsen bij een gelijke gassnelheid. Een kritische vloeistof-holdup tussen de pulsen is noodzakelijk voor de stabiliteit van de pulsen. Deze voedingsstrategie is de enige voedingsstrategie waarbij relatief hoge frequenties van een variërende vloeistofsnelheid in de reactor kunnen worden bereikt.

#### **Stof- en warmteoverdracht**

Locale tijdsgemiddelde stof- en warmteoverdrachtscoëfficiënten tussen de vloeistof en de pakking zijn bepaald in zowel het trickle flow regime als het pulsing flow regime. In het trickle flow regime nemen de stof- en warmteoverdracht toe met toenemende gas- en vloeistofsnelheden. De overgang naar pulsing flow wordt gekenmerkt door een substantiële toename in de stof- en warmteoverdracht. Stof- en warmteoverdrachtscoëfficiënten in de pulsen zijn 2 tot 3 maal zo groot als die tussen de pulsen in. De stof- en warmteoverdrachtscoëfficiënten tussen de pulsen zijn constant omdat de lineaire vloeistofsnelheid tussen de pulsen constant is. De lineaire vloeistofsnelheid bepaalt zowel de stof- en warmteoverdrachtscoëfficiënten in trickle en pulsing flow.

Zelfs in het pulsing flow regime bestaan er substantiële verschillen tussen lokaal gemeten stof- en warmteoverdrachtscoëfficiënten. Dit wordt veroorzaakt door verschillen in de lokale porositeit en de aanwezigheid van stagnante vloeistof-holdup die wordt vastgehouden op de contactpunten tussen de verschillende deeltjes. Het blijkt dat pulsen op de reactorschaal uniform zijn, maar dat er op deeltjesschaal substantiële verschillen voorkomen.

De stof- en warmteoverdrachtscoëfficiënten tijdens pulsing flow zijn redelijk goed te voorspellen met de penetratietheorie. Tevens wordt de analogie tussen stof- en warmteoverdracht met de penetratietheorie beter beschreven dan met de op de grenslaag theorie gebaseerde Chilton-Colburn analogie.

#### **Dynamische modelvorming**

Om het effect van periodieke bedrijfsvoering op de prestaties van een trickle-bed reactor voor zowel vloeistof- als gasgelimiteerde reacties te bestuderen, is een dynamisch model ontwikkeld.

---

Diffusie in de katalysatordeeltjes is in het model opgenomen omdat de snelheid van interne diffusie in belangrijke mate bepaalt welke eigenschappen van het cyclisch vloeistofdebiet optimaal zijn. Het effect van periodieke bedrijfsvoering op conversie, selectiviteit en productiecapaciteit is bestudeerd.

In het geval van gasgelimiteerde reacties resulteert periodieke bedrijfsvoering in vergelijking met de optimale stationaire bedrijfsvoering in een belangrijke toename van zowel conversie als productiecapaciteit. Voor vloeistofgelimiteerde reacties daarentegen is stationaire bedrijfsvoering beter dan periodieke bedrijfsvoering. De optimale tijdsspannen van de hoge en lage vloeistofvoeding zijn sterk van elkaar afhankelijk. In vergelijking met langzame reacties is voor snelle reacties een relatief korte duur van het lage vloeistofdebiet en een relatief hoge verhouding tussen de duur van het hoge en lage vloeistofdebiet nodig.

Een relatief hoge frequentie van een variërende vloeistofsnelheid in de reactor is effectiever voor een hoge productiecapaciteit, conversie en selectiviteit. Met een toenemende frequentie van het vloeistofdebiet is de tijdsgemiddelde concentratie van de vloeistoffase reactant in de katalysator hoger en de tijdsgemiddelde concentratie van het product lager. Dit leidt tot een belangrijkere bijdrage van de gewenste reactie ten opzichte van de ongewenste reactie.

#### **Concluderende opmerkingen**

Voor zowel vloeistof- als gasgelimiteerde reacties zijn er verschillende niet-stationaire voedingsstrategieën ontwikkeld en onderzocht, die de stofoverdrachtssnelheid van de limiterende reactant vergroten. Voor vloeistofgelimiteerde reacties is de bedrijfsvoering van een trickle-bed reactor in het natuurlijke pulsing flow regime het meest geschikt omdat dan de katalysatorbenutting en de stofoverdracht tussen de vloeistof en de katalysator optimaal zijn. Tevens kan de 'fast mode of liquid-induced pulsing flow' bij hoge frequenties worden toegepast om de verblijftijd van de vloeistoffase in de reactor te vergroten. In het geval van gasgelimiteerde reacties kan door een cyclisch vloeistofdebiet de katalysatorbenutting gecontroleerd op een laag niveau gehouden worden zonder dat een niet-uniforme vloeistofverdeling plaatsvindt. De snelheid van stofoverdracht van de limiterende gasfase reactant wordt periodiek sterk verhoogd tijdens de lage vloeistofvoeding, omdat dan gedeeltelijke katalysatorbenutting optreedt. Met name de 'slow mode of liquid-induced pulsing flow' voorkomt de vorming van hot spots.

---

De ‘fast mode of liquid-induced pulsing flow’ kan worden toegepast indien een relatief hoge frequentie van de variërende vloeistofsnelheid in de trickle-bed reactor vereist is, zoals bijvoorbeeld voor selectiviteitsredenen. Meer algemeen worden een niet-uniforme vloeistofverdeling en de vorming van hot spots, de belangrijkste problemen tijdens een stationaire bedrijfsvoering in het trickle flow regime, door periodieke bedrijfsvoering voorkomen.

Omdat de periodieke bedrijfsvoering berust op het manipuleren van een externe variabele, kunnen bestaande trickle-bed reactoren relatief eenvoudig worden aangepast om de prestaties te verbeteren. Voor nieuw te ontwikkelen trickle-bed reactoren wordt een afname in de investeringskosten verwacht omdat vloeistof herverdelers en interne warmtewisselaars kunnen worden geëlimineerd. Tevens is het mogelijk reactoren kleiner uit te voeren en bij lagere drukken te bedrijven. Deze veronderstellingen duiden erop, dat periodieke bedrijfsvoering een algemene methode is en een brede toepassing zou kunnen vinden.

De resultaten beschreven in dit proefschrift zijn behulpzaam geweest in verband met het opzetten van het Europees project CYCLOP, dat als doel heeft het ontwikkelen van ontwerpregels en methoden van bedrijfsvoering voor niet-stationair bedreven trickle-bed reactoren.



---

# Contents

---

<b>1. General introduction on trickle-bed reactors</b>	<b>1</b>
1.1. Three-phase reactors	
1.2. Trickle-bed reactors	
1.3. Flow maldistribution	
1.4. Formation of hot spots	
1.5. Partial wetting effect	
1.6. Periodic operation of a trickle-bed reactor	
1.7. Scope and objective of the thesis	
1.8. Outline of the thesis	
Notation	
Literature cited	
<b>2. Nature and characteristics of pulsing flow</b>	<b>23</b>
2.1. Introduction	
2.2. Scope and objective	
2.3. Experimental setup and procedures	
2.4. Transition boundary	
2.5. Characterization of pulsing flow	
2.6. Nature of pulsing flow	
2.7. Concluding remarks	
Notation	
Literature cited	
A2. Pulsing flow characteristics for other packing materials	
<b>3. Local particle-liquid heat transfer coefficient</b>	<b>53</b>
3.1. Introduction	
3.2. Scope and objective	
3.3. Experimental setup and procedures	
3.4. Hydrodynamics	
3.5. Local particle-liquid heat transfer coefficient	
3.6. Particle-liquid heat transfer coefficient during pulsing flow	
3.7. Concluding remarks	
Notation	
Literature cited	



---

<b>4. The induction of pulses by cycling the liquid feed</b>	<b>69</b>
4.1. Introduction	
4.2. Scope and objective	
4.3. Experimental setup and procedures	
4.4. Steady state hydrodynamics	
4.5. Continuity shock waves	
4.6. Induction of pulses	
4.7. Concluding remarks	
Notation	
Literature cited	
<b>5. Liquid-induced pulsing flow: Development of feed strategies</b>	<b>89</b>
5.1. Introduction	
5.2. Scope and objective	
5.3. Experimental setup and procedures	
5.4. Continuity shock waves	
5.5. Slow mode of liquid-induced pulsing flow	
5.6. Fast mode of liquid-induced pulsing flow	
5.7. Evaluation of potential advantages	
5.8. Concluding remarks	
Notation	
Literature cited	
<b>6. Local particle-liquid mass transfer coefficient</b>	<b>115</b>
6.1. Introduction	
6.2. Scope and objective	
6.3. Experimental setup and procedures	
6.4. Hydrodynamics	
6.5. Time-average mass transfer coefficient	
6.6. Mass transfer coefficients in pulsing flow	
6.7. Heat and mass transfer analogy	
6.8. Distribution of local mass transfer coefficients	
6.9. Concluding remarks	
Notation	
Literature cited	
A6. Optimal electrochemical system	

---

**7. Dynamic modeling of periodically operated trickle-bed reactors** **145**

- 7.1. Introduction
  - 7.2. Scope and objective
  - 7.3. Model development
  - 7.4. Simulation parameters and steady state results
  - 7.5. Single step reaction
  - 7.6. Consecutive reaction
  - 7.7. Practical relevance of modeling results
  - 7.8. Concluding remarks
- Notation  
Literature cited

**8. Periodic operation: State of the art and perspectives** **179**

- 8.1. Introduction
  - 8.2. Hydrodynamic description of operation modes
  - 8.3. Gas-limited reactions
  - 8.4. Liquid-limited reactions
  - 8.5. Hot spot control by periodic operation
  - 8.6. Future challenges
  - 8.7. Concluding remarks
- Literature cited



---

## Chapter 1

---

# General Introduction on Trickle-Bed Reactors

---

### 1.1. Three-phase reactors

Processes based upon heterogeneously catalyzed reactions occur in a broad range of application areas and form the basis for the manufacturing of a large variety of intermediate and consumer-end products. Heterogeneously catalyzed gas-liquid reactions are often characterized by a high reactivity, hence internal and external mass transport rates are rate limiting. Therefore, an essential function of a three-phase reactor is the contacting between the phases.

Several potential reactor arrangements exist for the processing of heterogeneously catalyzed gas-liquid reactions. A fundamental classification of three-phase reactors is made depending on whether the catalyst is suspended (slurry reactor) or fixed (fixed-bed, monolith reactor).

#### 1.1.1. Slurry reactors

In a slurry reactor (Fig. 1.1a), small catalyst particles (1-200  $\mu\text{m}$ ) are suspended in the liquid by either a mechanical stirrer or by the gas flow. Slurry reactors can be operated batch-wise as well as (semi-) continuous. When the catalyst particles are sufficiently large to form a distinct third phase, a continuously operated slurry reactor is also called a three-phase fluidized bed. In some cases, the gas-liquid mixture is injected as a jet at high velocity to promote mixing and total utilization of the pure gas reactant. To assure a strong internal liquid circulation, a draft tube may be installed inside the reactor.

The catalyst load in slurry reactors is limited by the agitation power of the mechanical stirrer or by the gas flow. However, the small dimensions of the catalyst particles provide catalyst utilization factors that approach unity. Due to substantial mixing, high conversions can be realized by the staging of several reactors only. Temperature control is relatively simple due to the large amount of liquid present and the possibility to install coolers inside the reactor. One of the most difficult aspects of these reactors is the catalyst filtration step. However, in case of rapid catalyst deactivation, continuous catalyst removal and regeneration is crucial and slurry reactors are likely to be applied.

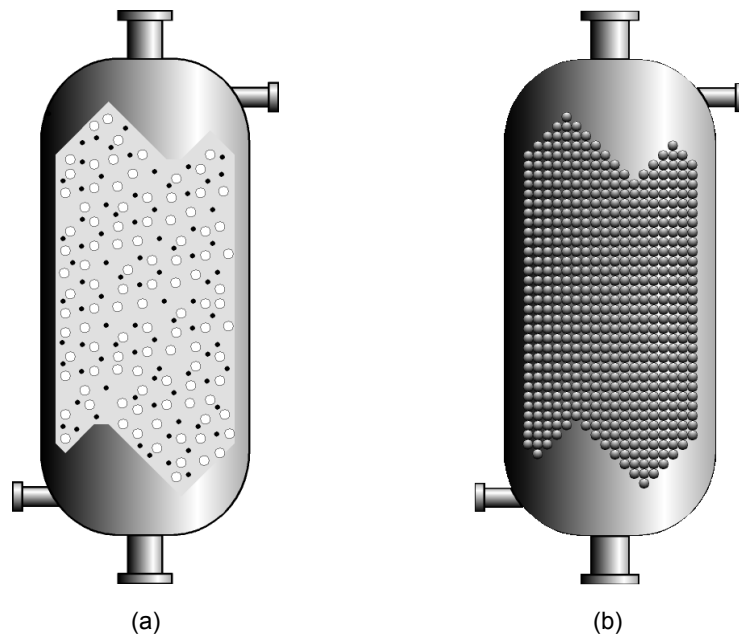


**Figure 1.1.** Schematic illustration of a (a) slurry bubble column and a (b) fixed bed reactor

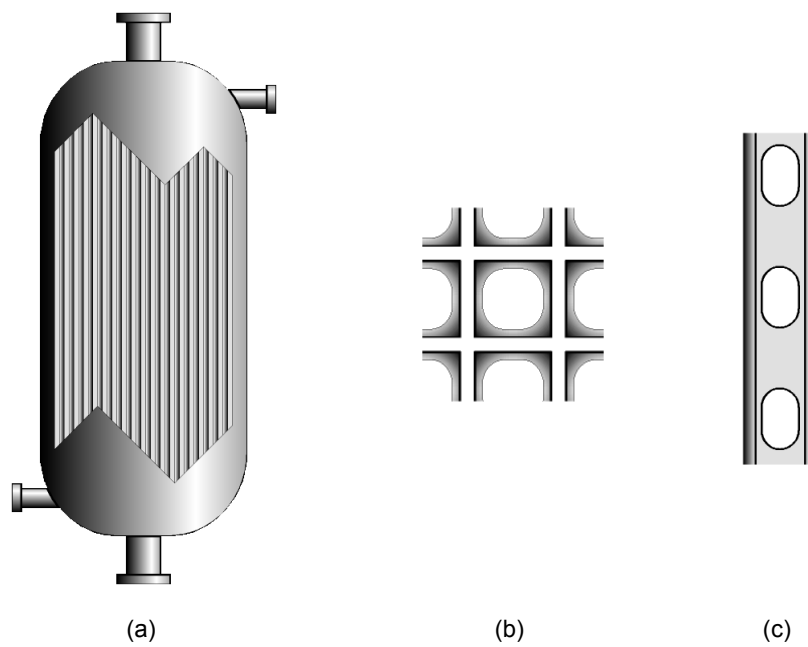


**Figure 1.2.** Schematic illustration of (a) a monolith reactor; (b) monolith structure with quadratic cells; (c) Taylor flow in a cylindrical capillary

The slurry reactor is widely implemented in the fine chemical and pharmaceutical industry for selective catalytic hydrogenations. Since in these industries, multipurpose manufacturing is an important issue, the operation is most often batch or semi-continuous. Bubbling slurry reactors are particularly employed in fermentation processes (Biardi and Baldi, 1999). Three-phase fluidized beds have been applied industrially in coal liquefaction.

#### **1.1.2. Fixed bed reactors**

A fixed bed reactor (Fig. 1.1b) consists of a cylindrical column in which a fixed bed of catalyst particles is randomly dumped. The catalyst (1–3 mm) may be spherical, cylindrical or have more sophisticated shapes like multilobes. Fixed bed reactors are characterized by a high catalyst load, while catalyst utilization is rather poor due to internal transport limitations in the relatively large particles. Smaller particles increase catalyst utilization but also cause increased pressure drop and thus higher compressor costs. Consequently, a shell catalyst that is only catalytically loaded in the outer layer is frequently applied. Due to the plug flow characteristics of a fixed bed reactor, very high conversions can be obtained. The poor radial heat transfer in commercial scale reactors implies that operation is essentially adiabatic (Biardi and Baldi, 1999) and therefore temperature control is rather difficult. Occasionally, partial evaporation of the liquid is used for cooling. Special care is required to prevent flow maldistribution, which can cause incomplete catalyst wetting in some parts of the bed. This may result in reduced overall production rates and poorer selectivity. For strongly exothermic reactions, more severe consequences as hot spot formation and possibly even runaways must be considered. The investment costs of a fixed bed reactor are rather low.

When a fixed bed is selected, the issue whether to employ cocurrent upflow or downflow operation must be considered. Operating a randomly packed bed reactor in the countercurrent mode is usually not feasible since flooding occurs at gas velocities far below industrial relevance. In cocurrent upflow, complete catalyst wetting at the expense of much larger liquid holdup is obtained compared to cocurrent downflow. The high liquid holdup increases the liquid film mass transfer resistance for the gaseous reactant and is undesirable if homogeneous liquid phase side-reactions occur. Due to complete catalyst wetting and a higher liquid holdup, heat transfer characteristics are much better in cocurrent upflow operation. In cocurrent upflow, the flow may induce local vibration or movement of the particles, which possibly results in attrition of the catalyst.

### 1.1.3. Monolith reactor

A monolith reactor (Fig. 1.2) consists of a bundle of parallel tubular channels of approximately 1 mm in diameter. The tubes are covered at the inside with a catalytically active wash coat of approximately 20-100  $\mu\text{m}$  thickness. Catalyst utilization is near complete due to the short diffusion distance in the catalytic wash coat. The catalyst load is less than in a fixed bed. In-situ catalyst regeneration is crucial, since the catalyst cannot be removed.

The pressure drop in a monolith reactor is about two orders of magnitude smaller compared to the pressure drop in a fixed bed reactor (Edvinson and Cybulski, 1994). Gas recirculation is therefore easy to achieve. The most delicate problem is to obtain a uniform distribution of flow at the reactor inlet. The relatively little experience with monolith reactors makes the design more accessible to uncertainties.

Monolith reactors are operated in the Taylor flow regime, in which alternate slugs of gas and liquid flow through the channels. The very thin liquid film between the catalyst and the gas slug ensures high overall gas-solid mass transfer rates. Monolith reactors are widely employed in the exhaust/gas cleaning. The hydrogenation of alkyl anthraquinone in hydrogenperoxide production is the only commercial example (Eka Nobel, Akzo Nobel).

### 1.1.4. Selection of optimal reactor configuration

The design of a reactor for a three-phase reaction system starts with catalyst design. The optimal particle size with respect to the production rate per unit reactor volume is obtained by a transport-reaction analysis. The selection of the reactor configuration is affected by the optimal particle size. Due to internal diffusion limitations, catalyst utilization diminishes with increasing catalyst size. When relatively small particles ( $< 1$  mm) are desirable, a slurry reactor is the most common choice. In this reactor type, catalyst effectiveness factors approaching unity can be achieved. A three-phase packed bed is then unlikely to be applied since small particles result in a high pressure drop. When relative large catalyst particles ( $> 2$  mm) are sufficient, a fixed bed reactor may be applied also. Providing that other motivations than an optimal catalyst size favor a fixed bed reactor, shell catalysts may be used. Volumetric gas-liquid mass transfer coefficients are comparable for slurry reactors and fixed bed reactors.

In general, the volumetric production capacity of a slurry reactor dominates the production capacity of a fixed bed reactor (Edvinson and Cybulski, 1994).

A slurry reactor is favorable in case of highly exothermic reactions, since heat removal is much better than in fixed bed reactors. Hence, as regards to safety considerations, a slurry reactor is then the best alternative.

In a fixed bed reactor, the liquid tends to approach plug flow and therefore a relatively high conversion can be obtained. In a slurry reactor, the residence time distribution is close to that of a continuously stirred tank reactor. By staging of several slurry reactors, higher conversions can be achieved at the expense of higher costs.

The necessary catalyst filtration step, which is technically difficult and expensive, favors the use of a three-phase packed bed reactor in terms of flexibility of operation and reduction of costs. However, when the catalyst life span is rather short, a slurry reactor is more flexible in operation. Another operation-linked advantage of a slurry reactor is its adaptability to continuous as well as to batch processes.

Knowledge on reactors with moving catalysts is less complete than for fixed bed reactors. Hence, the scale-up procedures are more accessible to uncertainties and it is not possible in general to relate the performance of a laboratory size unit to large-scale reactors via simple scale-up rules.

In many cases, the final choice is determined by the required selectivity. When the reaction product tends to undergo a consecutive reaction in the liquid phase, a packed bed is preferred because of its low liquid holdup. When the side reaction occurs inside the catalyst, small particles are desirable and subsequently the slurry reactor may be the final choice.

It is obvious that the elementary criteria for selecting a certain three-phase reactor configuration can be opposing. A trade-off between the desired production capacity, product quality, safety and flexibility in operation and the amount and quality of waste products is to be made. This means that in most cases not all the process “wants” can be met.

## **1.2. Trickle-bed reactors**

Trickle-bed reactors are the most widely used type of three-phase reactors. The gas and liquid cocurrently flow downward over a fixed bed of catalyst particles.



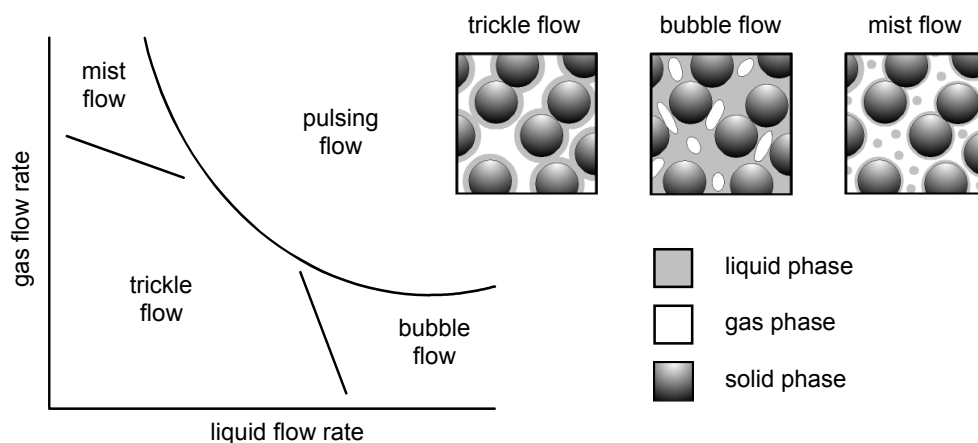


**Figure 1.3.** Schematic illustration of the location of the trickle, mist, bubble and pulsing flow regimes with respect to gas and liquid flow rates

Approximate dimensions of trickle-bed reactors are a height of 10 m and a diameter of 2 m. Trickle-bed reactors are employed in petroleum, petrochemical and chemical industries, in waste water treatment and biochemical and electrochemical processing (Al-Dahhan et. al., 1997). Table 1.1 lists some of the commercial processes carried out in trickle-bed reactors.

Most commercial trickle-bed reactors operate adiabatically at high temperatures and high pressures and generally involve hydrogen and organic liquids with superficial gas and liquid velocities up to 0.3 and 0.01 m s<sup>-1</sup> respectively. Kinetics and/or thermodynamics of reactions conducted in trickle-bed reactors often require high temperatures. Elevated pressures (up to 30 MPa) are required to improve the gas solubility and the mass transfer rates (Al-Dahhan et. al., 1997).

### 1.2.1. Flow regimes

In a trickle-bed, various flow regimes are distinguished, depending on gas and liquid flow rates, fluid properties and packing characteristics. According to Charpentier and Favier (1975, 1976), the four main flow regimes observed for non-foaming systems are trickle flow, pulsing flow, mist flow and bubble flow. The flow regime boundaries with respect to gas and liquid flow rates are schematically shown in Fig. 1.3. Each flow regime corresponds to a specific gas-liquid interaction thus having a great influence on parameters as liquid holdup, pressure drop and mass and heat transfer rates.

**Table 1.1.** Examples of commercial trickle-bed reactor processes

Trickle-bed process	Reference
Residuum and vacuum residuum desulfurization	(Meyers, 1996)
Catalytic dewaxing of lubestock cuts	(Meyers, 1996)
Sweetening of diesel, kerosine jet fuels, heating oils	(Meyers, 1996)
Hydrodemetallization of residues	(Trambouze, 1993)
Hydrocracking for production of high-quality middle distillate fuels	(Meyers, 1996)
Hydrodenitrofication	(Meyers, 1996)
Isocracking for the production of isoparaffin-rich naphta	(Meyers, 1996)
Production of lubricating oils	(Meyers, 1996)
Selective hydrogenation of butadiene to butene	(Charpentier, 1976)
Selective hydrogenation vinylacetylene to butadiene	(Charpentier, 1976)
Selective hydrogenation of phenyl acetylene to styrene	(Charpentier, 1976)
Selective hydrogenation of alkylanthraquinone to hydroquinone for the production of hydrogen peroxide	(Shah, 1979)
Hydrogenation of nitro compounds	(Germain et. al., 1979)
Hydrogenation of carbonyl compounds	(Germain et. al., 1979)
Hydrogenation of carboxylic acid to alcohols	(Germain et. al., 1979)
Hydrogenation of benzene to cyclohexane	(Germain et. al., 1979)
Hydrogenation of phenyl aniline to cyclohexylaniline	(Germain et. al., 1979)
Hydrogenation of glucose to sorbitol	(Germain et. al., 1979)
Hydrogenation of coal liquefaction extracts	(Germain et. al., 1979)
Hydrogenation of benzoic acid to hydrobenzoic acid	(Germain et. al., 1979)
Hydrogenation of caprolactone to hexanediol	(Germain et. al., 1979)
Hydrogenation of organic esters to alcohols	(Germain et. al., 1979)
Synthesis of butynediol from acetylene and aqueous formaldehyde	(Gianetto and Specchia, 1992)
Immobilized enzyme reactions	(Belhaj, 1984)
VOC abatement in air pollution control	(Diks and Ottengraf, 1991)
Wet air oxidation of formic acid, acetic acid and ethanol	(Baldi et. al., 1985)
Oxidation of sulphurdioxide	(Mata and Smith, 1981)
Oxidation of glucose	(Tahraoui, 1990)
Biochemical reactions and fermentations	(Bailey and Ollis, 1986)

The trickle flow regime prevails at relatively low gas and liquid flow rates. The liquid flows as a laminar film and/or in rivulets over the packing particles, while the gas passes through the remaining void space. At high gas and low liquid flow rates, transition to mist flow occurs. The liquid mainly travels down the column as droplets entrained by the continuous gas phase.

The bubble flow regime appears at high liquid flow rates and low gas flow rates, and is opposite in composition to mist flow. The liquid is the continuous phase and the gas moves in the form of dispersed bubbles. At moderate gas and liquid flow rates, the pulsing flow regime is obtained. This regime is characterized by the successive passage of liquid-rich and gas-rich regions through the bed.

Despite the steady state appearance of the trickle, bubble and spray flow regimes, the physical and chemical processes, when viewed on spatial scales much smaller than the reactor, are inherently unsteady. In fact, the observed macroscale flow regimes can be attributed to various combinations of microscale flow patterns, which are the outcome of local competition between liquid and gas in the packing interstices (Melli et. al., 1990; Tsochatzidis and Karabelas, 1994). In the pulsing flow regime, the unsteady state behavior is more pronounced because the spontaneous arising non-uniformity of the flow pattern manifests itself at the macroscale.

### **1.2.2. Pulsing flow**

The interesting flow regime termed pulsing flow prevails at higher gas and liquid flow rates compared to trickle flow. This flow regime is characterized by the passage of liquid-rich bubbly waves called pulses, followed by relative quiet periods resembling trickle flow. These pulses move downwards with a velocity of about  $1 \text{ m s}^{-1}$ . Pulse frequencies are typically 1–10 Hz and pulse lengths about 0.1 m (Blok and Drinkenburg, 1982; Tsochatzidis and Karabelas, 1995; Rao and Drinkenburg, 1983).

The pulses are characterized by high particle-liquid mass transfer rates (Chou et. al., 1979; Rao and Drinkenburg, 1985; Tsochatzidis and Karabelas, 1994). Since the gas is dispersed as bubbles inside the pulses, high gas-liquid interfacial areas and gas-liquid mass transfer rates arise (Fukushima and Kusaka, 1977; Hirose et. al., 1974; Blok et. al., 1984). Inside the pulses, wetting is complete and hence already developing hot spots are periodically flushed with liquid. Moreover, the pulses continuously mobilize the stagnant liquid holdup up to the point where its stagnant nature disappears. Since the stagnant liquid holdup represents about 10% to 30% of the total liquid holdup in trickle flow operations (Sicardi et. al., 1980; Colombo et. al., 1976), its more active character during pulsing flow will enhance reactor performance, especially for undesired consecutive reactions. Axial dispersion is less compared to trickle flow due to increased radial mixing and disappearance of stagnant liquid holdup (Lerou et. al., 1980).

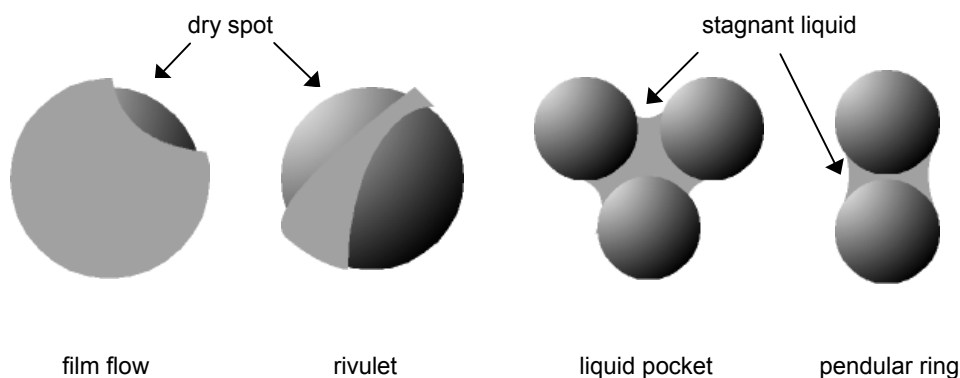


**Figure 1.4.** Schematic illustration of the several liquid flow textures encountered during trickle flow operation

### 1.3. Flow maldistribution

Liquid phase maldistribution is an important factor in the design, scale-up and operation of trickle-bed reactors (McManus et. al., 1993). For reasons such as an ineffective liquid inlet distributor, packing anisotropy, catalyst fines, changing liquid physical properties or physical obstructions, large sections of the bed may be bypassed by liquid (Stanek et. al., 1981; Moller et. al., 1996). Proper design of liquid distributors and redistribution of liquid in quench boxes and other devices can deal with this problem. Liquid maldistribution may result in two undesirable effects. With no supply of the liquid phase reactant to the dry parts of the bed, essentially no reaction in these regions occurs and the reactor is not fully utilized. In contrast, if a sufficient amount of liquid is vaporized, reaction still proceeds in these unwetted regions. Without the liquid phase removing the reaction heat, however, this may result in hot spot formation. A basic understanding of the impact of liquid maldistribution on reactor performance is thus essential.

In the trickle flow regime, the liquid is present as films, rivulets, pendular structures and liquid pockets (Zimmerman and Ng, 1986; Ravindra et. al., 1997), the latter two being highly stagnant in nature (Fig. 1.4). Even for an “ideal” liquid distribution at the top of the column, rivulets form downstream due to non-uniform porosity and the capillary pressure effect. Rivulets formed at low liquid flow rates gradually expand with increasing liquid flow rate. Large catalyst particles, uneven catalyst loading and a non-uniform liquid inlet distribution enhance channeling.

Pre-wetting of the bed is an important factor for improving the liquid distribution during operating conditions (Moller et. al., 1996; Ravindra et. al., 1997; Jiang et. al., 1999).

It is appropriate to distinguish between bed-scale and particle-scale partial wetting. During trickle flow, non-irrigated, partially irrigated as well as completely irrigated (regions of) catalyst particles coexist (Crine and Marchot, 1983). Almost complete wetting is established at high liquid flow rates. Knowledge of the importance and distribution of bed-scale and particle-scale wetting is indispensable for a correct calculation of the reactor performance. A realistic description of the flow conditions and the resulting interactions with the mechanisms of heat and mass transfer is crucial for a fundamental understanding of reactor performance.

#### **1.4. Formation of hot spots**

Trickle-bed reactors are often applied to perform strong exothermic reactions such as the hydrogenation of unsaturated hydrocarbons. One of the major disadvantages of trickle-bed reactors is their poor capability to eliminate the heat involved with reaction. Considering the low heat capacity of the gas, the liquid eliminates this heat. In case the generated heat is not adequately removed, hot spots may be created. These hot spots cause the catalyst particles to sinter, which decreases its activity and surface area. This results in a reduced catalyst life span as well as an increase in operating costs. In addition, hot spots can cause serious safety problems as they can damage the reactor casing and can lead to a reactor runaway. Undesirable side reactions are promoted due to non-uniform temperature distributions and varying residence time of the reactants. For these reasons, it is essential to determine when and how these hot spots are formed so that they can be avoided.

Hot spots are observed in industrial scale trickle-bed reactors running highly exothermic reactions (Goossens et. al., 1997; Jaffe, 1976; Barkelew and Gambhir, 1984) and laboratory-scale reactors (Julcour et. al., 2001; McManus et. al., 1993; Hanika et. al., 1976; Satterfield and Ozel, 1973; Germain et. al., 1974; Weekman, 1976; Hanika, 1999). The formation of hot spots is the result of flow maldistribution causing non-uniform irrigation of the catalyst. In a dry region, reaction between volatile components proceeds, its rate being usually higher compared to liquid phase conditions.

Since the liquid phase is absent, the reaction heat is not removed. The higher reaction rate accelerates heat production and hence hot spot enlargement is often observed (Hanika, 1999).

The elimination of hot spot formation is extremely important from its safe operation point of view. One possibility is the application of smaller catalyst particles to improve wetting and internal mass transfer (Hanika, 1999). Another method to control temperature excursions is cycling the liquid feed concentration (Hanika, 1999). By a decrease in the reactant concentration when a pre-determined maximum bed temperature is reached, a temperature decrease in the whole system is achieved. Periodically flooding the trickle-bed cuts off the development of hot spots also. Additionally, the operation of a trickle-bed reactor in the pulsing flow regime may be utilized to eliminate hot spots.

### **1.5. Partial wetting effect**

Most reaction systems can be classified as being liquid reactant or gas reactant limited (Mills and Dudukovic, 1980; Khaldikar et. al., 1996). For liquid-limited reactions, the highest possible wetting efficiency results in the fastest transport of the liquid phase reactant to the catalyst. Liquid-limited reactions are frequently encountered in high-pressure operations in petroleum processing and in processes in which a diluted liquid phase reactant must be converted, as in hydrodesulfurization and oxidation of organic compounds in waste water treatment.

Gas-limited reactions occur when the gaseous reactant is slightly soluble in the liquid and at moderate operating pressures (Beaudry et. al., 1987). Since for a completely wetted particle, the gaseous reactant must overcome both the gas-liquid and liquid-solid mass transfer resistances, partial wetting facilitates a much more effective transport of the gaseous reactant at the dry surface. At higher Thiele moduli, when the reaction rate is large compared to the internal diffusion rate, external mass transfer greatly affects the observed reaction rate. The reduction of the mass transfer resistance for the rate-limiting gaseous reactant on partially wetted catalyst pellets leads to (much) higher observed reaction rates (studies summarized in table 1.2). The global reaction rate can be approximated by the sum of contributions from wetted and non-wetted external surfaces by using the wetting efficiency as a weighting factor (Ishigaki and Goto, 1999; Sedriks and Kenney, 1973):

$$r_{\text{obs}} = f_w r_l (C_L) + (1 - f_w) r_l (C_L^*) \quad [1.1]$$

The first term in eq. 1.1 refers to the reaction rate in the wetted fraction ( $f_w$ ) of the catalyst where the surface concentration of the gaseous reactant approaches the concentration in the liquid phase ( $C_L$ ). The second term in eq. 1.1 corresponds to the reaction rate in the non-wetted fraction ( $1-f_w$ ) of the catalyst, where the surface concentration of the gaseous reactant can usually be approached by vapor-liquid equilibrium ( $C_L^*$ ), since gas solid mass transfer resistances can be assumed negligibly small. Internal catalyst wetting is complete due to capillary forces. For highly exothermic reactions with a volatile liquid phase reactant, the contribution of a gas phase reaction over an externally and internally dry catalyst is significant or even dominates the overall reaction rate (studies summarized in table 1.2). The global reaction rate is now expressed as:

$$r_{\text{obs}} = f_w r_l (C_L) + (1 - f_w) r_g (C_G) \quad [1.2]$$

The second term in eq. 1.2 corresponds to the reaction rate in the externally and internally non-wetted fraction ( $1-f_w$ ) of the catalyst at gas phase concentration ( $C_G$ ). For the hydrogenation of 1-methylnaphtalene for example, Ishigaki et. al. (1999) suggested the existence of 15%-38% completely dry catalyst particles.

Incomplete wetting of the catalyst particles leads to a non-uniform concentration of the reactants and product at the outer surface of the catalyst. As a result, the concentration profiles inside the pores are non-symmetrical. Conventional catalyst effectiveness factor concepts are therefore not applicable for partially wetted catalyst particles. Several models to specify the effectiveness factor for partially wetted catalyst particles are proposed in literature (e.g. Herskowitz et. al., 1979; Mills and Dudukovic, 1980; Ramachandran and Smith, 1979; Herskowitz, 1981; Zhu and Hofmann, 1997; Goto et. al., 1981). In case of liquid-limited reactions, higher wetting efficiencies result in higher catalyst effectiveness factors. Intermediate external wetting results in large increases in the catalyst effectiveness factor for gas-limited reactions. However, at very poor wetting, the reaction becomes liquid limited.

Specifying the wetting efficiency as such is not sufficient to determine the catalyst effectiveness factor (Ring and Missen, 1989; Yentekakis and Vayenas, 1987). The number and distribution of wetted zones on a catalyst particle must be specified to calculate effectiveness factors.

**Table 1.2.** Summary of experimental and modeling studies concerning the partial wetting effect

Reaction system	internal/external non-wetting	reference
hydrogenation of 1- methylnaphthalene	external and internal gas-phase reaction	Ishigaki et. al. (1999)
oxidation of ethanol	external, hydrophobic / hydrophilic catalyst	Horowitz et. al. (1999)
oxidation of ethanol	external	Goto and Mabuchi (1984)
oxidation of ethanol	external	Tukac et. al. (1989)
hydrogenation of 1,5,9-cyclododecatriene	external	Julcour et. al. (2001)
hydrogenation of benzene	external and internal gas phase reaction	Satterfield and Ozel (1973)
hydrogenation of cronataldehyde	gas phase reaction external and internal	Sedriks and Kenney (1973)
hydrodesulfurization of dibenzothiophene	gas phase reaction external	Ring and Missen (1989)
hydrogenation of alpha-methylstyrene	external and internal gas phase reaction	Castellari et. al. (1997)
hydrogenation of 2,4 dinitrotoluene	external	Rajashekharam et. al. (1998)
hydrogenation of alpha-methylstyrene	external	Funk et. al. (1991)
hydrogenation of cyclohexene	external and internal gas-phase reaction	Watson and Harold (1994)
oxidation of phenol	external	Pintar et. al. (1997)



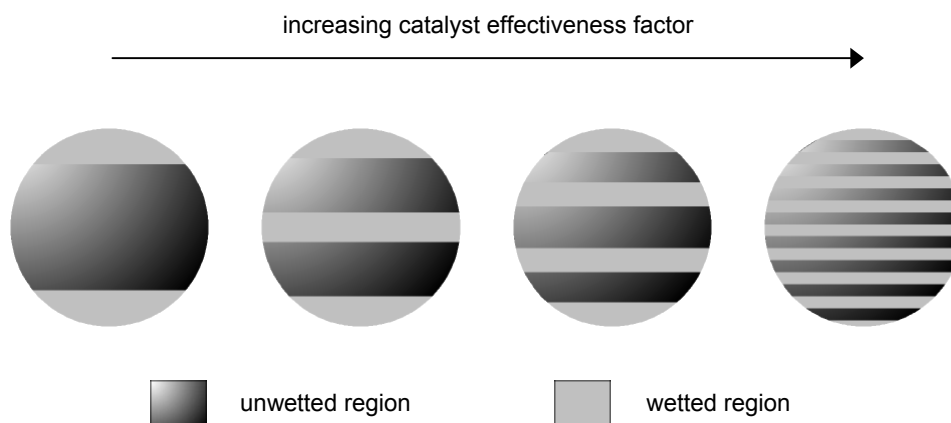


**Figure 1.5.** Illustration of the increase in catalyst effectiveness factor with increasing number of wetted regions at constant wetting efficiency

At a given wetting efficiency, the catalyst effectiveness factor increases with an increasing number of wetted regions, reaching a limiting value at an infinite number of uniformly distributed wetted zones (Fig. 1.5). Kouris et. al. (1998) modeled the effect of time-varying wetting efficiency on the effectiveness factor. In the high frequency limit, when the particle is unable to follow the rapid changes in wetting, it reaches a stationary state that depends on the time-averaged wetting efficiency. This relaxed steady state approximates the steady state obtained for the limiting case of an infinite number of uniformly distributed wetted zones. These frequencies of periodic wetting correspond to the frequencies of pulsing flow. Therefore, it was concluded that during pulsing flow, the highest possible catalyst effectiveness factors are achieved.

It could be of some advantage to design a trickle-bed reactor for partial wetting in case of gas-limited reactions. It is possible that some existing beds in industry owe their performance by this type of mechanism, whether by design or not (Sedriks and Kenney, 1973). The main problem is to attain partial wetting without gross maldistribution, which usually leads to unpredictable and uncontrollable reactor performance. If large sections of the bed are completely dry, the reaction becomes severely limited by liquid-phase reactant transfer (Beaudry et. al., 1987). On the other hand, on dry areas well fed by volatile reactants, hot spots may occur. Given the complexity of the hydrodynamics and the importance of the extent and distribution of wetting, this is unlikely to be reliable on a priori analysis.

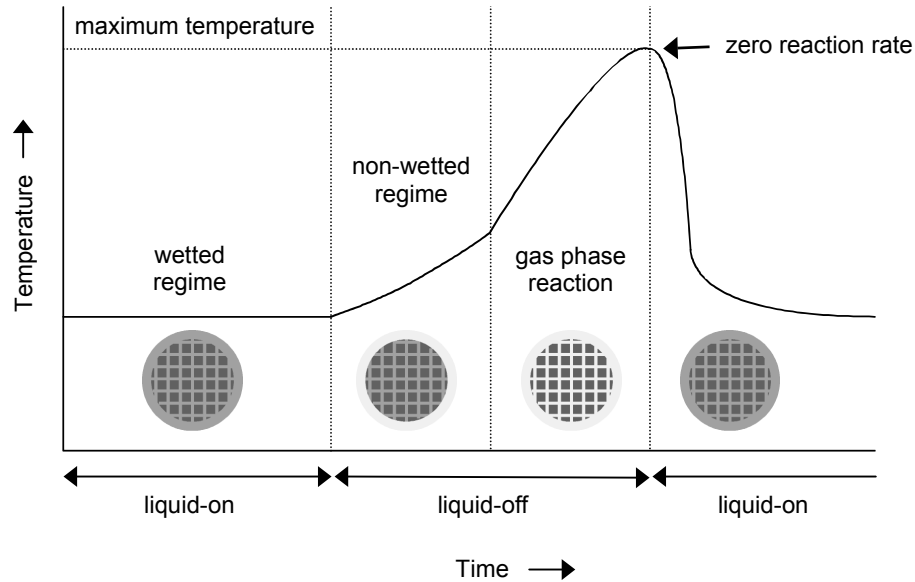


**Figure 1.6.** Effect of periodic operation on the temperature of the catalyst bed

## 1.6. Periodic operation of a trickle-bed reactor

Trickle-bed reactors are usually operated at steady state conditions. Recent studies have demonstrated reactor performance improvement over the optimal steady state under forced time-varying liquid flow rates. In this mode of operation, the bed is periodically flushed with liquid, while the gas phase is fed continuously. The liquid adds a transport resistance for the gaseous reactant that is often rate controlling for sparingly soluble gaseous reactants. The liquid phase, however, is essential to the system and cannot be eliminated. By periodic operation of a trickle-bed reactor, the transport resistance for the gaseous reactant is periodically reduced.

The use of a trickle-bed reactor packed with activated carbon has been recognized as a promising technology for the removal of  $\text{SO}_2$  (Lee et al., 1995). The water flow continuously restores the catalyst by converting the strongly adsorbed  $\text{SO}_3$  to  $\text{H}_2\text{SO}_4$ . To overcome the drawback of the transport resistances added by the liquid phase, Haure et. al. (1989) used the concept of periodic flushing of a trickle-bed. During the liquid flush, the product is removed from the catalyst, while in between flushes, the gaseous reactants can more easily adsorb on the catalyst. With this mode of operation, increases in oxidation rates up to 50% were achieved.

To demonstrate the advantages of periodic operation for a reaction, in which both gas and liquid phases contain reactants, the hydrogenation of  $\alpha$ -methyl styrene was studied by Lange et. al. (1994), Castellari and Haure (1995) and Gabarain et. al. (1997). Increases in reaction rates up to 400 % were obtained.

The basic mechanisms for this performance improvement are discussed upon the temperature profile presented in Fig. 1.6. During the flush, the bed is isothermal and the reaction heat is removed by the liquid phase. Wetting is near complete and the reaction proceeds between the dissolved gaseous reactant and the liquid reactant. When the flush ends, the bed partially drains and reaction proceeds between the liquid-phase reactant inside the catalyst and the continuously flowing gas phase. Partial wetting conditions arise, enhancing the transport of the gaseous reactant to the catalyst surface. The interruption of the liquid flow reduces heat removal and elevates the bed temperature. Under these conditions, even evaporation of the liquid phase may occur. When all the liquid is drained and/or evaporated, a change in the reaction mechanism from mass transfer limited to a gas-phase reaction over a dry catalyst is realized. This results in a further temperature increase. The temperature reaches a maximum since eventually, depletion of the liquid phase reactant reduces the reaction rate. The product occupying the catalytic sites may inhibit the reaction. Moreover, the bed cools down as the liquid feed is switched on and a subsequent cycle is started.

## 1.7. Scope and objective of the thesis

At present, steady state operation in the trickle flow regime is most common in industrial applications. Steady state operations play a very important role in chemical engineering due to the ease of material and energy recycling and the ability of set point control. Nevertheless, it is very unlikely that steady state operations provide the best in conversion and selectivity as discussed before. Since progress in automatic process control nowadays brings essentially every forcing function within reach, there is no need to keep the process steady state from that point of view. Also the recyclability of mass and energy is still possible for non-steady operations if cycle times are within reasonable bounds.

The objective of the study described in this thesis is essentially process intensification of a trickle-bed reactor by nonsteady state operation. Process intensification includes enhanced conversion, selectivity and production capacity. Additionally, safety in operation, e.g. control of hot spot formation and flow distribution is an important issue.

A decrease in investment costs may be achieved when the system is kept as simple as possible, e.g. without liquid redistributors, injection of cold gaseous reactant for temperature control, intercooling of fluids between reactor sections by heat exchangers and operation at the lowest possible pressure. It is (will be) the ultimate goal to achieve these objectives by one single technology.

To further develop the objectives it is necessary to categorize reactions and evaluate the conditions that lead to performance improvement. For gas-limited reactions, it is advantageous to reduce the mass transfer resistance added by the liquid phase, without the danger of gross liquid maldistribution. For liquid-limited reactions, the highest possible wetting efficiency and particle-liquid mass transfer rates are favorable. For process intensification it is required to improve the mass transfer characteristics of the limiting reactant. Simultaneously, flow maldistribution and the formation of hot spots must be prevented or at least controlled. If this can be achieved by manipulation of some external variable, no changes in reactor configuration are required. This may lead to a reduction of investment costs. Moreover, it would be quite advantageous when existing trickle-bed reactors could simply be modified to meet the requirements for performance improvement. The present study aims at achieving these objectives by a simple square wave cycling of the liquid feed, e.g., the manipulation of an external variable.

The present study aims at controlling the wetting efficiency in time and utilizing the advantages associated with pulsing flow in order to meet the demands for process intensification. The possibility of a forced induction of pulses is examined. This ultimately results in the development of several feed strategies, which combine the artificial induction of pulses and a segregation of the wetting efficiency in time (not in space, as during trickle flow with maldistribution). Particle-liquid heat and mass transfer rates are determined. The effect of periodic operation on reactor performance is examined by a dynamic modeling study.

## **1.8. Outline of the thesis**

This thesis has been set-up in such a way, that each chapter can be read separately. As a consequence, some crucial background knowledge is repeated in the introduction of subsequent chapters.

The present chapter deals with the general backgrounds on liquid maldistribution, hot spot formation, the partial wetting effect and the promising periodic operation of a trickle-bed reactor. Due to the overwhelming amount of literature on trickle-bed reactors, this chapter gives by no means a complete overview of the field; it more or less serves as an illustration of the relevance of the objective.

The hydrodynamic characteristics and nature of pulsing flow are the subject of the second chapter. Experimental data on pulse properties such as velocity, frequency, liquid holdup and length for various packing materials are presented. Based on these hydrodynamic properties, more insight is gained concerning the nature of pulsing flow. Chapter 3 deals with particle-liquid heat transfer rates determined by custom-made sensors. Special attention is given to particle-liquid heat transfer rates during pulsing flow. In chapter 4 the initial efforts to induce pulses by cycling the liquid feed in a column of 1 m height are described. Pulse induction by cycling the liquid feed is termed liquid-induced pulsing flow. Based on these results, it is anticipated that column length plays a very important role in the process of liquid-induced pulsing flow. Therefore, the process of liquid-induced pulsing flow is investigated in a column of 3.2 m height. These results are presented in chapter 5. In this chapter, a distinction between a slow and a fast mode of induced pulsing flow is made, resulting in a description of the different possible feed strategies. Particle-liquid mass transfer rates, obtained by an electrochemical method, are reported in chapter 6. Additionally, the analogy between heat and mass transfer is investigated. To examine the effect of periodic operation on reactor performance, a dynamic modeling study is presented in chapter 7. Finally, chapter 8 discusses the state of the art and perspectives for periodic operation of a trickle-bed reactor. The need of future research is pointed out.

## Notation

$C_L$	liquid phase concentration gaseous reactant	$[\text{mol m}^{-3}]$
$C_L^*$	equilibrium liquid phase concentration gaseous reactant	$[\text{mol m}^{-3}]$
$C_G$	gas phase concentration gaseous reactant	$[\text{mol m}^{-3}]$
$f_w$	wetting efficiency	$[-]$
$r_g$	reaction rate internally dry catalyst	$[\text{mol kg}^{-1} \text{s}^{-1}]$
$r_i$	reaction rate internally wetted catalyst	$[\text{mol kg}^{-1} \text{s}^{-1}]$
$r_{\text{obs}}$	observed reaction rate	$[\text{mol kg}^{-1} \text{s}^{-1}]$

## Literature cited

- Al-Dahhan M.H., Larachi F., Dudukovic M.P. and Laurent A., High-pressure trickle-bed reactors, a review, *Ind. Eng. Chem. Res.*, **36**, 3292-3314, 1997
- Bailey J.E. and Ollis D.F., *Biochemical Engineering Fundamentals*, 2<sup>nd</sup> ed., Mc Graw-Hill, New York, 1986
- Baldi G., Gianetto A., Sicardi S., Specchia V. and Mazzarino I., Oxidation of ethyl alcohol in trickle-bed reactors, *Can. J. Chem. Eng.*, **63**, 62, 1985
- Barkelew C.H. and Gambhir B.S., Stability of trickle-bed reactors, *ACS Symp. Ser.*, **237**, 31, 1984
- Beaudry E.G., Dudukovic M.P. and Mill P.L., Trickle-bed reactors: liquid diffusional effects in a gas-limited reaction, *AIChE J.*, **33**, 1435-1447, 1987
- Biardi G. and Baldi G., Three-phase catalytic reactors, *Catalysis today*, **52**, 223-234, 1999
- Blok J.R., Koning C.E. and Drinkenburg A.A.H., Gas-liquid mass transfer in fixed-bed reactors with cocurrent downflow operating in the pulsing flow regime, *AIChE J.*, **30**, 393-401, 1984
- Blok J.R. and Drinkenburg A.A.H., Hydrodynamic properties of pulses in two-phase downflow operated packed columns, *Chem. Eng. J.*, **25**, 89-99, 1982
- Castellari A.T., Cechini J.O., Gabarain L.J. and Haure P.M., Gas-phase reaction in a trickle-bed reactor operated at low liquid flow rates, *AIChE J.*, **43**, 813-1818, 1997
- Castellari A.T. and Haure P.M., Experimental study of the periodic operation of a trickle bed reactor, *AIChE J.*, **41**, 1593-1597, 1995
- Charpentier J.C., Recent progress in two phase gas-liquid mass transfer in packed beds, *Chem. Eng. J.*, **11**, 161-181, 1976
- Charpentier J.C. and Favier M., Some liquid holdup experimental data in trickle bed reactors for foaming and non-foaming hydrocarbons, *AIChE J.*, **21**, 1213-1218, 1975
- Chou T.S., Worley F.L. and Luss D., Local particle-liquid mass transfer fluctuations in mixed-phase cocurrent downflow through a fixed bed in the pulsing regime, *Ind. Chem. Eng. Fund.*, **18**, 279-283, 1979
- Crine M. and Marchot P., Cocurrent downward gas-liquid flows in granular packed beds. Part I: Description of liquid flow structures, *Int. Chem. Eng.*, **23**, 663-671, 1983
- Diks R.M. and Ottengraf S.P., Verification of a simplified model for removal of dichloromethane from waste gases using a biological trickling filter, *Bioprocess Eng.*, **6**, 131, 1991
- Dudukovic M.P., Larachi F. and Mills P.L., Multiphase reactors – revisited, *Chem. Eng. Sci.*, **54**, 1975-1995, 1999
- Fukushima S. and Kusaka K., Liquid phase volumetric mass transfer coefficient and boundary of hydrodynamic flow region in packed column with cocurrent downward flow, *J. Chem. Eng. Japan*, **10**, 468-474, 1977
- Funk G.A., Harold M.P. and Ng K.M., Experimental study of reaction in a partially wetted catalyst pellet, *AIChE J.*, **37**, 202-214, 1991
- Gabarain L., Castellari A.T., Cechini J., Tobolski A. and Haure P.M., Analysis of rate enhancement in a periodically operated trickle-bed reactor, *AIChE J.*, **43**, 166-172, 1997
- Germain A., L'Homme G. and Lefebvre A., The trickle flow and bubble flow reactors in chemical processing, In *Chemical Engineering of Gas-liquid-solid Catalyst Reactions*, L'Homme G.A., CEBEDOC, Liege, Belgium, p 265, 1979
- Gianetto A. and Specchia V., Trickle-bed reactors: State of art and perspectives, *Chem. Eng. Sci.*, **47**, 3197-3213, 1992

- Goosens E., Donker R. and van den Brink F., Reactor runaway in pyrolysis gasoline hydrogenation. Proc. 1<sup>st</sup> Int. Symp. Hydrotreatment Hydrocracking of oil fractions, Feb 17-19, Oostende Belgium
- Goto S. and Mabuchi K., Oxidation of ethanol in gas-liquid cocurrent upflow and downflow reactors, *Can. J. Chem. Eng.*, 62, 865-869, 1984
- Goto S., Lakota A. and Levec L., Effectiveness factors on nth order kinetics on trickle-bed reactors, *Chem. Eng. Sci.*, 36, 157-162, 1981
- Hanika J., Sporka K., Ruzicka V. and Pistek R., Dynamic behavior of an adiabatic trickle-bed reactor, *Chem. Eng. Sci.*, 32, 525-528, 1977
- Hanika J., Safe operation and control of trickle-bed reactor, *Chem. Eng. Sci.*, 54, 4653-4659, 1999.
- Haure P.M., Hudgins R.R. and Silveston P.L., Periodic operation of a trickle-bed reactor, *AIChE J.*, 35, 1437-1444, 1989
- Herskowitz M. and Smith J.M., Liquid distribution in trickle-bed reactors, *AIChE J.*, 24, 439-454, 1978
- Herskowitz M., Carbonell R.G. and Smith J.M., Effectiveness factors and mass transfer in trickle-bed reactors, *AIChE J.*, 39, 302-321, 1979
- Herskowitz M., Wetting efficiency in trickle-bed reactors: The overall effectiveness factor of partially wetted catalyst particles, *Chem. Eng. Sci.*, 36, 1665-1671, 1981
- Hirose T., Toda M. and Sato Y., Liquid phase mass transfer in packed bed reactor with cocurrent gas-liquid downflow, *J. Chem. Eng. Japan*, 7, 187-192, 1974
- Horowitz G.I., Cukierman A.L. and Cassanello M.C., Flow regime transition in trickle beds packed with particles of different wetting characteristics – check-up on new tools, *Chem. Eng. Sci.*, 52, 3747-3755, 1997
- Ishigaki S. and Goto S., Vapor-phase kinetics and its contribution to global three-phase reaction rate in hydrogenation of 1-methylnaphtalene, *Catalysis Today*, 48, 31-40, 1999
- Jaffe S.B., *Ind. Eng. Chem. Proc. Des. Dev.*, 15, 410, 1976
- Jiang Y., Khadiilkar M.R., Al-Dahhan M.H. and Dudukovic M.P., Two-phase flow distribution in 2D trickle-bed reactors, *Chem. Eng. Sci.*, 54, 2409-2419, 1999
- Julcour C., Jaganathan R., Chaudhari R.V., Wilhelm A.M. and Delmas H., Selective hydrogenation of 1,5,9-cyclododecatriene in up- and downflow fixed-bed reactors: experimental observations and modeling, *Chem. Eng. Sci.*, 56, 557-564, 2001
- Khaldikar M.R., Wu Y.X., Al-Dahhan M.H., Dudukovic M.P. and Colakyan M., Comparison of trickle bed and upflow performance at high pressure. Model predictions and experimental observations, *Chem. Eng. Sci.*, 51, 2139, 1996
- Kouris Ch., Neophytides St., Vayenas C.G. and Tsamopoulos J., Unsteady state operation of catalytic particles with constant and periodically changing degree of external wetting, *Chem. Eng. Sci.*, 53, 3129-3142, 1998
- Lange R., Hanika J., Stradiotto D., Hudgins R.R. and Silveston P.L., Investigations of periodically operated trickle-bed reactors, *Chem. Eng. Sci.*, 49, 5615-5621, 1994
- Lee K.J., Hudgins R.R. and Silveston P.L., A cycled trickle bed reactor for SO<sub>2</sub> oxidation, *Chem. Eng. Sci.*, 50, 2523-2530, 1995
- Lerou J.J., Glasser D. and Luss D., Packed-bed liquid phase dispersion in pulsed gas-liquid downflow, *Ind. Eng. Chem. Fund.*, 19, 66-71, 1980
- Mantle M.D., Sederman A.J. and Gladden M.F., Single- and two-phase flow in fixed-bed reactors: MRI flow visualization and lattice-Boltzmann simulations, *Chem. Eng. Sci.*, 56, 523-529, 2001

## General Introduction on Trickle-Bed Reactors

---

- Mata A.R. and Smith J.M., Oxidation of sulfur oxide in trickle-bed reactor, *Chem. Eng. J.*, 22, 229, 1981
- McManus R.K., Funk G.A., Harold M.P. and Ng K.M., Experimental study of reaction in trickle-bed reactors with liquid maldistribution, *Ind. Eng. Chem. Res.*, 32, 570, 1993
- Melli T.R., de Santos J.M., Kolb W.B. and Scriven L., Cocurrent downflow in networks of passages, microscale roots of macroscale flow regimes, *Ind. Eng. Chem. Res.*, 29, 2367-2379, 1990
- Meyers R.A., *Handbook of petroleum refining processes*, 2<sup>nd</sup> ed., McGraw-Hill, New York, 1996
- Mills P.L. and Dudukovic M.P., Analysis of catalyst effectiveness in trickle bed reactors processing volatile or nonvolatile reactants, *Chem. Eng. Sci.*, 35, 2267, 1980
- Moller L.B., Halken C., Hansen J.A. and Bartholdy J., Liquid and gas distribution in trickle-bed reactors, *Ind. Eng. Chem. Res.*, 35, 926-930, 1996
- Pintar A., Bercic G. and Levec J., Catalytic liquid-phase oxidation of aqueous phenol solutions in a trickle-bed reactor, *Chem. Eng. Sci.*, 52, 4143-4153, 1997
- Ramachandran P.A. and Smith J.M., Effectiveness factors in trickle-bed reactors, *AIChE J.*, 25, 538-542, 1979
- Rao V.G. and Drinkenburg A.A.H., Pressure drop and hydrodynamic properties of pulses in two-phase gas-liquid downflow through packed beds, *Can. J. Chem. Eng.*, 61, 158-167, 1983
- Rao V.G. and Drinkenburg A.A.H., Solid-liquid mass transfer in packed beds with cocurrent gas-liquid downflow, *AIChE J.*, 31, 1059-1068, 1985
- Rasjashekharam M.V., Jaganathan R. and Chaudhari R.V., A trickle-bed reactor model for hydrogenation of 2,4 dinitrotoluene: experimental verification, *Chem. Eng. Sci.*, 53, 787-805, 1998
- Ravindra P.V., Rao D.P. and Rao M.S., Liquid flow texture in trickle-bed reactors: An experimental study, *Ind. Eng. Chem. Res.*, 36, 5133-5145, 1997
- Ring Z.E. and Missen R.W., Trickle-bed reactor performance: An experimental study of partial wetting effect, *AIChE J.*, 35, 1821-1828, 1989
- Ruzicka J. and Hanika J., Partial wetting and forced reaction mixture transition in a model trickle-bed reactor, *Catalysis Today*, 20, 476-484, 1994
- Satterfield C.N. and Ozel F., Direct solid-catalyzed reaction of a vapor in an apparently completely wetted trickle bed reactor, *AIChE J.*, 19, 1259-1261, 1973
- Sedriks W. and Kenney C.N., Partial wetting in trickle-bed reactors – the reduction of crotonaldehyde over a palladium catalyst, *Chem. Eng. Sci.*, 28, 559-568, 1973
- Stanek V., Hanika J., Hlavacek V. and Trnka O., The effect of liquid distribution on the behavior of a trickle-bed reactor, *Chem. Eng. Sci.*, 36, 1045-1067, 1981
- Trambouze P., Engineering of hydrotreating processes, in *Chemical Reactor Technology for Environmentally Safe Reactors and Products*, De Lasa H.I., Dogu G., Ravella A., NATO Advanced Study Institute Series E, Plenum, New York, p 425, 1993
- Tsochatzidis N.A. and Karabelas A.J., Study of pulsing flow in a trickle bed using the electrodiffusion technique, *J. Appl. Electrochem.*, 24, 670-675, 1994
- Tsochatzidis N.A., Karabelas A.J., Properties of pulsing flow in a trickle bed, *AIChE J.*, 41, 2371-2382, 1995
- Tsochatzidis N.A. and Karabelas A.J., Experiments in trickle-beds at the micro and macro scale. Flow characterization and onset of pulsing, *Ind. Eng. Chem. Res.*, 33, 1299-1309, 1994
- Tukac V. and Hanika J., The effect of mass transfer on the oxidation of ethanol in a trickle-bed reactor, *Int. Chem. Eng.*, 29, 177-181, 1989



- Watson P.C. and Harold M.P., Rate enhancement and multiplicity in a partially wetted and filled pellet: experimental study, *AIChE J.*, 40, 97-111, 1994
- Wu Y., Khaldikar M.R., Al-Dahhan M.R. and Dudukovic M.P., Comparison of upflow and downflow two-phase flow packed bed reactors with and without fines, *Ind. Eng. Chem. Res.*, 35, 397, 1996
- Yentekakis I.V. and Vayenas C.G., Effectiveness factors for reactions between volatile and non-volatile components in partially wetted catalysts, *Chem. Eng. Sci.*, 42, 1323-1332, 1987
- Zhu X. and Hofmann H., Effect of wetting geometry on overall effectiveness factors in trickle beds, *Chem. Eng. Sci.*, 52, 4511-4524, 1997

---

## Chapter 2

---

# Nature and Characteristics of Pulsing Flow

---

### Abstract

Pulsing flow is well known for its advantages in terms of an increase in mass and heat transfer rates, complete catalyst wetting and a decrease in axial dispersion compared to trickle flow. The operation of a trickle-bed reactor in the pulsing flow regime is favorable in terms of a capacity increase and the elimination of hot spots. Extending the knowledge on the hydrodynamic nature and characteristics of pulsing flow stands at the basis of further exploitation of the effects of this flow regime on reactor performance.

An analysis of the hydrodynamics of pulsing flow reveals that pulse properties as liquid holdup, velocity and duration, are invariant to the liquid flow rate at a constant gas flow rate. The pulse frequency, however, increases with increasing liquid flow rate. The relative contribution of the pulses and the parts of the bed in between pulses to an average measured property can thus be obtained. By implementation of this concept it is shown that the linear liquid velocity inside the pulses is very high and is probably responsible for the enhanced mass and heat transfer rates. The liquid holdup in the parts of the bed in between pulses equals the liquid holdup at the transition to pulsing flow at all gas flow rates. The same trend holds for the linear liquid velocity in between pulses. Pulsing flow then is a hybrid of two transition states. The pulses reside at the transition to bubble flow, while the parts of the bed in between pulses reside at the transition to trickle flow.

This chapter is based on the following publications:

Boelhouwer J.G., Piepers H.W. and Drinkenburg A.A.H., Nature and characteristics of pulsing flow in trickle-bed reactors, Chem. Eng. Sci., submitted for publication

Boelhouwer J.G., Piepers H.W. and Drinkenburg A.A.H., Nature and characteristics of pulsing flow in trickle-bed reactors, paper 337g, AIChE Annual meeting, Los Angeles, CA, U.S.A., 2000

## 2.1. Introduction

Packed bed reactors with two-phase gas-liquid downflow, termed trickle-bed reactors, are frequently selected in chemical reactor design, especially for hydrogenations and oxidations. Trickle-bed reactors may be operated in several flow regimes, depending on the flow rates of the phases, characteristics of the packed bed and the fluid physical properties. At present, trickle flow is the most common flow regime encountered in industrial applications. The interaction between the phases is rather poor. Flow maldistribution and hot spot formation are the major problems experienced during trickle flow operations.

A more favorable flow regime, termed pulsing flow, is obtained at higher gas and liquid flow rates. The pulses are characterized by large mass and heat transfer rates (Lemay et. al., 1975; Chou et. al., 1979; Tsochatzidis and Karabelas, 1994; Rao and Drinkenburg, 1985; Marcandelli et. al., 1999). Increased catalyst wetting and a continuous mixing between parallel flowing rivulets diminish flow maldistribution. In addition, the formation of local hot spots is reduced, leading to an intrinsically safer process and diminished catalyst deactivation. The pulses continuously mobilize the stagnant liquid holdup up to the point where its stagnant nature disappears. Since the stagnant liquid holdup represents about 10 to 30% of the total liquid holdup in trickle flow operations (Colombo et. al., 1976), its more dynamic character during pulsing flow will enhance reactor performance. Axial dispersion is considerably less compared to trickle flow, due to effective radial mixing between the different parallel flowing liquid streams and disappearance of stagnant liquid holdup (Lerou et. al., 1980; Fukushima and Kusaka, 1977). Especially undesired consecutive reactions are reduced to lower levels due to better overall plug flow behavior. A further advantage of pulsing flow is the much higher effective radial conductivity as shown by Lamine et. al. (1996). Wu et. al. (1995) employed a simple theoretical model to predict the selectivity and yield for consecutive and parallel reactions under pulsing flow conditions. In some cases, depending on the pulse frequency, significant changes in both yield and selectivity occur. They experimentally verified these model results for the selective hydrogenation of phenylacetylene to styrene and ethylbenzene (Wu et. al., 1999). It was demonstrated that pulsing flow has a positive effect, particularly on selectivity, with respect to trickle flow.

Some data on pulse characteristics are reported in early studies by Weekman and Myers (1964) and Sato et. al. (1973).

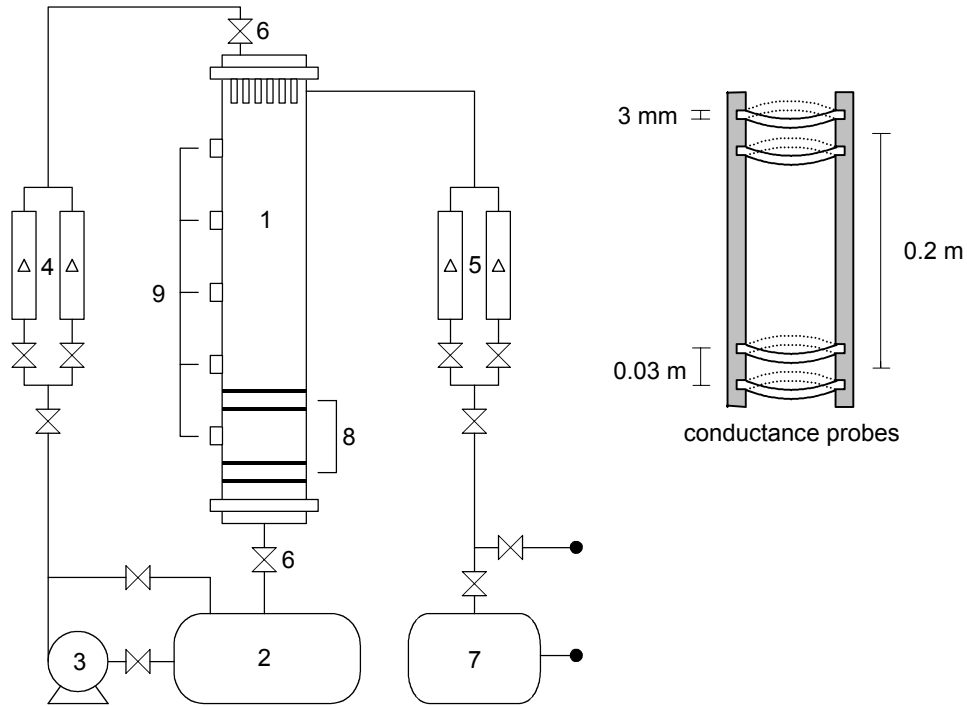


**Figure 2.1.** Schematic illustration of the experimental equipment (1: column; 2: liquid storage tank; 3: liquid pump; 4: liquid flow meter; 5: gas flow meter; 6: magnetic valve; 7: pressure vessel; 8: conductivity probes; 9: pressure taps)

In more recent studies, pulse properties were experimentally determined by conductance techniques and correlations for these properties were developed (Blok and Drinkenburg, 1982; Rao and Drinkenburg, 1983; Tsochatzidis and Karabelas, 1995; Bartelmus et. al., 1998).

## 2.2. Scope and objective

Extending the knowledge on the hydrodynamic nature and characteristics of pulsing flow stands at the basis of further exploitation of the effects of this flow regime on reactor performance. Despite the numerous publications concerning the hydrodynamics of pulsing flow, only two studies explore the advantages of pulsing flow in a reaction system (Wu et. al., 1999; Sims et. al., 1994). In this chapter, experimental results on pulse properties are presented. A quantitative knowledge of pulse characteristics is essential for modeling reactions during pulsing flow.

**Table 2.1.** Properties of the packed beds

packing material	column diameter	porosity	specific area
3.0 mm glass spheres	0.05 m	0.40	1200 m <sup>-1</sup>
6.0 mm glass spheres	0.11 m	0.38	620 m <sup>-1</sup>
10.0 x (6.5-5.0) mm Raschig rings	0.11 m	0.67	924 m <sup>-1</sup>

### 2.3. Experimental setup and procedures

A schematic illustration of the experimental equipment is shown in Fig. 2.1. The experiments were performed in Plexiglas columns of 0.11 and 0.05 m inner diameter. Three different packing materials were employed of which the properties are summarized in Table 2.1. The packing is supported at the bottom of the column by a stainless steel screen. Air and water were uniformly distributed at the top of the column. The experiments were conducted at room temperature and near-atmospheric pressure. Gas and liquid flow rates were measured by calibrated flowmeters.

Instantaneous cross-sectionally averaged liquid holdup was determined with a conductance technique developed and implemented by Tsochatzidis et. al. (1992) and Tsochatzidis and Karabelas (1995). Both columns were equipped with 2 conductance probes, separated by a distance of 0.2 m. Each probe consisted of two flush-mounted ring electrodes of 3 mm width and 3 cm apart to achieve satisfactory spatial resolution. A schematic illustration of the probe arrangement is presented in Fig. 2.1. In order to suppress electrode polarization and capacitance effects, a sufficiently high frequency a.c. voltage excitation of 25 respectively 30 kHz was applied to the probes. Therefore, the measured electrical impedance across the electrode pair is essentially resistive in nature (Tsochatzidis et. al., 1992; Andreussi et. al., 1999). The signal from each probe is uniquely related to the conductance of the medium between the ring electrodes and thus to the amount of liquid. Lock-in amplifiers (model 5105 Princeton Applied Research) were used to measure the output signal of the probes. As reference signal, the same a.c. high frequency voltage excitation applied to the probes was fed to the lock-in amplifier. The lock-in amplifier essentially acts as a narrow band pass filter, which removes much of the unwanted noise. The d.c. output level of the lock-in amplifier is proportional to the input signal of the probes. The conductivity probes were calibrated by tracer injections and by the stop-flow method. Both calibration methods proved to be very reproducible and provided identical results.

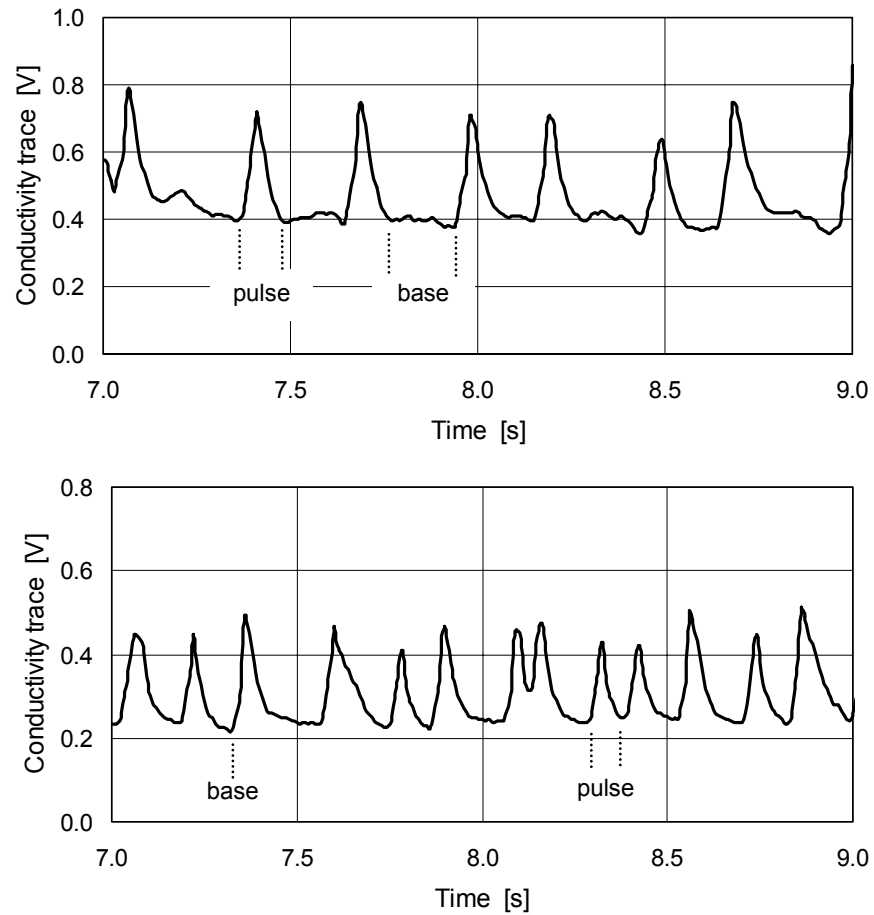


**Figure 2.2.** Example of measured conductivity traces (a:  $U_i = 0.0102 \text{ m s}^{-1}$ ;  $U_g = 0.37 \text{ m s}^{-1}$ ; b:  $U_i = 0.0102 \text{ m s}^{-1}$ ;  $U_g = 0.61 \text{ m s}^{-1}$ ; packing material: GS 3.0 mm)

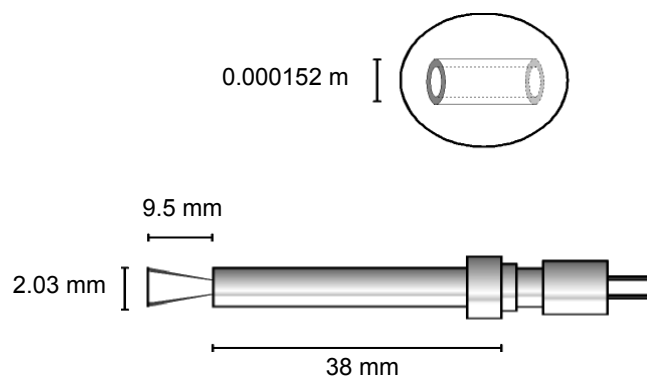


**Figure 2.3.** Schematic illustration of the cylindrical hot film anemometer (TSI 1210 60W)

Two examples of measured conductivity traces recorded during a relatively low and high pulse frequency are plotted in Fig. 2.2. Pulses are clearly observable as the large peaks. Two different definitions of the pulse liquid holdup were applied. The pulse liquid holdup was either defined as the maximum occurring liquid holdup or the holdup integrated over the pulse. At low pulse frequencies, the parts of the bed in between pulses, termed “base”, are rather flat. At relatively high pulse frequencies, distinction between pulses becomes difficult, due to overlap between pulses. In this case, the liquid holdup in between pulses is defined as the minimum holdup in between pulses. The pulse frequency was obtained by evaluation of the number of pulses present in the conductivity trace. Pulse velocities were obtained by the cross correlation of two conductivity traces measured at different axial positions in the column.

A hot film cylindrical shaped anemometer (TSI, model 1210 60W), schematically shown in Fig. 2.3, was used to provide some qualitative information concerning the gas-liquid distribution during pulsing flow. The anemometer was situated inside the packing interstices. The output of the anemometer is directly related to the amount of heat transfer to the surrounding medium.

Before conducting any experiments, the column was operated in the pulsing flow regime for at least 1 hour to ensure a perfectly pre-wetted bed. For a period of at least 5 minutes, both pressure drop and liquid holdup data were collected with a sample frequency of 100 Hz.

## 2.4. Transition boundary

In Fig. 2.4, the transition boundary from trickling to pulsing flow is plotted for all packing materials. The transition is established at approximately 0.1 m above the bottom of the column. By increasing the gas flow rate, the point of pulse inception moves upward in the column. The transition boundaries for 3.0 and 6.0 mm spheres only slightly differ. The transition boundary for Raschig Rings as packing material is located at much higher gas and liquid flow rates, due to the much higher porosity. Blok et. al. (1983) observed that the transition to pulsing flow occurs at a certain critical linear liquid velocity. They proposed a threshold value of the Froude number at the transition boundary. Our results presented in Fig. 2.5 indicate that the linear liquid velocity at the transition boundary is constant, except at low gas flow rates. This critical linear liquid velocity is, however, equivalent for the three packing materials tested.

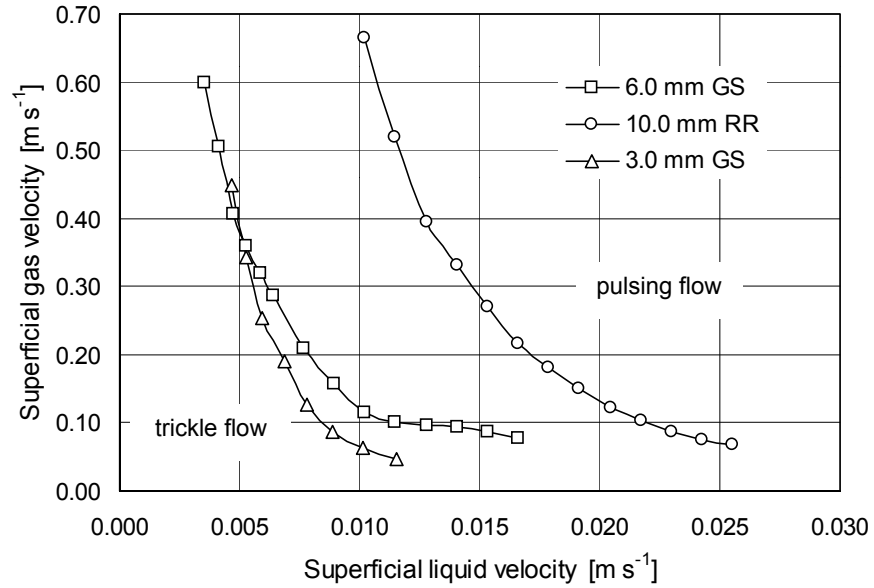


**Figure 2.4.** Transition boundary from trickle to pulsing flow in terms of superficial gas and liquid velocities

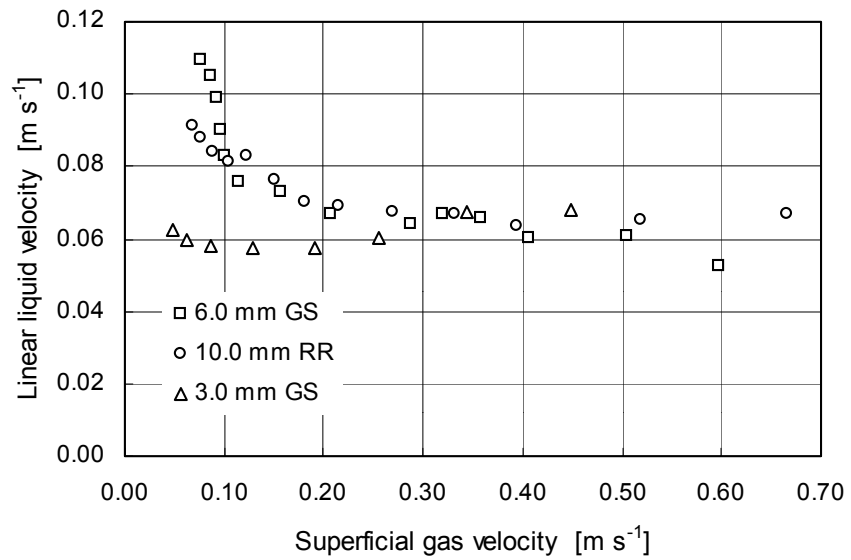


**Figure 2.5.** Transition boundary from trickle to pulsing flow in terms of superficial gas and linear liquid velocity



## 2.5. Characterization of pulsing flow

Pulse characteristics as liquid holdup, velocity, frequency and duration are experimentally determined for all packing materials. In this section, the results for 6.0 mm glass spheres as packing material are presented. The reader is referred to the appendix for the results concerning the other packing materials.

### 2.5.1. Liquid holdup and phase distribution

A plot of the pulse and base liquid holdup versus the superficial gas velocity is presented in Fig. 2.6. The pulse liquid holdup plotted in this figure is defined as the maximum liquid holdup in the pulse. The pulse liquid holdup continuously decreases linearly with increasing gas flow rate. With increasing gas flow rate, the base liquid holdup first decreases and subsequently remains constant. It is remarkable to notice that both pulse and base liquid holdup do not depend on the liquid flow rate. This observation likewise holds for the pulse liquid holdup when defined as the integrated holdup over a pulse. It seems that with increasing gas flow rate, pulse and base liquid holdup eventually approach the same value, which indicates that the pulsing flow boundary is reached. At these high gas velocities and low liquid holdups, mist flow will occur. With increasing liquid flow rate, at a constant gas flow rate, the pulse frequency increases up to the point where the distinction between separate pulses fades away and the bubble flow regime boundary is reached.

It is interesting to compare the liquid holdup at the transition boundary to the base liquid holdup at equivalent superficial gas velocities. This comparison is shown in Fig. 2.7. The base liquid holdup perfectly matches the liquid holdup at the transition to pulsing flow at all superficial gas velocities. Apparently, the parts of the bed in between pulses continuously reside at the transition boundary from trickle to pulsing flow.

Constant temperature anemometry was applied to gain qualitative information concerning the nature of pulsing flow. A typical example of an obtained signal is provided in Fig. 2.8. The large peaks in the signal correspond to the passage of pulses. Several peak and trough values in one pulse are observed. The trough values are caused by the passage of the dispersed gas bubbles inside the pulses. When such a bubble hits the probe, the heat transfer from the probe substantially decreases. The peak values correspond to liquid passing the probe. In between the pulses, two different levels in the output signal can be observed, 1.5 and 3.5 V.

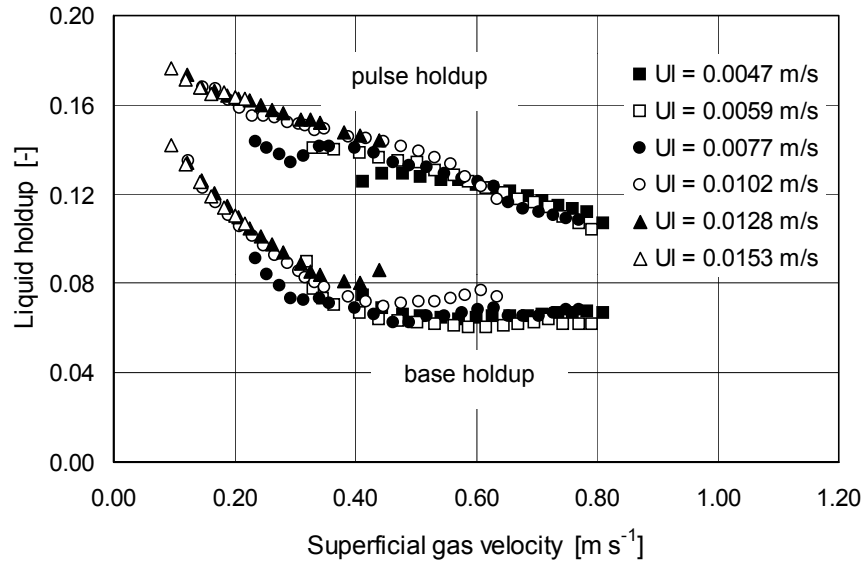


**Figure 2.6.** Pulse and base liquid holdup versus the superficial gas velocity (packing material: 6.0 mm glass spheres)

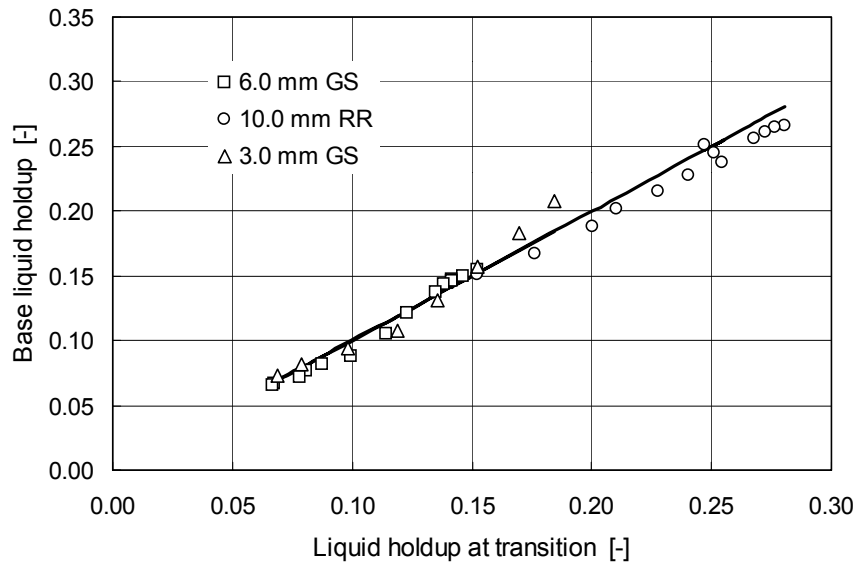


**Figure 2.7.** Comparison between the liquid holdup at the transition to pulsing flow and the base liquid holdup during pulsing flow at equivalent superficial gas velocity

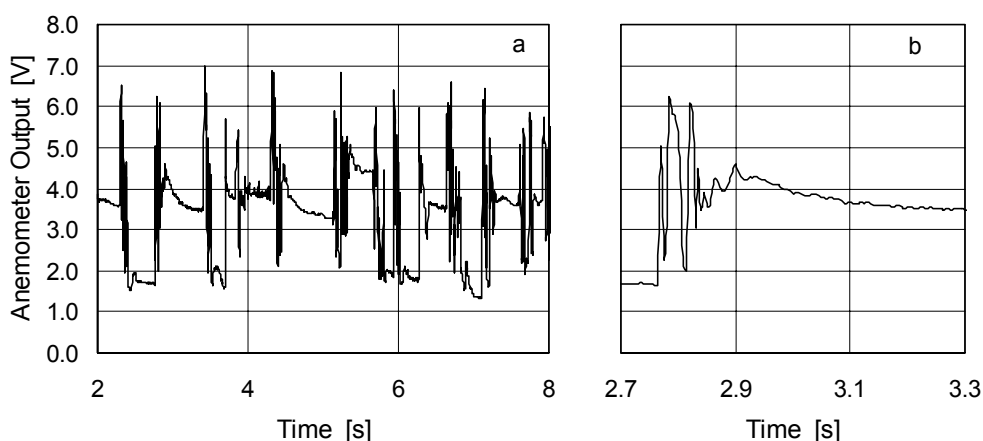


**Figure 2.8.** An example of an anemometer output signal during pulsing flow

These values correspond respectively to single-phase gas flow and single-phase liquid flow. The situation in between the pulses apparently changes randomly after the passage of a pulse; the probe is alternately exposed to liquid flow or gas flow. Wetting in between pulses seems rather poor, which is confirmed by the low liquid holdup in between pulses. In contrast, it is generally hypothesized that catalyst wetting is complete inside the pulses due to the continuous character of the liquid.

### 2.5.2. Pulse velocity

The pulse velocity versus the superficial gas velocity is plotted in Fig. 2.9. The pulse velocity increases with increasing gas flow rate, while the liquid flow rate seems to exhibit a negligible influence. The pulse velocity approaches a certain limiting value as also reported by Blok and Drinkenburg (1982) and Tsochatzidis and Karabelas (1995). For each packed bed, the minimum pulse velocity is  $0.6 \text{ m s}^{-1}$ . Different limiting pulse velocities at high gas flow rates exist for the different packing materials (see appendix).

Pulse velocity is determined at a fixed location. The point of pulse inception, however, moves closer to the top of the column when the gas flow rate is increased. Since acceleration of pulses must occur, final pulse velocities at the point of measurement are probably not realized at gas flow rates just beyond the transition to pulsing flow. This effect may be the cause for the weak influence of the liquid flow rate on pulse velocity just beyond the transition.

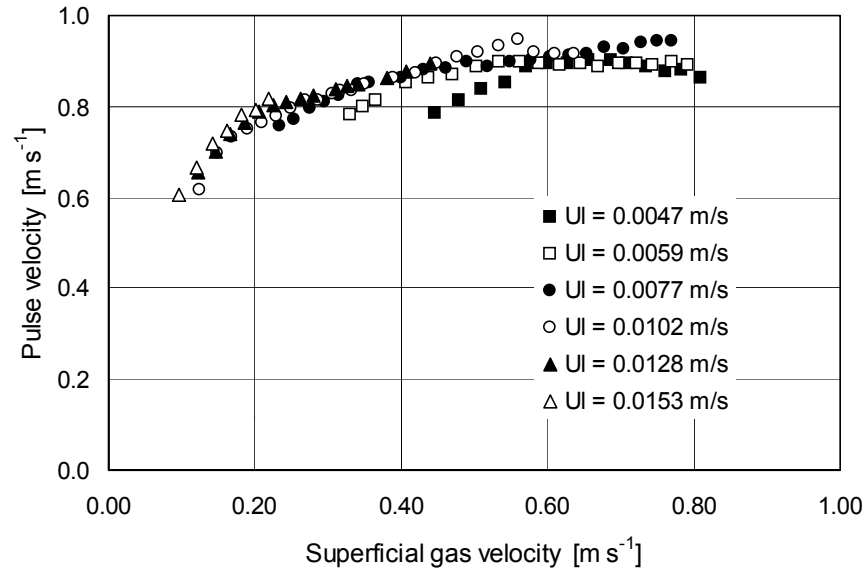


**Figure 2.9.** Pulse velocity versus the superficial gas velocity (packing material: 6.0 mm glass spheres)

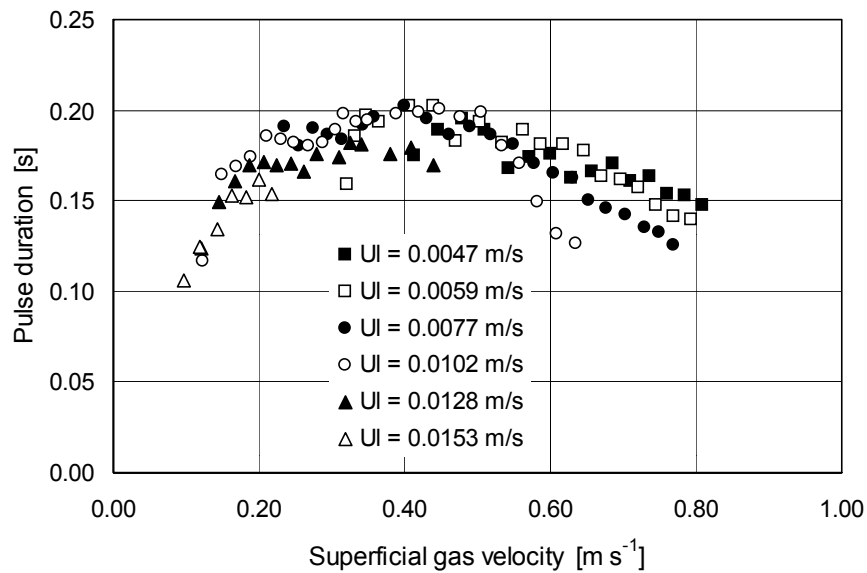


**Figure 2.10.** Pulse duration versus the superficial gas velocity (packing material: 6.0 mm glass spheres)

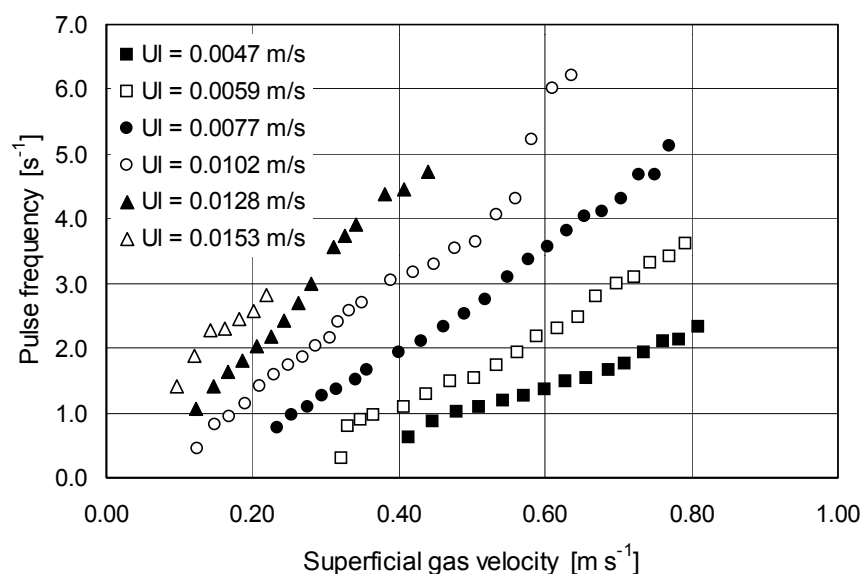


**Figure 2.11.** Pulse frequency versus the superficial gas velocity (packing material: 6.0 mm glass spheres)

### 2.5.3. Pulse duration

The pulse duration versus the superficial gas flow rate is plotted in Fig. 2.10. Pulse duration first increases with increasing gas flow rate, then reaches a maximum and subsequently decreases. Like pulse liquid holdup and pulse velocity, pulse duration is not significantly affected by the liquid flow rate. Some spread on measured pulse durations is noticed, especially at relatively high gas flow rates. This results from the relatively high pulse frequencies that cause a certain overlap between pulses. This makes it difficult to determine the exact pulse (and base) duration by analysis of the conductivity signals. Pulse duration thus have a tendency to become smaller with increasing pulse frequency. This will be discussed in more detail in chapter 5.

### 2.5.4. Pulse frequency

Pulse frequency versus the superficial gas velocity is depicted in Fig. 2.11. The pulse frequency increases roughly linear with increasing gas flow rate. Moreover, an increase in pulse frequency is observed when the liquid flow rate is increased. The pulse frequency is the only pulse property that is affected by the liquid flow rate.

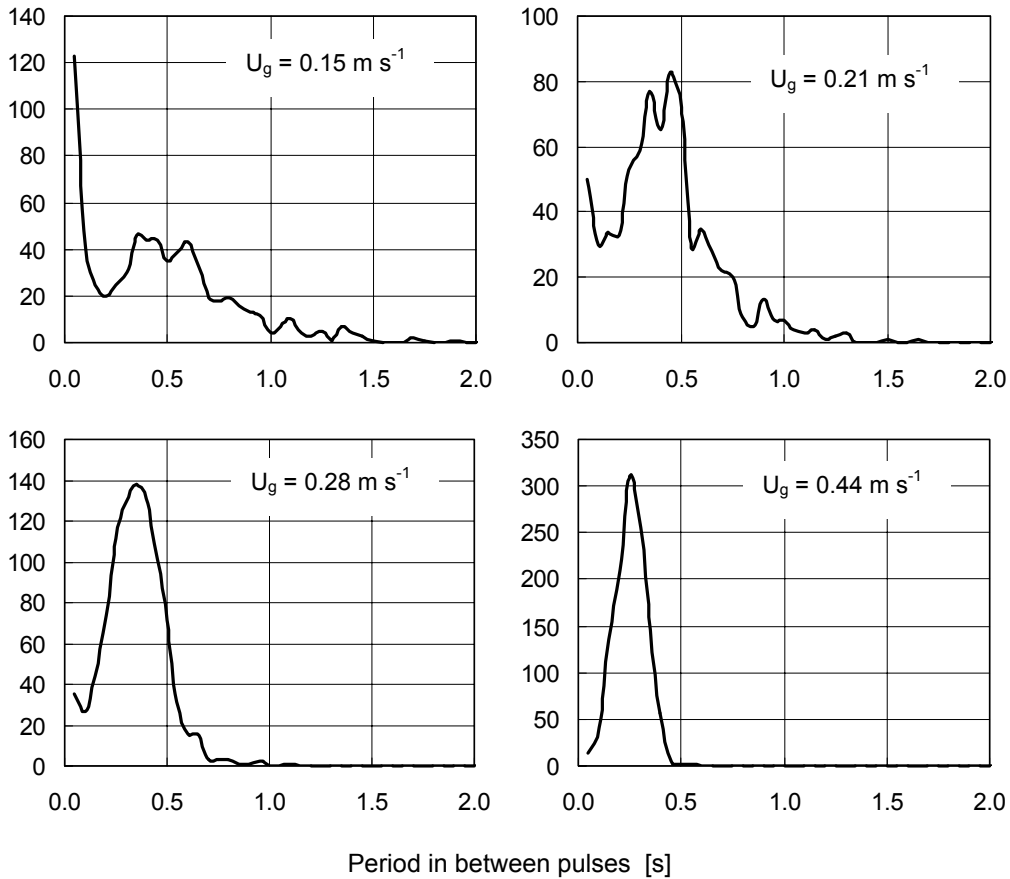


**Figure 2.12.** Effect of superficial gas velocity on the distribution of time intervals between subsequent pulses ( $U_l = 0.0128 \text{ m s}^{-1}$ ; packing material: 6.0 mm glass spheres)

Blok and Drinkenburg (1982) proposed that the pulses transport all liquid in excess of the critical linear liquid velocity, at which the transition to pulsing flow occurs. Moreover they assumed a constant ratio between pulse and base liquid holdup. Pulse frequency should then linearly depend on the linear liquid velocity. Our data on pulse frequency support their hypothesis only for relatively low gas flow rates. The assumption of a constant ratio between pulse and base liquid holdup is certainly not satisfied, especially at higher gas flow rates. However, since it is observed that the base liquid holdup continuously matches the liquid holdup at the transition to pulsing flow, there might be such a critical linear liquid velocity as proposed by Blok and Drinkenburg (1982).

The effect of increasing gas flow rate on the distribution of the time intervals between subsequent pulses is presented in Fig. 2.12. At the lowest gas flow rate, just beyond the transition to pulsing flow, mainly double pulses are initiated. Upon increasing the gas flow rate, double pulse formation diminishes and eventually, a sharp frequency is obtained at high gas flow rates. Pulsing flow becomes more regular upon increasing the gas flow rate.

### 2.5.5. Concluding remarks

As the experimental results on pulse properties indicate, the properties of the pulses solely depend on the superficial gas flow rate. The liquid flow rate seems to exhibit no, or at least a negligible influence on pulse and base liquid holdup, velocity and duration. Equivalent experimental results were obtained by Blok and Drinkenburg (1983), Rao and Drinkenburg (1985) and Tsochatzidis and Karabelas (1995). The only pulse property that depends on the superficial liquid velocity is the pulse frequency. Since as well the maximum liquid holdup of a pulse, the pulse duration as the integrated pulse liquid holdup is invariant to the liquid flow rate, pulse shape will correspondingly not be affected by the liquid flow rate either. At a constant gas flow rate, pulses are identical.

Danckworth et. al. (1990, 1992) analyzed the nonlinear behavior of two-phase flow in packed beds by bifurcation and singularity theory of a macroscopic model to describe the qualitative nature of pulses. Their calculations show that pulses are square-wave solutions of high liquid holdup. The pulse and base liquid holdup and the pulse velocity solely depend on the total superficial velocity  $U_t (= U_l + U_g)$ . Since in the pulsing flow regime, the superficial gas velocity is 20 to 240 times higher compared to the superficial liquid velocity, pulse and base liquid holdup and pulse velocity almost entirely depend on the gas flow rate. Our results on liquid holdup (Fig. 2.6) and pulse velocity (Fig. 2.9) strongly agree with these model results.

## 2.6. Nature of pulsing flow

As shown in the previous section, pulses are (nearly) identical at a certain gas flow rate, regardless the applied liquid flow rate. Solely the pulse frequency depends on the liquid flow rate. Since the hydrodynamic pulse properties are not affected by the liquid flow rate, it is argued that correspondingly other properties, such as pressure drop and heat and mass transfer rates, inside and in between the pulses are not affected by the liquid flow rate either.

This implies that the increase in such an average property at a certain constant gas flow rate with increasing liquid flow rate is solely due to an increase in pulse frequency, not a change in the properties of the pulses themselves. This provides a means to obtain the relative contribution of the pulses and the parts of the bed in between pulses to an average measured property. An average property  $\alpha$  during pulsing flow is composed of the value inside the pulse ( $\alpha_p$ ) and in between the pulses ( $\alpha_b$ ) as:

$$\alpha = f_p (t_p \alpha_p + t_b \alpha_b) \quad [2.1]$$

In this equation,  $f_p$  is the pulse frequency and  $t_p$  and  $t_b$  are respectively the pulse and base duration. Solely  $\alpha_b$  and  $\alpha_p$  are unknown, but independent on the liquid flow rate at a constant gas flow rate. By comparing  $\alpha$  for two different liquid flow rates at a constant gas flow rate,  $\alpha_b$  and  $\alpha_p$  can be eliminated:

$$\alpha_p = \frac{1}{t_p (t_{b2} - t_{b1})} \left[ \frac{t_{b2}}{f_{p1}} \alpha_1 - \frac{t_{b1}}{f_{p2}} \alpha_2 \right] \quad [2.2]$$

$$\alpha_b = \frac{\alpha - f_p t_p \alpha_p}{f_p t_b} \quad [2.3]$$

By comparing the average property  $\alpha$  at  $n$  different liquid flow rates at a constant gas flow rate,  $(n/2)(n-1)$  values of  $\alpha_p$  and  $\alpha_b$  are obtained. This procedure can be used with confidence at relatively low pulse frequencies only since the overlap between pulses at relatively high pulse frequencies prevents accurate determination of the pulse and base duration. Therefore, this procedure is applied for the results accompanied with pulse frequencies up to 4 Hz.

### 2.6.1. Liquid holdup

By the above-described procedure pulse and base liquid holdup can be calculated by using the time-average liquid holdup. The calculated pulse liquid holdup is the integrated value over the pulse. The calculated values are compared to the experimentally determined values in Fig. 2.13. A good agreement between experimental and calculated values is found. For the other packing materials, satisfactory agreement between experimentally determined and calculated pulse and base liquid holdup was obtained also.



This provides confidence to the statement that pulse properties are invariant to the liquid flow rate at a certain gas flow rate.

### **2.6.2. Superficial liquid velocity**

The calculated superficial liquid velocity inside and in between pulses is shown in Fig. 2.14. Superficial liquid velocities inside the pulses are quite high, while superficial liquid velocities in between pulses are rather low. This is confirmed by visual observation of the liquid flow at the column outlet. At the moment a pulse leaves the column, a large amount of liquid is collected in the gas-liquid separator, while in between pulses almost no liquid leaves the column. The low liquid velocity in between pulses implies poor wetting characteristics, as was also concluded by the measurements with hot film anemometry. The high liquid velocity inside the pulses and the continuous character of the liquid imply total catalyst wetting as generally assumed in literature.

The superficial liquid velocity in the column varies between two values corresponding to the pulse and the base, regardless of the applied liquid feed rate. The hydrodynamic character of a pulse resembles bubble flow. Upon increasing the liquid flow rate at a constant gas flow rate, the pulse frequency increases up to the point where the distinction between separate pulses fades away and the bubble flow regime boundary is reached. The hydrodynamic properties of the pulses, however, remain unchanged upon increasing the liquid flow rate. This suggests that the gas and liquid flow rates characterizing the pulses reside at the transition boundary to bubble flow. The bubble flow character of a pulse is then the result of the high superficial liquid velocity inside the pulse. The base liquid holdup equals the holdup at the transition to pulsing flow at all gas flow rates. Pulsing flow then is a hybrid of two transition states. The pulses reside at the transition to bubble flow while the bases reside at the transition to trickle flow.

### **2.6.3. Pressure gradient**

The calculated pressure gradient over the pulse and base is plotted in Fig. 2.15. The pressure gradients over the pulse and over the base both increase with increasing gas flow rate.

### **2.6.4. Linear liquid velocity**

The linear liquid velocity inside the pulses and in the parts of the bed in between pulses is plotted in Fig 2.16 versus the superficial gas velocity. Rather high linear liquid velocities characterize the pulse while in between pulses the linear liquid velocity is approximately constant.

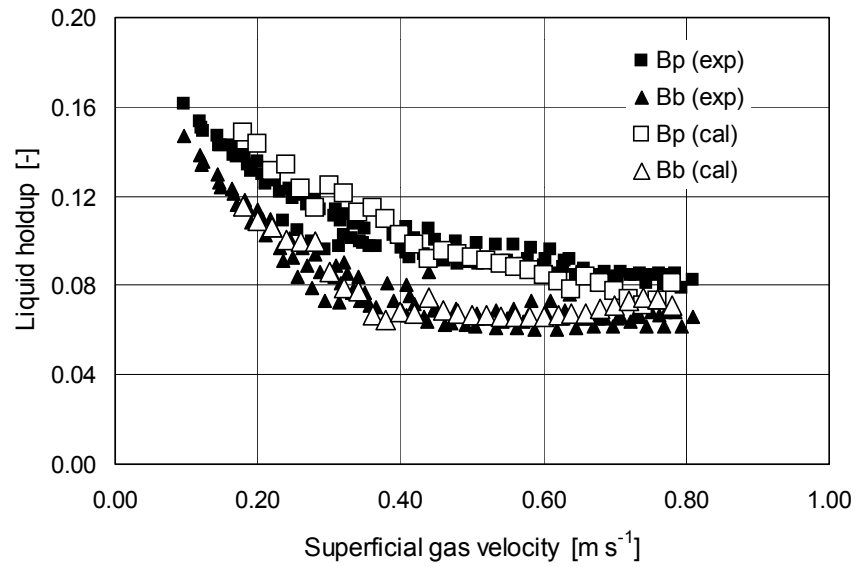


**Figure 2.13.** Comparison between experimentally determined and calculated liquid holdup inside and in between pulses (packing material: 6.0 mm glass spheres)

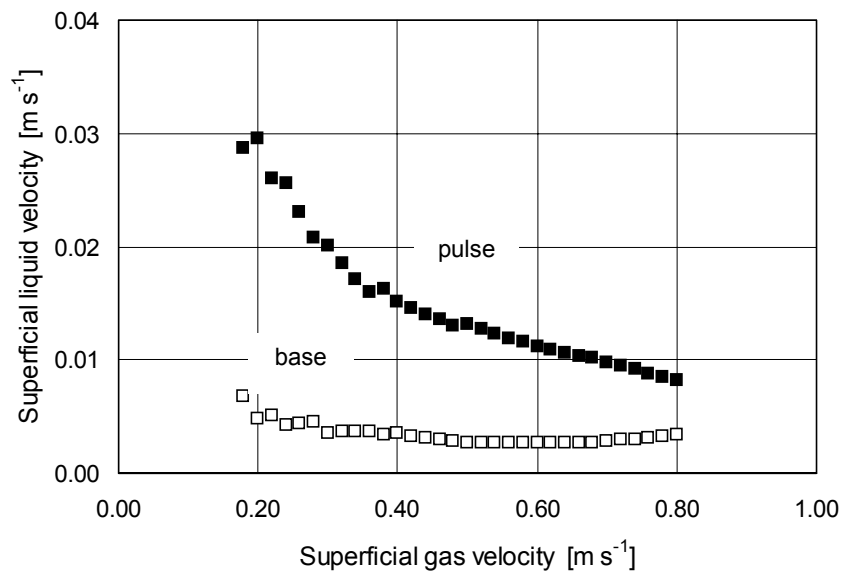


**Figure 2.14.** Calculated superficial liquid velocity in between and inside the pulses (packing material: 6.0 mm glass spheres)

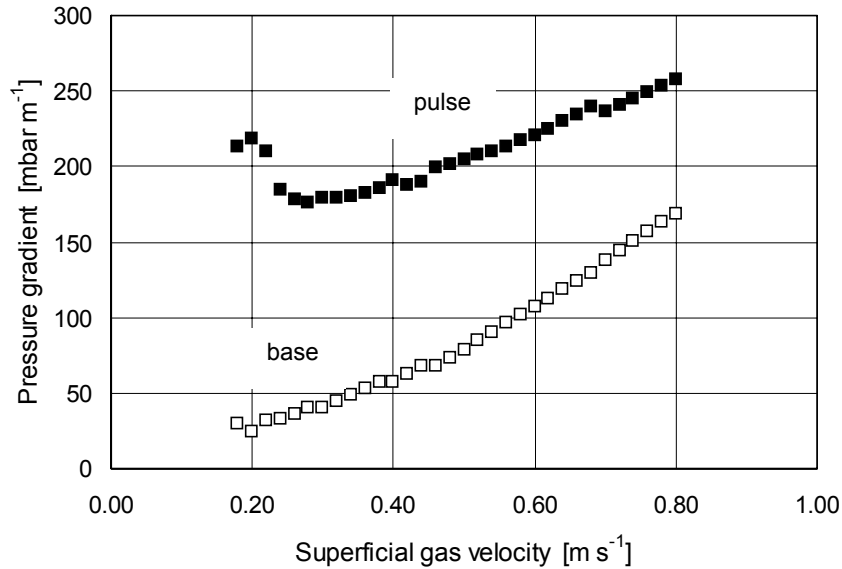


**Figure 2.15.** Calculated pressure gradient in between and inside the pulses (packing material: 6.0 mm glass spheres)

The linear liquid velocity inside the pulses decreases with increasing gas flow rate. The linear liquid velocity in between pulses for all packing materials is plotted in Fig. 2.17. It is striking to notice that the linear liquid velocity in between pulses is approximately constant and equal for all packed bed characteristics tested. Comparison between the linear liquid velocity at the transition boundary to pulsing flow (Fig. 2.5) and the linear liquid velocity in between pulses shows fair agreement. Somewhat higher linear liquid velocities are encountered at the transition to pulsing flow. However, since the base liquid holdup equals the holdup at the transition to pulsing flow at all gas flow rates (Fig. 2.7), this will probably apply to the linear liquid velocity in between pulses as well. The somewhat lower calculated linear liquid velocities may be caused by the inaccuracy in establishing the parameters in eqs. 2.2 and 2.3. One might argue that the linear liquid velocity shown in Fig. 2.17 is the maximum velocity possible in the bed to maintain the trickle flow regime. All liquid in excess is transported as pulses.

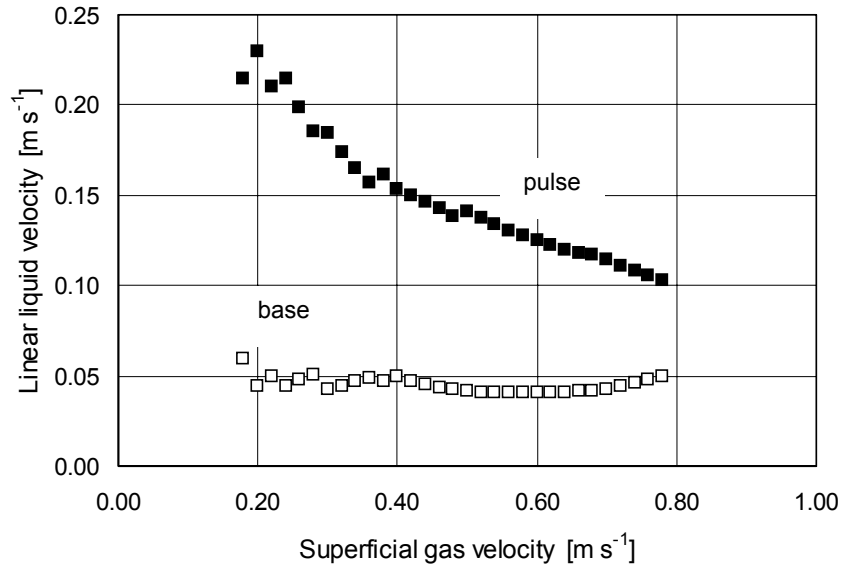


**Figure 2.16.** Calculated linear liquid velocity in between and inside the pulses (packing material: 6.0 mm glass spheres)

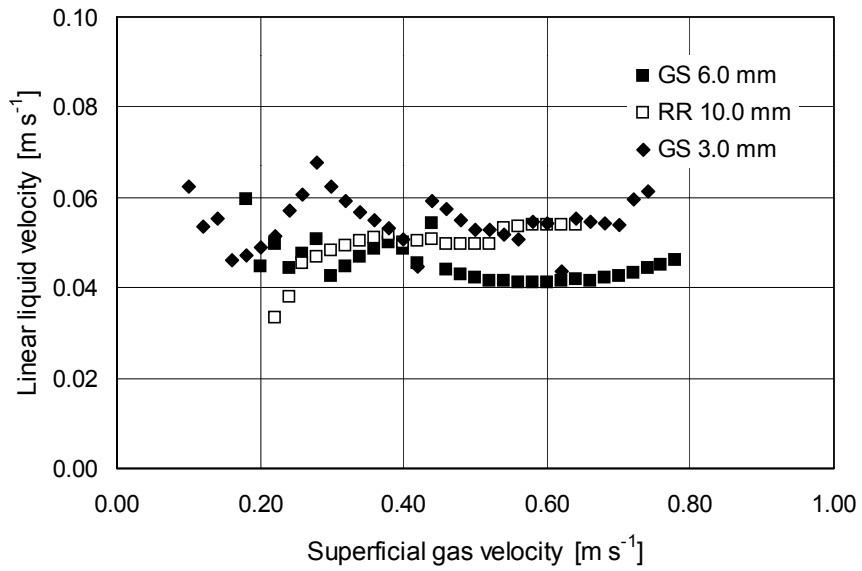


**Figure 2.17.** Calculated linear liquid velocity in between pulses for all packing materials tested

## 2.7. Concluding remarks

The properties of pulses are (nearly) invariant to the liquid flow rate. This is confirmed by experimental results of Blok and Drinkenburg (1983), Rao and Drinkenburg (1985) and Tsochatzidis and Karabelas (1995) and modeling results of Danckworth et. al. (1990, 1992). This result provides a procedure to obtain the relative contribution of the pulses and the parts of the bed in between pulses to an average measured property. This procedure shows some aspects about the nature of pulsing flow. The linear liquid velocity inside the pulses is rather high and decreases with increasing gas flow rate. The high linear liquid velocity inside the pulses may be responsible for the enhanced mass and heat transfer rates achieved during pulsing flow. The liquid holdup in between pulses equals the liquid holdup at the transition to pulsing flow at all gas flow rates. The same trend holds for the linear liquid velocity in between pulses. Pulsing flow then is a hybrid of two transition states. The pulses reside at the transition to bubble flow while the bases reside at the transition to trickle flow.

The gas penetrates the pulse from behind and is subsequently dispersed as bubbles, as is clearly demonstrated by the use of hot film anemometry. This results in large gas-liquid interfacial areas and surface renewal rates compared to trickle flow. Additional advantages as high mass and heat transfer rates, diminished axial dispersion, a more uniform distribution of liquid and periodic flushing of the catalyst, cause pulsing flow to be a promising mode of operation.

### Notation

$f_p$	pulse frequency	$[s^{-1}]$
$t_b$	base duration	$[s]$
$t_p$	pulse duration	$[s]$
$U_g$	superficial gas velocity	$[m\ s^{-1}]$
$U_l$	superficial liquid velocity	$[m\ s^{-1}]$
$\alpha$	average parameter	
$\alpha_b$	base value of average parameter	
$\alpha_p$	pulse value of average parameter	
$\beta_b$	liquid holdup in between pulses	$[-]$
$\beta_p$	liquid holdup inside pulses	$[-]$

## Literature cited

- Andreussi P., Donfrancesco A. and Messia M., An impedance method for the measurement of liquid holdup in two-phase flow, *Int. J. Multiphase Flow*, 14, 777-185, 1988
- Bartelmus G., Gancarczyk A. and Stasiak M., Hydrodynamics of cocurrent fixed-bed three-phase reactors: Part I. The effect of physicochemical properties of the liquid on pulse velocity, *Chem. Eng. Proc.*, 37, 331-341, 1998
- Blok J.R. and Drinkenburg A.A.H., Hydrodynamic properties of pulses in two-phase downflow operated packed columns, *Chem. Eng. J.*, 25, 89-99, 1982
- Blok J.R., Varkevisser J. and Drinkenburg A.A.H., Transition to pulsing flow, holdup and pressure drop in packed columns with cocurrent gas-liquid downflow, *Chem. Eng. Sci.*, 38, 687-699, 1983
- Chou T.S., Worley F.J. and Luss D., Local particle-liquid mass transfer fluctuations in mixed-phase cocurrent downflow through a fixed bed in the pulsing regime, *Ind. Eng. Chem. Fund.*, 18, 279-283, 1979
- Colombo A.J., Baldi G. and Sicardi S., Solid liquid contacting effectiveness in trickle-bed reactors, *Chem. Eng. Sci.*, 31, 1101, 1976
- Danckworth D.C., Kevrekidis I.G. and Sundaresan S., Dynamics of pulsing flow in trickle beds, *AIChE J.*, 36, 605-621, 1990
- Danckworth D.C. and Sundaresan S., Time dependent vertical gas-liquid flow in packed beds, *Chem. Eng. Sci.*, 47, 337-346, 1992
- Fukushima S. and Kusaka K., Liquid phase volumetric and mass transfer coefficient and boundary of hydrodynamic flow region in packed column with cocurrent downward flow, *J. Chem. Eng. Japan*, 10, 468-474, 1977
- Lamine A.S., Gerth L., Le Gall H. and Wild G., Heat transfer in a packed bed reactor with cocurrent downflow of a gas and a liquid, *Chem. Eng. Sci.*, 51, 3813-3827, 1996
- Lemay Y., Pineault G. and Ruether J.A., Particle-liquid mass transfer in a three-phase fixed bed reactor with cocurrent flow in the pulsing regime, *Ind. Eng. Chem. Proc. Des. Dev.*, 14, 280-285, 1975
- Lerou J.J., Glasser D. and Luss D., Packed bed liquid phase dispersion in pulsed gas-liquid downflow, *Ind. Eng. Chem. Fund.*, 19, 66, 1980
- Marcandelli C., Wild G., Lamine A.S. and Bernard J.R., Measurement of local particle-fluid heat transfer coefficient in trickle-bed reactors, *Chem. Eng. Sci.*, 54, 4997-5002, 1999
- Rao V.G. and Drinkenburg A.A.H., Pressure drop and hydrodynamic properties of pulses in two-phase gas-liquid downflow through packed beds, *Can. J. Chem. Eng.*, 61, 158-167, 1983
- Rao V.G. and Drinkenburg A.A.H., Solid-liquid mass transfer in packed beds with cocurrent gas-liquid downflow, *AIChE J.*, 31, 1059-1068, 1985
- Sato Y., Hirose F., Takahashi F., Tosa M. and Hashiguchi Y., Flow patterns and pulsation properties of cocurrent gas-liquid downflow in packed beds, *J. Chem. Eng. Japan*, 6, 315-320, 1973
- Sims W.B., Gasket S.W. and Luss D., Effect of flow regime and liquid velocity on conversion in a trickle bed reactor, *Ind. Eng. Chem. Res.*, 33, 2530-2539, 1994
- Tsochatzidis N.A. and Karabelas A.J., Properties of pulsing flow in a trickle bed, *AIChE J.*, 41, 2371-2382, 1995
- Tsochatzidis N.A., Karapantsios T.D., Kostoglou M.V. and Karabelas A.J., A conductance probe for measuring liquid fraction in pipes and packed beds, *Int. J. Multiphase flow.*, 18, 653-667, 1992

- Tsochatzidis N.A. and Karabelas A.J., Study of pulsing flow in a trickle bed using the electrodiffusion technique, *J. Appl. Electrochem.*, 24, 670-675, 1994
- Wu R., McCready M.J. and Varma A., Influence of mass transfer coefficient fluctuation frequency on performance of three-phase packed-bed reactors, *Chem. Eng. Sci.*, 50, 3333-3344, 1995
- Wu R., McCready M.J. and Varma A., Effect of pulsing on reaction outcome in a gas-liquid catalytic packed-bed reactor, *Catalysis Today*, 48, 195-198, 1999
- Weekman V.W. and Myers J.E., Fluid flow characteristics of cocurrent gas-liquid flow in packed beds, *AIChE J.*, 10, 951-957, 1964

## A2. Pulsing flow characteristics for other packing materials

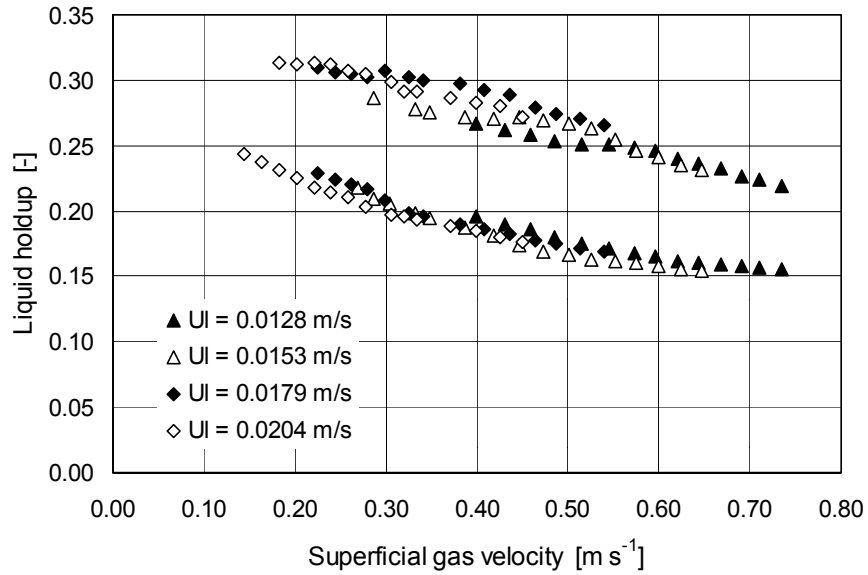


**Figure A2.1.** Liquid holdup versus the superficial gas velocity (packing material: 10.0 mm Raschig Rings)

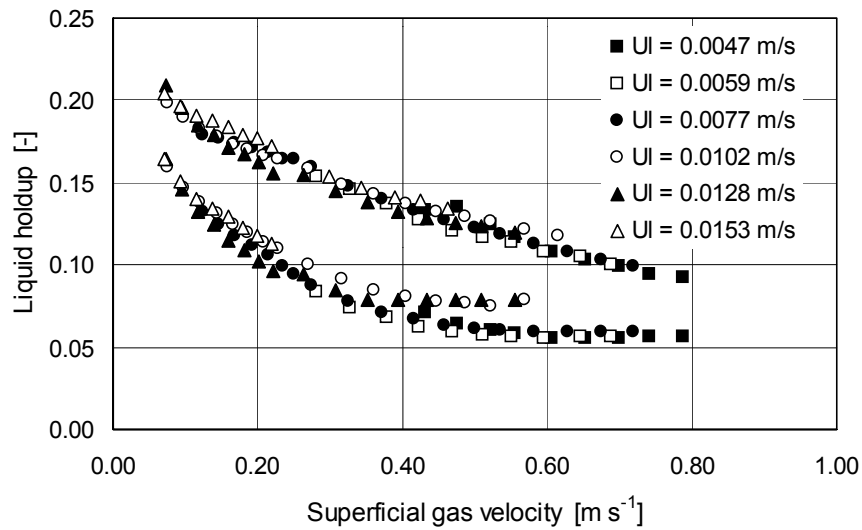


**Figure A2.2.** Liquid holdup versus the superficial gas velocity (packing material: 3.0 mm glass spheres)



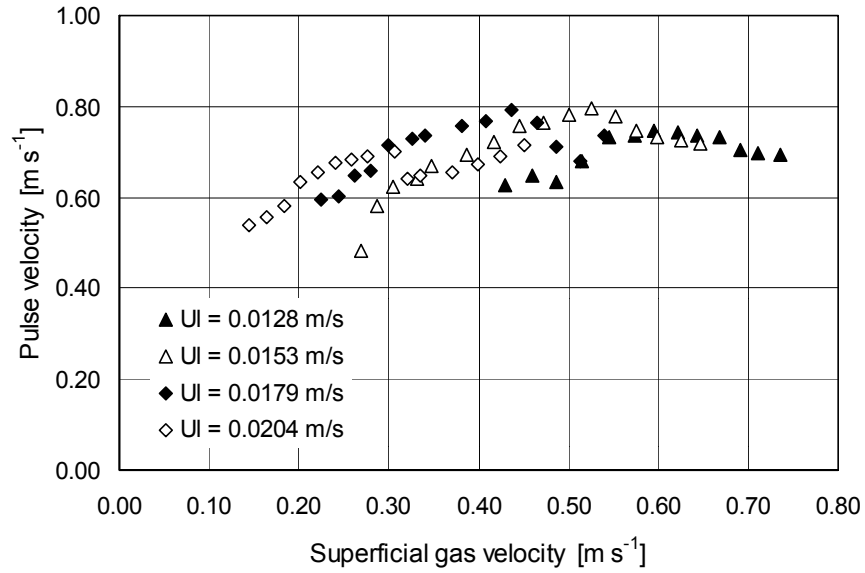


**Figure A2.3.** Pulse velocity versus the superficial gas velocity (packing material: 10.0 mm Raschig Rings)

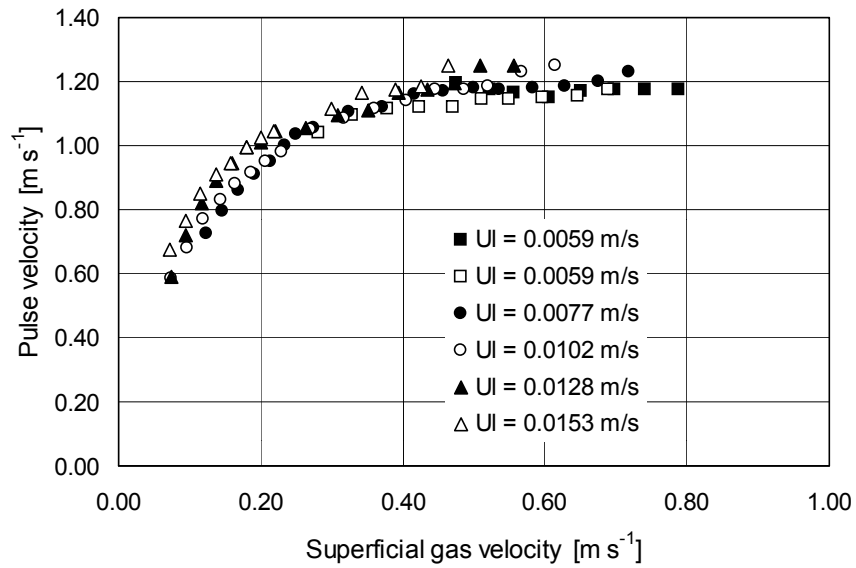


**Figure A2.4.** Pulse velocity versus the superficial gas velocity (packing material: 3.0 mm glass spheres)

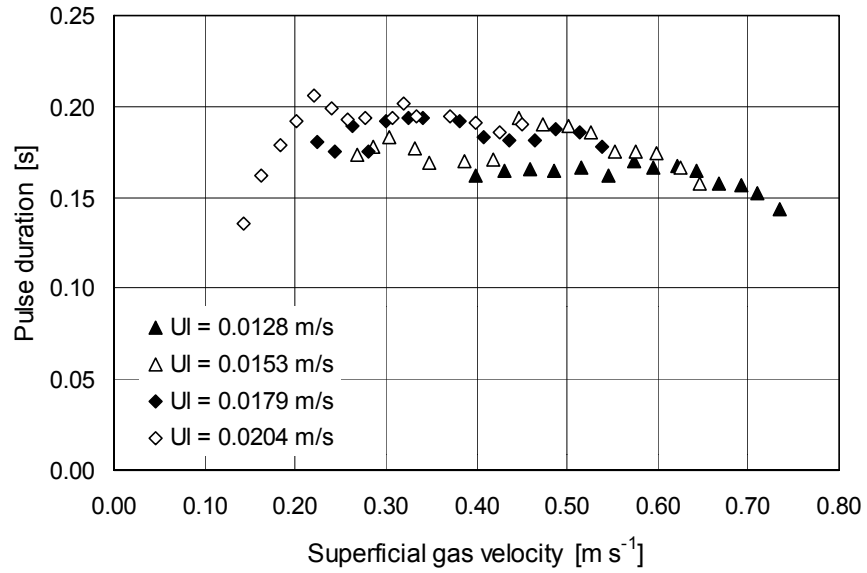


**Figure A2.5.** Pulse duration versus the superficial gas velocity (packing material: 10.0 mm Raschig Rings)

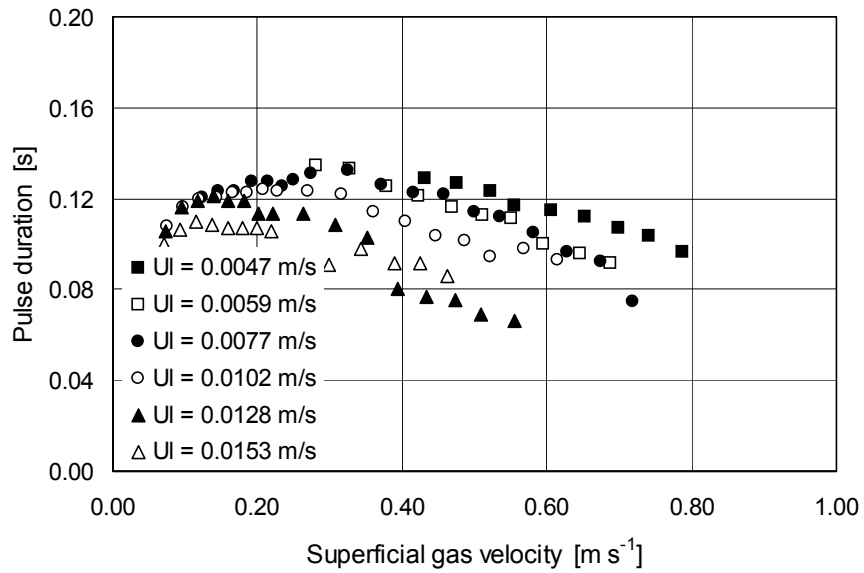


**Figure A2.6.** Pulse duration versus the superficial gas velocity (packing material: 3.0 mm glass spheres)

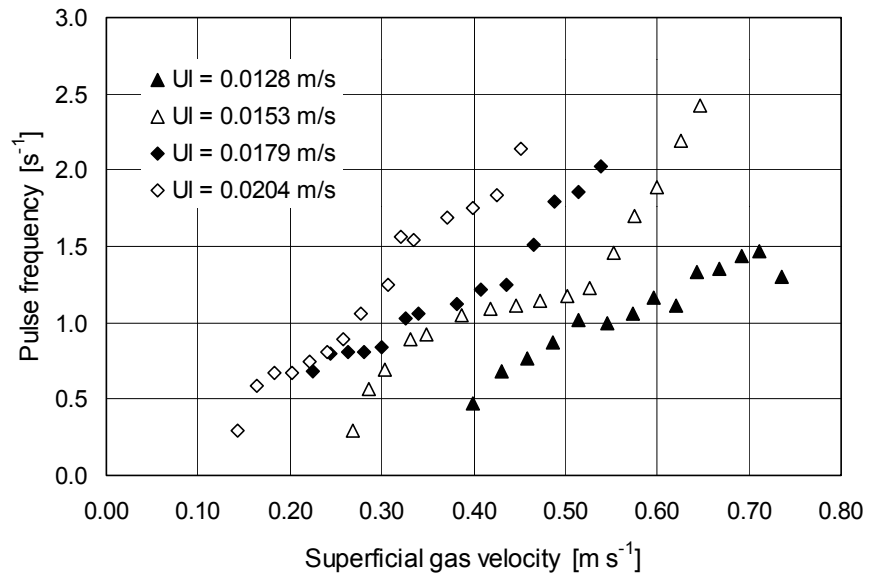


**Figure A2.7.** Pulse frequency versus the superficial gas velocity (packing material: 10.0 mm Raschig Rings)

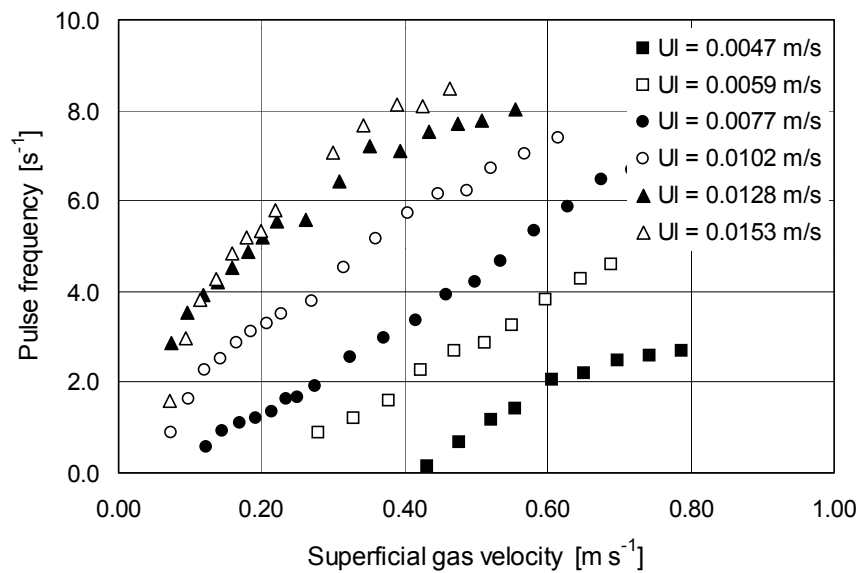


**Figure A2.8.** Pulse frequency versus the superficial gas velocity (packing material: 3.0 mm glass spheres)

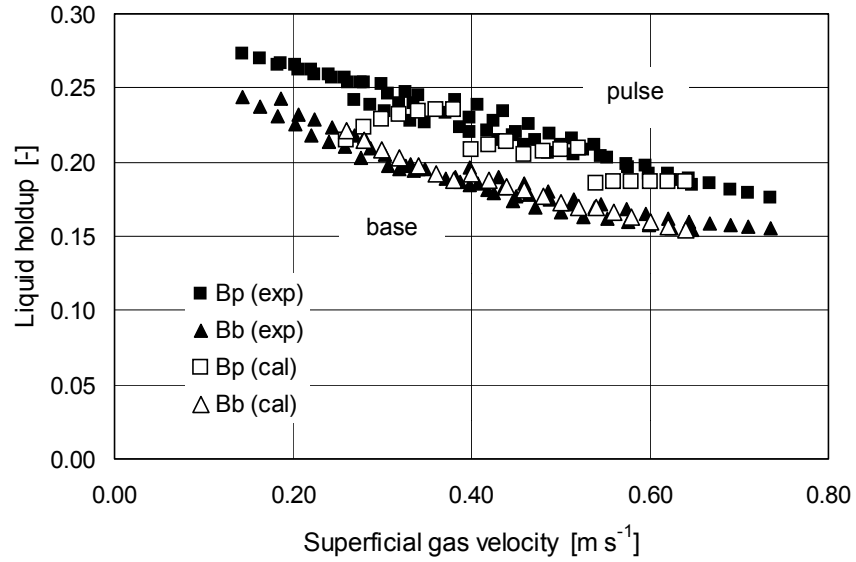


**Figure A2.9.** Comparison between experimentally determined and calculated liquid holdup inside and in between pulses (packing material: 10.0 mm Raschig Rings)

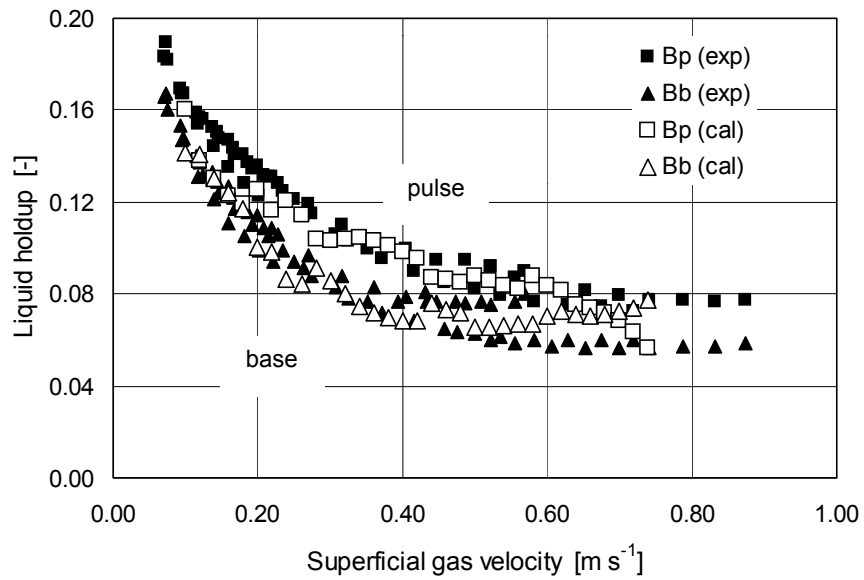


**Figure A2.10.** Comparison between experimentally determined and calculated liquid holdup inside and in between pulses (packing material: 3.0 mm glass spheres)

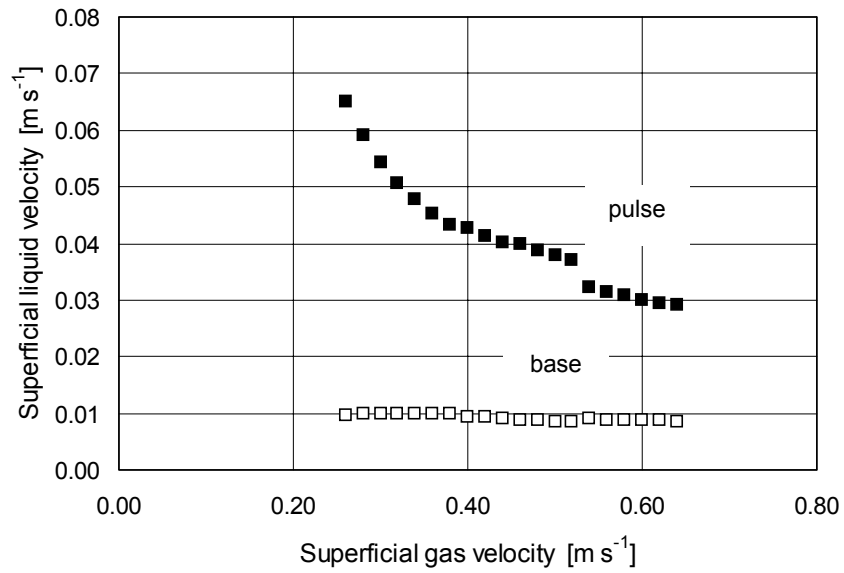


**Figure A2.11.** Calculated superficial liquid velocity in between and inside the pulses (packing material: 10.0 mm Raschig Rings)

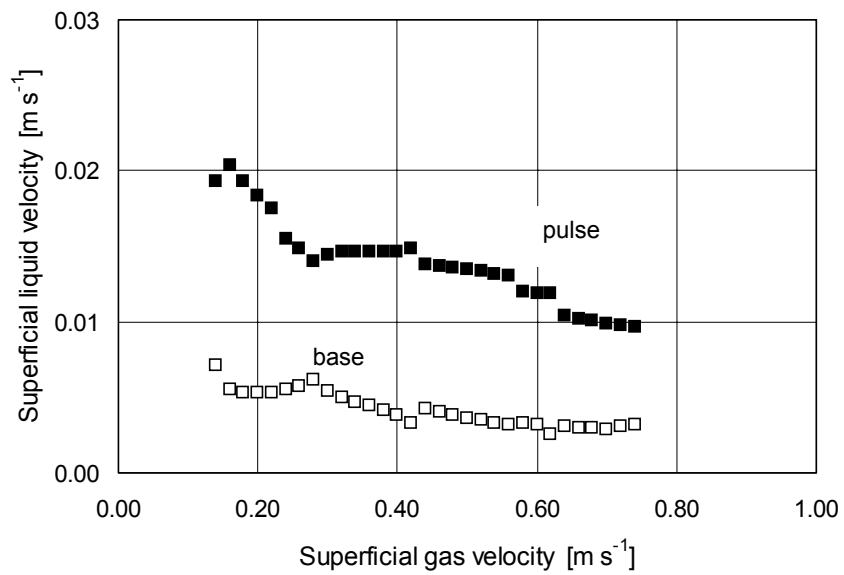


**Figure A2.12.** Calculated superficial liquid velocity in between and inside the pulses (packing material: 3.0 mm glass spheres)

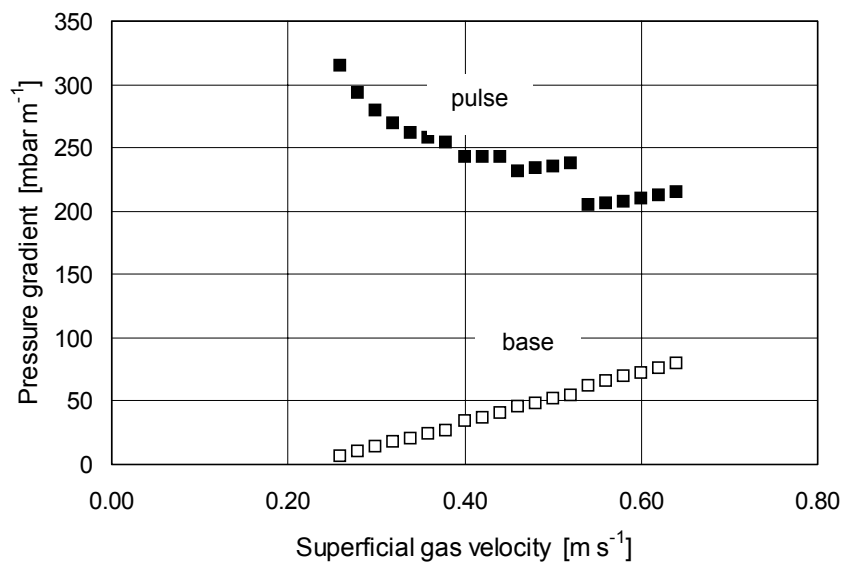


**Figure A2.13.** Calculated pressure gradient in between and inside the pulses (packing material: 10.0 mm Raschig Rings)

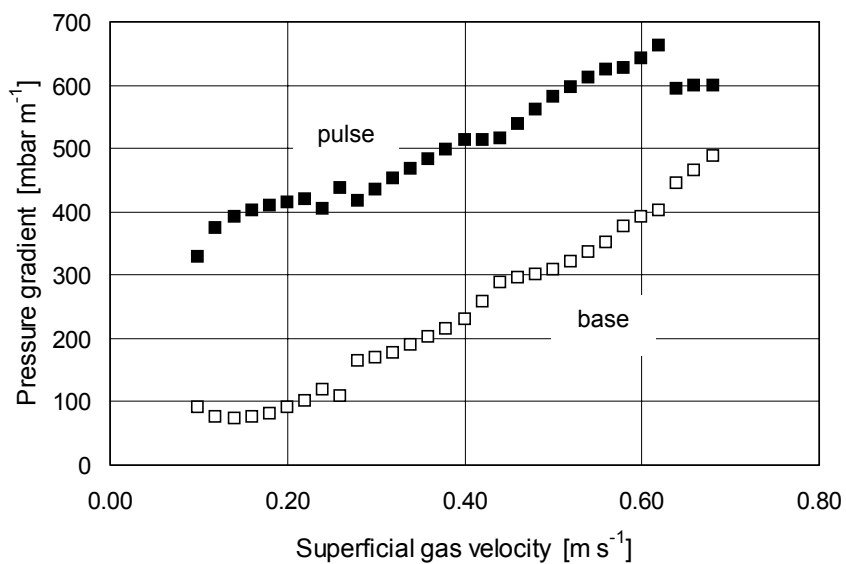


**Figure A2.14.** Calculated pressure gradient in between and inside the pulses (packing material: 3.0 mm glass spheres)

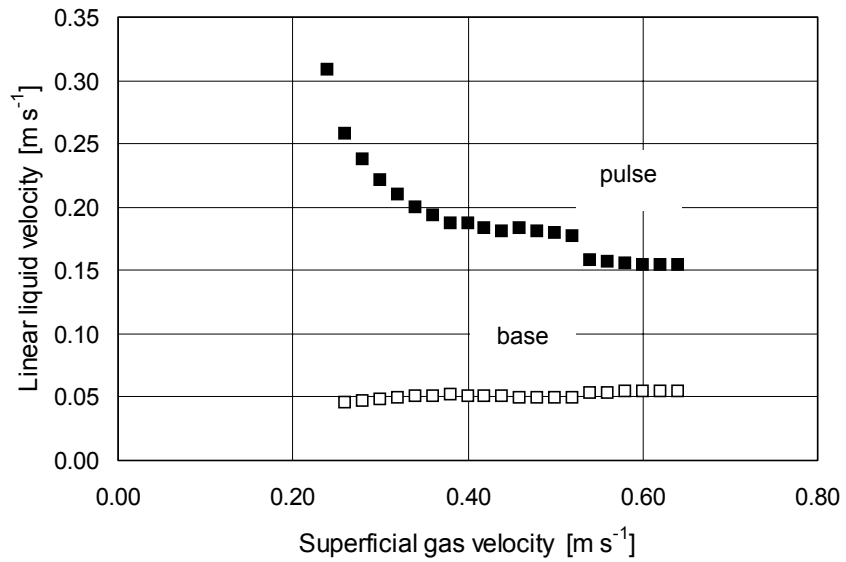


**Figure A2.15.** Calculated linear liquid velocity in between and inside the pulses (packing material: 10.0 mm Raschig Rings)

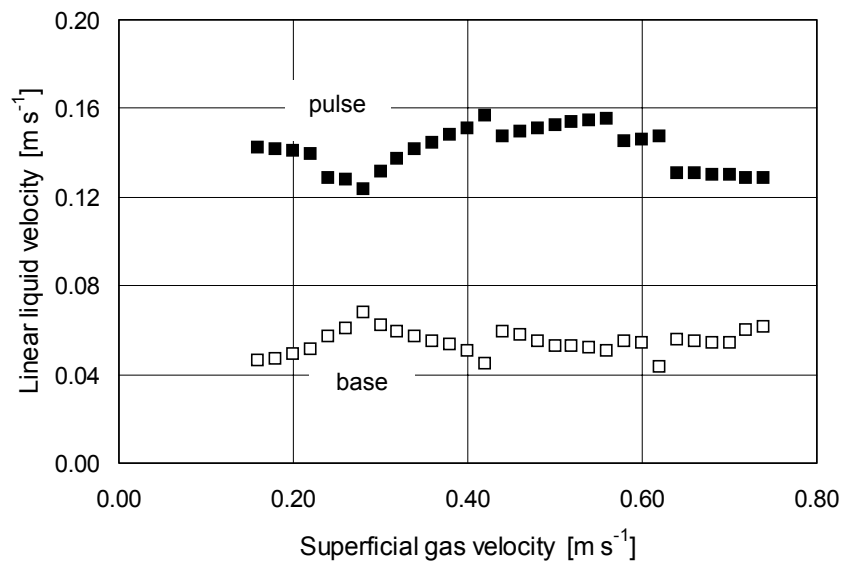


**Figure A2.16.** Calculated linear liquid velocity in between and inside the pulses (packing material: 3.0 mm glass spheres)

---

## Chapter 3

---

# Local Particle-Liquid Heat Transfer Coefficient

---

### Abstract

Trickle-bed reactors are generally operated in the trickle flow regime during which a tendency for flow maldistribution exists. Consequently, unwetted regions of catalyst particles may be created in which, in case of a volatile liquid phase reactant, the reaction rate is much higher as compared to the wetted zones. This possibly results in hot spot formation. Subsequently, safety problems, catalyst deactivation and reduced selectivities may originate.

Local time-averaged particle-liquid heat transfer rates are determined with custom-made probes in the trickle and pulsing flow regimes. In the trickle flow regime, the local heat transfer coefficient increases with both increasing liquid and gas flow rate. The transition to pulsing flow is accompanied by a substantial increase in heat transfer rates. The linear liquid velocity is identified as the main parameter that governs heat transfer rates in both flow regimes. Particle-liquid heat transfer coefficients inside pulses are 2 to 3 times higher than in between pulses. The high particle-liquid heat transfer coefficient inside the pulses is the result of the high linear liquid velocity inside the pulses. Particle-liquid heat transfer rates in between pulses are constant due to the constant linear liquid velocity. Heat transfer rates considerably depend on the local structure of the packed bed. Heat transfer coefficients in terms of Nusselt numbers strongly correlate with  $Re^{0.8}$ .

Pulsing flow results in high particle-liquid heat transfer rates and a periodic flushing of the catalyst particles. Therefore, the operation of a trickle-bed reactor in the pulsing flow regime assesses the possibility to prevent hot spot formation. Safety problems, catalyst deactivation and less than optimal selectivities can be avoided.

This chapter is based on the following publications:

- Boelhouwer J.G., Piepers H.W. and Drinkenburg A.A.H., Particle-liquid heat transfer in trickle-bed reactors, *Chem. Eng. Sci.*, **56**, 1181-1187, 2001
- Boelhouwer J.G., Piepers H.W. and Drinkenburg A.A.H., Nature and characteristics of pulsing flow in trickle-bed reactors, *Chem. Eng. Sci.*, submitted for publication
- Boelhouwer J.G., Piepers H.W. and Drinkenburg A.A.H., Particle-liquid heat transfer in trickle-bed reactors, paper 333f, AIChE Annual Meeting, Los Angeles, CA, U.S.A., 2000



### 3.1. Introduction

A trickle-bed reactor is a type of three-phase reactors in which a gas and a liquid phase cocurrently flow downward over a packed bed of catalyst particles. These trickle-bed reactors are often applied to perform strong exothermic reactions as the hydrogenation of unsaturated hydrocarbons (Hanika, 1999). One of the major disadvantages of trickle-bed reactors is their poor capability to eliminate the heat involved with reaction. Considering the low heat capacity of the gas, the reaction heat is most often removed by the liquid phase, although sometimes evaporation of the liquid is used. When the generated heat is not adequately removed, hot spots are created and catalyst deactivation may occur. The formation of hot spots must be prevented regarding safety considerations, e.g. no runaway is allowed to occur. Deactivation of the catalyst causes problems with selectivity, production capacity and flexibility in operation.

Trickle-bed reactors are usually operated in the trickle flow regime. It is well known that during trickle flow operation, a tendency for flow maldistribution and phase segregation exists (Sapre et. al., 1990; Stanek et. al., 1981; Moller et. al., 1996). Flow maldistribution may result in the formation of unwetted regions of catalyst particles. Depending on the volatility of the liquid-phase reactants, the reaction rate in these regions may be much higher as compared to the wetted zones. The higher reaction rate in turn accelerates the heat production and hence hot spot enlargement is often observed (Hanika, 1999). The operation of a trickle-bed reactor in the pulsing flow regime is well known for its large increase in mass transfer rates (Chou et. al., 1979; Ruether et. al., 1980; Rao and Drinkenburg, 1985; Tsochatzidis and Karabelas, 1994). Correspondingly, enhanced heat transfer rates are expected to occur during pulsing flow. Additionally, pulsing flow is accompanied by an increased wetting of the catalyst particles and a radially uniform distribution of the phases, which prevents the formation of unwetted regions and hence the development of hot spots.

Only few studies in literature deal with particle-liquid heat transfer rates in trickle-bed reactors. The main reason is probably the difficulty to find an accurate experimental method. Kirillov and Ogarkov (1980) report limited data on particle-liquid heat transfer and claim that the hydrodynamic flow regime strongly affects heat transfer rates. Heat transfer rates seem to decrease in the high interaction regime. Sapre et. al. (1990) and Anderson et. al. (1992) used a large cylindrical sensor to measure flow maldistribution in trickle-bed reactors based on solid-liquid heat transfer.

The difference in size between their probe and the packing disturbs the flow and their results hardly seem relevant for particle-liquid heat transfer. A recent experimental study of Marcandelli et. al. (1999) indicates an increase in heat transfer rates upon the transition from the low to the high interaction regime.

### **3.2. Scope and Objective**

The operation of a trickle-bed reactor in the pulsing flow regime assesses the possibility to prevent the formation of hot spots due to a periodic flushing of the catalyst particles. It is also expected that pulsing flow results in relatively high particle-liquid heat transfer rates analogous to enhanced mass transfer rates. Safety problems, catalyst deactivation and reduced selectivities can possibly be avoided.

The objective of the work presented in this chapter is to experimentally determine time-averaged local particle-liquid heat transfer coefficients in the trickle and pulsing flow regime. Moreover, the effect of the radial distribution of heat transfer rates is investigated. Special attention is given to particle-liquid heat transfer during pulsing flow, since pulsing flow is a promising mode of operation.

### **3.3. Experimental set-up and procedures**

The experiments were performed in a Plexiglas column of 0.11 m inner diameter and a packed height of 1.0 m. A schematic illustration of the experimental equipment is presented in Fig. 3.1. The packing material consisted of 6.0 mm glass spheres. A porosity of 0.38 and a specific packing area of  $620 \text{ m}^{-1}$  characterized the packed bed. Air and water were uniformly distributed at the top of the column. The experiments were conducted at room temperature and near atmospheric pressure. A conductance technique, described in detail in chapter 2, was used to instantaneously measure cross-sectionally averaged liquid holdup. For a period of at least 5 minutes, conductivity traces were collected with a sampling rate of 100 Hz.

A custom-made probe capable of time-average measurement of local particle-liquid heat transfer rates is developed. The size and shape of the probe is identical to a packing particle (6.0 mm sphere) to avoid disturbances of the liquid film. A schematic illustration of the sensor is presented in Fig. 3.2.

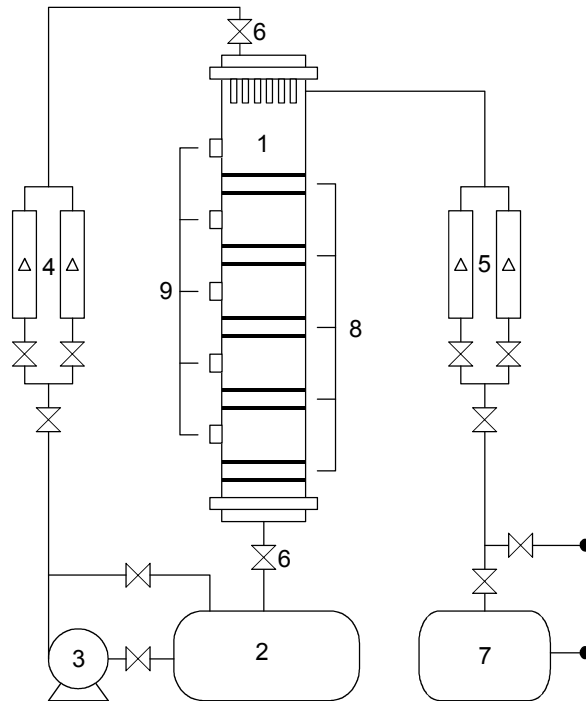


**Figure 3.1.** Schematic illustration of the experimental equipment (1: column; 2: liquid storage tank; 3: liquid pump; 4: liquid flow meters; 5: gas flow meters; 6: magnetic valve; 7: pressure vessel; 8: conductivity probes; 9: pressure taps)

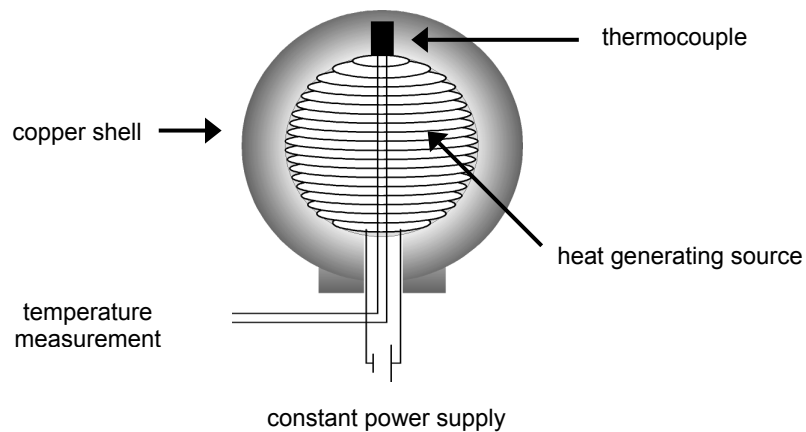


**Figure 3.2.** Schematic illustration of the custom-made probe for measurement of local time-average particle-liquid heat transfer coefficient

The probe consists of a hollow copper particle of approximately 1.0 mm thickness in which a spherical-shaped heat-generating source is installed. In the copper shell, at the vicinity of the outer surface of the probe, a thermocouple capable of accurate temperature measurement is situated. Temperature gradients in the copper shell are negligible ( $Bi \ll 1$ ). A constant power is applied to the heat-generating source. Both the dissipated power and the temperature were recorded and stored in a computer with a sample-frequency of 10 Hz. The experimentally obtained time-averaged heat transfer coefficient can be calculated by applying the following equation:

$$\alpha_p = \frac{1}{a_p} \frac{\sum_t Q_p}{\sum_t (T_p - T_l)} \quad [3.1]$$

In this equation,  $Q_p$  is the dissipated power,  $a_p$  the geometrical surface area of the probe,  $T_p$  the surface temperature of the probe and  $T_l$  the temperature of the liquid. Actually, the apparent heat transfer coefficient is obtained, since wetting of the probe may be incomplete and additional heat transfer to stagnant liquid may occur. Preliminary calculations following the approach of Yagi and Kunii (1957) established that there existed a negligible rate of heat transfer by direct conduction between the sensor and the bed of glass spheres. This is due to the low thermal conductivity of the glass.

A total of 5 probes are situated in the trickle-bed at various radial positions for measurement of local heat transfer coefficients. The wires connecting the probes with the control-unit were mounted in packing particles to avoid disturbances of the liquid film. Before performing any experiments, the column was operated in the pulsing flow regime for at least 1 hour to ensure a perfectly pre-wetted bed. After the gas and liquid flow were established, a short period was necessary for the probe to reach its stationary condition. After the stationary condition was accomplished, the measurement was started. Local time-average particle-liquid heat transfer coefficients were determined for a wide range of gas and liquid flow rates. The liquid holdup was measured in the same range of gas and liquid flow rates in order to calculate linear liquid velocities.

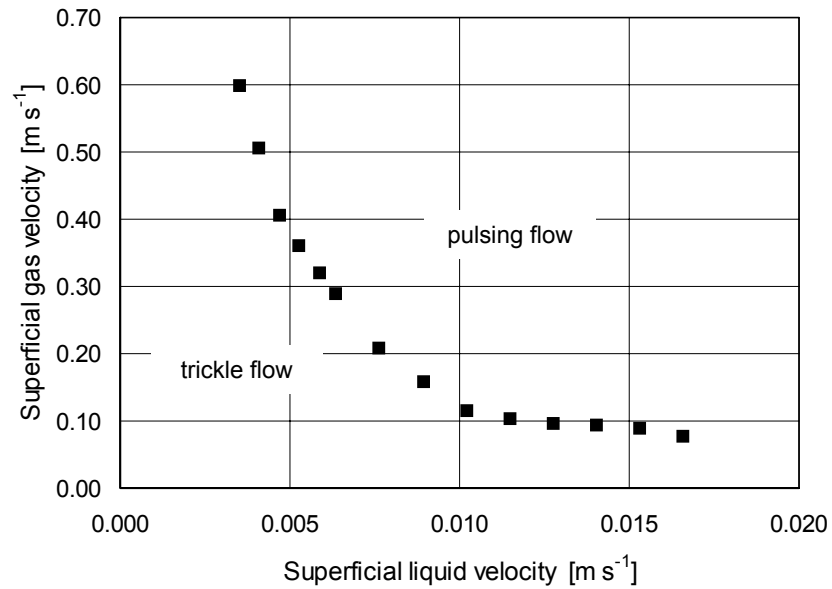


**Figure 3.3.** Transition boundary from trickle to pulsing flow in terms of superficial gas and liquid velocities

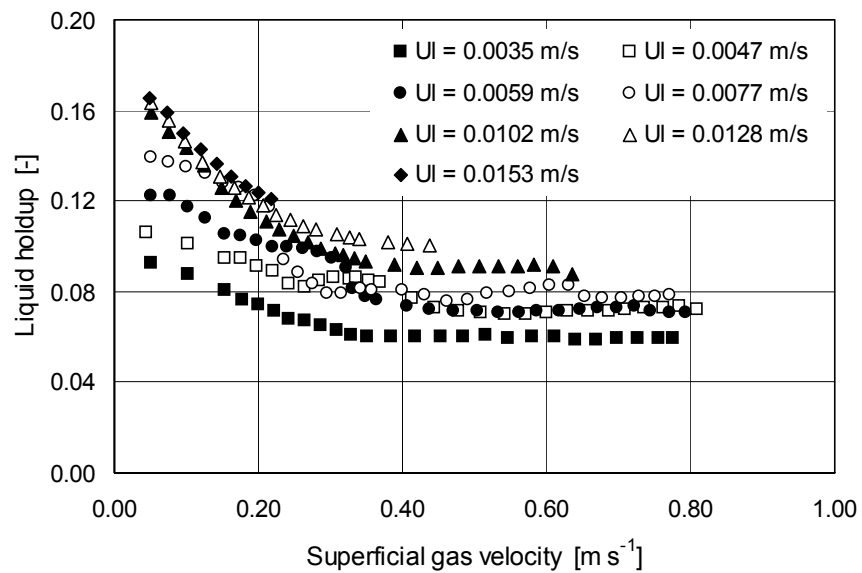


**Figure 3.4.** Liquid holdup versus the superficial gas velocity

### 3.4. Hydrodynamics

The two main flow regimes visually observed in the column are trickle and pulsing flow. The transition boundary from trickle to pulsing flow is presented in Fig. 3.3. The hydrodynamic nature of the flow regime is expected to exhibit a strong influence on particle-liquid heat transfer rates.

The liquid holdup, defined as the fraction of the empty column occupied with liquid, is plotted in Fig. 3.4 as a function of gas and liquid flow rates. The liquid holdup data are taken at approximately the same height in the packed bed as where the probes are located. In the trickle flow regime, liquid holdup increases with increasing liquid flow rate and slightly decreases with increasing gas flow rate. In the pulsing flow regime, however, liquid holdup first decreases strongly with increasing gas flow rate and subsequently becomes approximately constant at relatively high gas flow rates. Our experimental data concerning liquid holdup are consistent with the data of Blok et. al. (1983) and Tsochatzidis and Karabelas (1995). It must be noted that, although time-average liquid holdup in the pulsing flow regime increases with increasing liquid flow rate, the liquid holdup inside and in between pulses is invariant to the liquid flow rate. Time-average liquid holdup solely increases with increasing liquid flow rate due to an increase in pulse frequency. For more details regarding liquid holdup during pulsing flow, the reader is referred to chapter 2.

### 3.5. Local particle-liquid heat transfer coefficient

#### 3.5.1. Time-average heat transfer coefficient

Particle-liquid heat transfer coefficients as a function of gas and liquid flow rates are presented in Fig. 3.5. The presented data are the average values of de 5 probes. Heat transfer rates increase with both increasing gas and liquid flow rate. In the trickle flow regime, the effect of the gas flow rate is rather weak, while the transition to pulsing flow results in an increase in the local average heat transfer rates. These trends are confirmed by the study of Marcandelli et. al. (1999).

A plot of the particle-liquid heat transfer coefficient versus the linear liquid velocity ( $U_l/\beta$ ) is given in Fig. 3.6. The solid markers represent heat transfer coefficients in the trickle flow regime while the open markers represent data in the pulsing flow regime.

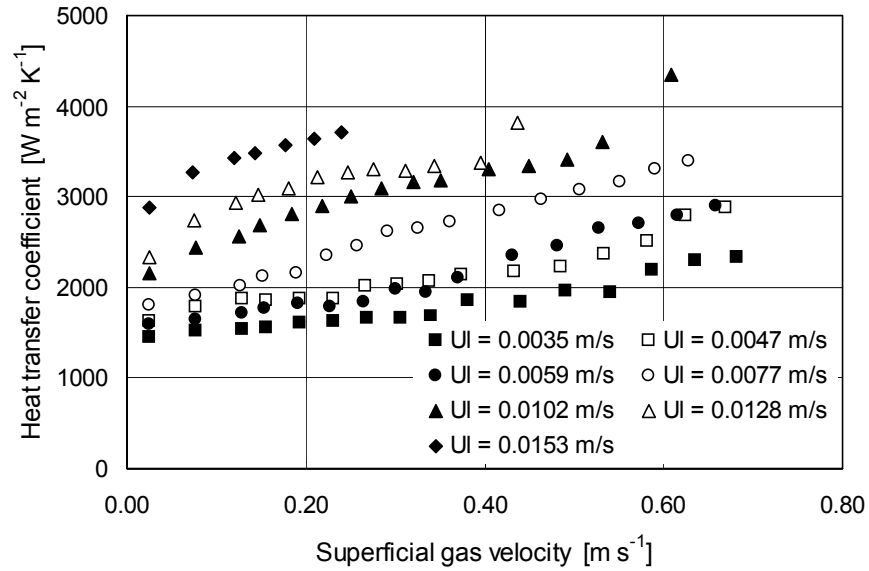


**Figure 3.5.** Time-average particle-liquid heat transfer coefficient versus superficial gas and liquid velocities

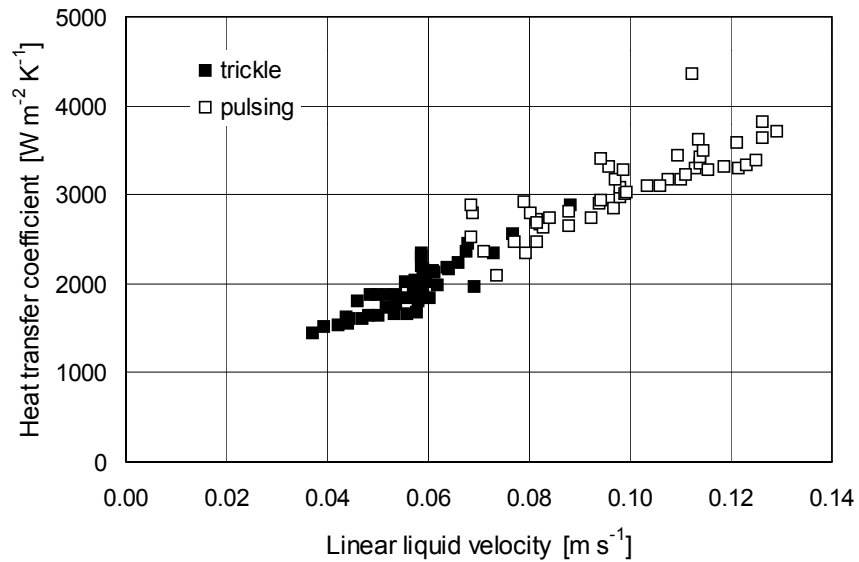


**Figure 3.6.** Time-average particle liquid heat transfer coefficient versus the linear liquid velocity

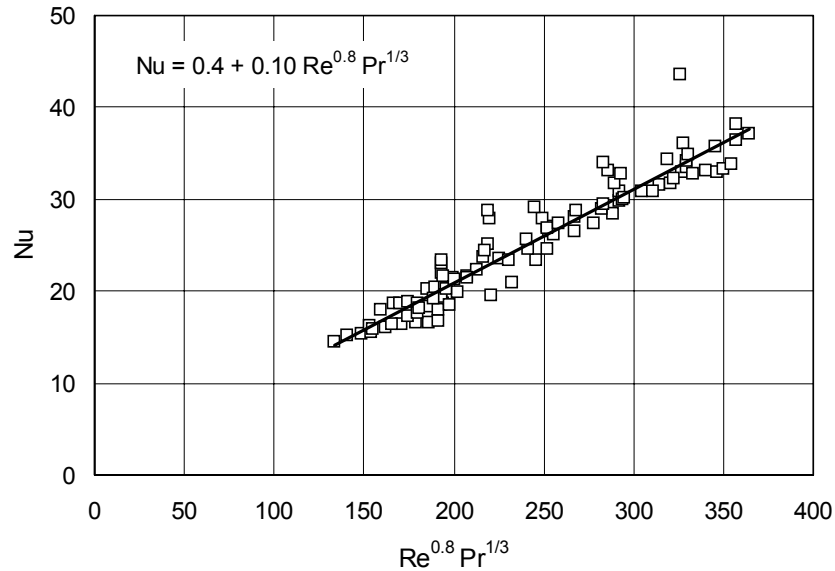


**Figure 3.7.** Correlation of particle-liquid heat transfer coefficient in terms of the Nu-number

A rather sharp distinction can be made between the heat transfer coefficients for the trickle and pulsing flow regime with respect to the linear liquid velocity. Heat transfer coefficients at linear liquid velocities above approximately  $0.07 \text{ m s}^{-1}$  are associated with pulsing flow. The data presented in this figure imply that the linear liquid velocity is the main parameter that governs heat transfer coefficients. No principal difference (in the form of a sudden jump) seems to exist between heat transfer rates in the trickle and pulsing flow regime, although the hydrodynamic behavior differs considerably.

### 3.5.2. Correlation of results

The experimental data in terms of a Nu-number averaged over the 5 probes strongly correlate with  $Re^{0.8} Pr^{1/3}$ , as shown in Fig. 3.7:

$$Nu = 0.4 + 0.10 Re^{0.8} Pr^{0.33} \quad [3.2]$$

The Re-number is based on the linear liquid velocity and the particle diameter. The Pr-number is only varied in a narrow range, due to small temperature variations of the liquid in the experiments.



Hence, this parameter has no significant distinction in the results presented in this figure. The correlation between  $Nu$  and  $Re^{0.8}$  is common for heat transfer in turbulent flow and is characteristic for good radial mixing. Ruether et. al. (1980) presented a correlation for particle-liquid mass transfer in which a power of 0.77 for the  $Re$ -number was found. The  $Re$ -number in this correlation is also based on the linear liquid velocity. All other published correlations for mass transfer coefficients are expressed as functions of both the liquid and gas  $Re$ -numbers. However, it is very likely that for mass transfer coefficients also, the effect of the gas flow rate is embedded in the liquid holdup and hence in the linear liquid velocity. It must be noted that for zero  $Re$ -number, the  $Nu$ -number in packed beds approaches a value less than 2 because liquid maldistribution plays an important role (Martin, 1978).

### 3.5.3. Radial distribution of particle-liquid heat transfer

A plot of the particle-liquid heat transfer coefficient versus the linear liquid velocity for 4 of the probes is presented in Fig. 3.8. The lowest heat transfer rates are observed close to the wall of the column and in the center of the bed. The differences between the measured heat transfer rates at different positions in the bed are substantial, as was also noted by Marcandelli et. al. (1999, 2000). The same magnitude in local differences is encountered for particle-liquid mass transfer rates for which more information is available (Chou et. al., 1979; Gabitto and Lemcoff, 1987; Tsochatzidis and Karabelas, 1994).

Three main phenomena may be responsible for the observed local differences in heat (and mass) transfer rates. The contact area between the probe and the dynamic liquid is probably different for each probe due to flow maldistribution. Different wetting efficiencies will result in different apparent heat transfer rates. Since heat transfer to stagnant liquid will occur also, differences in contact area between the probes and the stagnant liquid will affect the measured particle-liquid heat transfer coefficient. At the point of contact between two particles, a pocket of stagnant liquid holdup is present. More neighboring particles result in an increase in the total stagnant liquid holdup held at the contact points, and hence in an increase in the contact area between the probe and the stagnant liquid. An additional reason is that the linear liquid velocity is based on the cross-sectionally averaged liquid holdup. Actual liquid velocities around the probes may differ substantially depending on the local structure of the packed bed (Gabitto and Lemcoff, 1987; Moller et. al., 1996; Herskowitz and Smith, 1978; Wang et. al., 1998).

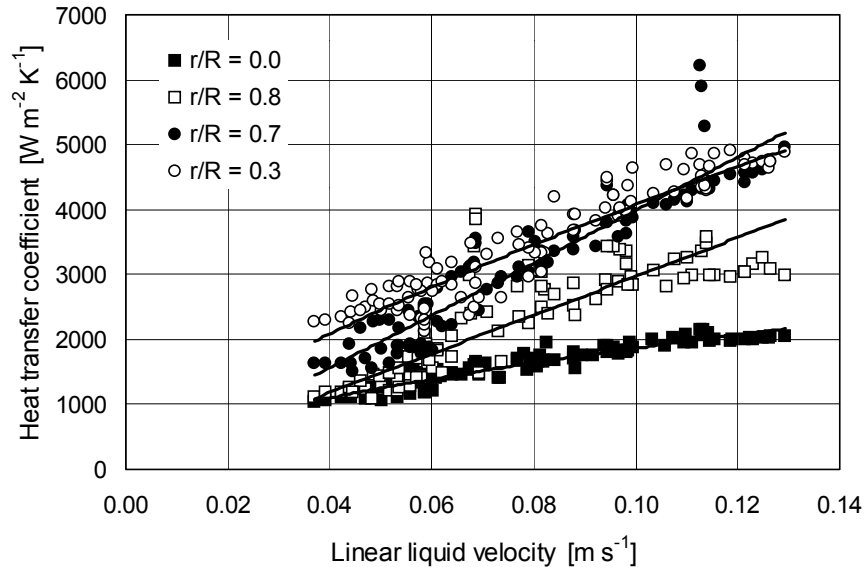


**Figure 3.8.** Particle-liquid heat transfer coefficient versus the linear liquid velocity at different radial positions in the bed

### 3.6. Particle-liquid heat transfer coefficient during pulsing flow

In chapter 2, a procedure to obtain the relative contribution of the pulses and the parts of the bed in between pulses to a measured time-average parameter is presented. The fact that the hydrodynamic properties of the pulses are identical at a constant gas flow rate, regardless the applied liquid flow rate, form the basis for this procedure. The increase in a time-average property at a constant gas flow rate with increasing liquid flow rate is solely due to an increase in the pulse frequency, not a change in the properties of the pulses themselves. For more details concerning this procedure, the reader is referred to chapter 2.

By implementing this procedure to time-averaged particle-liquid heat transfer rates, heat transfer coefficients inside and in between pulses are obtained. The results are plotted versus the superficial gas flow rate in Fig. 3.9. Heat transfer coefficients in between pulses are constant while heat transfer coefficients inside pulses are much higher and decrease with increasing gas flow rate. By applying this same procedure to the time-average linear liquid velocity, linear liquid velocities inside and in between pulses are calculated (chapter 2).

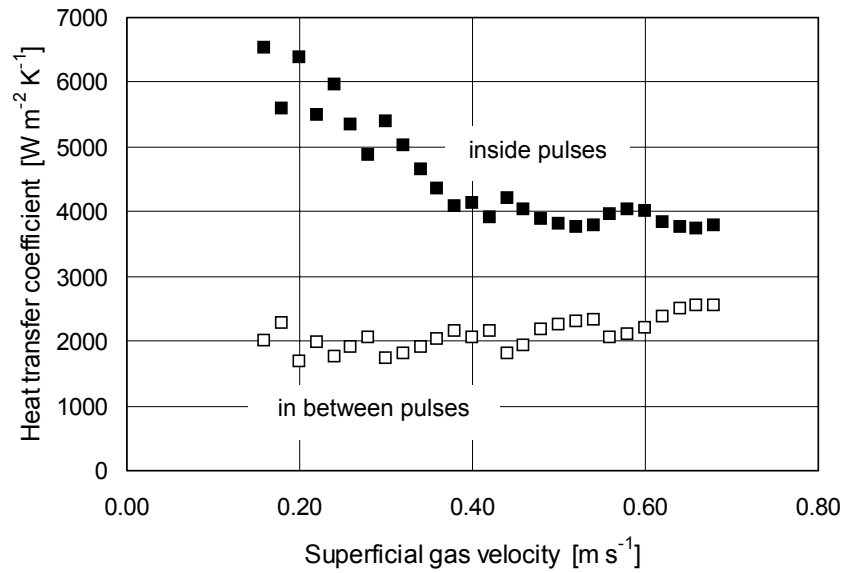


**Figure 3.9.** Calculated particle-liquid heat transfer coefficient inside and in between pulses versus the superficial gas velocity

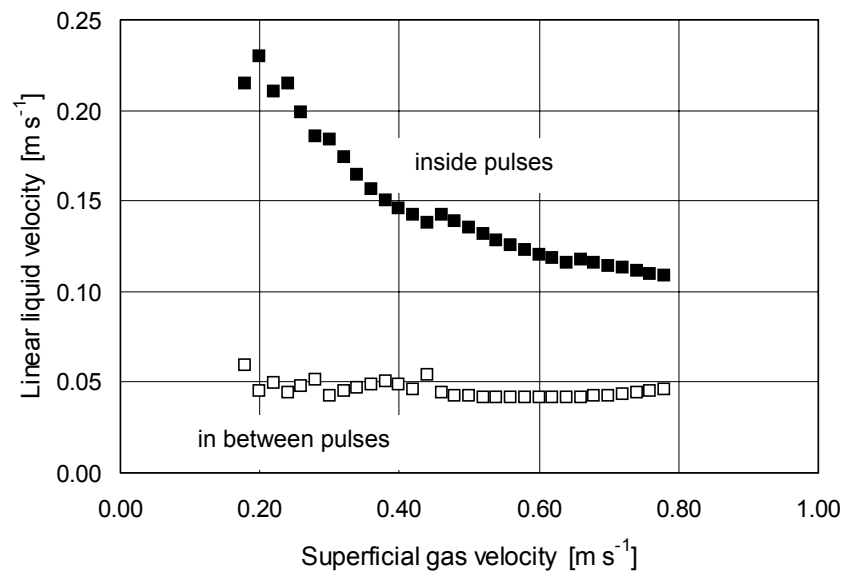


**Figure 3.10.** Calculated linear liquid velocity inside and in between pulses versus the superficial gas velocity

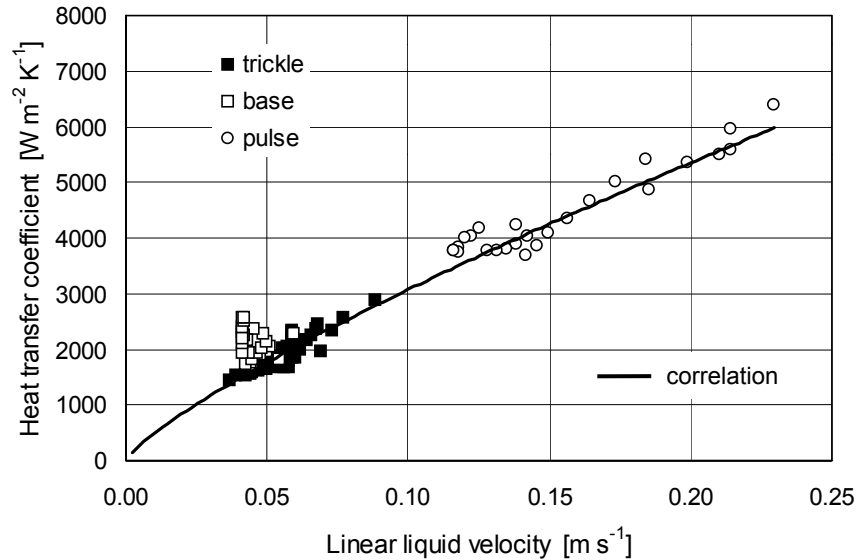


**Figure 3.11.** Comparison of particle-liquid heat transfer coefficient inside and in between pulses with correlation for time-average particle-liquid heat transfer coefficient

The results are presented in Fig. 3.10. Obviously the same trends prevail, as for heat transfer coefficients inside and in between pulses. Heat transfer rates in between pulses are constant since the linear liquid velocity in between pulses is fixed. Heat transfer coefficients inside the pulses decrease with increasing gas flow rate since the linear liquid velocity decreases with increasing gas flow rate also.

In Fig. 3.11, the calculated heat transfer coefficients inside and in between pulses are plotted versus the calculated linear liquid velocity inside and in between pulses. Additionally, the proposed correlation and the heat transfer coefficients obtained in the trickle flow regime are presented in this figure for comparison. Heat transfer coefficients inside and in between pulses obey the proposed correlation for time-average heat transfer coefficients, although the calculated linear liquid velocity and heat transfer coefficients are independently obtained. This suggests that the higher linear liquid velocity inside the pulses causes the increase in heat (and mass) transfer rates inside the pulses. It must be noted that the heat transfer coefficients in between pulses are somewhat higher compared to the correlation. This may be caused by the higher wetting efficiency in between pulses compared to trickle flow at equivalent linear liquid velocities.

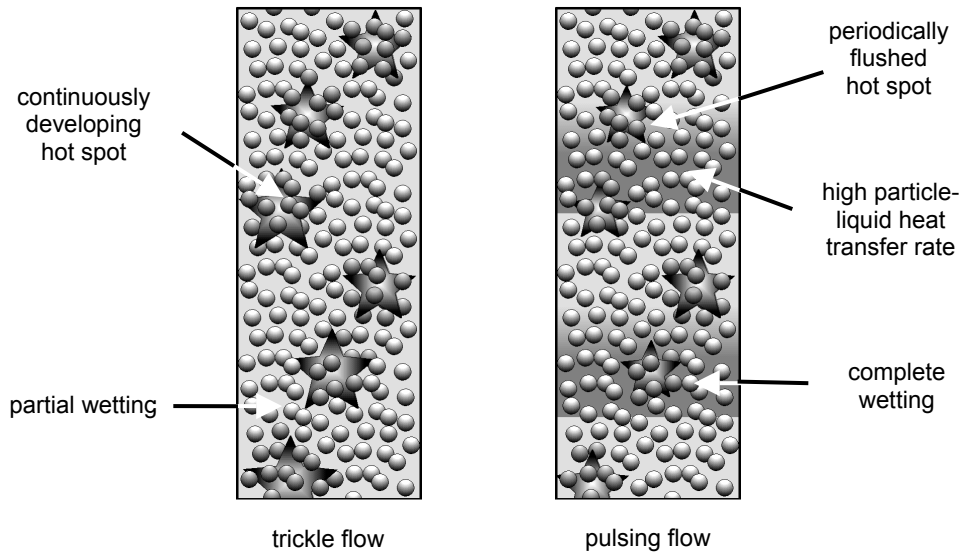


**Figure 3.12.** Concept of periodic flushing of (developing) hot spots during pulsing flow

Wetting in between pulses is higher compared to steady flow at equivalent linear liquid velocities since a pulse very recently completely wetted the packing and draining needs time.

### 3.7. Concluding remarks

In this chapter, experimental results on particle-liquid heat transfer rates in trickle-bed reactors are presented. The transition from trickle to pulsing flow is accompanied by a substantial increase in heat transfer rates. The linear liquid velocity is identified as the main parameter that governs heat transfer coefficients. No principal difference in heat transfer mechanism exists between trickle and pulsing flow although the hydrodynamic behavior is totally different. Heat transfer rates inside the pulses are 2 to 3 times higher than in between the pulses. Calculated heat transfer coefficients inside and in between pulses obey the same correlation with linear liquid velocity as time-average heat transfer coefficients. This suggests that the increase in heat (and mass) transfer rates inside the pulses is mainly the result of the higher linear liquid velocity inside the pulses.

The local structure of the packed bed considerably influences local heat transfer rates. Care must be taken in applying the presented correlation, since a limited number of locally obtained data stand at the basis of the correlation.

The operation of a trickle-bed reactor in the pulsing flow regime results in high particle-liquid heat transfer rates and a periodic flushing of the catalyst particles, as schematically shown in Fig. 3.12. The operation of a trickle-bed reactor in the pulsing flow regime assesses the possibility to prevent the formation of hot spots. Safety problems, catalyst deactivation and reduced selectivities can be avoided.

### Notation

$a_p$	surface area custom-made probe	[m <sup>2</sup> ]
$c_{pl}$	specific heat of liquid	[J kg <sup>-1</sup> K <sup>-1</sup> ]
$d_p$	particle diameter	[m]
Nu	Nusselt number ( $\alpha_p d_p \lambda_l^{-1}$ )	[-]
Pr	Prandtl number ( $c_{pl} \mu_l \lambda_l^{-1}$ )	[-]
$Q_p$	heat production custom-made probe	[W]
Re	Reynolds number ( $\rho_l v_l d_p \mu_l^{-1}$ )	[-]
$T_l$	liquid temperature	[K]
$T_p$	surface temperature custom-made probe	[K]
$U_l$	superficial liquid velocity	[m s <sup>-1</sup> ]
$v_l$	linear liquid velocity	[m s <sup>-1</sup> ]
$\alpha_p$	heat transfer coefficient	[W m <sup>-2</sup> K <sup>-1</sup> ]
$\beta$	liquid holdup	[-]
$\lambda_l$	liquid thermal conductivity	[W m <sup>-1</sup> K <sup>-1</sup> ]
$\mu_l$	liquid viscosity	[Pa s]
$\rho_l$	liquid density	[kg m <sup>-3</sup> ]

### Literature cited

- Anderson D.H., Krambeck F.J. and Sapre A.V., Development of trickle-bed heat transfer correlation for flow measurement probe, *Chem. Eng. Sci.*, 47, 3501-3508, 1992
- Blok J.R., Varkevisser J. and Drinkenburg A.A.H., Transition to pulsing flow, holdup and pressure drop in packed columns with cocurrent gas-liquid downflow, *Chem. Eng. Sci.*, 38, 687-699, 1983

- Chou T.S., Worley F.J. and Luss D., Local particle-liquid mass transfer fluctuations in mixed-phase cocurrent downflow through a fixed bed in the pulsing regime, *Ind. Eng. Chem. Fund.*, 18, 279-283, 1979
- Gabitto J.F. and Lemcoff N.O., Local solid-liquid mass transfer coefficients in a trickle-bed reactor, *Chem. Eng. J.*, 35, 69-74, 1987
- Hanika J., Safe operation and control of trickle-bed reactor, *Chem. Eng. Sci.*, 54, 4653-4659, 1990
- Herskowitz M. and Smith J.M., Liquid distribution in trickle-bed reactors, *AIChE J.*, 24, 439-454, 1978
- Kirillov V.A. and Ogarkov B.L., Investigation of the processes of heat and mass transfer in a three-phase fixed bed of catalyst, *Int. Chem. Eng.*, 20, 478-485, 1980
- Marcandelli C., Wild G., Lamine A.S. and Bernard J.R., Measurement of local particle-fluid heat transfer coefficient in trickle-bed reactors, *Chem. Eng. Sci.*, 54, 4997-5002, 1999
- Marcandelli C., Lamine A.S., Bernard J.R. and Wild G., Liquid distribution in trickle bed reactor, *Oil & Gas Sci. Tech.*, 55, 407-415, 2000
- Martin H., Low Peclet number particle-to-fluid heat and mass transfer in packed beds, *Chem. Eng. Sci.*, 33, 913-919, 1978
- Moller L.B., Halken C., Hansen J.A. and Bartholdy J., Liquid and gas distribution in trickle-bed reactors, *Ind. Eng. Chem. Res.*, 35, 926-930, 1996
- Rao V.G. and Drinkenburg A.A.H., Solid-liquid mass transfer in packed beds with cocurrent gas-liquid downflow, *AIChE J.*, 31, 1059-1067, 1985
- Ruether J.A., Yang C.S. and Hayduk W., Particle mass transfer during cocurrent downward gas-liquid flow in packed beds, *Ind. Eng. Chem. Proc. Des. Dev.*, 19, 103-107, 1980
- Sapre A.V., Anderson D.H. and Krambeck F.J., Heater probe technique to measure flow maldistribution in large scale trickle-bed reactors, *Chem. Eng. Sci.*, 45, 2263-2268, 1990
- Stanek V., Hanika J., Hlavacek V. and Trnka O., The effect of liquid distribution on the behavior of a trickle-bed reactor, *Chem. Eng. Sci.*, 36, 1045-1067, 1981
- Tsochatzidis N.A. and Karabelas A.J., Study of pulsing flow in a trickle bed using the electrodiffusion technique, *J. Appl. Electrochem.*, 24, 670-675, 1994
- Tsochatzidis N.A., Karabelas A.J., Properties of pulsing flow in a trickle bed, *AIChE J.*, 41, 2371-2382, 1995
- Wang Y.F., Mao Z.S. and Chen J., Scale and variance of radial liquid maldistribution in trickle beds, *Chem. Eng. Sci.*, 53, 1153-1162, 1998
- Yagi S. and Kunii D., Studies on effective thermal conductivities in packed beds, *AIChE J.*, 3, 373-381, 1957

---

## Chapter 4

---

# The Induction of Pulses by Cycling the Liquid Feed

---

### Abstract

The operation of a trickle-bed reactor in the pulsing flow regime is well known for its advantages in terms of increased mass and heat transfer rates, complete catalyst wetting and total mobilization of the stagnant liquid. However, the operation in the pulsing flow regime requires fairly high gas and liquid flow rates, resulting in relatively short liquid phase residence times. This chapter describes the exploration of controlled pulse induction by cycling the liquid feed.

Due to the step-change in liquid flow rate, continuity shock waves are initiated in the column. At sufficiently high gas flow rates, the inception of pulses occurs within the shock wave. This mode of operation to force pulse initiation is termed liquid-induced pulsing flow. Analysis of the performed experiments indicates that besides gas and liquid flow rates, an additional criterion for pulse inception is the available length for disturbances to grow into pulses. For self-generated pulsing flow this results in the upward movement of the point of pulse inception with increasing gas flow rate. For liquid-induced pulsing flow, higher gas flow rates are necessary to induce pulses as the length of the shock wave decreases. For both self-generated and liquid-induced pulsing flow the relation between the necessary gas flow rate and the available length for pulse formation is identical.

By cycling the liquid feed it is possible to induce pulses at average throughputs of liquid associated with trickle flow during steady state operation. The advantages associated with pulsing flow may then be utilized to improve reactor performance in terms of a capacity increase and hot spot elimination, while liquid phase residence times are comparable to trickle flow. Moreover, with liquid-induced pulsing flow, the pulse frequency and thus the time constant of the pulses can be externally set.

This chapter is based on the following publications:

- Boelhouwer J.G., Piepers H.W. and Drinkenburg A.A.H., Enlargement of the pulsing flow regime by periodic operation of a trickle-bed reactor, *Chem. Eng. Sci.*, **54**, 4661-4667, 1999  
Boelhouwer J.G., Piepers H.W. and Drinkenburg A.A.H., The induction of pulses in trickle-bed reactors by cycling the liquid feed, *Chem. Eng. Sci.*, **56**, 2605-2614, 2001  
Boelhouwer J.G., Piepers H.W. and Drinkenburg A.A.H., Liquid-induced pulsing flow in trickle-bed reactors, proceedings AIChE Annual Meeting, paper 304c, Dallas, TX, U.S.A., 1999



## 4.1. Introduction

A trickle-bed reactor is a commonly employed type of three-phase catalytic reactors in which a gas and a liquid phase cocurrently flow downward through a fixed bed of catalyst particles. A trickle-bed reactor is usually operated in the trickle flow regime, which is characterized by a rather poor interaction between the phases. Mass transfer resistances for the gaseous reactant often govern the overall reaction rate. Periodic operation may be applied to reduce these mass transfer resistances and thus enhances the performance of a trickle-bed reactor. One of most simple methods of unsteady state operation is an on-off cycling of the liquid feed. With this mode of operation, significant increases in reaction rate are obtained (Haure et. al. 1989, Lee et. al., 1995; Castellari and Haure, 1995). Performance improvement results from reduction of mass transfer resistances for the gaseous reactant, elevated temperatures and the appearance of a gas phase reaction over an almost dry catalyst during the liquid-off period (Gabarain et. al., 1997).

Pulsing flow can be considered as a spontaneously arising nonsteady state behavior of the reactor. Wu et. al. (1999) showed that an increase in selectivity for the hydrogenation of phenylacetylene to styrene results from the change in flow regime from trickle to pulsing flow. Enhancement of the selectivity could originate on account of the dynamic interaction between the fluctuations in mass transfer and reaction on similar time scales, as was predicted theoretically by Wu et. al. (1995). Another explanation is a decrease in axial dispersion and mobilization of the stagnant liquid holdup by the pulses.

The physical mechanism responsible for pulse inception often suggested in literature is the occlusion of the packing channels by the liquid and subsequently blowing off the liquid obstruction by the gas flow. Based on this concept, several models are proposed to clarify the conditions at which the transition to pulsing flow occurs (Sicardi and Hoffman, 1979, 1980; Blok et. al., 1983; Ng, 1986; Cheng and Yuan, 1999). These models attempt to explain the transition on the basis of a microscopic view of two-phase flow in an individual packing channel. It is not clear how these microscopic occlusions of several packing channels result in the macroscopic non-uniform behavior of pulsing. The first to adapt a macroscopic view to interpret the transition from trickling to pulsing flow were Grosser et. al. (1988). They employed a macroscopic model of two-phase flow in a packed bed and demonstrated that a loss of stability of the uniform state occurs. They identified this loss of stability as the transition boundary. According to Krieg et. al. (1995), traveling waves of high liquid holdup comparable to pulses are already present in the trickle flow regime.

**Table 4.1.** Properties of the packed beds

packing material	diameter	packed height	porosity	specific area
glass spheres	6 mm	1.20 m	0.36	640 m <sup>-1</sup>
glass spheres	3 mm	1.04 m	0.40	1200 m <sup>-1</sup>

A stability analysis predicts the conditions of onset of these traveling disturbances that eventually grow into pulses only if sufficient column length is available.

## 4.2. Scope and objective

The operation of a trickle-bed reactor in the pulsing flow regime has many advantages compared to the operation in the trickle flow regime. The drawback of pulsing flow is the relative short residence time of the liquid phase due to the relatively high gas and liquid velocities required to achieve this flow regime. These short residence times may counterbalance the advantages of pulsing flow. To overcome this drawback, a cycled liquid feed may be utilized to induce pulses at throughputs of liquid that would lead to trickle flow only during steady state operation. The advantages associated with pulsing flow may then be utilized to increase reactor performance, while liquid phase residence times remain comparable to trickle flow.

The aim of the work described in this chapter is to explore the possibility of a controlled pulse induction by cycling the liquid feed. Additionally, it is expected that the pulse frequency can be externally controlled by the liquid feed cycle frequency. Matching the time scales of pulses with the time scales of reaction may enhance selectivity.

## 4.3. Experimental setup and procedures

A schematic illustration of the experimental equipment is presented in Fig. 4.1. The experiments were performed in a Plexiglas column of 0.11 m inner diameter. The packing material consisted of 3.0 mm and 6.0 mm glass spheres of which the packing characteristics are listed in Table 4.1. The packing was supported at the bottom of the column by a stainless steel screen. Air and water were uniformly distributed at the top of the column.

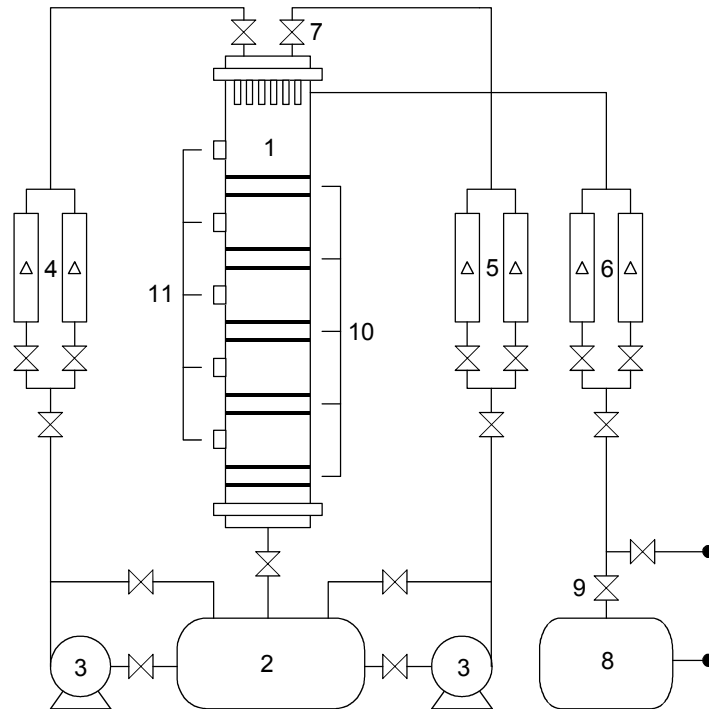


**Figure 4.1.** Schematic illustration of the experimental equipment (1: column; 2: liquid storage tank; 3: liquid pump; 4: liquid flow meter primary feed line; 5: liquid flow meter secondary feed line; 6: gas flow meter; 7: magnetic valve activated by electronic timer; 8: pressure vessel; 9: pressure regulator; 10: conductivity probes; 11: pressure taps)

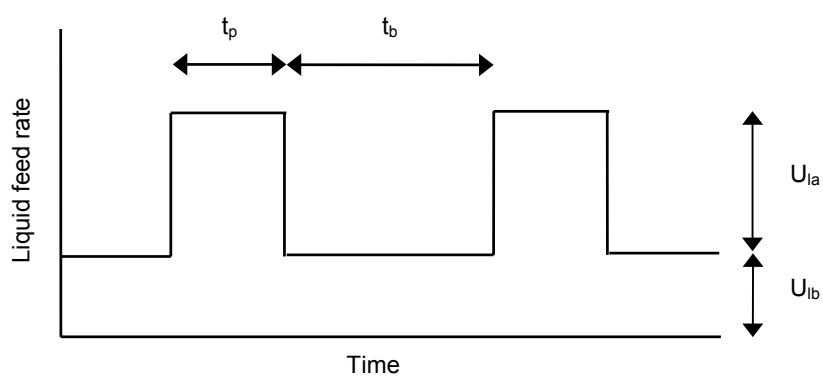


**Figure 4.2.** Schematic illustration of the characterization of the cycled liquid feed ( $U_{lb}$ : base liquid feed;  $U_{la}$ : additional liquid feed;  $t_b$ : duration of base liquid feed;  $t_p$ : duration of additional liquid feed)

For the air supply, a pressure vessel was kept on 7 bars by a compressor to minimize fluctuations in the gas flow rate due to pressure fluctuations in the column. The experiments were conducted at room temperature and near atmospheric pressure.

For the liquid feed, two distinct feed lines were applied. The primary feed line was used to introduce a continuous liquid feed to the column while the secondary feed line provided an additional liquid feed for a certain period. With this set-up a square-wave cycled liquid feed was achieved. The cycled liquid feed is characterized by 4 parameters, schematically shown in Fig. 4.2. A magnetic valve in the secondary feed line, activated by an electronic timer, was adapted to regulate the feed periods of respectively the high ( $U_{lp}$ ) and low ( $U_{lb}$ ) liquid feed. High and low liquid feed rates were measured by calibrated flow meters.

Preliminary experiments indicated a slight increase in pressure at the top of the column when the additional liquid feed was supplied. This increase in pressure somewhat reduces the superficial gas flow rate at the top of the column. The variation in gas flow rate at the column top due to pressure fluctuations is, however, very small. The reported superficial gas velocities in this study are calculated by using the pressure at the top of the column at the moment the additional liquid feed is ended. Pressure fluctuations in unsteady state operated trickle-bed reactors are inherent to this mode of operation. Along the column axis, superficial gas velocities vary due to fluctuations in liquid holdup and pressure drop.

A conductance technique, described in detail in chapter 2, was used to provide instantaneous measurement of cross-sectionally averaged liquid holdup. The column was equipped with 5 sets of conductance probes, flush-mounted in the column wall at distances of 0.2 m, to measure liquid holdup at various axial positions. The conductivity probes were calibrated by tracer injections and by the stop-flow method. Both calibration methods proved to be very reproducible and no significant difference existed between the calibration result. Pressure drop was measured by pressure transducers that were connected to several pressure taps separated by distances of 0.2 m. For a period of at least 5 minutes, liquid holdup and pressure data were simultaneously recorded and stored in a computer with a sampling rate of 100 Hz.

Before performing any experiments, the column was operated in the pulsing flow regime for at least 1 hour to ensure a perfectly pre-wetted bed. Liquid holdup during trickle flow was measured for 6 different liquid flow rates and a wide range of gas flow rates.

The transition to self-generated pulsing flow was established at several axial positions in the bed to examine the upward movement of the point of pulse inception with increasing gas flow rate. This was accomplished by visual observation and by monitoring of the signals from 2 neighboring conductivity probes. Transition to pulsing flow at a certain axial position was acknowledged in case the lower conductivity probe clearly showed large fluctuations in liquid holdup while the upper probe showed an almost unvarying liquid holdup.

The hydrodynamics during liquid feed cycling were examined for a broad range of cycled feed characteristics. At fixed cycled liquid feed characteristics, the gas flow rate was gradually increased until eventually, natural pulses were observed. With this procedure, the effect of unsteady state operation on the hydrodynamics at gas flow rates not sufficient for pulse inception was examined and subsequently, the minimum gas flow rate required for induced pulsing was determined. The pulse frequency was obtained by evaluation of the number of pulses present in the conductivity signal.

#### **4.4. Steady state hydrodynamics**

As will be revealed later, accurate liquid holdup data in the trickle flow regime are essential to understand the hydrodynamic phenomena observed during a cycled liquid feed. In Fig. 4.3, the liquid holdup, defined as the fraction of the empty column occupied with liquid, is plotted versus the superficial gas velocity for 3.0 mm glass spheres as packing material. Liquid holdup increases with increasing liquid flow rate and decreases with increasing gas flow rate. A somewhat lower liquid holdup was observed for 6.0 mm glass spheres as packing material, since the liquid is less supported by the smaller specific packing area.

In Fig. 4.4, the transition boundary from trickling to pulsing flow is presented for both packing materials. The transition is established at approximately 0.1 m above the bottom of the column. There is no noticeable difference between the transition boundaries for 3.0 and 6.0 mm glass spheres.

A general observation reported in literature is the upward movement of the point of pulse inception with increasing gas flow rate. In Fig. 4.5, the effect of increasing gas flow rate on the axial position of the point of pulse inception is presented. It is generally assumed that this upward movement of the point of pulse inception with increasing gas flow rate is due to the pressure drop over the bed. Volumetric gas flow rates are higher at the bottom of the column.

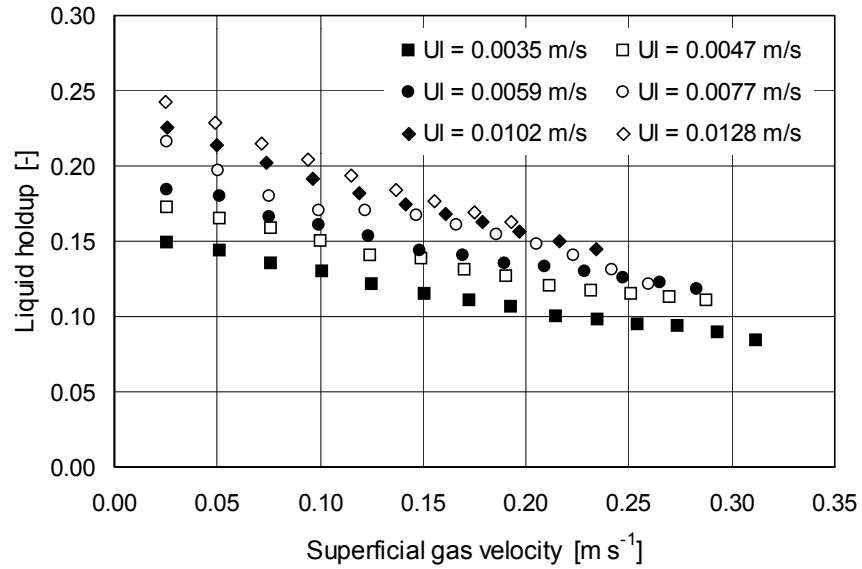


**Figure 4.3.** Liquid holdup during trickle flow versus superficial gas velocity (packing material: 3.0 mm glass spheres)

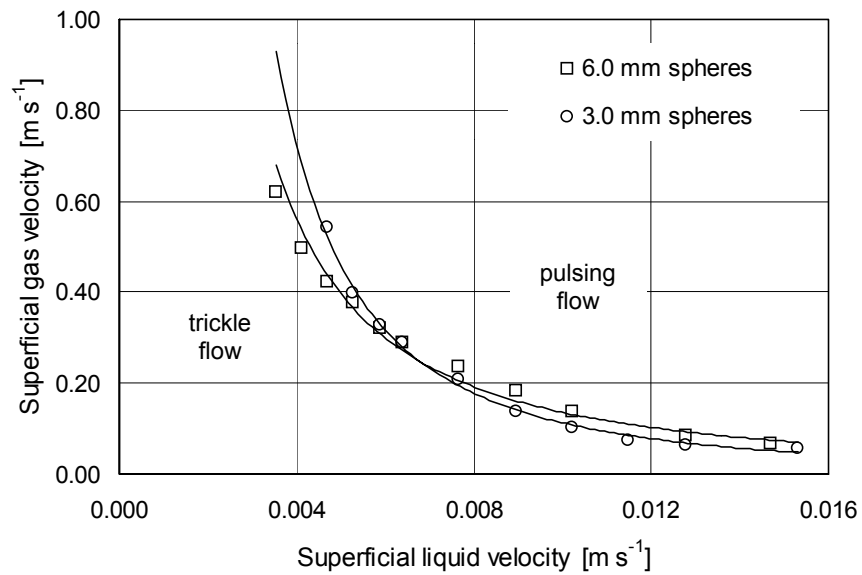


**Figure 4.4.** Transition boundary from trickle to pulsing flow versus superficial gas and liquid velocities

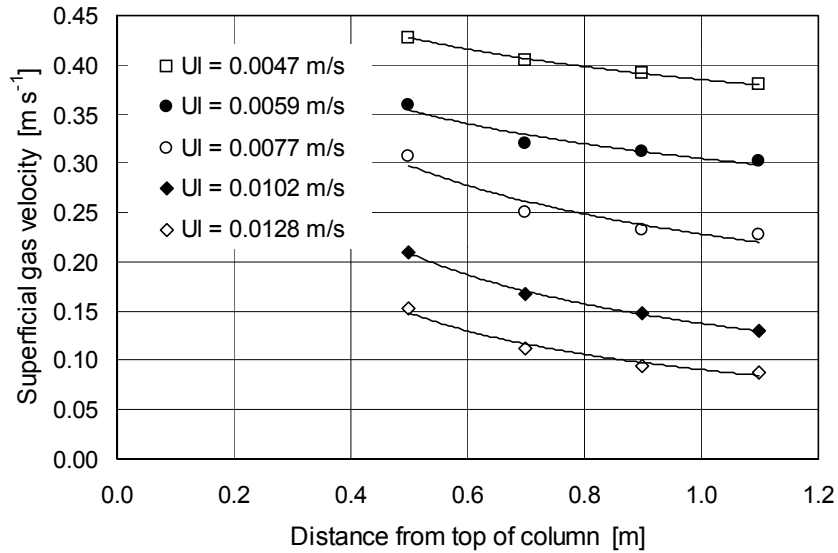


**Figure 4.5.** Effect of superficial gas velocity on the axial position of the point of pulse inception

In Fig. 4.5 it is observed that a relatively large increase in gas flow rate is needed to shift the point of pulse inception upward, much larger than pressure drop can account for. Visual observations illustrate that even though pulses are first generated near the bottom of the column, traveling disturbances are already present above the point of pulse inception. These findings agree with the observations of Krieg et. al. (1995) that traveling disturbances are also present in the trickle flow regime. They consider that the transition to pulsing flow corresponds to only a quantitative change in the strength of these waves. Convective disturbances grow with distance and eventually become observable and are thus recognized as pulses, at a position that depends on flow conditions.

Apparently, with increasing gas flow rate, the required bed length for disturbances to grow into detectable pulses decreases. Hence, the point of pulse inception moves upward in the column. Besides gas and liquid flow rates, available bed length may be identified as a fundamental parameter for pulse generation.

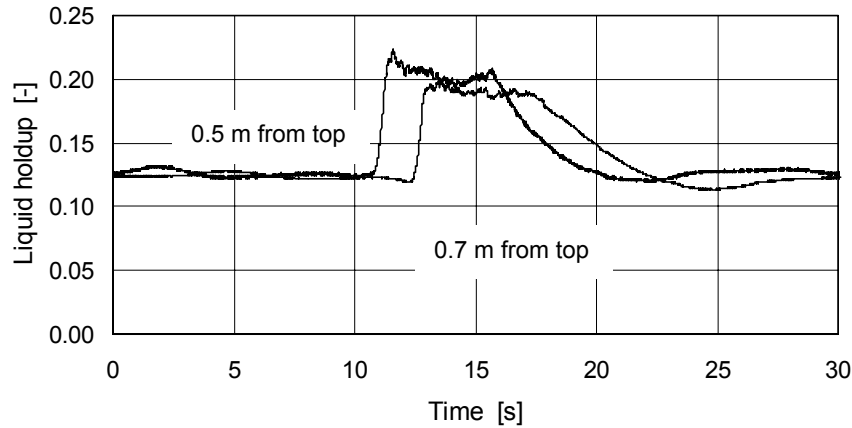


**Figure 4.6.** Example of liquid holdup traces during a cycled liquid feed ( $U_{lb} = 0.0035 \text{ m s}^{-1}$ ;  $U_{lp} = 0.0102 \text{ m s}^{-1}$ ;  $t_p = 5 \text{ s}$ ;  $t_b = 20 \text{ s}$ ;  $U_g = 0.10 \text{ m s}^{-1}$ ; packing material: 3.0 mm glass spheres)

## 4.5. Continuity shock waves

In order to determine the conditions under which pulses are generated during a cycled liquid feed, it is desired to investigate the effect of liquid feed cycling on the hydrodynamics at gas flow rates not capable to force pulse initiation. An example of liquid holdup traces during a cycled liquid feed obtained at two conductivity probes is given in Fig. 4.6. The supply of the additional liquid feed for a certain period results in a liquid-rich region moving down the bed. The front of this region is characterized by an abrupt increase in liquid holdup. A more gradual decrease in liquid holdup characterizes the back of the liquid-rich region. The liquid-rich region lasts for a period approximately equal to  $t_p$ .

### 4.5.1. Liquid holdup

A parity plot of the liquid holdup in the liquid-rich region versus the steady state liquid holdup at equivalent liquid flow rates is presented in Fig. 4.7. The liquid holdup of the liquid-rich region is identical to the liquid holdup obtained during steady state operation at equivalent liquid feed rates. Presumably, the liquid-rich region is a steady state condition.

### 4.5.2. Continuity shock waves

By evaluating the time lag between two signals of neighboring conductivity probes, the velocity of the moving liquid front is obtained.



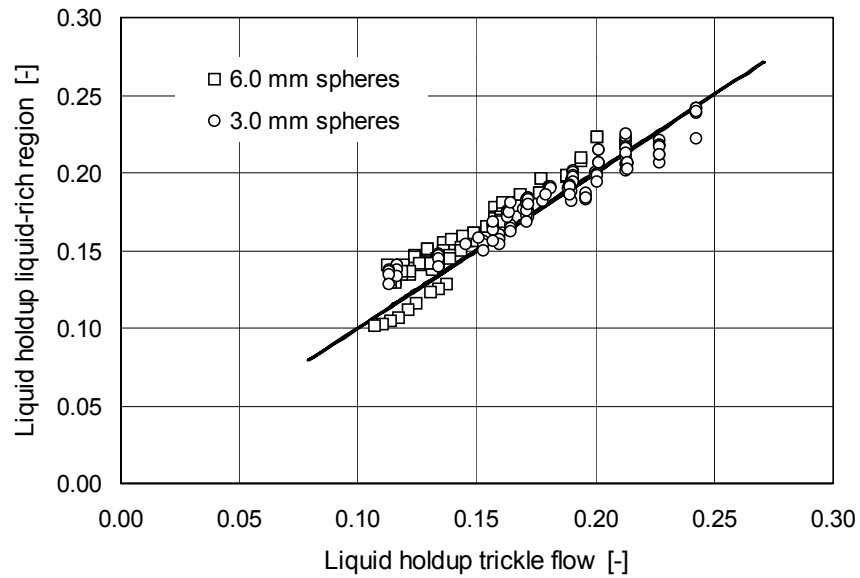


**Figure 4.7.** Comparison between liquid holdup during steady state trickle flow and liquid holdup within the liquid-rich region at equivalent superficial liquid velocities

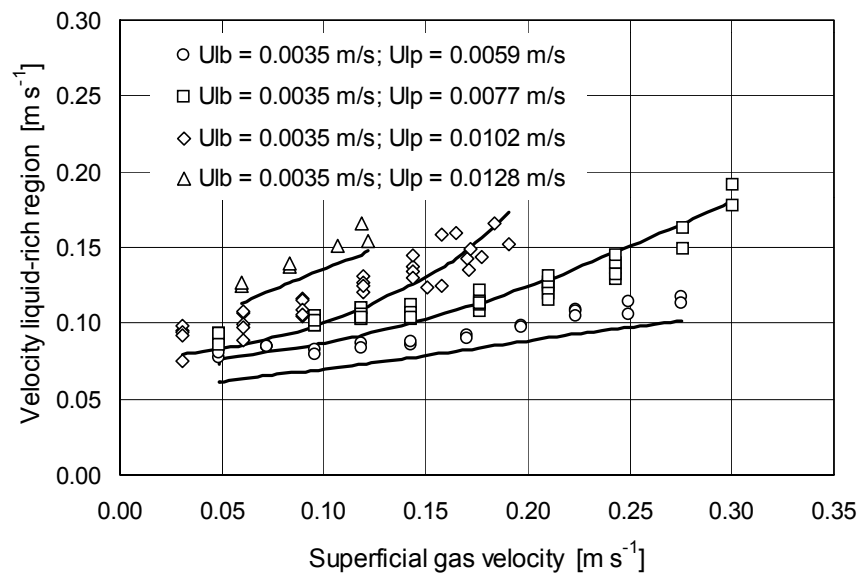


**Figure 4.8.** Velocity of the liquid-rich region versus the superficial gas velocity ( $t_b = 20$  s;  $t_p = 1 - 10$  s;  $U_{lb} = 0.0035$  m s<sup>-1</sup>; packing material: 6.0 mm spheres)

The experimentally determined linear velocity of the liquid-rich region is plotted in Fig. 4.8 versus the superficial gas velocity for 6.0 mm spheres as packing material. The velocity increases with both increasing gas flow rate and with an increasing difference between  $U_{lb}$  and  $U_{lp}$ . The velocity of the liquid-rich region, altering roughly between 0.1 and 0.2 m s<sup>-1</sup>, is much higher as compared to the linear liquid velocity (superficial liquid velocity divided by liquid holdup) that varies between 0.02 and 0.08 m s<sup>-1</sup>. Due to liquid feed cycling, some kind of waves are initiated in the column.

It seems useful to investigate the possibility of the formation of continuity shock waves due to the step-change in liquid flow rate. Continuity waves occur whenever the flow rate of a substance depends on the amount of that substance present. Continuity waves often emerge in systems where gravity and pressure drop are balanced against drag forces, as is the case with liquid flow in packed beds. One steady state simply propagates into another one and there are no dynamic effects of inertia or momentum (Wallis, 1969). Waves can either propagate continuous changes or can involve a step-change or finite discontinuity. The latter are termed shock waves. According to Wallis (1969), the velocity of a shock wave, derived from continuity considerations obeys the following equation:

$$V_s = \frac{U_{lp} - U_{lb}}{\beta_p - \beta_b} \quad [4.1]$$

According to equation 4.1, the shock wave velocity is directly related to the difference between liquid flow rates and the difference between the resulting liquid holdups. The effect of the gas flow rate on shock wave velocity is embedded in the liquid holdup.

To calculate the shock wave velocity, the experimentally obtained liquid holdup during trickle flow is applied. The solid lines in Fig. 4.8 depict the calculated velocity of the liquid-rich region conform equation 4.1. A good agreement exists between experimentally and calculated values, as well qualitatively as quantitatively. A comparison of all the experimental data with calculated values is shown in Fig. 4.9. Calculated values become more accurate with increasing difference between  $\beta_b$  and  $\beta_p$ . Since this difference varies in a narrow range (between 0.03 and 0.1), the use of correct liquid holdup data is important, because the accuracy severely affects calculated shock wave velocities.

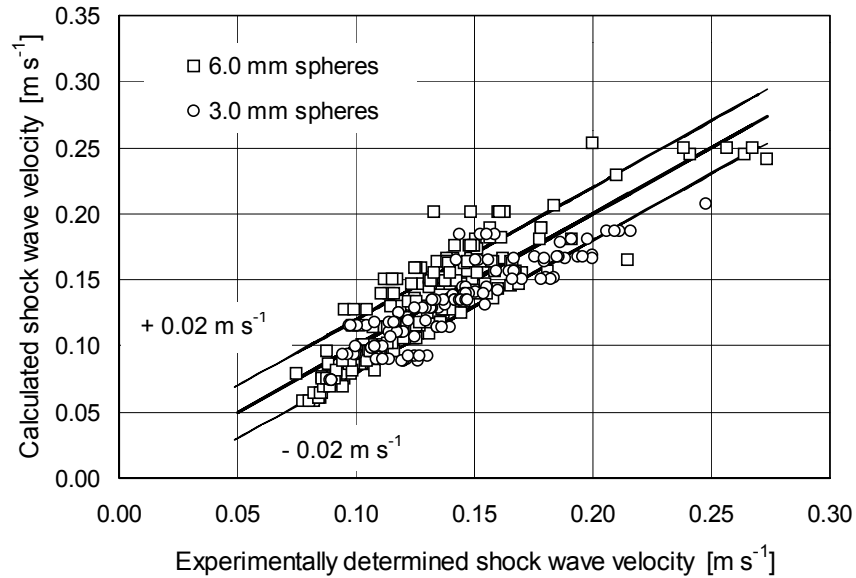


**Figure 4.9.** Comparison between the experimentally determined and calculated shock wave velocity ( $U_{lb} = 0.0035 - 0.0077 \text{ m s}^{-1}$ ;  $U_{lp} = 0.0059 - 0.0128 \text{ m s}^{-1}$ ;  $U_g = 0.03 - 0.30 \text{ m s}^{-1}$ ;  $t_b = 20 \text{ s}$ ;  $t_p = 2 - 15 \text{ s}$ )

In summary, due to the step-change in liquid flow rate, liquid-rich continuity shock waves are initiated in the column. As a result, two different steady states can coexist. These steady states are separated by a moving boundary of which the velocity can be obtained on the basis of continuity considerations.

#### 4.6. Induction of pulses

Due to the step-change in liquid flow rate, liquid-rich continuity shock waves are initiated in the column. At sufficiently high gas flow rates, inception of natural pulses occurs. The process of pulse induction is shown in the liquid holdup traces presented in Fig. 4.10. In the trace obtained at 0.5 m beneath the top of the column no pulse is present, while in the trace obtained at 0.7 m beneath the top, a pulse is evidently visible. Hence it is concluded that pulses are initiated within the front of the shock wave.

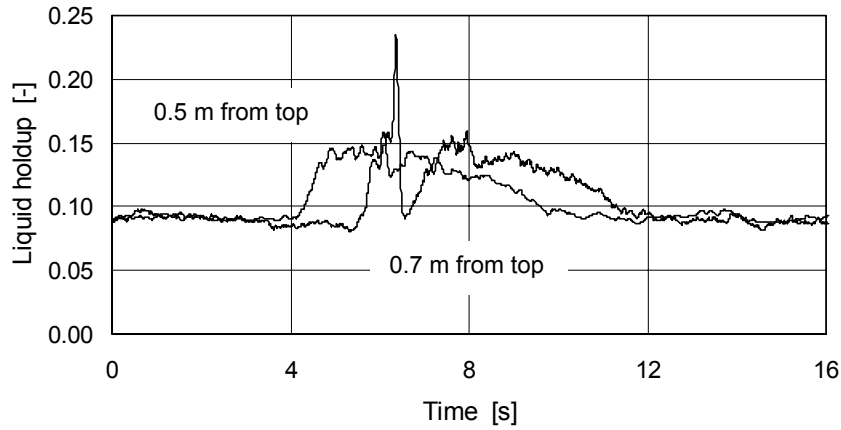


**Figure 4.10.** Example of the measured liquid holdup during liquid-induced pulsing flow ( $U_{lb} = 0.0035 \text{ m s}^{-1}$ ;  $U_{lp} = 0.0077 \text{ m s}^{-1}$ ;  $U_g = 0.29 \text{ m s}^{-1}$ ;  $t_b = 20 \text{ s}$ ;  $t_p = 3 \text{ s}$ ; packing material: 6.0 mm spheres)

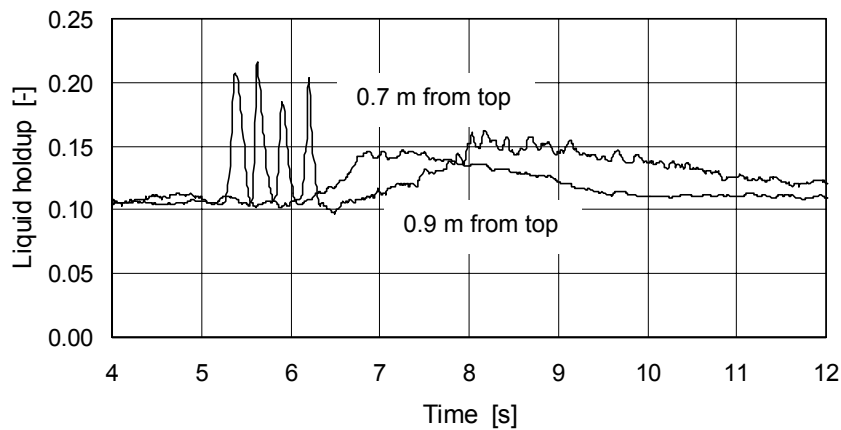


**Figure 4.11.** Example of the measured liquid holdup during liquid-induced pulsing flow ( $U_{lb} = 0.0035 \text{ m s}^{-1}$ ;  $U_{lp} = 0.0128 \text{ m s}^{-1}$ ;  $U_g = 0.26 \text{ m s}^{-1}$ ;  $t_b = 20 \text{ s}$ ;  $t_p = 2 \text{ s}$ ; packing material: 6.0 mm spheres)

This is confirmed by visual observation. Since the velocity of the initiated pulses is much higher than the shock wave velocity, pulses will eventually leave the shock wave, as illustrated in the liquid holdup traces presented in Fig. 4.11. The initiated pulses have abandoned the shock wave, but remain stable. Occasionally the initiated pulses fade away upon leaving the shock wave.

However, since the column height is rather short, it cannot be assured at this moment whether pulses remain stable in columns of larger height or not. Pulse induction by cycling the liquid feed is termed liquid-induced pulsing flow<sup>(1)</sup>.

#### 4.6.1. Required gas flow rate

The necessary gas flow rate for pulse induction depends on  $t_p$ . However, it is more convenient to employ the length of the shock wave in the discussion that follows. The length of the shock wave is calculated by:

$$l_s = V_s t_p \quad [4.2]$$

The shock wave velocity at the transition to liquid-induced pulsing flow, applied in equation 4.2, is obtained by extrapolation of the values determined at lower gas flow rates (Fig. 4.8). The required gas flow rate for pulse induction versus the length of the shock wave is plotted in Fig. 4.12. The necessary gas flow rate is completely governed by  $U_{lp}$ , since pulses are initiated within the shock waves. For relatively high  $t_p$ , the column will eventually be entirely filled with the liquid-rich shock wave. The column is then operated in the natural pulsing flow regime for a certain period. The required minimal gas velocity equals the velocity needed for transition to self-generated pulsing flow near the bottom of the column. Upon increasing  $t_p$ , the required gas flow rate remains constant. However for relatively short shock wave lengths compared to the column height, a higher gas velocity is necessary to induce pulses. The gas flow rate needed increases with decreasing shock wave length, although the cycled liquid feed rates are unchanged.

These results indicate that not a combination of gas flow rate and liquid flow rate as such determines whether pulses are initiated or not, but the available length for disturbances to grow into pulses must be included.

With decreasing  $t_p$  and hence decreasing shock wave length, increasing gas flow rates are necessary to induce pulses. Pulses are always initiated at the front of the shock wave, as observed in Fig. 4.10. A similar phenomenon is observed for self-generated pulsing flow during which the point of pulse inception moves upwards with increasing gas flow rate.

<sup>(1)</sup> Artificial pulse induction is feasible by cycling the gas feed also. This process is termed gas-induced pulsing flow. The work on the induction of pulses by cycling the gas feed is not included in this thesis but is in preparation for publication as:

Boelhouwer J.G., Piepers H.W. and Drinkenburg A.A.H, The induction of pulses in trickle-bed reactors by cycling the gas feed, in preparation for publication

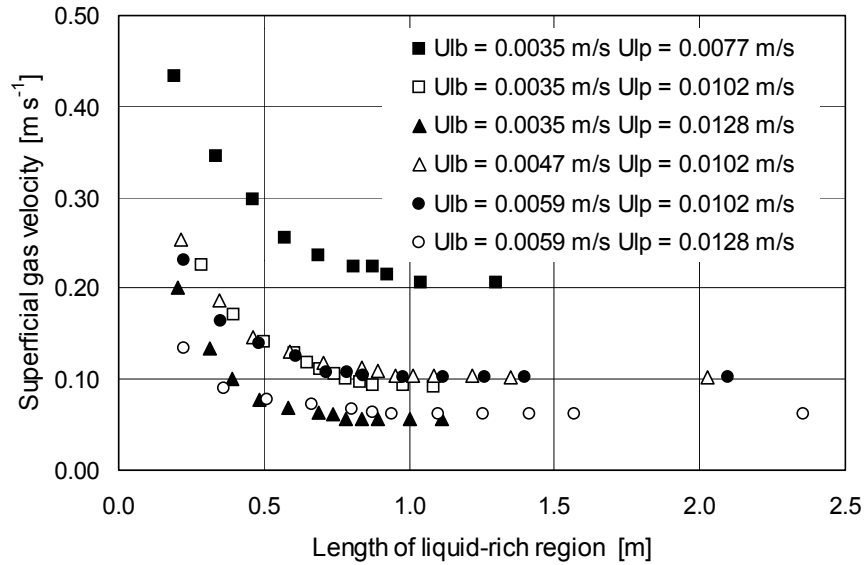


**Figure 4.12.** Relation between the necessary gas flow rate for induced pulsing flow and the length of the liquid-rich region (packing material: 6.0 mm glass spheres)

As well for self-generated pulsing flow as for liquid-induced pulsing flow, there seems to be a relation between necessary gas flow rate and available length for pulse formation. For liquid-induced pulsing flow, the necessary gas flow rate for pulse induction equals the necessary gas flow rate for natural pulsing flow when the shock wave length is about 0.15 m less than the bed height. Additionally, the point of pulse inception for natural pulsing flow never reaches the top of the bed. The highest observed location of pulse inception is about 0.15 m below the top of the bed. It seems that the upper part of the bed does not actively participate in the process of pulse formation. It is expected that this part of the bed is needed to arrive at the necessary distribution of the phases. The length of this distribution zone is approximately 0.15 m for both packing materials.

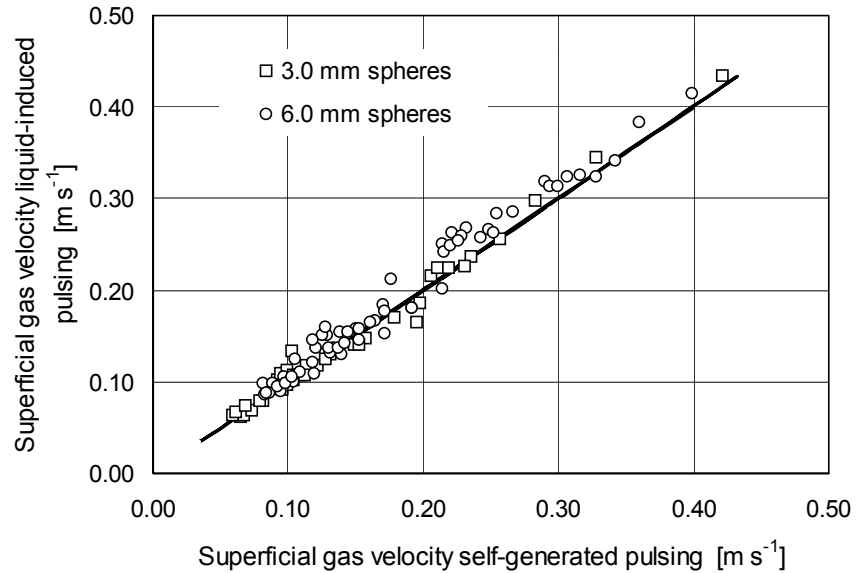
Assuming that the upper 0.15 m does not participate in the process of pulse formation, it is possible to establish the interdependence between gas flow rate and available length for pulse formation for self-generated pulsing flow. The data in Fig. 4.5 must be shifted 0.15 m horizontally towards the top of the column. Subsequently the relation between the necessary gas velocity and available length for pulse formation for self-generated pulsing flow is established.

In Fig. 4.13, a comparison of the superficial gas velocities required for self-generated respectively liquid-induced pulsing flow at equivalent available lengths for pulse formation is presented for both packing materials. Considering the fact that the point of pulse inception during self-generated pulsing flow could only be measured at fixed points along the column axis, the line denoting the necessary gas velocity for self-generated pulsing flow is obtained by interpolation of the modified results of Fig. 4.5. The agreement between the required gas flow rates for natural and liquid-induced pulsing flow is surprisingly good. It must be noted that the applied correction of 0.15 m to account for the length of the initial distribution zone is indispensable to match the data in Fig. 4.13. Uncertainty exists in determining the exact location of the point of pulse inception for natural pulsing flow, since this position randomly fluctuates. Transition to pulsing flow at a certain axial position was acknowledged when the lower conductivity probe clearly showed large fluctuations in liquid holdup while the upper probe showed an almost unvarying liquid holdup. Hence, the uncertainty in determining the location of the point of pulse inception is  $\pm 0.1$  m, which is close to the 0.15 m length of the distribution zone. Nevertheless it is reasonable to conclude that the interdependence between the superficial gas velocity and the necessary length for pulse formation is equivalent for both self-generated and liquid-induced pulsing flow.

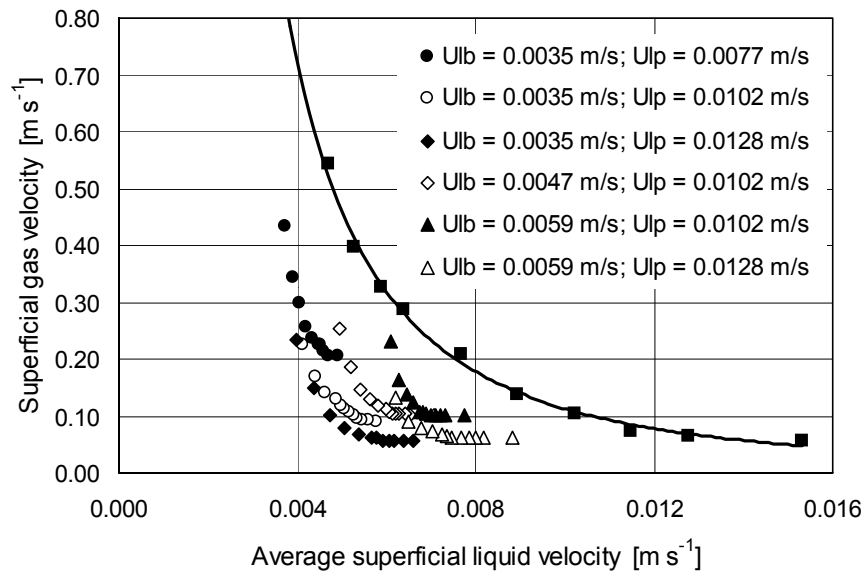
#### 4.6.2. Features of induced pulsing flow

Fig. 4.14 provides the results of the enlargement of the pulsing flow regime by cycling the liquid feed for 3.0 mm glass spheres as packing material. Similar results are obtained for the 6.0 mm glass spheres as packing material. The solid line, denoting the transition boundary to self-generated pulsing flow, is taken at approximately 0.1 m from the bottom of the column. It is possible to induce pulses at average liquid flow rates associated with trickle flow during steady state operation. Hence, although throughputs of liquid are equal, the prevailing flow regime is pulsing instead of trickle flow. The advantages associated with pulsing flow may be utilized to improve reactor performance. Since average liquid flow rates are reduced, the residence time of the liquid phase is comparable to trickle flow operation.

Another feature of liquid-induced pulsing flow is the possibility to tune the pulse frequency and therefore the time constant of the pulses. In Fig. 4.15, the number of pulses generated during one liquid feed cycle is plotted versus the shock wave length for 3.0 mm glass spheres as packing material.



**Figure 4.13.** Comparison between necessary superficial gas velocity for self-generated and liquid-induced pulsing flow at equivalent available lengths for pulse formation ( $U_{lb} = 0.0035 - 0.0077 \text{ m s}^{-1}$ ;  $U_{lp} = 0.0059 - 0.0128 \text{ m s}^{-1}$ ;  $t_b = 20 \text{ s}$ ;  $t_p = 2 - 8 \text{ s}$ )



**Figure 4.14.** Enlargement of the pulsing flow regime by cycling the liquid feed ( $t_b = 20 \text{ s}$ ;  $t_p = 0.5 - 15 \text{ s}$ ; packing material: 3.0 mm spheres)



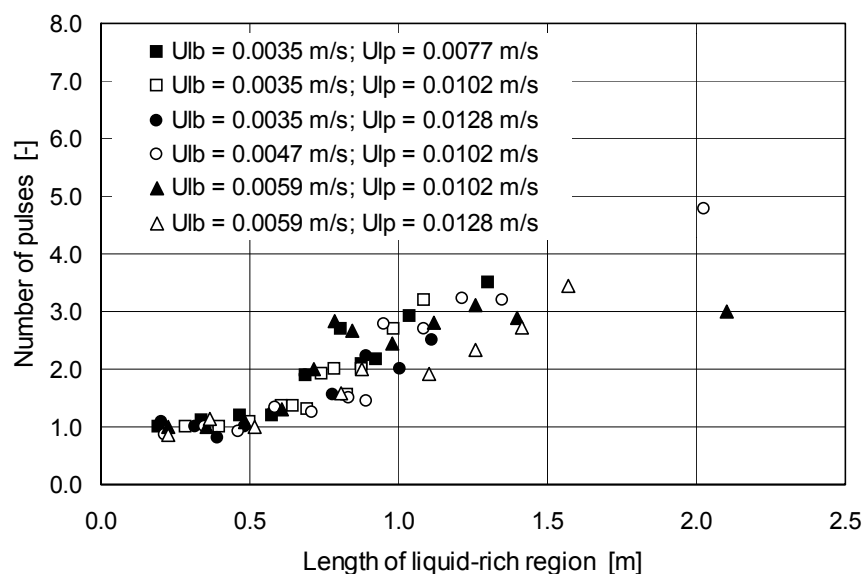


**Figure 4.15.** Number of pulses generated during one liquid feed cycle as a function of the shock wave length (packing material: 3.0 mm spheres)

Apparently, only 1 pulse per liquid feed cycle is generated in case the shock wave length is less than approximately 0.5 m. For lengths exceeding 0.5 m, the number of pulses increases roughly linearly with increasing length. A comparable plot is obtained for 6.0 mm glass spheres as packing material. In this case, the critical length below which just one pulse is generated during a liquid feed cycle is approximately 0.6 m.

#### 4.7. Concluding remarks

The main result presented in this chapter is that it is possible to induce pulses by cycling the liquid feed. The many advantages of pulsing flow may then be utilized to increase reactor performance while the residence time of the liquid remains comparable to trickle flow operation. By applying relatively short periods of the high liquid flow rate, the pulse frequency can be externally set by the liquid feed cycling frequency. This tuning of the pulses is an important issue in the optimization of selectivity in catalytic reactions. Higher selectivities can be achieved when the time constant of pulsing is comparable to the time constant of important physical and chemical processes (Wu et. al., 1995, 1999).

The formation of observable pulses is the result of the growth of convective instabilities with distance into pulses. With increasing gas flow rate, the necessary length for pulse formation decreases. This phenomenon is responsible for the upward movement of the point of pulse inception for self-generated pulsing flow. This same phenomenon is found to control the process of liquid-induced pulsing flow. By cycling the liquid feed, continuity shock waves are initiated in the column. As a result, for relatively short  $t_p$ , two regions of different liquid holdup are present in the column. At sufficiently high gas flow rates, pulses are initiated within the front of shock wave. With decreasing shock wave length, higher gas velocities are necessary to induce natural pulses. For both self-generated and liquid-induced pulsing flow, the relationship between the necessary length for pulse formation and the required gas flow rate is equivalent.

One might argue that only for relatively short  $t_p$ , when the shock wave length is less compared to the bed height, the term induced-pulsing flow might be used. In case the shock wave length is larger than the column height, the column is essentially alternately operated in the trickle and natural pulsing flow regime.

Since the velocity of the initiated pulses is much higher than the shock wave velocity, pulses will eventually leave the shock wave. In most cases the pulses remain stable and move to the bottom of the column. In some cases, however, the pulses fade away. At present, it is not possible to assure that the induced pulses remain stable in columns of larger height. Furthermore, the stability of the initiated continuity shock waves may be questioned. Although they appear sharp at the front, the back of the shock waves is characterized by a more gradual decrease in liquid holdup. This suggests that the shock waves leave some liquid behind at the tail. This process may be at the expense of the liquid amount carried by the shock wave. It is certainly desirable to investigate the process of liquid-induced pulsing flow in columns of large height. This is the subject of the next chapter.

## Notation

$l_s$	length of liquid-rich region	[m]
$t_b$	period of low liquid flow	[s]
$t_p$	period of high liquid flow	[s]
$U_g$	superficial gas velocity	[m s <sup>-1</sup> ]
$U_{la}$	superficial additional liquid feed velocity	[m s <sup>-1</sup> ]
$U_{lb}$	superficial low liquid feed velocity	[m s <sup>-1</sup> ]

$U_{lp}$	superficial high liquid feed velocity	$[m\ s^{-1}]$
$V_s$	shock wave velocity	$[m\ s^{-1}]$
$\beta_b$	liquid holdup corresponding to low liquid flow rate	[-]
$\beta_p$	liquid holdup corresponding to high liquid flow rate	[-]

### Literature cited

- Blok J.R., Varkevisser J. and Drinkenburg A.A.H., Transition to pulsing flow, holdup and pressure drop in packed columns with cocurrent gas-liquid downflow, *Chem. Eng. Sci.*, **38**, 687-699, 1983
- Castellari A.T. and Haure P.M., Experimental study of the periodic operation of a trickle-bed reactor, *AIChE J.*, **41**, 1593-1597, 1995
- Cheng Z.M. and Yuan W.K., Necessary condition for pulsing flow inception in a trickle bed, *AIChE J.*, **45**, 1394-1400, 1999
- Gabarain L., Castellari A.T., Cechini J., Tobolski A. and Haure P.M., Analysis of rate enhancement in a periodically operated trickle-bed reactor, *AIChE J.*, **43**, 166-172, 1997
- Grosser K., Carbonell R.G. and Sundaresan S., Onset of pulsing in two-phase cocurrent downflow through a packed bed, *AIChE J.*, **34**, 1850-1860, 1988
- Haure P.M., Hudgins R.R. and Silveston P.L., Periodic operation of a trickle-bed reactor, *AIChE J.*, **35**, 1437-1444, 1989
- Krieg D.A., Helwick J.A., Dillon P.O. and McCready M.J., Origin of disturbances in cocurrent gas-liquid packed bed flows, *AIChE J.*, **41**, 1653-1666, 1995
- Lee J.K., Hudgins R.R. and Silveston P.L., A cycled trickle-bed reactor for SO<sub>2</sub> oxidation, *Chem. Eng. Sci.*, **50**, 2523-2530, 1995
- Ng K.M., A model for flow regime transitions in cocurrent down-flow trickle-bed reactors, *AIChE J.*, **32**, 115-122, 1986
- Sicardi S., Gerhard H. and Hoffman H., Flow regime transition in trickle-bed reactors, *Chem. Eng. J.*, **18**, 173-182, 1979
- Sicardi S. and Hoffman H., Influence of gas velocity and packing geometry on pulsing inception in trickle-bed reactors, *Chem. Eng. J.*, **20**, 251-253, 1980
- Wallis G.B., One-dimensional two-phase flow, McGraw-Hill Inc., 122-135, 1969
- Wu R., McCready M.J. and Varma A., Influence of mass transfer coefficient fluctuation frequency on performance of three-phase packed-bed reactors, *Chem. Eng. Sci.*, **50**, 3333-3344, 1995
- Wu R., McCready M.J. and Varma A., Effect of pulsing on reaction outcome in a gas-liquid catalytic packed-bed reactor, *Catalysis Today*, **48**, 195-198, 1999

---

## Chapter 5

---

# Liquid-Induced Pulsing Flow Development of Feed Strategies

---

### Abstract

Gas-limited reactions occur when the gaseous reactant is slightly soluble in the liquid phase and at moderate operating pressures. Since for a completely wetted catalyst particle, the gaseous reactant must overcome both the gas-liquid and liquid-solid mass transfer resistances, partial wetting facilitates a much more effective transport of the gaseous reactant at the dry catalyst surface. The main problem during steady state operation is to attain partial wetting without gross liquid maldistribution, which usually leads to unpredictable and uncontrollable reactor performance. Based on a square-wave cycled liquid feed, two feed strategies are developed that involve the artificial induction of natural pulses and a separation of the wetting efficiency in time. The feed strategies aim at increasing the mass transfer rate of the limiting gaseous reactant and simultaneous prevention of flow maldistribution and hot spot formation. The feed strategies are distinguished by a relatively fast and slow cycling of the liquid feed.

Cycling the liquid feed results in the formation of continuity shock waves. The shock waves decay by leaving liquid behind their tail. This process of decay limits the frequency of the cycled liquid feed to rather low values since at relatively high frequencies, total collapse of the shock waves occurs. By the induction of natural pulses inside the shock waves, the mass and heat transfer rates during the liquid flush will be improved. Shorter flushes can therefore be applied and the usual encountered periodic operation is optimized. This first feed strategy is termed the slow mode of liquid-induced pulsing flow.

The second feed strategy termed the fast mode of liquid-induced pulsing flow may be viewed as an extension of natural pulsing flow. Individual natural pulses are induced at an externally set pulse frequency less than 1 Hz. The characteristics of the induced pulses equal the pulse characteristics of natural pulsing flow at equivalent gas flow rates. A critical liquid holdup in between pulses is necessary for the induced pulses to remain stable.

This chapter is based on the following publication:

Boelhouwer J.G., Piepers H.W. and Drinkenburg A.A.H., Liquid-induced pulsing flow in trickle-bed reactors, Chem. Eng. Sci., submitted for publication

## 5.1. Introduction

Trickle-bed reactors are usually operated at steady state conditions in the trickle flow regime. Recent experimental studies have demonstrated reactor performance improvement over the optimal steady state under forced time-varying liquid flow rates. In this mode of operation, the bed is periodically flushed with liquid, while the gas phase is fed continuously. This on-off feed strategy increases reactor performance in case the rate-limiting reactant is in the gas phase. The gaseous reactants can more easily adsorb on the catalyst since the mass transfer resistance added by the liquid phase is periodically reduced. During the liquid flush, heat and products are removed from the catalyst. Haure et. al. (1989) and Lee et. al. (1995) used this concept for the oxidation of SO<sub>2</sub> to sulfuric acid. Increases in oxidation rates up to 50% were achieved. During the periodic operation, higher bed temperatures were encountered compared to steady state operation. Only half of the rate enhancement could be attributed to these higher temperatures. The additional improvement is due to an increase in the mass transfer of oxygen to the catalyst. To demonstrate the advantages of periodic operation on a reaction in which both the gas and liquid phase contain reactants, the hydrogenation of  $\alpha$ -methyl styrene was studied by Lange et. al. (1994), Castellari and Haure (1995), Gabarain et. al. (1997) and Lange et. al. (1999). Increases in reaction rates up to 400% were obtained.

Periodic operation may be considered as the opportunity to operate the reactor for a certain period at conditions that create high reaction rates but is not feasible as steady state operation. Of course, steady state operation at a zero liquid flow rate is not possible. However, advantage of the enhanced reaction rates during zero liquid flow is obtained, since the liquid flush periodically supplies the liquid phase reactant to the catalyst. At low liquid flow rates, the steady state may be a gas-phase reaction over a dry catalyst (Castellari et. al., 1997; Satterfield and Ozel, 1973). Since heat removal during a low liquid flow rate is very poor, the reaction heat may completely evaporate the liquid phase, resulting in high reaction rates. In this case, advantage is obtained of a condition that is not feasible as steady state in terms of a reactor runaway.

In chapter 4, the possibility of the induction of natural pulses by cycling the liquid feed was described. Liquid feed cycling results in the formation of liquid-rich shock waves moving down the bed. At sufficiently high gas flow rates, natural pulses are initiated within the shock waves. This process is termed liquid-induced pulsing flow.

Since sufficient column length is needed for disturbances to grow into pulses, higher gas flow rates are necessary to induce pulses as the length of the shock wave decreases. When the length of the shock wave is comparable to or larger than the column height, the gas flow rate necessary for pulse inception equals the gas flow rate needed for natural pulsing flow. The column is then essentially alternately operated in the trickle and natural pulsing flow regime. The experiments described in chapter 4 were performed in a column of 1 m height. Some questions emerged concerning the stability of the initiated shock waves. Furthermore, since the velocity of the induced natural pulses exceeds the shock wave velocity, pulses leave the shock wave. In most cases, the induced pulses remained stable but occasionally the pulses vanished upon leaving the liquid-rich shock wave. Experiments in columns of larger height are required to study the stability of both the shock waves and the induced pulses.

## 5.2. Scope and objective

Experiments in a column of 3.2 m height were performed to examine the effect of column height on the stability of both the shock waves and the induced natural pulses. Two different modes of liquid-induced pulsing flow are considered, distinguished by a relatively slow and fast cycling of the liquid feed.

The slow mode of liquid-induced pulsing flow may be considered as the optimization of the (on-off) periodic operation described in the introduction. The aim is to induce pulses inside the liquid flushes to optimize the heat and mass transfer rates during the flush. Since the higher reaction rates occur during the period of zero (low) liquid feed, shorter flushes further improve reactor performance. The avoidance of hot spot formation is particularly important because of a substantial temperature increase during the period of zero (low) liquid feed. Given that natural pulses are characterized by complete catalyst wetting and high heat transfer rates, it is believed that the slow mode of liquid-induced pulsing flow benefits safety in periodic operation.

The fast mode of liquid-induced pulsing flow can be obtained in columns of large height only. This mode of operation may be perceived as an extension of natural pulsing flow since individual natural pulses can be induced at an externally set pulse frequency.

The objective of the present investigation is the characterization of the hydrodynamics of both the slow and fast mode of liquid-induced pulsing flow in a column of 3.2 m height. Furthermore, the potential advantages of these feed strategies on reactor performance are evaluated.

### 5.3. Experimental setup and procedures

A schematic illustration of the experimental equipment is presented in Fig. 5.1. The experiments were performed in a Plexiglas column of 0.11 m inner diameter and a packed height of 3.2 m. The packing material consisted of 6.0 mm glass spheres. A porosity of 0.37 and a specific packing area of  $630 \text{ m}^{-1}$  characterized the packed bed. The packing was supported at the bottom of the column by a stainless steel screen. Air and water were uniformly distributed at the top of the column. The air was obtained from the 7 bar central air distribution system. A pressure regulator was used to reduce the pressure from 7 to 2 bars. For the liquid feed, two different feed lines were applied. The primary feed line was used to provide a continuous liquid feed to the column while the secondary feed line provided an additional liquid feed for certain periods. In this manner, a square-wave cycled liquid feed was achieved. The cycled liquid feed is characterized by 4 parameters, schematically shown in Fig. 5.2. A magnetic valve in the secondary feed line activated by an electronic timer was employed to regulate the feed times of respectively the high ( $U_{lp}$ ) and low ( $U_{lb}$ ) liquid feed rates. High and low liquid feed rates were measured by calibrated flow meters.

Unsteady state operation of trickle-bed reactors is inherently accompanied by pressure fluctuations and hence varying gas flow rates at the top of the column. For the fast mode of liquid-induced pulsing flow, these pressure fluctuations are negligible. For the slow mode of periodic operation, however, significant pressure fluctuations occur (up to 0.05 bar). The reported superficial gas velocities for the slow mode periodic operation are calculated by using the pressure at the top of the column at the moment the additional liquid feed is ended, e.g. at the highest possible pressure at the column top.

A conductance technique, described in detail in chapter 2, was used to provide instantaneous measurements of cross-sectionally average liquid holdup. The column was equipped with 8 sets of conductance probes to measure liquid holdup at various axial positions. The conductivity probes were calibrated by both the tracer method and the stop-flow method.

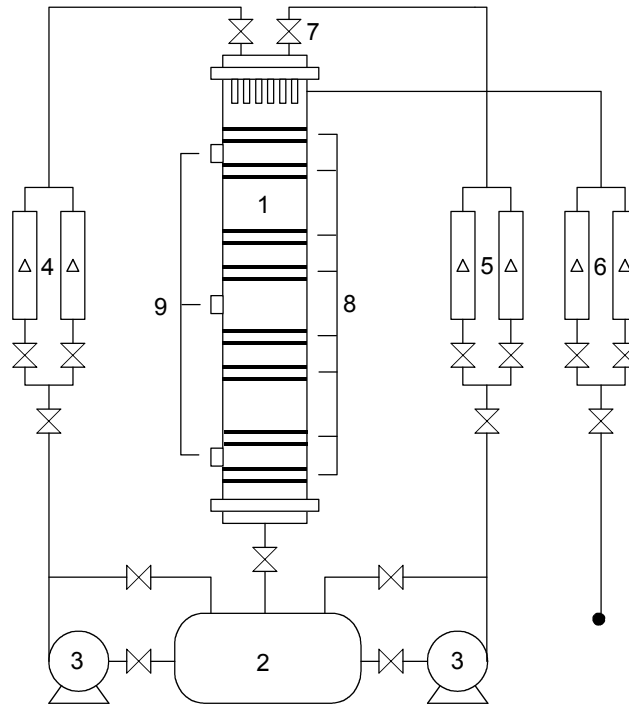


**Figure 5.1.** Schematic illustration of the experimental equipment (1: packed column; 2: liquid storage tank; 3: liquid pump; 4: liquid flow meters primary feed line; 5: liquid flow meters secondary feed line; 6: gas flow meters; 7: magnetic valve activated by electronic timer; 8: conductivity probes; 9: pressure taps)

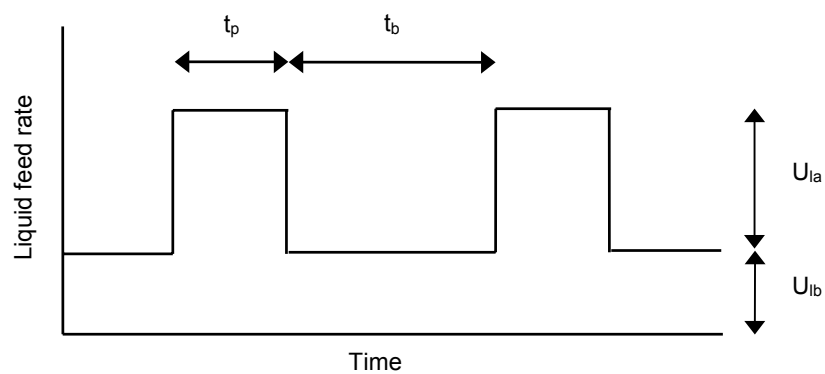


**Figure 5.2.** Schematic illustration of the characterization of the cycled liquid feed ( $U_{lb}$ : base liquid feed;  $U_{la}$ : additional liquid feed;  $t_b$ : duration of base liquid feed;  $t_p$ : duration of additional liquid feed)



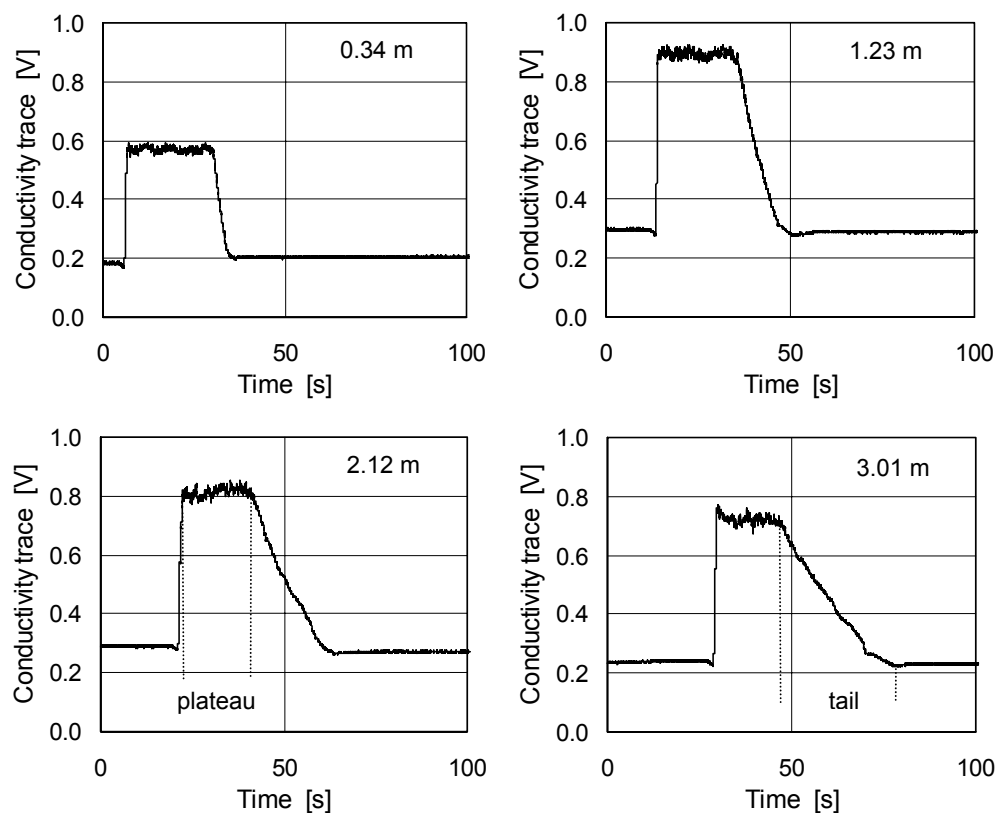


**Figure 5.3.** Conductivity traces at various distances from the column top for a relatively slow cycling of the liquid feed ( $t_p = 25$  s;  $t_b = 100$  s)

Both calibration methods were very reproducible and provided identical results. Conductivity traces were recorded and stored in a computer with a sampling rate of 100 Hz. Before performing any experiments, the column was operated in the pulsing flow regime for at least 1 hour to ensure a perfectly pre-wetted bed. The hydrodynamics of continuity shock waves and the slow and fast mode of liquid-induced pulsing flow were examined for a broad range of cycled liquid feed characteristics. Necessary gas flow rates for pulse induction were established by increasing the gas flow rate in small steps at fixed cycled liquid feed characteristics until natural pulses were initiated. The pulse frequency was obtained by evaluation of the number of pulses present in the conductivity signal. Pulse velocities were obtained by the cross correlation of two conductivity traces measured at different axial positions in the column.

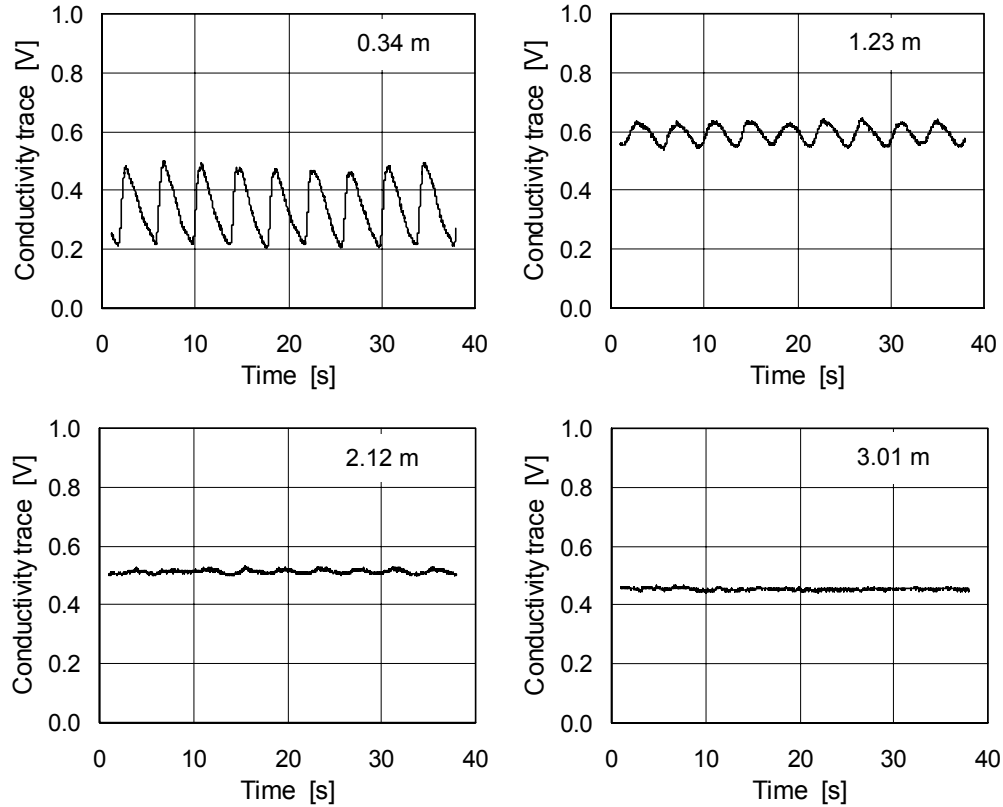


**Figure 5.4.** Conductivity traces at various distances from the column top for a relatively fast cycling of the liquid feed ( $t_p = 1$  s;  $t_b = 3$  s)

### 5.3. Continuity shock waves

#### 5.3.1. Qualitative description of the process

Due to the step change in liquid flow rate, continuity shock waves are initiated in the column (chapter 4). In Fig. 5.3, conductivity traces at 4 different axial positions along the column axis are presented. It is evident that the shock waves decay while moving down the bed. The shape of these traces suggests that the shock waves decay by leaving liquid behind their tail. This process is at the expense of the liquid amount carried by the wave and results in a decrease in the duration of the shock wave plateau and subsequently in an increase in the duration of the shock wave tail. The shock wave plateau and tail are defined in Fig. 5.3. The front of the shock waves remains sharp.

When shorter periods of high liquid feed are applied, total collapse of the shock waves is observed, as shown in Fig. 5.4. Eventually, this results in entire disintegration of the shock waves and steady state trickle flow emerges. Repeated experiments demonstrate that the rate of decay increases with increasing difference in  $U_{lp}$  and  $U_{lb}$ . Especially the on-off cycled liquid feed generates the most unstable shock waves.

### 5.3.2. Shock wave velocity

According to Wallis (1969), the velocity of a shock wave, derived from continuity considerations, obeys the following equation:

$$V_s = \frac{U_{l,p} - U_{l,b}}{\beta_p - \beta_b} \quad [5.1]$$

According to equation 5.1, the shock wave velocity is directly related to the difference between liquid flow rates and the difference between the resulting liquid holdups. The effect of the gas flow rate on shock wave velocity is embedded in the liquid holdup. A comparison between the calculated and experimentally determined shock wave velocities is presented in Fig. 5.5. The agreement is satisfactory. Shock wave velocity remains constant along the column height and is not affected by the process of decay as long as a shock wave plateau is observed.

### 5.3.3. Shock wave decay

Although the shock wave front is stable, the shock waves decay by leaving liquid behind at the tail. This process is at the expense of the amount of liquid carried by the shock wave. The process of decay results in a decrease in the length of the shock wave 'plateau' and consequently in an increase in the length of the tail. As a consequence, the integral heat and mass transfer rates during the shock wave will decrease as it moves down the column. In Fig. 5.6, an example of the decrease in the duration of the shock wave plateau versus the bed height is plotted. This figure clearly demonstrates that the process of decay is linear with respect to the distance traveled by the shock wave. With increasing difference between  $U_{lp}$  and  $U_{lb}$ , the shock waves decay more severely. Since the shock wave velocity remains unchanged, the decrease in length of the shock wave plateau is a linear process with time also. The rate of shock wave decay correlates reasonably well with the shock wave velocity as depicted in Fig. 5.7.

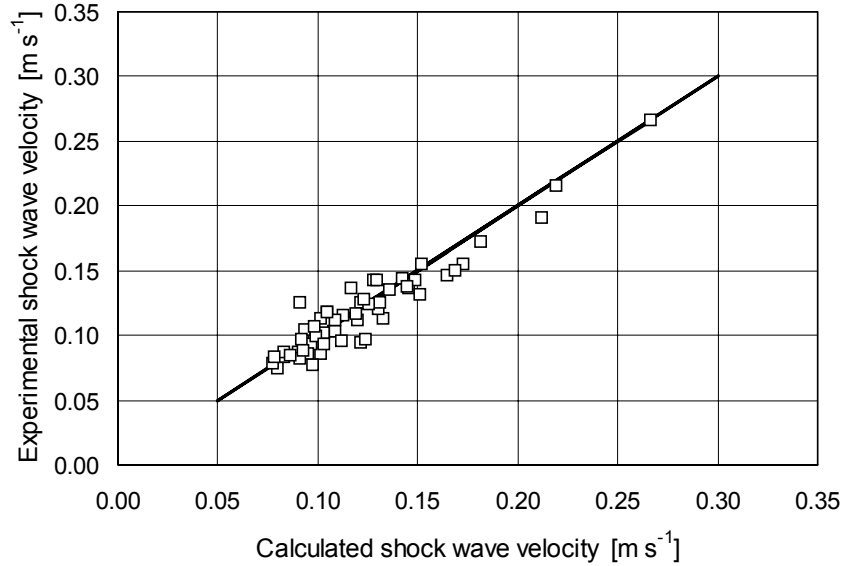


**Figure 5.5.** Comparison between experimentally determined and calculated shock wave velocity

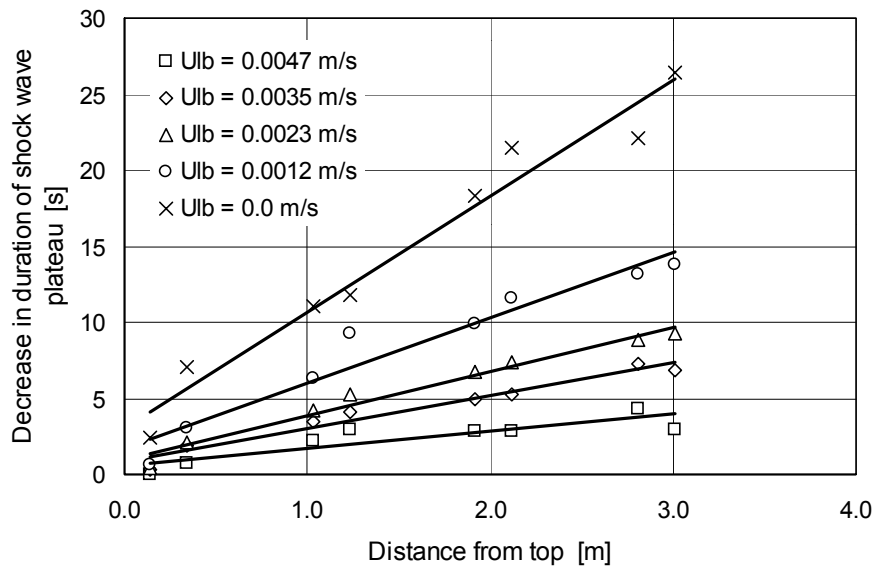


**Figure 5.6.** Decrease in the duration of shock wave plateau versus the distance from the column top ( $U_p = 0.0058 \text{ m s}^{-1}$ ;  $U_g = 0.12 \text{ m s}^{-1}$ )

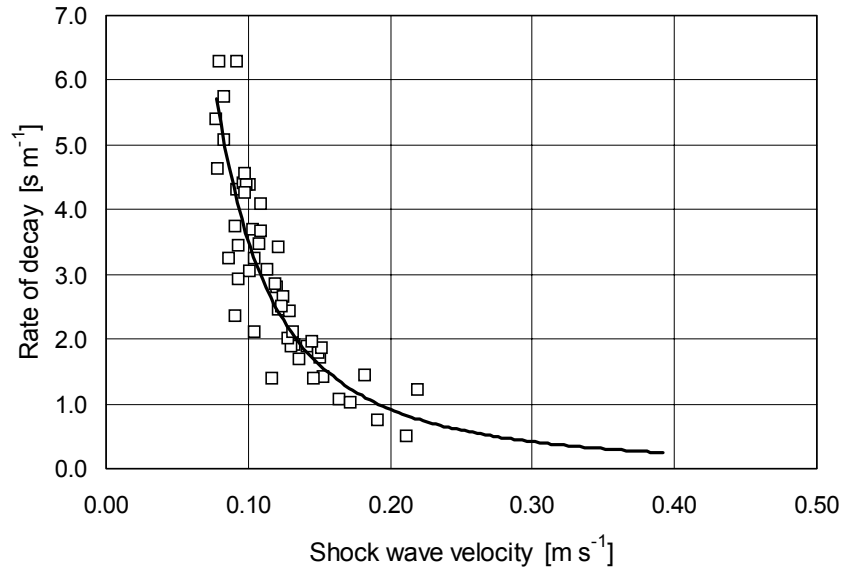


**Figure 5.7.** Correlation of the rate of shock wave decay with the shock wave velocity

Due to the decay of the shock waves, the length of the tail increases with traveled distance. In case  $t_b$  is sufficiently short, the increase in the tail length may result in the overlap of successive shock waves. Shock wave overlap causes the periods of zero (low) liquid flow rates to disappear and subsequently the positive effects owing to periodic operation will vanish. Therefore, it is of importance to quantify the minimum  $t_b$  needed to avoid overlap of the shock waves. Since the tail approaches a triangular shape, the increase in the tail length can be estimated to be twice the decrease in the length of the shock wave plateau. The final duration of the shock wave tail at the bottom of the column is almost completely governed by  $U_{lb}$ , as shown in Fig. 5.8. The highest  $U_{lb}$  minimizes the process of decay, but the lowest possible  $U_{lb}$  maximizes reaction rate enhancement during periodic operation. Fig. 5.8 clearly shows that the decaying process in columns of large height limits the cycle periods.

#### 5.3.4. Concluding remarks

Cycling the liquid feed results in the formation of continuity shock waves. The shock waves decay while moving down the bed by leaving liquid behind their tail. This process is at the expense of the liquid amount carried by the wave.

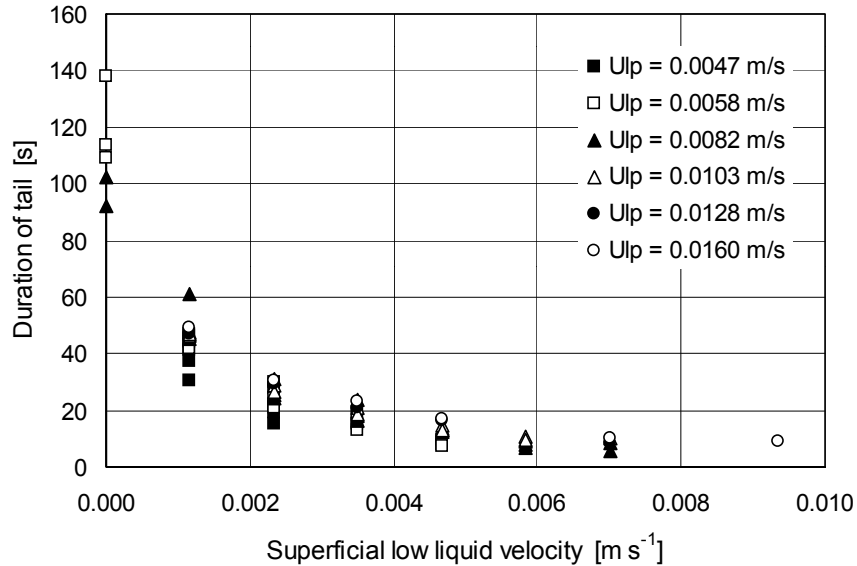


**Figure 5.8.** Effect of  $U_{lb}$  on the duration of the shock wave tail at the bottom of the column

The integral heat and mass transfer rates during the shock waves will therefore decrease with increasing traveled distance. The process of decay results in the formation of a long tail. When the applied  $t_b$  is insufficient, overlap between successive shock waves occurs, which diminishes the positive effects of periodic operation. If a relatively low  $t_p$  is applied, complete collapse of the shock waves is observed and steady state trickle flow emerges. The frequency of the cycled liquid feed is thus limited to relatively low values. The periods of the high and low liquid feed applied in literature studies vary between 30 seconds and 30 minutes. For the larger periods of cycling, the process of decay will be of minor importance. For the shorter periods, however, the process of decay is essential and must be accounted for in columns of large height.

## 5.4. Slow mode of liquid-induced pulsing flow

### 5.4.1. Introduction

During the periodic operation, the higher reaction rates occur during the portion of the feed cycle at zero (low) liquid flow rate.

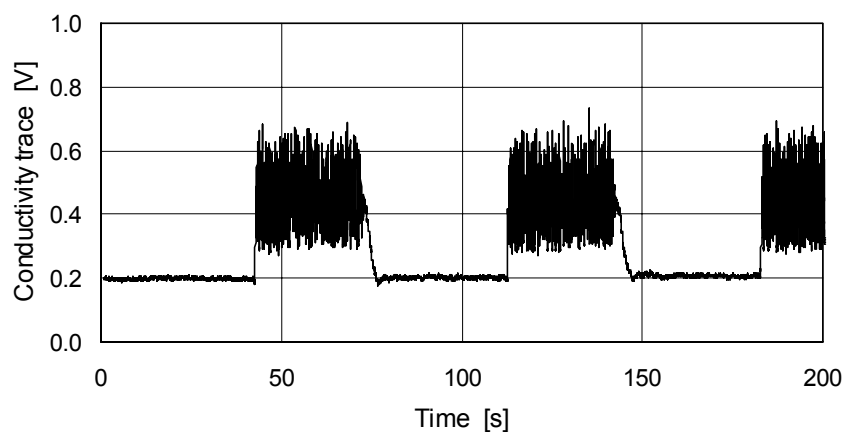


**Figure 5.9.** Example of a conductivity trace obtained during the slow mode of liquid-induced pulsing flow

The period of high liquid flow rate is necessary to remove the heat and products from the catalyst and to supply fresh liquid phase reactants. Reactor performance under periodic operation is enhanced if these processes occurring during the flush are optimized and shorter flushes can be achieved. When pulses are induced within the liquid flush, the mass and heat transfer rates are significantly enhanced. This mode of operation is termed the slow mode of liquid-induced pulsing flow.

#### 5.4.2. Qualitative description of the process

At sufficiently high gas flow rates, the inception of pulses occurs within the shock waves. An example of a conductivity trace obtained during the slow mode of liquid-induced pulsing flow is denoted in Fig. 5.9. Since the pulses move much faster than the shock wave, they leave the shock wave at the front. At the moment the pulses leave the shock wave, they immediately fade away, leaving a blob of liquid behind. The shock wave on its turn incorporates this blob of liquid and a new pulse may be initiated. Only for the highest applied  $U_{lb} = 0.0047 \text{ m s}^{-1}$ , the pulses remain stable upon leaving the shock wave. The stability of natural pulses outside the shock waves at relatively high  $U_{lb}$  clarifies that in chapter 4 it was established that in most cases, pulses remained stable upon leaving the shock waves. Relatively high  $U_{lb}$  ( $0.0035\text{-}0.0077 \text{ m s}^{-1}$ ) were applied. Some critical liquid holdup in between shock waves seems necessary for pulses to remain stable.

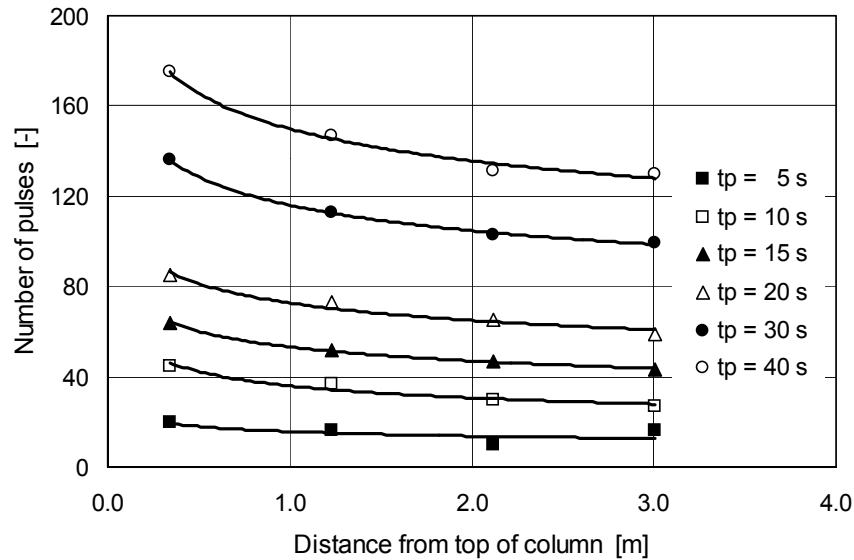


**Figure 5.10.** Decrease in the number of pulses versus the distance from the column top during the slow mode of liquid-induced pulsing flow ( $U_b = 0.0023 \text{ m s}^{-1}$ ;  $U_{lp} = 0.0082 \text{ m s}^{-1}$ ;  $U_g = 0.47 \text{ m s}^{-1}$ )

The decrease in the number of pulses present in the shock wave versus the distance from the column top is denoted in Fig. 5.10. The length of the shock wave plateau decreases due to the process of decay. Pulses leaving the shock wave at the front cause an additional loss of liquid holdup. The decreasing shock wave length results in a decrease in the number of pulses present in the shock wave. In case the shock waves are comparable to or shorter in length than the bed height, different flow regimes coexist in the column and the term liquid-induced pulsing flow is appropriate. In case sufficiently high  $t_p$  causes shock waves to be much larger than the column height, the column is essentially alternately operated in the trickle and natural pulsing flow regime. The process of decay limits the cycling frequency.

## 5.5. Fast mode of liquid-induced pulsing flow

### 5.5.1. Introduction

In the previous section, the slow mode of liquid-induced pulsing was described, which can be perceived as an optimization of the periodic operation using shock waves. This mode of operation is characterized by rather long cycle periods.



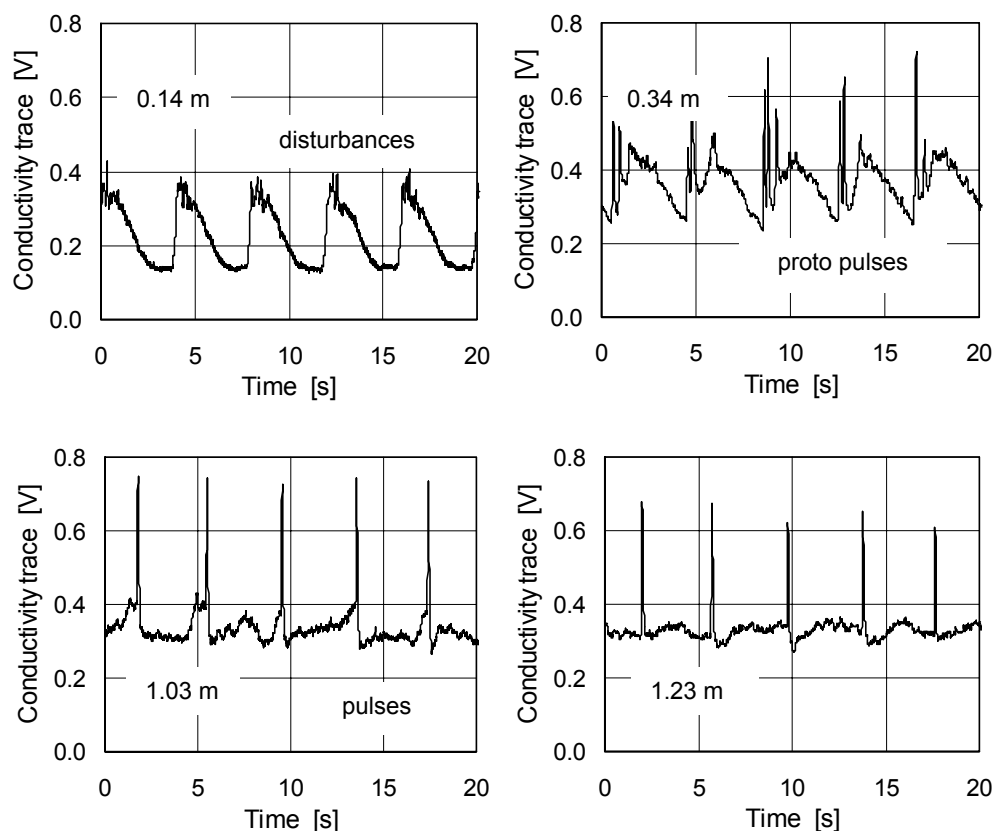


**Figure 5.11.** Conductivity traces at various distances from the column top presenting the process of pulse induction by the fast mode of liquid-induced pulsing flow

Fast liquid feed cycling does not seem to be feasible due to the lack of shock wave stability (see Fig. 5.4). Preliminary experiments, however, demonstrated another possibility to achieve a fast mode of periodic operation, consisting of the induction of individual natural pulses by liquid feed cycling. This feed strategy is termed the fast mode of liquid-induced pulsing flow since a very short  $t_p$  and much higher cycle frequencies are applied.

### 5.5.2. Qualitative description of process

By applying a high liquid feed for 1 or 2 seconds, continuity shock waves are initiated at the top of the column. Since these shock waves are unstable, complete collapse of the initiated shock waves is observed within a short distance (0.5 m) with respect to the top of the column.

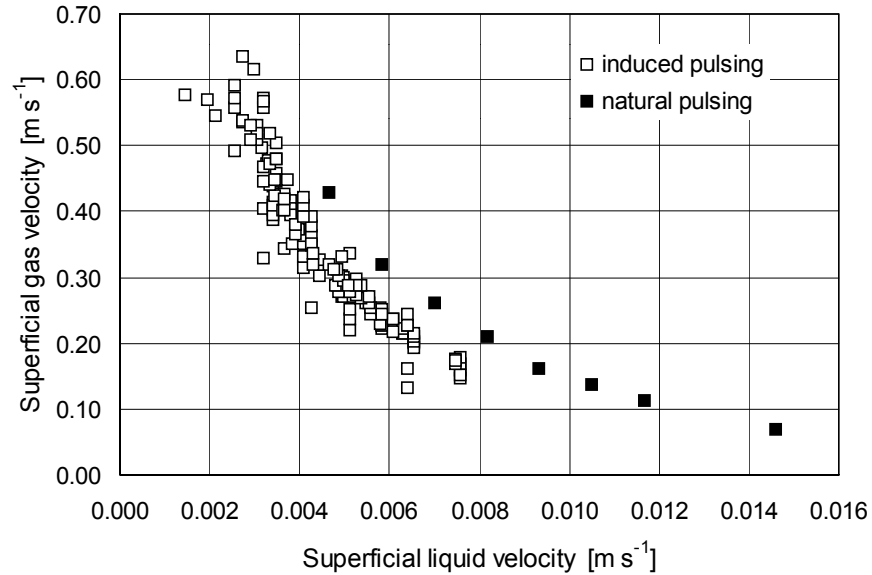


**Figure 5.12.** Comparison between the transition boundary to natural pulsing flow and the fast mode of liquid-induced pulsing flow

At sufficiently high gas flow rates, inception of pulses occurs within the shock waves in the upper region of the column where the individual shock waves are still observable. In the remainder of the column, a steady state trickle flow regime develops due to collapse of the shock waves. The initiated pulses, however, remain stable and move down from beginning to end through the column. This process of pulse induction is shown in Fig. 5.11 in terms of conductivity traces. Within the shock waves, disturbances are present. These disturbances form so-called proto-pulses, which eventually grow into pulses. A fast cycling of the liquid feed results in a quasi steady state in which pulses exist. The transition from trickle to induced pulsing flow is compared to the transition boundary for natural pulsing flow in Fig. 5.12. Required gas flow rates are about 25% lower compared to natural pulsing flow at equivalent (average) liquid flow rates. During the fast mode of liquid-induced pulsing flow, pulses are initiated within the shock waves at the column top. The liquid flow rate inside the shock waves is higher than the average liquid flow rate. At higher liquid flow rates, lower gas flow rates are sufficient for pulse initiation.

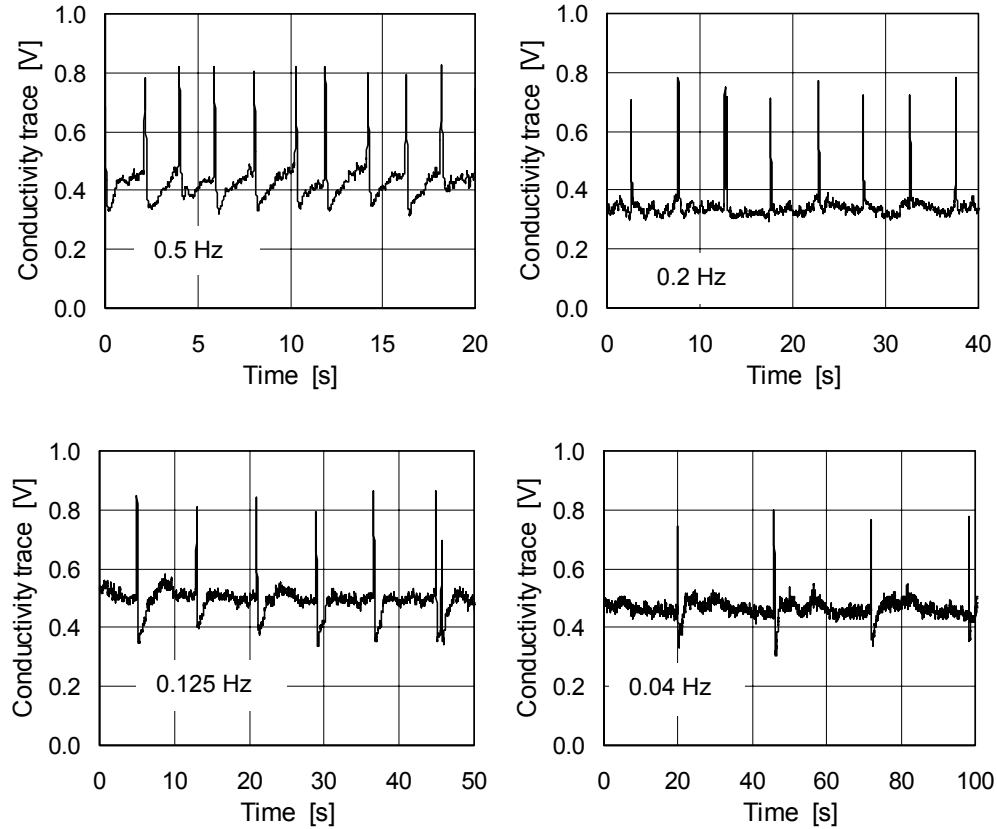


**Figure 5.13.** Examples of conductivity traces during the fast mode of liquid-induced pulsing flow to demonstrate the ability of pulse frequency control

### 5.5.3. Pulse frequency

By applying the fast mode of liquid-induced pulsing flow, all pulse frequencies less than 1 Hz can be realized. Some examples of pulse frequencies during the fast mode of liquid-induced pulsing flow are presented in terms of conductivity traces in figure 5.13. Since pulse frequencies during natural pulsing flow vary between 1 and 10 Hz, a very broad range of pulse frequencies can be assessed in combination with the fast mode of liquid-induced pulsing flow. Frequencies between 0.1 and 1 Hz can be obtained by applying an  $U_{lb}$  less than  $0.0047 \text{ m s}^{-1}$ . For higher  $U_{lb}$ , virtually all frequencies less than 1 Hz are possible. The sensitivity of the artificial pulse frequency to the gas flow rate is presented in Fig. 5.14. The time on the horizontal axis denotes the period in between successive induced pulses. The pulse frequency is externally set to 0.5 Hz by the cycled liquid feed ( $t_p = 1 \text{ s}$ ,  $t_b = 1 \text{ s}$ ).

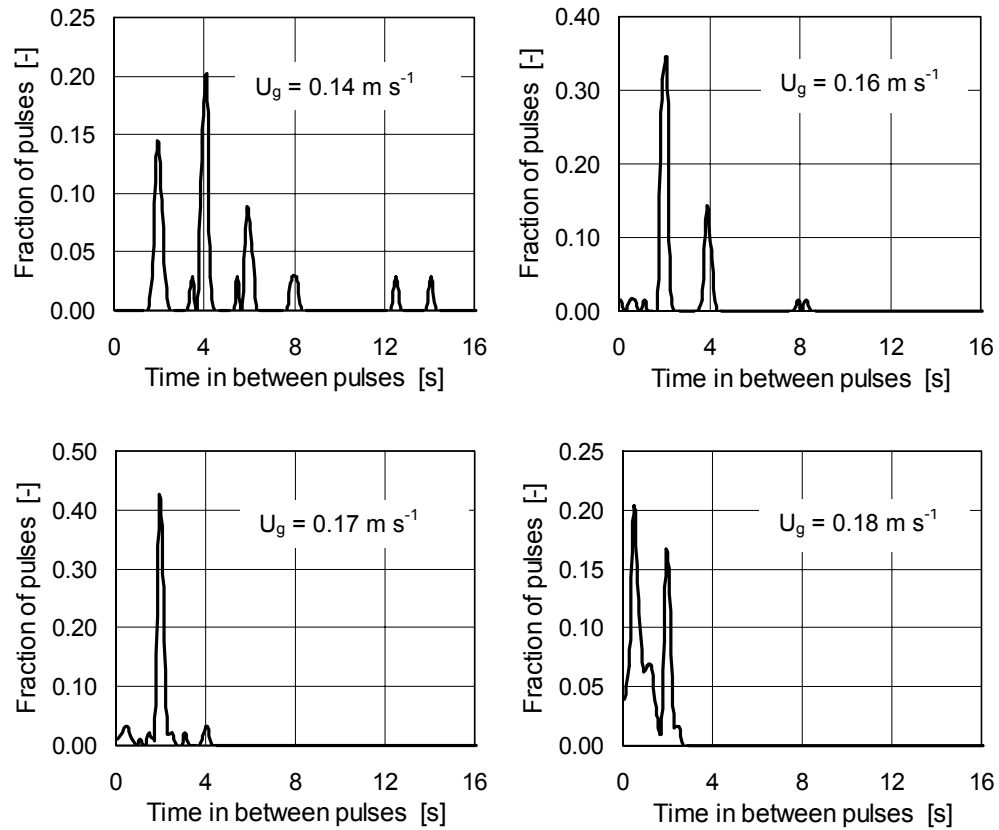


**Figure 5.14.** Effect of superficial gas velocity on the distribution of periods between successive pulses during the fast mode of liquid-induced pulsing flow

At the lowest gas flow rate, peaks are obtained at time intervals that are a multiple of the externally set period of 2 s. Apparently, pulses are not initiated within each feed cycle or vanish. At a higher gas flow rate, pulses are observed at 2 and 4 s only; pulses are induced more regularly. By a further increase in the gas flow rate, a sharp peak resembling the externally set cycled liquid feed frequency is obtained. Upon increasing the gas flow rate even further, an additional peak at low time intervals is observed. This corresponds to double pulse initiation. Further increase in the gas flow rate favors double pulse formation and eventually even triple pulse formation. Although this double and triple pulse formation is controllable, this is not further investigated.

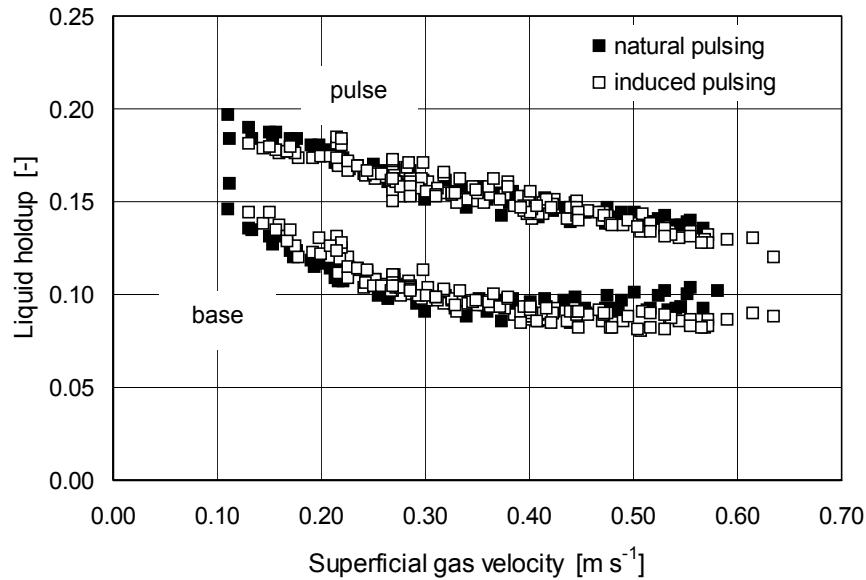


**Figure 5.15.** Comparison between pulse and base liquid holdup for natural pulsing flow and the fast mode of liquid-induced pulsing flow

#### 5.5.4. Liquid holdup

The liquid holdup in between and inside the pulses (from now on termed respectively pulse and base liquid holdup) during the fast mode of liquid-induced pulsing flow are compared to the pulse and base liquid holdup for the natural pulsing flow regime in Fig. 5.15. Both pulse and base liquid holdup during natural pulsing flow do not depend on the liquid flow rate, as is also reported in chapter 2. Pulse and base liquid holdup during the fast mode of liquid-induced pulsing flow perfectly coincide with the data concerning natural pulsing flow. This suggests that the hydrodynamic properties of the induced pulses are identical compared to natural pulsing flow.

The base liquid holdup provides the necessary conditions for pulses to remain stable in terms of a critical liquid holdup (chapter 2). In Fig. 5.16, the liquid holdup at the transition boundary to natural pulsing flow is compared to the liquid holdup in between pulses for both natural pulsing flow and the fast mode of liquid-induced pulsing flow. The base liquid holdup equals the liquid holdup at the transition boundary to natural pulsing flow at equivalent gas flow rates.

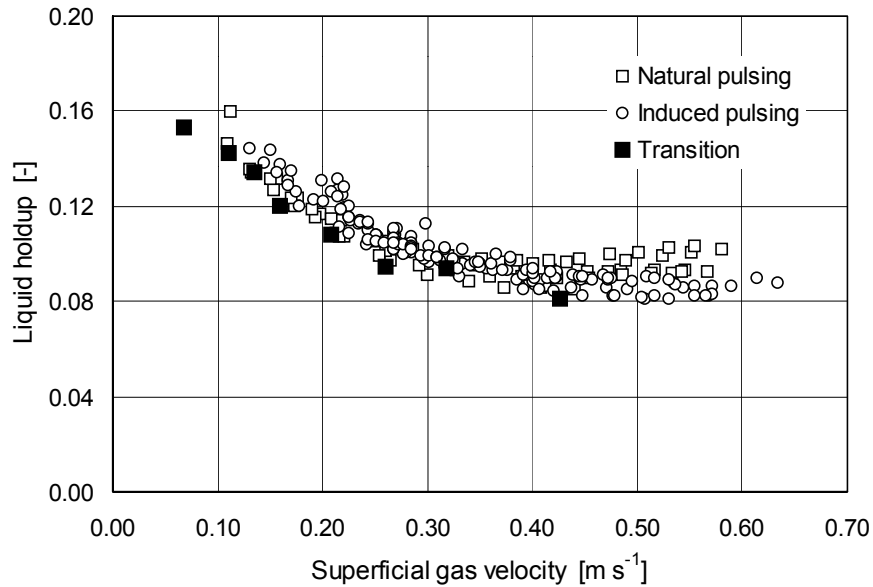


**Figure 5.16.** Comparison between the liquid holdup at the transition to natural pulsing flow with the base liquid holdup during natural pulsing flow and the fast mode of liquid-induced pulsing flow

At fixed  $U_{lp}$ ,  $U_{lb}$  and  $t_p$ , the quasi steady state liquid holdup, resulting from the collapse of shock waves, decreases with increasing  $t_b$ . A sufficiently long  $t_b$  is thus needed to achieve the critical quasi steady state liquid holdup for pulses to remain stable. This limits the pulse frequencies that can be accomplished. The highest applied  $U_{lb}$  ( $0.0047 \text{ m s}^{-1}$ ) on itself takes care of this critical liquid holdup. Therefore, in this case, all pulse frequencies less than 1 Hz are possible.

##### 5.5.5. Pulse velocity

The pulse velocity is determined at two axial positions in the column. The results are presented in Fig. 5.17. Pulse velocity solely depends on the gas flow rate, as is the case for natural pulsing flow (chapter 2). Higher pulse velocities are measured in the lower section of the column. Acceleration of the pulses occurs as they descend the column. A comparison between pulse velocities for both natural pulsing flow and the fast mode of liquid-induced pulsing flow is made in Fig. 5.18. The data coincide, being that the pulse velocities at the two axial positions in the column cover the range of pulse velocities measured in the natural pulsing flow regime.

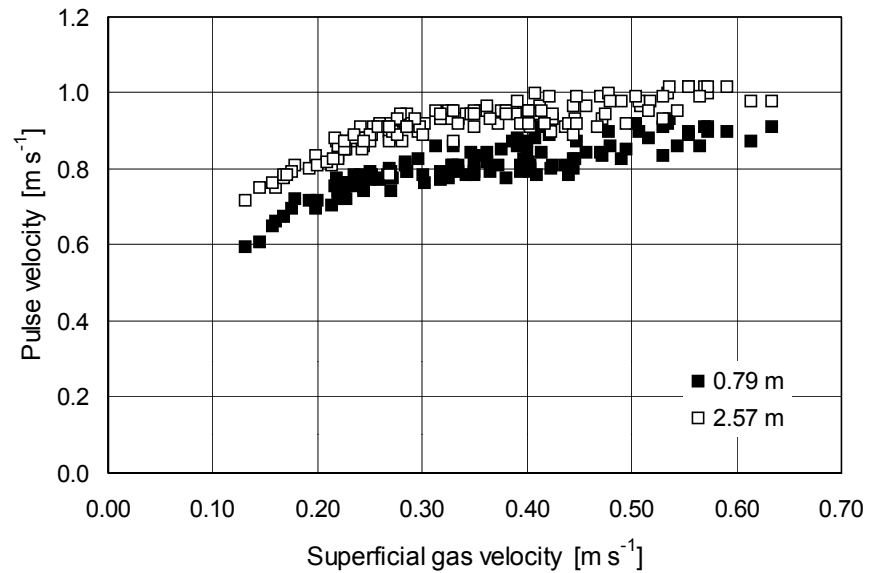


**Figure 5.17.** Relation between pulse velocity and superficial gas velocity for the fast mode of liquid-induced pulsing flow at 0.79 and 2.57 m from the column top

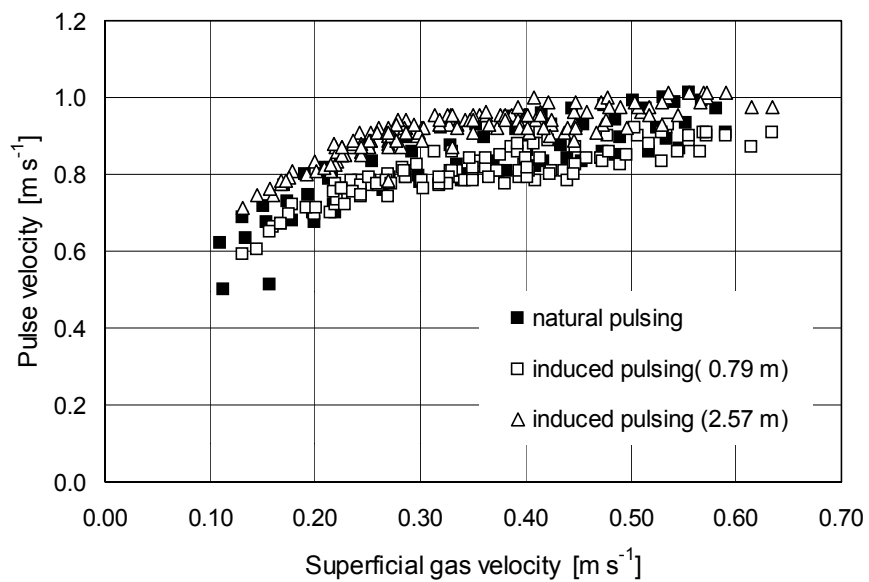


**Figure 5.18.** Comparison between the pulse velocity for natural pulsing flow and the fast mode of liquid-induced pulsing flow

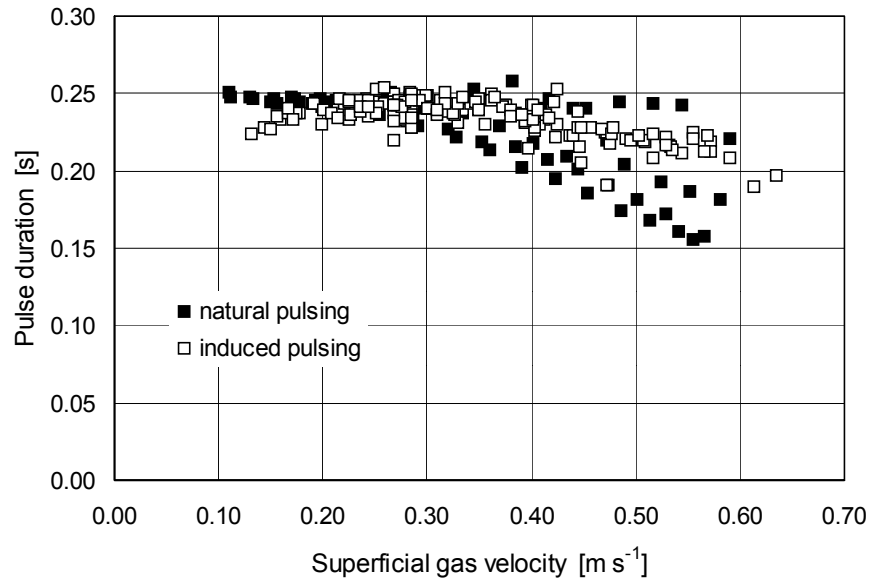


**Figure 5.19.** Comparison between the pulse duration for natural pulsing flow and the fast mode of liquid-induced pulsing flow

The spread in pulse velocity for natural pulsing flow is much broader than for liquid-induced pulsing flow. The location of the point of pulse inception for natural pulsing depends on the gas and liquid flow rates. Since the pulse velocity is measured at a fixed location in the bed, it is affected by the location of the point of pulse inception that determines the available time for pulse acceleration. With liquid-induced pulsing flow, the point of pulse inception is fixed and hence all pulses exhibit the same period of acceleration. The small but detectable influence of the liquid flow rate on pulse velocity during natural pulsing flow is caused by the variable age of the pulses; pulse velocity during natural pulsing flow is independent of the liquid flow rate.

#### 5.5.6. Pulse duration

A comparison of the pulse duration for natural and liquid-induced pulsing flow is shown in Fig. 5.19. It is obvious that the data coincide. Once more it is noticed that the spread on pulse duration for natural pulsing flow is considerably higher compared to liquid-induced pulsing flow, especially at high gas velocities. At relatively high pulse frequencies, pulses tend to overlap, which makes it impossible to obtain the actual pulse duration.



Since pulse frequency increases both with increasing gas and liquid flow rate, pulse duration during natural pulsing flow appears to be affected by the liquid flow rate at high gas and liquid flow rates. The low pulse frequencies during the fast mode of liquid-induced pulsing flow, however, assure that no overlap of individual pulses occurs. It is therefore believed that the pulse duration obtained during the fast mode of liquid-induced pulsing flow is the true pulse duration and applicable to natural pulsing flow.

#### **5.5.7. Concluding remarks**

By applying a short period of the high liquid flow rate, it is possible to induce pulses and externally control the pulse frequency. All pulse frequencies less than 1 Hz can be achieved by this mode of operation. It is shown that the properties of the induced pulses are identical to those of natural pulses. The induced pulses remain stable if the quasi steady state liquid holdup resulting from shock wave collapse equals the liquid holdup at the transition boundary to natural pulsing flow. This feed strategy is the only fast mode of periodic operation possible since pulses are stable while shock waves decay.

The hydrodynamics of the fast mode of liquid-induced pulsing flow also reveal that pulse duration and pulse velocity during natural pulsing flow are completely independent of the liquid flow rate. The slight impact of the liquid flow rate on measured pulse velocity and pulse duration during natural pulsing flow is due to pulse acceleration respectively overlap between pulses that blur the measurements.

### **5.6. Evaluation of potential advantages**

Gas-limited reactions occur when the gas phase reactant is slightly soluble in the liquid phase and at moderate operating pressures. Since for a completely wetted catalyst particle, the gas phase must overcome both the gas-liquid and liquid-solid mass transfer resistances, partial wetting facilitates a much more effective transport of the gaseous reactant at the dry catalyst surface. The main problem during steady state operation is to attain partial wetting without gross liquid maldistribution, which usually leads to unpredictable and uncontrollable reactor performance.

Cycling the liquid feed results in temporal variations in the wetting efficiency of the catalyst particles, without the problem of gross liquid maldistribution. During the non-wetted part of the feed cycle, the gaseous reactant has increased access to the catalyst.

During the wetted part of the feed cycle, the heat and products are removed from the catalyst and fresh liquid phase reactant is supplied. Since the higher reaction rates prevail during the non-wetted part of the feed cycle, shorter flushes increase reactor performance even more. Shorter necessary flushes can be achieved by the slow mode of liquid-induced pulsing flow, since the pulses enhance the rate of heat removal and mass transfer of the products and reactants. Especially, the danger of hot spot formation is prevented during the slow mode of liquid-induced pulsing flow, since the pulses are characterized by complete catalyst wetting and high particle-liquid heat transfer rates. This heat elimination is of particular interest since during the low part of the feed cycle, the liquid does not or slightly remove the reaction heat and a significant temperature rise of the catalyst bed prevails.

A rather important criterion limiting the duration of the liquid-off period may be the selectivity for consecutive reactions ( $A \rightarrow P \rightarrow Q$ ). During the liquid-off period, the desired product P is initially produced. Since the product is not removed from the catalyst, the reaction to the unwanted product Q becomes increasingly significant. Additionally, since the reaction heat is not removed, higher catalyst temperatures prevail. In case the activation energy of the second (undesired) reaction is higher than the activation energy of the first (desired) reaction, higher bed temperatures reduce selectivity. To avoid selectivity problems, there will be an upper limit of the dry period. Selectivity problems may therefore require a relatively fast cycling of the liquid feed to reduce the residence time of the desired product inside the catalyst. Unfortunately, no studies about periodic operation of a trickle-bed for consecutive reactions are reported in literature <sup>(1)</sup>.

In general, the frequency of the cycled liquid feed must increase as the heat production rate increases, as the reaction rate increases and as the selectivity of consecutive reactions is important. Due to the lack of stability of the shock waves, the frequency is limited to rather low values. A 'fast' mode of periodic operation is, however, feasible by the artificial induction of individual natural pulses. This feed strategy is termed the fast mode of liquid-induced pulsing flow. Due to the very low liquid holdup in between pulses, it is believed that partial wetting or at least very thin liquid films exist in between the induced pulses. Moreover, the pulses are characterized by large increases in volumetric gas-liquid mass transfer rates (Blok et. al., 1984; Fukushima and Kusaka, 1977; Hirose et. al., 1974) which benefits the overall transport of the gaseous reactant to the catalyst.

<sup>(1)</sup> Work on consecutive reactions during periodic operation is in progress (Lange and Hanika, 2001)

The fast mode of liquid-induced pulsing flow may be perceived as an extension of natural pulsing flow. All pulse frequencies less than 1 Hz can be achieved. With natural pulsing flow, frequencies between 1 and 10 Hz can be obtained. Wu et. al., (1995) used a theoretical model to predict the selectivity and yield for consecutive and parallel reactions under pulsing flow conditions. In some cases, depending on the pulse frequency, significant changes in both yield and selectivity occur. They experimentally verified these model results with the hydrogenation of phenylacetylene to styrene and ethylbenzene (Wu et. al., 1999). It was demonstrated that pulsing flow has a positive effect with respect to trickle flow, particularly on selectivity. Lee and Bailey (1974) modeled a complex heterogeneously catalyzed reaction under periodic variations of the reactant concentrations at the outer surface of the catalyst. Due to interacting concentration waves inside the catalyst, improved selectivity was obtained. It might very well be possible that periodic operation of a trickle-bed reactor leads to selectivity improvements for non-linear reaction kinetics. The possibility to obtain virtually every pulse frequency with the fast mode of liquid-induced pulsing flow creates the opportunity to match the time constant of pulsing with the time constant of reaction. The fast mode of induced-pulsing flow may therefore be a powerful mode of operation to increase reaction selectivity.

Applying the fast mode of liquid-induced pulsing flow diminishes flow maldistribution and the danger of hot spots. At very low frequencies, the reactor is essentially operated in the trickle flow regime while at certain periods pulses are induced, which assure good radial mixing between parallel flowing liquid streams. Redistribution of liquid in quench boxes and other devices may be eliminated by applying this feed strategy.

## 5.7. Concluding remarks

In this chapter, two feed strategies based on a cycled liquid feed are described. Both feed strategies involve the artificial induction of natural pulses and a separation of the wetting efficiency in time. The feed strategies are distinguished by a relatively fast and slow cycling of the liquid feed.

The slow mode of liquid-induced pulsing flow may be seen as an optimization of the usual encountered periodic operation, since shorter flushes may be applied. Especially, the danger of hot spot formation is prevented during the slow mode of liquid-induced pulsing flow, since the pulses are characterized by complete catalyst

wetting and high particle-liquid heat transfer rates. This heat elimination is of particular interest since during the low part of the feed cycle, the liquid does not remove the reaction heat and a significant temperature rise of the catalyst bed prevails.

The frequency of the cycled liquid feed is limited to rather low values due to the unstability of the shock waves. It is expected that especially for reasons of selectivity, a faster cycling of the liquid feed must be applied. By faster cycling of the liquid feed, residence times of the desired product in the catalyst are reduced while effective mass transport of the gaseous reactant still occurs. In this case, the fast mode of liquid-induced pulsing flow seems appropriate. The fast mode of liquid-induced pulsing flow may be seen as an extension of natural pulsing flow. Individual natural pulses can be induced at externally controlled frequencies less than 1 Hz. The possibility to obtain virtually all pulse frequencies with the fast mode of liquid-induced pulsing flow provides the opportunity to match the time constant of pulsing with the time constant of reaction, which possibly benefits selectivity.

Both the slow and fast mode of liquid-induced pulsing flow prevent flow maldistribution and hot spot formation due to complete catalyst wetting and high heat transfer rates characterizing the induced natural pulses. Although both feed strategies are mainly concerned with gas limited reactions, the operation in the natural pulsing flow regime at high pulse frequencies seems appropriate for liquid-limited reactions.

## Notation

$t_b$	duration of low liquid feed	[s]
$t_p$	duration of high liquid feed	[s]
$U_{la}$	superficial additional liquid feed velocity	[m s <sup>-1</sup> ]
$U_{lb}$	superficial low liquid feed velocity	[m s <sup>-1</sup> ]
$U_{lp}$	superficial high liquid feed velocity	[m s <sup>-1</sup> ]
$V_s$	shock wave velocity	[m s <sup>-1</sup> ]
$\beta_b$	liquid holdup in between shock waves	[-]
$\beta_p$	liquid holdup within shock waves	[-]

## Literature cited

- Blok J.R. and Drinkenburg A.A.H., Hydrodynamic properties of pulses in two-phase downflow operated packed columns, *Chem. Eng. J.*, 25, 89-99, 1982
- Blok J.R., Koning C.E. and Drinkenburg A.A.H., Gas-liquid mass transfer in fixed-bed reactors with cocurrent downflow operating in the pulsing flow regime, *AIChE J.*, 30, 393-401, 1984
- Castellari A.T. and Haure P.M., Experimental study of the periodic operation of a trickle bed reactor, *AIChE J.*, 41, 1593-1597, 1995
- Castellari A.T., Cechini J.O., Gabarain L.J. and Haure P.M., Gas-phase reaction in a trickle-bed reactor operated at low liquid flow rates, *AIChE J.*, 43, 813-1818, 1997
- Fukushima S. and Kusaka K., Liquid phase volumetric and mass transfer coefficient and boundary of hydrodynamic flow region in packed column with cocurrent downward flow, *J. Chem. Eng. Japan*, 10, 468-474, 1977
- Gabarain L., Castellari A.T., Cechini J., Tobolski A. and Haure P.M., Analysis of rate enhancement in a periodically operated trickle-bed reactor, *AIChE J.*, 43, 166-172, 1997
- Haure P.M., Hudgins R.R. and Silveston P.L., Thermal waves in the periodic operation of a trickle bed, *Chem. Eng. Sci.*, 45, 2255-2261, 1990
- Haure P.M., Hudgins R.R. and Silveston P.L., Periodic operation of a trickle-bed reactor, *AIChE J.*, 35, 1437-1444, 1989
- Hirose T., Toda M. and Sato Y., Liquid phase mass transfer in packed bed reactor with cocurrent gas-liquid downflow, *J. Chem. Eng. Japan*, 7, 187-192, 1974
- Khaldikar M.R., Wu Y.X., Al-Dahhan M.H., Dudukovic M.P. and Colakyan M., Comparison of trickle bed and upflow performance at high pressure. Model predictions and experimental observations, *Chem. Eng. Sci.*, 51, 2139, 1996
- Lange R., Hanika J., Stradiotto D., Hudgins R.R. and Silveston P.L., Investigations of periodically operated trickle-bed reactors, *Chem. Eng. Sci.*, 49, 5615-5621, 1994
- Lange R., Gutsche R. and Hanika J., Forced periodic operation of a trickle-bed reactor, *Chem. Eng. Sci.*, 54, 2569-2573, 1999
- Lange R. and Hanika J., personal communication
- Lee C.K. and Bailey J.E., Diffusion waves and selectivity modifications in cyclic operation of a porous catalyst, *Chem. Eng. Sci.*, 29, 1157-1163, 1974
- Lee K.J., Hudgins R.R. and Silveston P.L., A cycled trickle bed reactor for SO<sub>2</sub> oxidation, *Chem. Eng. Sci.*, 50, 2523-2530, 1995
- Mills P.L. and Dudukovic M.P., Analysis of catalyst effectiveness in trickle bed reactors processing volatile or nonvolatile reactants, *Chem. Eng. Sci.*, 35, 2267, 1980
- Satterfield C.N. and Ozel F., Direct solid-catalyzed reaction of a vapor in an apparently completely wetted trickle bed reactor, *AIChE J.*, 19, 1259-1261, 1973
- Tsochatzidis N.A., Karabelas A.J., Properties of pulsing flow in a trickle bed, *AIChE J.*, 41, 2371-2382, 1995
- Wallis G.B., One-dimensional two-phase flow, McGraw-Hill Inc., 122-135, 1969
- Wu R., McCready M.J. and Varma A., Effect of pulsing on reaction outcome in a gas-liquid catalytic packed-bed reactor, *Catalysis Today*, 48, 195-198, 1999
- Wu R., McCready M.J. and Varma A., Influence of mass transfer coefficient fluctuation frequency on performance of three-phase packed-bed reactors, *Chem. Eng. Sci.*, 50, 3333-3344, 1995

---

## Chapter 6

---

# Local Particle-Liquid Mass Transfer Coefficient

---

### Abstract

For highly active catalysts, fast reactions and/or relatively large catalyst particles, the liquid film becomes the controlling resistance. Especially for liquid-limited reactions, high wetting efficiencies and particle-liquid mass transfer coefficients are favored.

Particle-liquid mass transfer coefficients during trickle, bubble and pulsing flow are determined. Compared to trickle flow, pulsing and bubble flow result in considerably higher particle-liquid mass transfer coefficients. The linear liquid velocity governs mass transfer rates. Even in the pulsing flow regime, large differences in local mass transfer coefficients exist. This is attributed to non-uniformities in the local voidage distribution.

The scatter in mass transfer coefficients predicted by literature correlations is not random. Correlations proposed for systems characterized by high Sc-numbers predict much lower particle-liquid mass transfer rates than correlations proposed for systems characterized by low Sc-numbers. Apparently, the effect of the Sc-number is not correctly accounted for.

The penetration theory is useful in calculating both particle-liquid heat and mass transfer coefficients during pulsing flow. Additionally, the analogy between heat and mass transfer rates proposed by penetration theory outperforms the Chilton-Colburn analogy.

The operation of a trickle-bed reactor in the pulsing flow results in a large increase in mass transfer rates and complete catalyst wetting. The operation of a trickle-bed reactor in the natural pulsing flow regime is therefore more suitable for externally mass transfer controlled reactions than trickle flow operation.

This chapter is based on the following publications:

- Boelhouwer J.G., Piepers H.W., Hoogenstrijd B.W.J.L., Janssen L.J.J. and Drinkenburg A.A.H., Comments on the electrochemical method to determine particle-liquid mass transfer rates in trickle-bed reactors, Chem. Eng. Sci., submitted for publication  
Boelhouwer J.G., Piepers H.W. and Drinkenburg A.A.H., Local particle-liquid mass transfer in trickle-bed reactors, in preparation

## 6.1. Introduction

In a trickle-bed reactor, a gas and a liquid phase cocurrently flow downward over a fixed bed of catalyst particles. For highly active catalysts, fast reactions and/or relatively large catalyst particles, the liquid film becomes the controlling resistance (Rao and Drinkenburg, 1985; Ruether et. al., 1980). The operation of a trickle-bed reactor in the pulsing flow regime results in a large increase in mass transfer rates (Chou et. al., 1979; Ruether et. al., 1980; Rao and Drinkenburg, 1985) and is therefore more suitable for externally mass transfer controlled reactions.

Two techniques are generally applied for mass transfer measurements in trickle-bed reactors, which are based on the determination of the rate of (a) dissolution of a soluble packing or the rate of (b) an electrochemical redox reaction. The electrochemical method offers the advantage of obtaining instantaneous measurements and is thus very convenient for measuring mass transfer rates under dynamic conditions. Upon increasing the potential between two electrodes, the intrinsic rate of an electrochemical reaction is increased. This is observed as an increase in the current density. At relatively high electrode potentials, the current reaches a saturation level termed the limiting current. Upon a further increase in the electrode potential, the current remains constant until eventually hydrogen and oxygen evolution occur. The limiting current plateau indicates that liquid-solid mass transfer of the electro-active species from the bulk solution to the electrode surface is the rate-limiting factor. The limiting current is a direct measure of the mass transfer coefficient. The counter electrode is much larger than the working electrode to assure mass transfer limitations occur at the working electrode only. Mizushina (1981) and Selman and Tobias (1978) presented detailed reviews concerning the application of the limiting current technique in mass transfer measurement.

## 6.2. Scope and objective

The objective of the study described in this chapter is to experimentally determine local particle-liquid mass transfer coefficients in the trickle and pulsing flow regimes. The spread in local mass transfer rates in the bed is investigated. Special attention is given to particle-liquid mass transfer during pulsing flow, since pulsing flow is a promising mode of operation for liquid-limited reactions. The analogy between heat and mass transfer is evaluated.

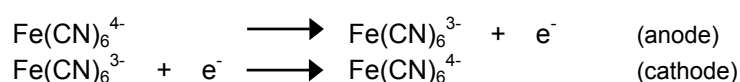
**Table 6.1.** Physical properties of the electrolytic solutions and water.

liquid	viscosity [mPa s]	density [kg m <sup>-3</sup> ]	surface tension [mN m <sup>-1</sup> ]
water	1.00	1000	72.0
Na <sub>2</sub> SO <sub>4</sub>	1.28	1154	59.0
NaOH	0.97	1020	42.0

### 6.3. Experimental set-up and procedures

The experiments were performed in a Plexiglas column of 0.11 m inner diameter and a packed height of 1.0 m. A schematic illustration of the experimental equipment is presented in Fig. 6.1. The packing material consisted of 6.0 mm glass spheres. A porosity of 0.36 and a specific packing area of 640 m<sup>-1</sup> characterized the packed bed. Air and the electrolytic solution were uniformly distributed at the top of the column. The experiments were performed at room temperature and near atmospheric pressure.

The electrolytic solution was a mixture of 0.01M potassium ferricyanide<sup>(1)</sup>, 0.01 M potassium ferrocyanide<sup>(1)</sup> and a large excess of 0.5 M sodium sulfate as supporting electrolyte. Sodium sulfate is an indifferent electrolyte that reduces the migration current and the ohmic potential drop. The anode was a nickel sphere of 6.0 mm diameter. A thin nickel foil with a large surface area was used as the cathode. The potential of the working electrode is measured as the overpotential with respect to a small nickel reference electrode. The reactions at the anode, respectively cathode are:



This electrochemical system deviates from the systems usually employed for mass transfer measurement in trickle-bed reactors. Generally, a cathodic working electrode is applied (Chou et. al., 1979; Rao and Drinkenburg, 1985; Tsochatzidis and Karabelas, 1994). Since in these studies air is employed as the gas-phase, the reduction of oxygen at the cathode can lead to serious overestimation of the particle-liquid mass transfer coefficient. Therefore, in this study, an anodic working electrode is applied. Details concerning the reduction of oxygen at the cathode are discussed in the appendix to this chapter.

<sup>(1)</sup> The official designation of ferricyanide resp. ferrocyanide is hexacyanoferrate(III) and hexacyanoferrate(II)



The physical properties of the electrolytic system are summarized in Table 6.1.

A total of 5 anodes was situated in the column at various radial positions to measure local mass transfer coefficients. Before performing any experiments, the column was operated in the pulsing flow regime for at least 1 hour to ensure a perfectly pre-wetted bed. After the gas and liquid flow were established, the measurement was started. Current-potential curves were recorded with a digital potentiostat (Autolab, PGSTAT20, EcoChemie) to determine the range of electrode potentials at which the limiting current is present. An example of such a current-potential curve is shown in Fig. 6.2. Subsequently, measurement of the limiting current in time was employed with a sample rate of 100 Hz. Local particle-liquid mass transfer coefficients were determined for a wide range of gas and liquid flow rates in the trickle, pulsing and bubble flow regimes. Local particle-liquid mass transfer coefficients are calculated by:

$$k_{s,app} = f_w k_s = \frac{I_L}{a_p F C_1} \quad [6.1]$$

In this equation,  $I_L$  is the limiting current,  $a_p$  the anode surface area,  $F$  the Faraday constant and  $C_1$  the bulk concentration of ferrocyanide. The obtained apparent mass transfer coefficient ( $k_{s,app}$ ) is actually the product of the mass transfer coefficient ( $k_s$ ) and the fractional wetting ( $f_w$ ) of the anode. The response time of the anode can be estimated by the ratio of the diffusivity of the ferrocyanide ions to the square of the observed mass transfer coefficient. The measured mass transfer coefficient during pulsing flow is about  $3 \cdot 10^{-5} \text{ m s}^{-1}$  resulting in a response time of the anode of approximately 0.5 s. Therefore, this method is capable of measuring fluctuations in the mass transfer coefficient up to 2 Hz.

#### 6.4. Hydrodynamics

The hydrodynamics of the aqueous  $\text{Na}_2\text{SO}_4$ -solution substantially differ from water as the liquid phase. The flow regime boundaries for both the air-water and air- $\text{Na}_2\text{SO}_4$ -system are presented in Fig. 6.3. Compared to the air-water system, the trickle flow regime is restricted to considerably lower gas and liquid flow rates. Additionally, bubble flow is obtained, which is absent for the air-water system. A comparison of the physical properties for water and the  $\text{Na}_2\text{SO}_4$ -solution is shown in Table 6.1.

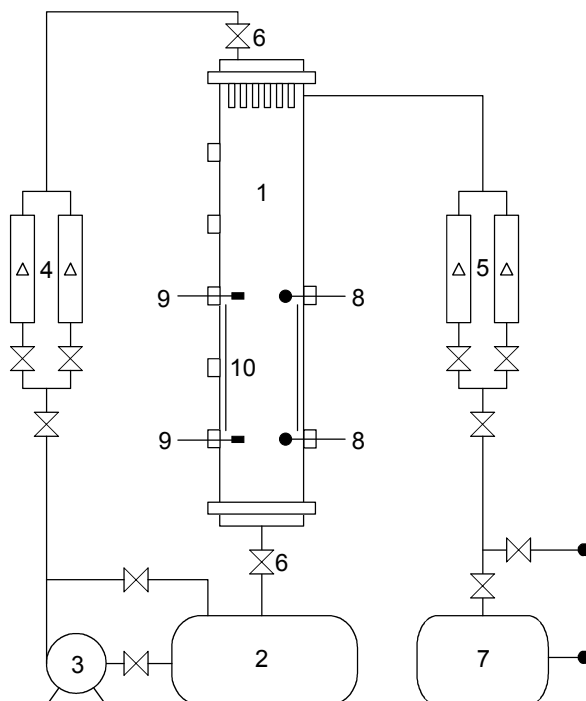


**Figure 6.1.** Schematic illustration of the experimental equipment (1: column; 2: liquid storage tank; 3: liquid pump; 4: liquid flow meter; 5: gas flow meter; 6: magnetic valve; 7: pressure vessel; 8: anode; 9: reference electrode; 10: counterelectrode)

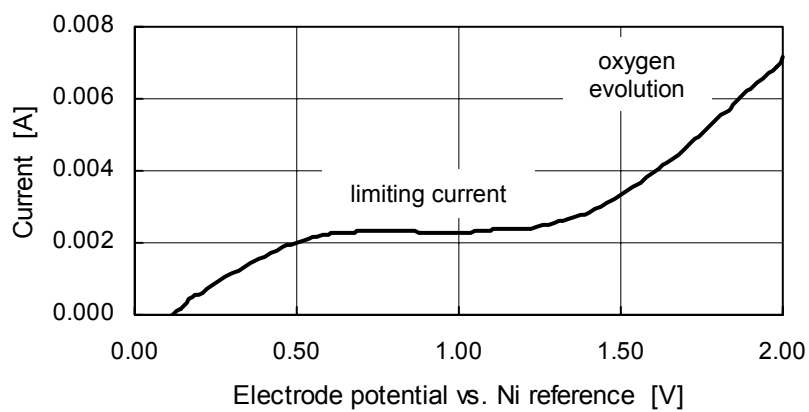


**Figure 6.2.** Typical example of a potential-current curve showing the limiting current plateau

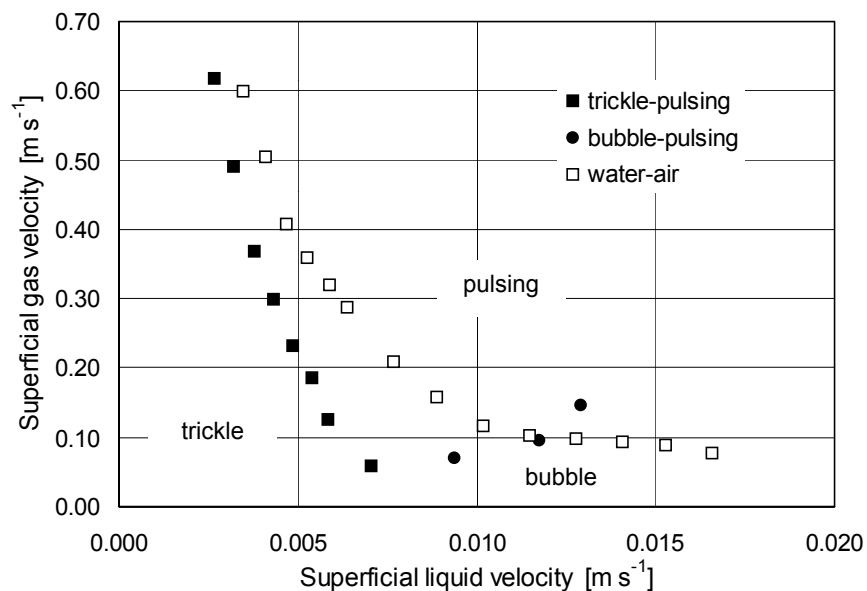


**Figure 6.3.** Transition boundaries in terms of superficial gas and liquid velocities for the water-air, respectively  $\text{Na}_2\text{SO}_4$ -solution-air system (solid markers:  $\text{Na}_2\text{SO}_4$ -solution; open markers: water)

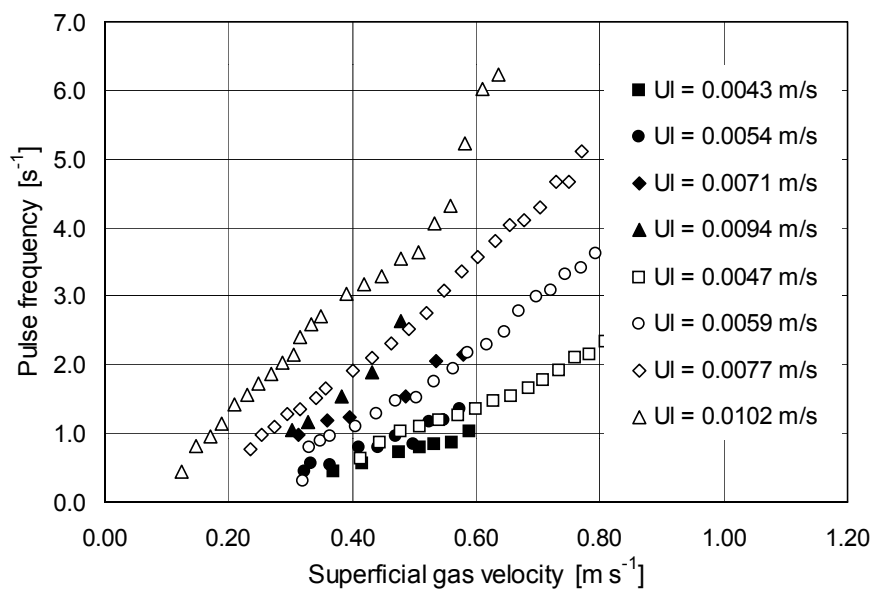


**Figure 6.4.** Pulse frequency versus superficial gas velocity (solid markers:  $\text{Na}_2\text{SO}_4$ -solution; open markers: water)

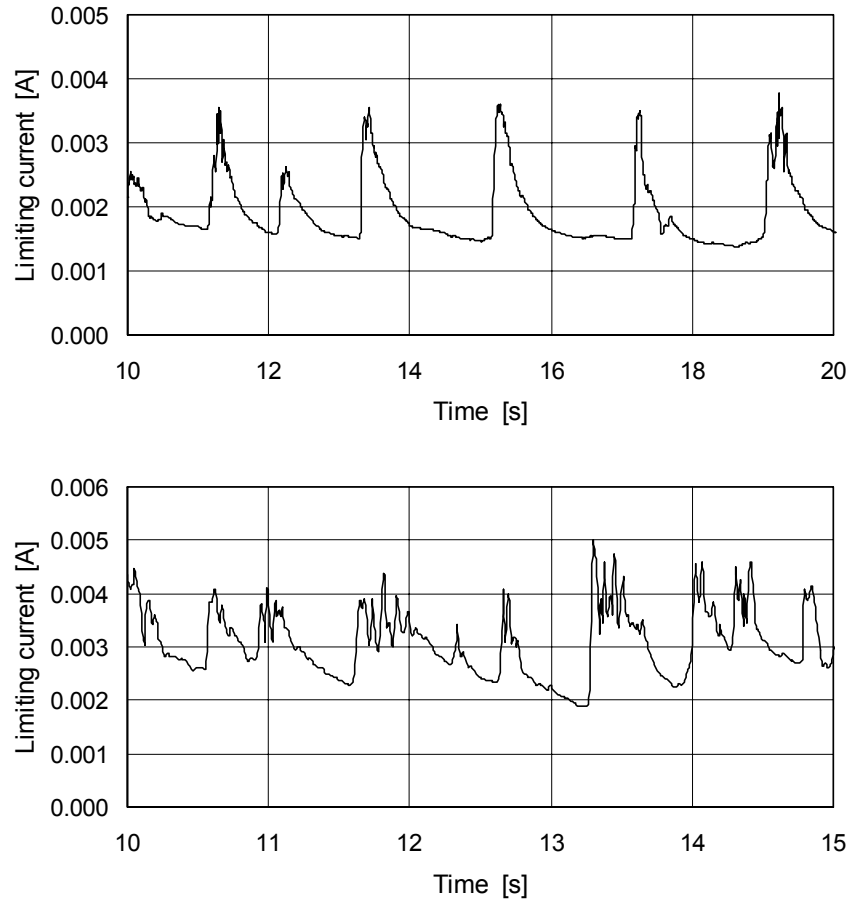


**Figure 6.5.** Typical examples of recorded mass transfer traces during pulsing flow (a:  $U_l = 0.0054 \text{ m s}^{-1}$ ;  $U_g = 0.36 \text{ m s}^{-1}$ ; b:  $U_l = 0.0071 \text{ m s}^{-1}$ ;  $U_g = 0.35 \text{ m s}^{-1}$ ).

The pulsing flow regime shifts to significantly lower liquid velocities when the liquid viscosity and density are increased (Talmor, 1977; Tosun, 1984). Regarding the effect of surface tension, disagreement in the reported studies exists (e.g. Iliuta et. al., 1999). Possibly, such is caused by dynamic surface tension differences (Zuiderweg and Harmens, 1958). The pulse frequency versus the superficial gas velocity for both systems is presented in Fig. 6.4. In case of water as liquid, considerably higher pulse frequencies are observed. Tsochatzidis et. al., (1998) report that pulse frequency decreases with increasing viscosity.

Typical traces representing local mass transfer coefficient during pulsing flow are presented in Fig. 6.5. The pulse front is characterized by a steep increase in the mass transfer rate. Tsochatzidis and Karabelas (1994) noticed that the drop in liquid holdup at the back of the pulse is much steeper than the drop in mass transfer rates. Apparently, the anodes experience a prolonged effect of the high mass transfer rates due to the pulses. At relatively high gas flow rates, pulses as large as 0.5 m in length are visually observed.

## 6.5. Time-average mass transfer coefficient

### 6.5.1. Average mass transfer coefficient

Particle-liquid mass transfer coefficients, averaged in time and position, versus the superficial gas velocity are presented in Fig. 6.6. Mass transfer coefficients increase both with increasing gas and liquid flow rate. In the trickle flow regime, the effect of the gas flow rate is rather weak. The transition to the pulsing and bubble flow regimes, results in a substantial increase in the average mass transfer rates. The highest particle-liquid mass transfer rates are encountered in the bubble flow regime.

Particle-liquid heat transfer rates were successfully correlated in terms of the linear liquid velocity (Chapter 3). To calculate the linear liquid velocity, knowledge of the liquid holdup is required. For this purpose, several published liquid holdup correlations are used. The correlations were chosen based on two criteria. The liquid holdup correlation should satisfactorily predict the measured liquid holdup for the air-water system, presented in chapter 2. Additionally, the correlations must account for the effect of the liquid physical properties. A plot of the particle-liquid mass transfer coefficient versus the linear liquid velocity ( $U_l/\beta$ ) is presented in Fig. 6.7. For all correlations used, the mass transfer coefficient seems to be completely governed by the linear liquid velocity. The particle-liquid mass transfer coefficients correlate with the linear liquid velocity of which the power varies between 0.7 and 0.9, depending on the applied liquid holdup correlation. For particle-liquid heat transfer coefficients, a power of 0.8 was found.

### 6.5.2. Mass transfer coefficients in trickle flow

The mass transfer coefficients obtained in the trickle flow regime are compared to a number of published correlations in Fig. 6.8. Obviously, a large scatter in the mass transfer coefficient, predicted by the several correlations exists.

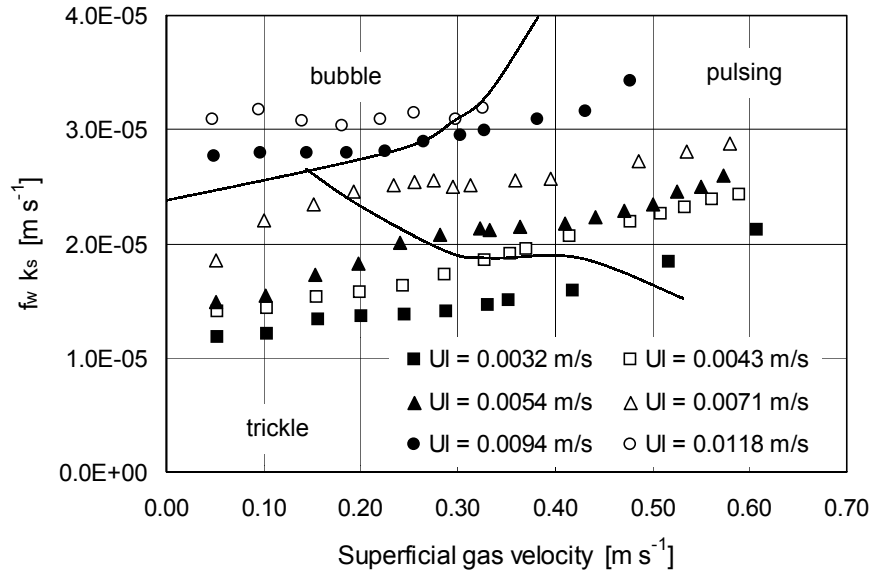


**Figure 6.6.** Average particle-liquid mass transfer coefficient versus the superficial gas velocity

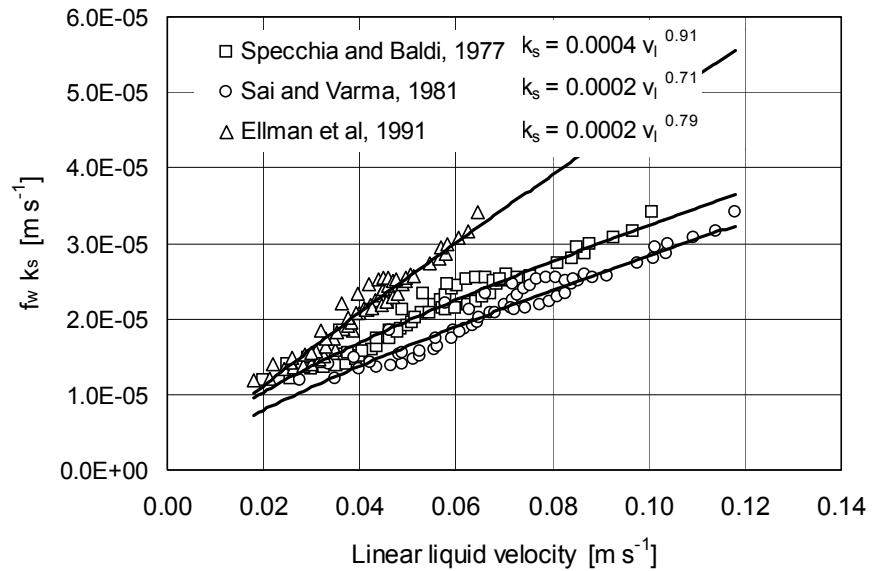


**Figure 6.7.** Mass transfer coefficient versus the linear liquid velocity calculated on the basis of several liquid holdup correlations

However, a trend is recognized when the predicted mass transfer coefficients are compared to the Sc-numbers characterizing the experimental system in which the data were obtained. The lowest mass transfer coefficients are predicted by the correlations measured for systems characterized by the highest Sc-numbers, while the highest mass transfer coefficients are predicted by the correlations obtained for systems characterized by the lowest Sc-numbers. Apparently, the effect of the Sc-number is not correctly accounted for in the several correlations. Mass transfer coefficients measured by the dissolution technique are generally associated with large Sc-numbers since the components used to measure mass transfer rates (e.g. benzoic acid) are characterized by relatively small diffusion coefficients. Mass transfer coefficients determined by the electrochemical method are generally associated with relatively large diffusion coefficients (except the correlation of Latifi et. al., 1988, who applied the electrochemical technique in an organic liquid phase).

### 6.5.3. Correlation of results

Particle-liquid mass transfer coefficients seem to be entirely governed by the linear liquid velocity calculated on the basis of several published liquid holdup correlations. However, the applicability of these liquid holdup correlations to systems with different physical properties as for which they were obtained, may be questioned. This is clearly shown in Fig. 6.7, in which a considerable difference in calculated linear liquid velocity is noticed for the three liquid holdup correlations tested. Consequently, attempts should be made to find the relation between the mass transfer coefficient and external well-known parameters such as gas and liquid flow rates and packing properties. The mass transfer data in the trickle, pulsing and bubble flow regime are satisfactorily correlated by:

$$\frac{f_w \text{Sh}}{\text{Sc}^{1/3}} = 0.84 \text{Re}_l^{0.63} \text{Re}_g^{0.21} \quad [6.2]$$

A comparison of the proposed correlation with the experimental data is presented in Fig. 6.9. The correlation represents the mass transfer coefficients obtained in all flow regimes. Usually one encounters different correlations for different flow regimes. The gas and liquid flow rates characterizing the transition boundaries separating the several flow regimes strongly depend on the fluid physical properties and packing characteristics. Equation 6.2 can be applied without a priori knowledge of the prevailing flow regime at a given set of gas and liquid flow rates.

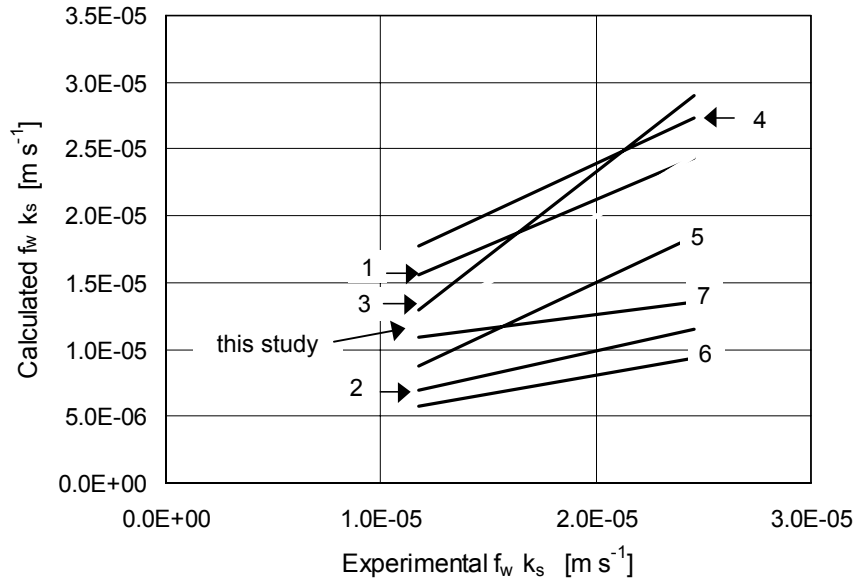


**Figure 6.8.** Comparison between experimentally determined mass transfer coefficient during trickle flow with a number of published correlations (1: Burghardt et. al, 1995:  $Sc = 1560$ ; 2: Goto et. al., 1975:  $Sc = 14124$ ; 3: Yoshikawa et. al., 1981:  $Sc = 334$ ; 4: Tan and Smith, 1982:  $Sc = 974$ ; 5: Satterfield et. al., 1978:  $Sc = 10000$ ; 6: Latifi et. al., 1988:  $Sc = 40921$ ; 7: Lakota and Levec, 1990:  $Sc = 14124$ )

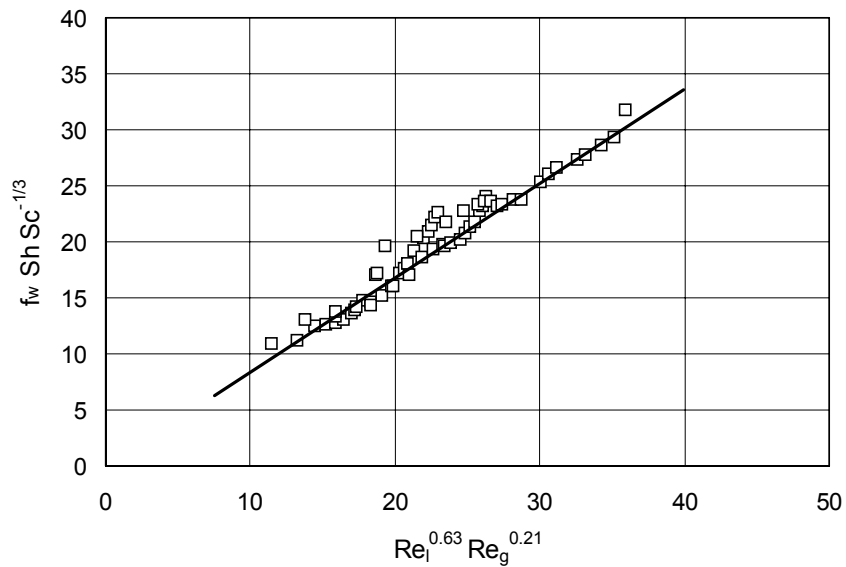


**Figure 6.9.** Comparison of experimental and correlated particle-liquid mass transfer data for trickle, pulsing and bubble flow



## 6.6. Mass transfer coefficients in pulsing flow

### 6.6.1. Pulse and base mass transfer coefficient

The maximum mass transfer coefficient inside the pulse and the mass transfer coefficient in between pulses (base) is plotted in Fig. 6.10. The base mass transfer coefficient is unaffected by both gas and liquid flow rates. The pulse mass transfer coefficient increases with both gas and liquid velocity, although it seems that at high gas velocities, the effect of the liquid flow rate diminishes. The pulse mass transfer coefficient is about 2 to 3 times higher than the base mass transfer coefficient. The same ratio is obtained for heat transfer coefficients as reported in chapter 3.

A comparison of the measured mass transfer coefficients during pulsing flow with a number of published correlations is presented in Fig. 6.11. The correlations predict higher values. The correlations are based on mass transfer coefficients obtained with NaOH as supporting electrolyte. In Table 6.1 it is shown that the physical properties of this solution are comparable to water, except for gas-liquid surface tension. Lower viscosities result in higher pulse frequencies. Therefore the pulse frequency in these systems is probably larger than for Na<sub>2</sub>SO<sub>4</sub> as electrolytic solution. Higher pulse frequencies lead to higher time-average mass transfer coefficients. Unfortunately, no data on pulse frequency were reported. Although the correlations were obtained for identical electrolytic solutions, different diffusion coefficients were used to establish the correlations (Rao and Drinkenburg, 1985:  $D = 5.5 \cdot 10^{-10} \text{ m}^2 \text{ s}^{-1}$ ; Chou et. al., 1979:  $D = 6.7 \cdot 10^{-10} \text{ m}^2 \text{ s}^{-1}$ ; Burghardt et. al., 1995:  $D = 7.06 \cdot 10^{-10} \text{ m}^2 \text{ s}^{-1}$ ). This largely influences the Sh and Sc numbers used to propose correlations for their experimental results. Additionally, Rao and Drinkenburg (1985) and Chou et. al. (1979) used air as the gas-phase and applied a cathodic working electrode. Since the liquid is continuously recycled, it is saturated with oxygen. In the appendix to this chapter it is shown that for a cathodic working electrode, oxygen reduction leads to serious overprediction of mass transfer coefficients.

### 6.6.2. Penetration theory

While numerous empirical correlations exist, which permit the determination of mass transfer coefficients in trickle-bed reactors, it is nevertheless of interest to explore these events from a theoretical point of view.

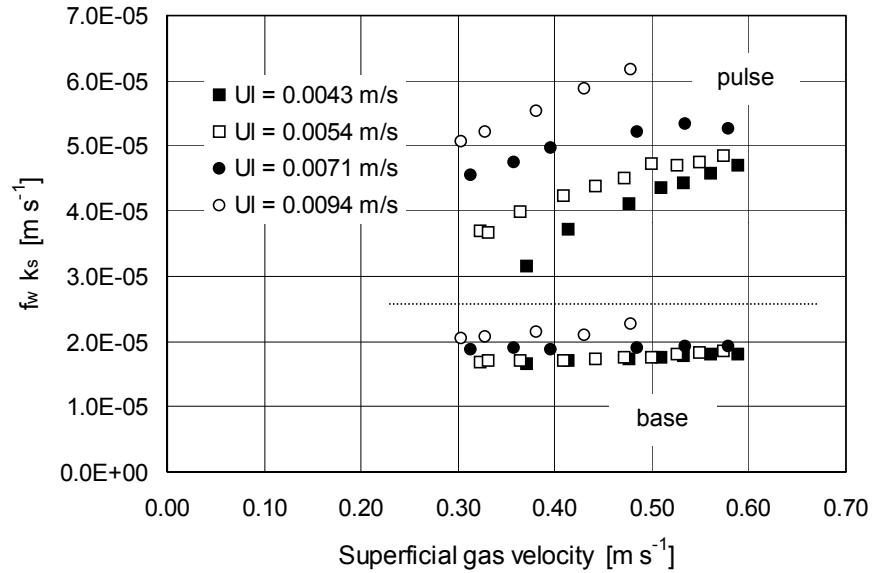


**Figure 6.10.** Pulse and base particle-liquid mass transfer coefficients versus the superficial gas velocity

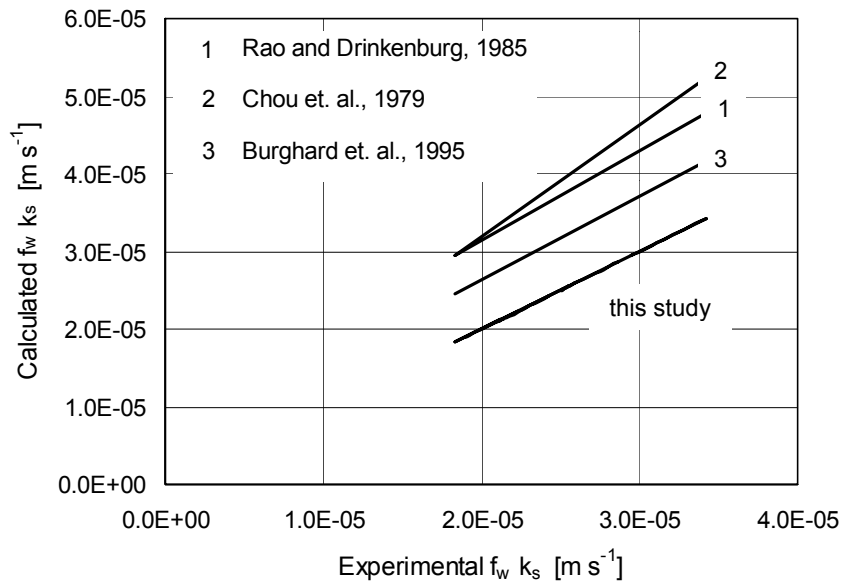


**Figure 6.11.** Comparison between experimentally determined particle-liquid mass transfer coefficient during pulsing flow with a number of published correlations

The penetration theory relates the average mass transfer coefficient to the diffusivity ( $D$ ) and the average time of fluid element exposure to sink or source ( $\tau$ ) by:

$$k_s = 2 \sqrt{\frac{D}{\pi\tau}} \quad [6.3]$$

For pulsing flow, the average time that a fluid element is exposed to direct contact with the anode may be estimated by the reciprocal pulse frequency. Each time a pulse passes, the fluid element is incorporated into the bulk liquid and a new fluid element is transferred to the surface of the anode. A comparison between theoretical and experimentally determined mass transfer coefficients is presented in Fig. 6.12. Penetration theory reasonably predicts the measured time-average mass transfer coefficients. Penetration theory can be applied for heat transfer coefficients also:

$$\alpha_p = 2 \sqrt{\frac{\lambda \rho c_p}{\pi\tau}} \quad [6.4]$$

A plot of the measured heat transfer coefficient obtained from chapter 3 versus the theoretical heat transfer coefficient is shown in Fig. 6.13. Especially at the higher pulse frequencies, a satisfactory agreement exists for theoretical and experimentally determined heat transfer coefficients.

Penetration theory assumes that the fluid element exposed to the source or sink is regarded as semi-infinite, which means that the final penetration depth of the diffusing species in the fluid element during the contact time must be smaller than the thickness of the fluid element. The pulse frequencies at which penetration theory may be applied can be estimated for respectively mass and heat transfer by:

$$Fo_{mt} = \frac{D}{f_p \delta^2} < 0.1 \quad [6.5]$$

$$Fo_{ht} = \frac{a}{f_p \delta^2} < 0.1 \quad [6.6]$$

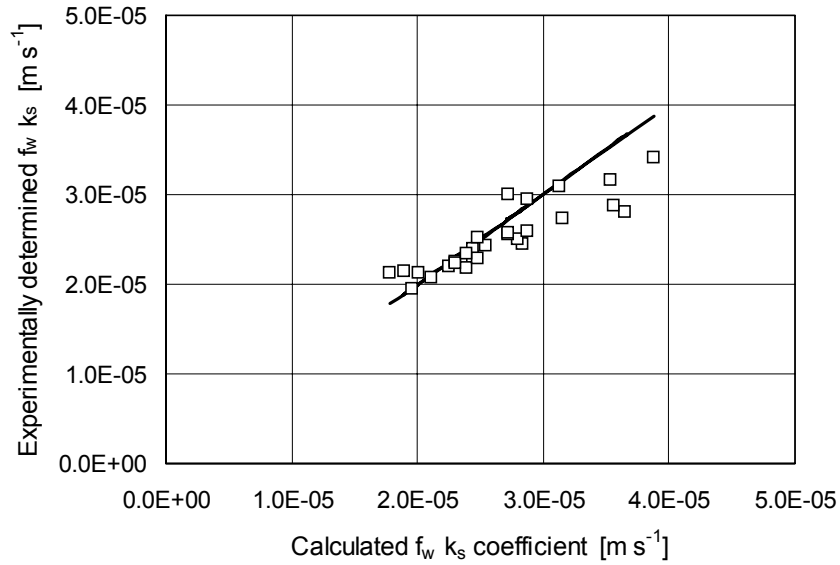


**Figure 6.12.** Comparison between experimentally determined and calculated mass transfer coefficient during pulsing flow

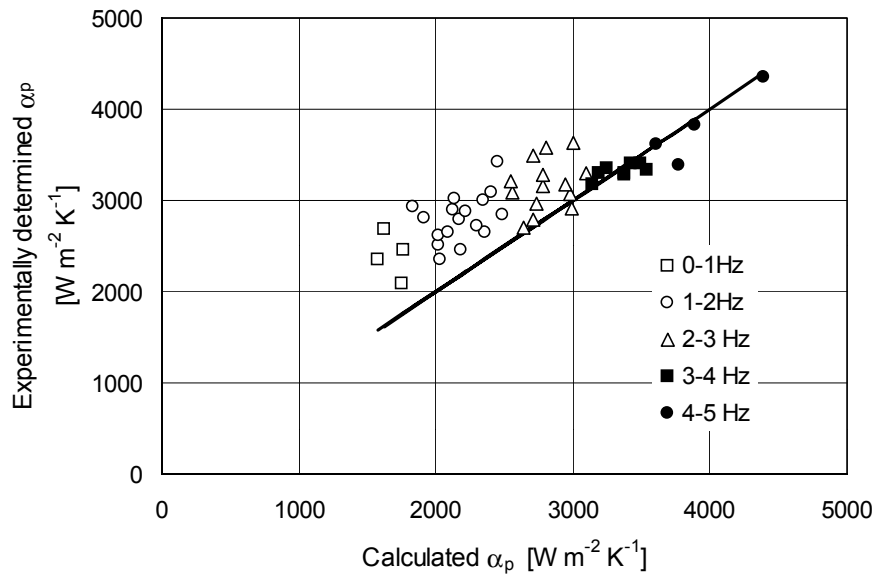


**Figure 6.13.** Comparison between experimentally determined and calculated heat transfer coefficient during pulsing flow at various pulse frequencies

In equations 6.5 and 6.6,  $\delta$  is the thickness of the fluid elements,  $f_p$  the pulse frequency and  $a$  is the thermal diffusivity. In case the thickness of the fluid element is estimated by dividing the liquid holdup by the specific packing area, penetration theory may be applied for mass transfer during pulsing flow at pulse frequencies higher than 0.1 Hz and for heat transfer at pulse frequencies higher than 20 Hz. The difference between the critical pulse frequency for heat and mass transfer arises because of the relatively high thermal diffusivity compared to mass diffusivity. Nevertheless, at pulse frequencies less than 20 Hz, penetration theory reasonably predicts heat transfer coefficients during pulsing flow. For organic liquids, thermal diffusivities are about one order of magnitude less compared to the thermal diffusivity of water. The concept of penetration is therefore expected to hold better for particle-liquid heat transfer in organic liquids, since equation 6.6 then holds for lower pulse frequencies.

## 6.7. Heat and mass transfer analogy

### 6.7.1. Chilton-Colburn analogy

Instead of performing both heat and mass transfer measurements, an analogy can be used to calculate the heat transfer coefficient from the mass transfer coefficient, or vice versa. The Chilton-Colburn analogy, based on boundary layer theory, is most popular and states that:

$$\frac{Sh}{Sc^{1/3}} = \frac{Nu}{Pr^{1/3}} \quad [6.7]$$

The analogy between mass and heat transfer rates is tested for the air-water system. The proposed mass transfer correlation is used to calculate the heat transfer coefficients conform the Chilton-Colburn analogy. The calculated heat transfer coefficients are compared to the experimentally determined heat transfer coefficients in Fig. 6.14. The predicted heat transfer coefficients are much higher than the experimentally determined heat transfer coefficients.

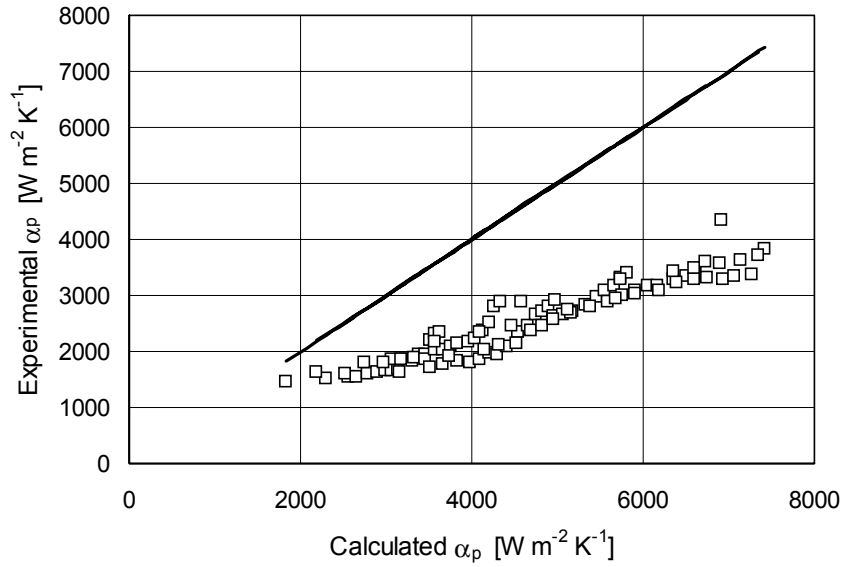


**Figure 6.14.** Experimentally determined heat transfer coefficient versus calculated (Chilton-Colburn analogy) heat transfer coefficient

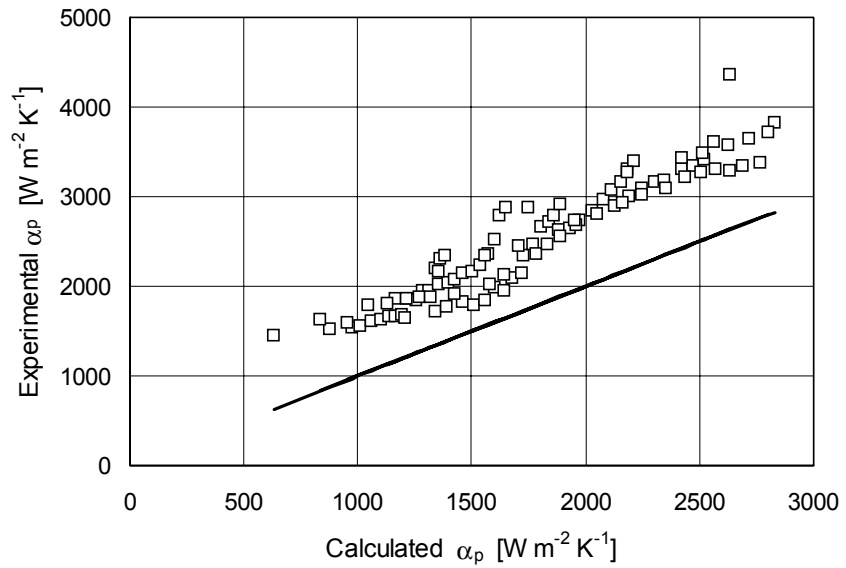


**Figure 6.15.** Experimentally determined heat transfer coefficient versus calculated (penetration theory) heat transfer coefficient

### 6.7.2. Penetration theory

The analogy between mass and heat transfer in trickle-bed reactors may be extracted from penetration theory. For this purpose it is assumed that penetration theory may also be applied as an approximation in the trickle flow regime for mass and heat transfer. The concept of surface renewal due to the pulses is then replaced by that of laminar liquid, which mixes at discontinuities in the packing. The analogy between heat and mass transfer may then be formulated as:

$$\frac{Sh}{Sc^{1/2}} = \frac{Nu}{Pr^{1/2}} \quad [6.8]$$

The analogy between mass and heat transfer based on the penetration theory is tested for the air-water system by applying the proposed mass transfer correlation to calculate the heat transfer coefficient. The calculated heat transfer coefficient is compared to the experimentally determined heat transfer coefficient in Fig. 6.15. The experimentally determined heat transfer coefficients are approximately 25% higher than the calculated heat transfer coefficients. Nevertheless, the analogy between heat and mass transfer based on penetration theory outperforms the Chilton-Colburn analogy.

## 6.8. Distribution of local mass transfer coefficients

In Fig. 6.16, the local mass transfer coefficients in the pulsing flow regime are plotted against the average mass transfer coefficient. Obviously, there exists a large spread in local particle-liquid mass transfer coefficients in the pulsing flow regime. Local differences during pulsing flow are somewhat smaller than during trickle flow. Local differences in the base mass transfer coefficients are somewhat larger than local differences in the pulse mass transfer coefficient. Still, substantial differences in the local mass transfer coefficient inside the pulses exist. However, all the anodes strongly sense the fluctuations in mass transfer due to the pulses.

Local differences in mass transfer coefficients in the trickle flow regime are usually attributed to differences in wetting efficiency. Wetting inside pulses is generally assumed to be complete. Still substantial differences in local mass transfer coefficients exist in the pulsing flow regime.

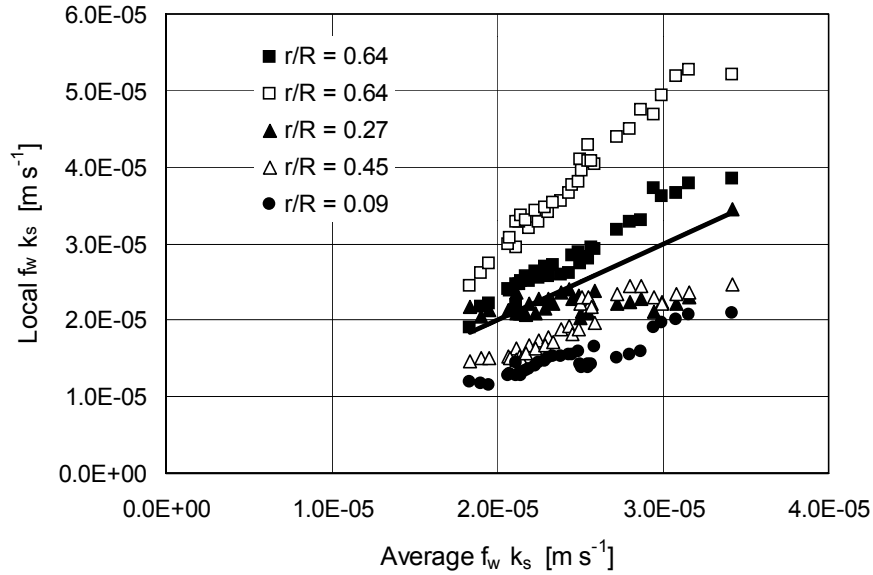


**Figure 6.16.** Local particle-liquid mass transfer coefficient versus average particle-liquid mass transfer coefficient in the pulsing flow regime

Therefore, it seems appropriate to attribute these differences to the local porosity around the sensor. The local bed voidage determines the linear liquid velocity around the probes. Gabitto and Lemcoff (1987) for example measured differences of 300% in local liquid velocities during pulsing flow and accordingly large variations in local mass transfer rates. Local voidage consists of large pore chambers ( $d_{pc}$ ) and small pore throats ( $d_{pt}$ ), of which the approximate diameters can be calculated by (Ng, 1986):

$$d_{pc} = \sqrt[3]{\frac{\epsilon}{1-\epsilon}} d_p \cong 5 \text{ mm} \quad [6.9]$$

$$d_{pt} = \sqrt{\frac{2}{\pi} \sin \frac{\pi}{3} - 0.5} d_p \cong 1.3 \text{ mm} \quad [6.10]$$



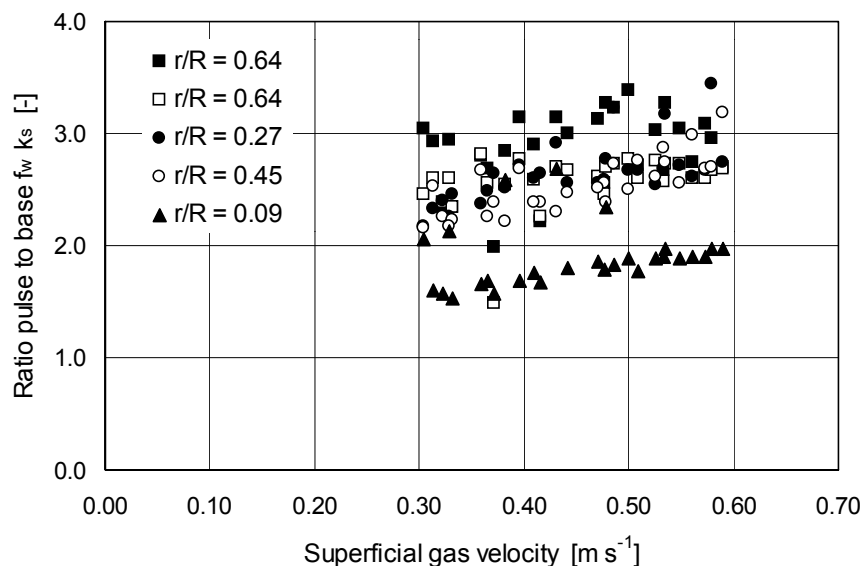


**Figure 6.17.** Ratio of pulse to base mass transfer coefficient at various positions in the bed in the pulsing flow regime.

It is visualized that when the anode is beneath some pore throats, less liquid reaches the anode than when it is surrounded by large pore chambers. Therefore, not only differences in average particle-liquid mass transfer coefficients exist, but also differences in the ratio of pulse to base mass transfer are expected to occur. The ratio of pulse to base mass transfer coefficients for all anodes is plotted in Fig. 6.17. There is a substantial difference in the ratio of pulse to base mass transfer for the several probes. Apparently, each probe experiences the pulse differently. Tsochatzidis and Karabelas (1994) and Sims et. al. (1993) also found substantial differences in the ratio of pulse to base mass transfer coefficients. Since each anode strongly senses the pulses, pulses are macroscopically uniform. On the particle scale, however, pulses are characterized by substantial non-uniformities.

## 6.9. Concluding remarks

Particle-liquid mass transfer coefficients during trickle, bubble and pulsing flow are determined. Pulsing and bubble flow result in considerably higher particle-liquid mass transfer coefficients than trickle flow.

The pulse mass transfer coefficient is 2 to 3 times higher than the base mass transfer coefficient. The linear liquid velocity governs mass transfer coefficients in all flow regimes. The data are correlated based on the superficial gas and liquid flow rates. This correlation can be applied for all flow regimes.

Literature correlations predict both lower and higher mass transfer coefficients in trickle flow than determined in this study. However, this scatter in data is not random. Correlations proposed for system characterized by high Sc-numbers predict far lower particle-liquid mass transfer rates than correlations proposed for systems characterized by low Sc-numbers.

The hydrodynamics for the electrolytic solution greatly differ from the hydrodynamics for the air-water system. Both the trickle-pulsing and the trickle-bubble transition boundaries are shifted towards much lower liquid flow rates. Additionally, pulse frequency is about 1.5 times less than for the air-water system. Since pulse frequency strongly depends on the liquid physical properties, care must be taken in applying correlations for mass transfer in the pulsing flow regime. The pulse frequency is implicitly included in these correlations. Pulse frequency strongly determines time-average particle-liquid mass transfer rates.

Pulses are macroscopically uniform since the mass transfer fluctuations due to the pulses are strongly sensed by all the anodes situated at different radial positions in the bed. Even in the pulsing flow regime, large differences in local mass transfer coefficients exist. This is attributed to non-uniformities in local voidage distribution. On the particle level, pulses are not uniform.

The penetration theory is useful in calculating both particle-liquid heat and mass transfer coefficients during pulsing flow. Additionally, the analogy between heat and mass transfer rates in all flow regimes proposed by penetration theory outperforms the Chilton-Colburn analogy.

## Notation

$a$	thermal diffusivity ( $\lambda_l \rho_l^{-1} c_{pl}^{-1}$ )	$[\text{m}^2 \text{s}^{-1}]$
$a_p$	surface area anode	$[\text{m}^2]$
$a_s$	specific packing area	$[\text{m}^{-1}]$
$C_1$	bulk concentration electrochemical active species	$[\text{mol m}^{-3}]$
$c_{pl}$	liquid specific heat	$[\text{J kg}^{-1} \text{K}^{-1}]$
$D$	diffusion coefficient	$[\text{m}^2 \text{s}^{-1}]$
$d_p$	particle diameter	$[\text{m}]$

$d_{pc}$	diameter pore chamber	[m]
$d_{pt}$	diameter pore throat	[m]
$I_l$	limiting current	[A]
$f_p$	pulse frequency	[s <sup>-1</sup> ]
F	Faraday constant	[C mol <sup>-1</sup> ]
Fo	Fourier number (defined by eq. 6.10 and 6.11)	[-]
$f_w$	wetting efficiency	[-]
$k_s$	particle-liquid mass transfer coefficient	[m s <sup>-1</sup> ]
Nu	Nusselt number ( $\alpha_p d_p \lambda_l^{-1}$ )	[-]
Pr	Prandtl number ( $c_{pl} \mu_l \lambda_l^{-1}$ )	[-]
Re <sub>g</sub>	gas Reynolds number ( $U_g \rho_g d_p \mu_g^{-1}$ )	[-]
Re <sub>l</sub>	liquid Reynolds number ( $U_l \rho_l d_p \mu_l^{-1}$ )	[-]
Sc	Schmidt number ( $\mu_l \rho_l^{-1} D^{-1}$ )	[-]
Sh	Sherwood number ( $k_s d_p D^{-1}$ )	[-]
$U_g$	superficial gas velocity	[m s <sup>-1</sup> ]
$U_l$	superficial liquid velocity	[m s <sup>-1</sup> ]
$\alpha_p$	particle-liquid heat transfer coefficient	[W m <sup>-2</sup> K <sup>-1</sup> ]
$\beta$	total liquid holdup	[-]
$\delta_l$	thickness total liquid film	[m]
$\varepsilon$	bed porosity	[-]
$\lambda_l$	liquid thermal conductivity	[W m <sup>-1</sup> K <sup>-1</sup> ]
$\mu_l$	viscosity	[Pa s]
$\rho_l$	density	[kg m <sup>-3</sup> ]
$\tau$	characteristic contact time	[s]

### Literature cited

- Brett C.M.A. and Brett A.M.O., *Electrochemistry*, Oxford University Press, 1993
- Burghardt A., Bartelmus G., Jaroszynski M. and Kolodziej A., Hydrodynamics and mass transfer in a three-phase fixed-bed reactor with cocurrent gas-liquid downflow, *Chem. Eng. J.*, **58**, 83-99, 1995
- Chou T.S., Worley F.J. and Luss D., Local particle-liquid mass transfer fluctuations in mixed-phase cocurrent downflow through a fixed bed in the pulsing regime, *Ind. Eng. Chem. Fund.*, **18**, 279-283, 1979
- Dharwadkar A. and Sylvester N.D., Liquid-solid mass transfer in trickle beds, *AIChE J.*, **23**, 376-378, 1977

## Local particle-liquid mass transfer coefficient

---

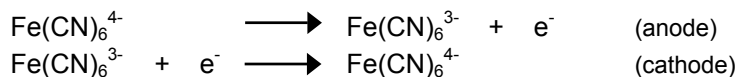
- Ellman M.J., Midoux G., Wild G., Laurent A. and Charpentier J.C., A new improved liquid holdup correlation for trickle bed reactors, *Chem. Eng. Sci.*, 45, 1677-1684, 1990
- Gabitto J.F. and Lemcoff N.O., Local solid-liquid mass transfer coefficients in a trickle-bed reactor, *Chem. Eng. J.*, 35, 69-74, 1987
- Goto S., Levec J. and Smith J.M., Mass transfer in packed beds with two-phase flow, *Ind. Eng. Chem. Proc. Des. Dev.*, 14, 473-478, 1975
- Hiraoka S., Yamada I., Ikeno H., Asano H., Nomura S., Okada T. and Nakamura H., Measurement of diffusivities of ferricyanide and ferrocyanide ions in dilute solution with KOH supporting electrolyte, *J. Chem. Eng. Jap.*, 14, 345-351, 1981
- Hodgman C.D., Weast R.C. and Lide D.R., *CRC handbook of chemistry and physics*, 79th ed., McGraw-Hill, New York, 1962
- Iliuta I., Ortiz-Arroyo A., Larachi F., Grandjean B.P.A. and Wild G., Hydrodynamics and mass transfer in trickle-bed reactors: an overview, *Chem. Eng. Sci.*, 54, 5329-5337, 1999
- Lakota A. and Levec J., Solid-liquid mass transfer in packed beds with cocurrent downward two-phase flow, *AIChE J.*, 36, 1444-1448, 1990
- Latifi M.A., Laurent A. and Storck A., Liquid-solid mass transfer in a packed bed with downward cocurrent gas-liquid flow: an organic liquid phase with high Schmidt number, *Chem. Eng. J.*, 38, 47-56, 1988
- Lemay Y., Pineault G. and Ruether J.A., Particle-liquid mass transfer in a three-phase fixed bed reactor with cocurrent flow in the pulsing regime, *Ind. Eng. Chem. Proc. Des. Dev.*, 14, 280-285, 1975
- Mizushima J., *Adv. Heat Transfer*, 7, 87-161, 1971
- Ng K.M., A model for flow regime transitions in cocurrent down-flow trickle-bed reactors, *AIChE J.*, 32, 115-122, 1986
- Perry R.H., Green D.W. and O Maloney J.G., *Perry's chemical engineers handbook*, 7th ed., McGraw-Hill, New York, 1997
- Rao V.G. and Drinkenburg A.A.H., Solid-liquid mass transfer in packed beds with cocurrent gas-liquid downflow, *AIChE J.*, 31, 1059-1068, 1985
- Ruether J.A., Yang C.S. and Hayduk W., Particle mass transfer during cocurrent downward gas-liquid flow in packed beds, *Ind. Eng. Chem. Proc. Des. Dev.*, 19, 103-107, 1980
- Sai P.S.T. and Varma Y.B.G., Flow pattern of the phases and liquid saturation in cocurrent downflow through packed beds, *Can. J. Chem. Eng.*, 60, 353-360, 1988
- Satterfield C.N., Liquid-solid mass transfer in packed beds with downward concurrent gas-liquid flow, *AIChE J.*, 24, 709-717, 1978
- Selman J.R. and Tobias C.W., *Advances in chemical engineering*, 10, Academic Press, New York, 211-318, 1978
- Sims W.B., Schulz F.G. and Luss D., Solid-liquid mass transfer to hollow pellets in a trickle bed, *Ind. Eng. Chem. Res.*, 32, 1895-1903, 1993
- Specchia V. and Baldi G., Pressure drop and liquid holdup for two-phase cocurrent downflow in packed beds, *Chem. Eng. Sci.*, 32, 515-523, 1977
- Talmor E., Two-phase downflow through packed beds. Part I: Flow maps, *AIChE J.*, 23, 868-874, 1977
- Tan C.S. and Smith J.M., A dynamic method for liquid-particle mass transfer in trickle beds, *AIChE J.*, 28, 190-195, 1982

- 
- Tosun G., A study of cocurrent downflow of nonfoaming gas-liquid systems in a packed bed. Part I. Flow regimes: Search for a generalized flow map, *Ind. Eng. Chem. Proc. Des. Dev.*, 23, 29-35, 1984
- Tsochatzidis N.A. and Karabelas A.J., Study of pulsing flow in a trickle bed using the electrodiffusion technique, *J. Appl. Electrochem.*, 24, 670-675, 1994
- Tsochatzidis N.A., Ntampeglitis K.I. and Karabelas A.J., Effect of viscosity on hydrodynamic properties of pulsing flow in trickle beds, *Chem. Eng. Commun.*, 166, 137-156, 1998
- Vazquez G., Alvarez E., Varela R., Cancela A. and Navaza J.M., Density and viscosity of aqueous solutions of sodium dithionite, sodium hydroxide, sodium dithionate + sucrose, and sodium dithionite + sodium hydroxide + sucrose from 25°C to 40°C, *J. Chem. Eng. Data*, 41, 244-248, 1996
- Washburn E.W., West C.J. and Bichowski F.R., *International critical tables of numerical data, physics and technology*, McGraw-Hill, New York, 1926
- Yoshikawa M., Iwai K., Goto S. and Teshima H., Liquid-solid mass transfer in gas-liquid cocurrent flows through beds of small packings, *J. Chem. Eng. Jap.*, 14, 444-450, 1981
- Zuiderweg F.I. and Harmens A., Influence of surface phenomena on the performance of distillation columns, *Chem. Eng. Sci.*, 9, 89-108, 1958

## A6. Optimal electrochemical system

### A6.1. Experimental setup

A schematic view of the thermostated electrolysis cell is presented in Fig. A6.1. A Pt rotating disc of 8.0 mm in diameter was used. Rotation rates varied between 4 and 64 rps. The counterelectrode consisted of a Pt-sheet of much larger dimensions than the rotating disc electrode in order to avoid transport limitations at the counterelectrode. The potential of the working electrode is measured as the overpotential with respect to a saturated calomel electrode (SCE). The investigated redox reactions are:



The electrolytic solution contained approximately 0.01 M of both  $\text{K}_3\text{Fe(CN)}_6$  and  $\text{K}_4\text{Fe(CN)}_6$  and 0.5 M NaOH as supporting electrolyte. A supporting electrolyte is necessary to eliminate migration effects and to minimize the ohmic potential drop (Mizushima, 1971; Selman and Tobias, 1978). Current-potential curves were recorded with a digital potentiostat (Autolab, PGSTAT20, EcoChemie). Negative current densities indicate a cathodic working electrode while positive current densities indicate an anodic working electrode.

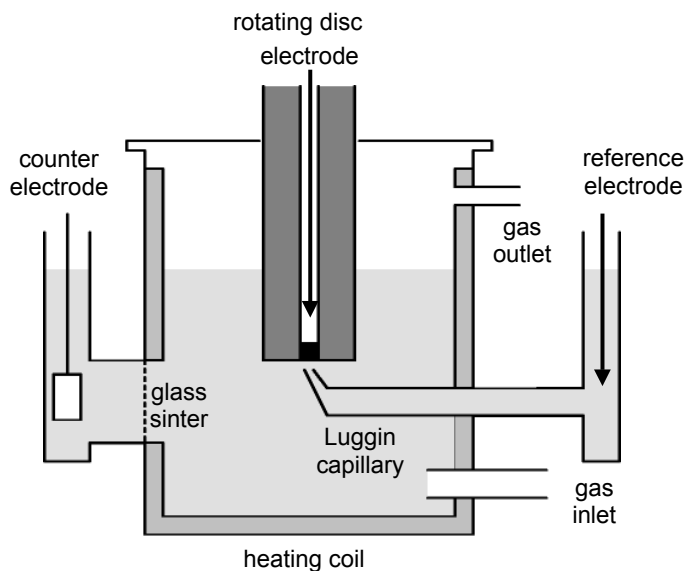


**Figure A6.1.** Schematic illustration of the rotating disc equipment

**A6.2. Effect of dissolved oxygen and supporting electrolyte**

The potential-current curves at various rotation speeds are plotted in Fig. A6.2. Limiting current plateaus are clearly visible. Higher disc rotation rates result in higher limiting currents since mass transfer is enhanced by rotation. At electrode potentials of approximately 0.6 V and -1.2 V, the effect of oxygen respectively hydrogen evolution becomes noticeable. In case the working electrode is cathodic, a shift in the limiting current plateau towards higher currents is observed at potentials below -0.3 V. This is the effect of reduction of dissolved oxygen. The following reaction occurs at the cathodic working electrode:



To substantiate the effect of dissolved oxygen, a reference experiment with a 0.5 M NaOH solution (no ferri/ferrocyanide) was conducted. The resulting potential-current curves are presented in Fig. A6.3. Obviously, the reduction of dissolved oxygen at the cathodic working electrode becomes significant below electrode potentials of -0.3 V.

The important assumption when measuring mass transfer is that the limiting current is a direct measure of the mass transfer rate of the electrochemical active species towards the working electrode. In case of a cathodic working electrode, the limiting current is the result of both reduction of ferricyanide and dissolved oxygen. Since the reduction of dissolved oxygen needs four electrons instead of one, the direct relationship between the limiting current and the mass transfer rate is unknown (one assumes that every electron participating in the limiting current is due to mass transfer of one ferricyanide ion). Mass transfer coefficients are therefore overestimated (about 20%).

The effect of dissolved oxygen can be eliminated by using an anodic working electrode instead of a cathodic working electrode as observed in Figs. A6.2. and A6.3. However, the limiting current plateau at the anodic working electrode in case of a NaOH-solution is rather narrow, making it more difficult to determine the limiting current. This is probably the reason that every reported study concerning particle-liquid mass transfer in trickle-bed reactors deals with a cathodic working electrode.

The potential at which hydrogen or oxygen evolution occurs at respectively the cathode or anode depends on the pH of the electrolytic solution. When using  $\text{Na}_2\text{SO}_4$  as supporting electrolyte instead of NaOH, the electrolytic solution will be neutral instead of basic.

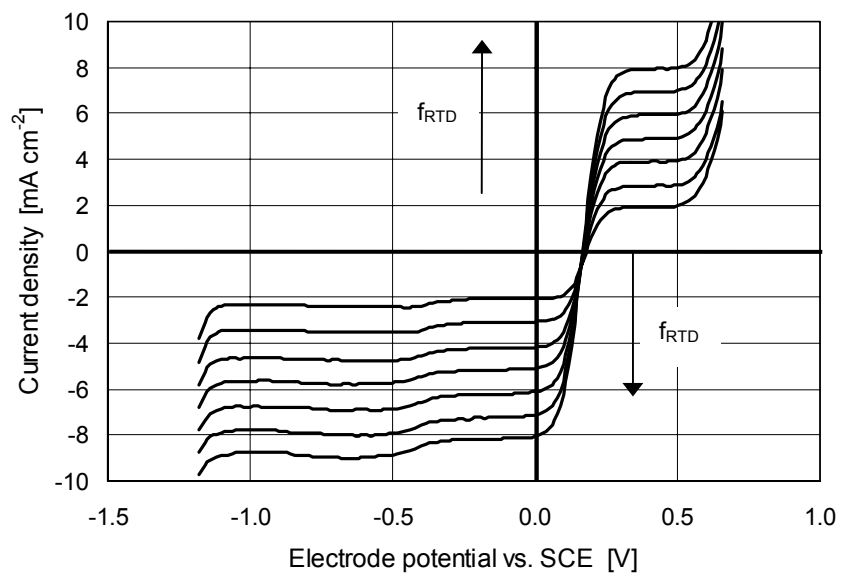


**Figure A6.2.** Potential-current curves for ferri/ferrocyanide in 0.5 M NaOH saturated with oxygen ( $f_{RTD} = 4, 9, 16, 25, 36, 49$  and  $64 \text{ s}^{-1}$ )

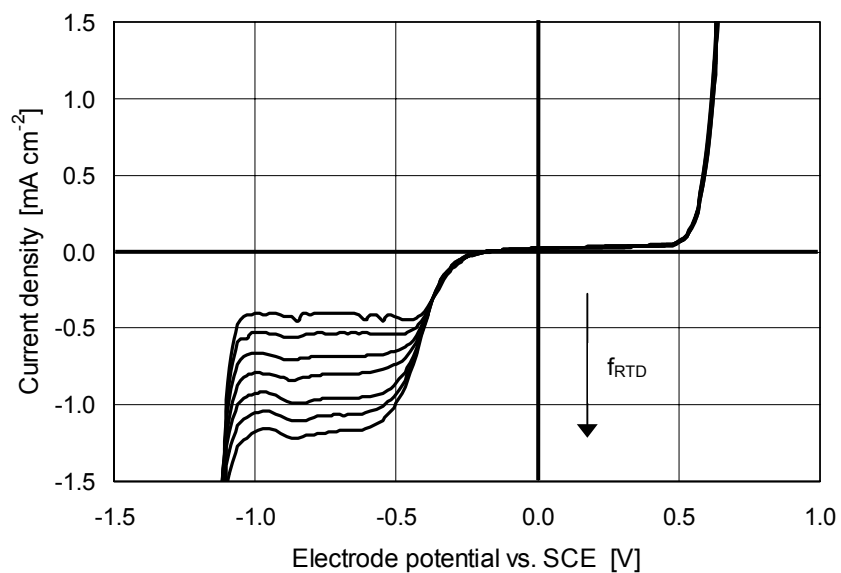


**Figure A6.3.** Potential-current curves for oxygen in 0.5 M NaOH ( $f_{RTD} = 4, 9, 16, 25, 36, 49$  and  $64 \text{ s}^{-1}$ )



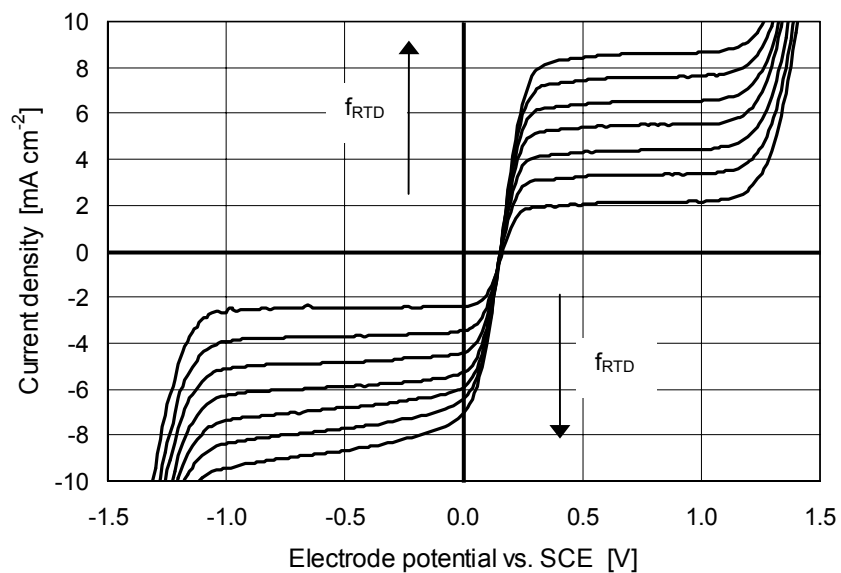


**Figure A6.4.** Potential-current curves for ferri/ferrocyanide in 0.5 M  $\text{Na}_2\text{SO}_4$  saturated with oxygen ( $f_{\text{RTD}} = 4, 9, 16, 25, 36, 49$  and  $64 \text{ s}^{-1}$ )

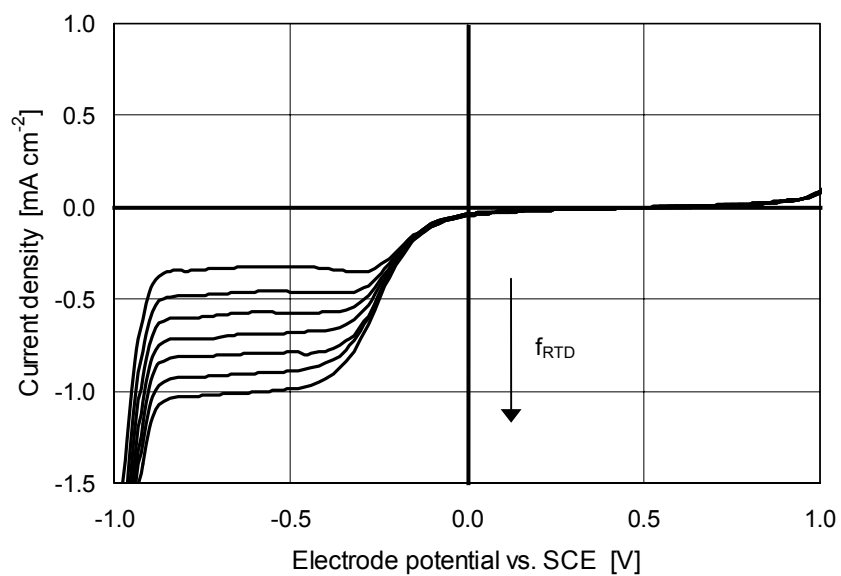


**Figure A6.5.** Potential-current curves for oxygen in 0.5 M  $\text{Na}_2\text{SO}_4$  ( $f_{\text{RTD}} = 4, 9, 16, 25, 36, 49$  and  $64 \text{ s}^{-1}$ )

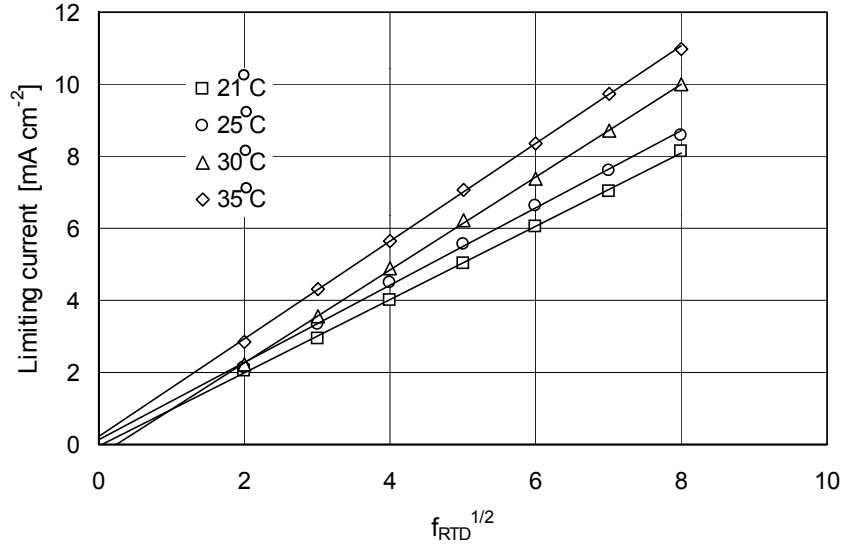


**Figure A6.6.** Limiting current density of ferrocyanide reduction as a function of rotation speed at various temperatures

Oxygen evolution at the anode now occurs at much higher electrode potentials. Hence the limiting current plateau is much broader. The potential-current curves for the solution containing 0.5 M Na<sub>2</sub>SO<sub>4</sub> as supporting electrolyte are presented in Fig. A6.4. The anodic limiting current plateau is much broader than the solution containing NaOH as supporting electrolyte. Moreover, it is difficult to determine the limiting current if the working electrode is cathodic, due to the reduction of dissolved oxygen. The potential-current curves for a 0.5 M Na<sub>2</sub>SO<sub>4</sub> reference solution saturated with oxygen is shown in Fig. A6.5. For electrode potentials below zero, the effect of oxygen reduction is, again, clearly visible.

### A6.3. Diffusion coefficient

At the limiting current plateau, the Levich equation can be applied to calculate the diffusion coefficient (Brett and Brett, 1993):

$$i_L = 0.62 n F D^{2/3} \nu^{-1/6} C_b (2\pi f_{RTD})^{1/2} \quad [A6.1]$$

A plot of  $i_L$  versus  $f_{RTD}^{1/2}$  is linear, as shown in Fig. A6.6 and the slope of the curve can be utilized to calculate the diffusion coefficient.

**Table A6.1.** Diffusion coefficients of ferricyanide and ferrocyanide in 0.5 M NaOH and 0.5 M Na<sub>2</sub>SO<sub>4</sub>.

temperature [K]	$D_{\text{ferri}} [\text{Na}_2\text{SO}_4]$ [ $10^{-10} \text{ m}^2 \text{ s}^{-1}$ ]	$D_{\text{ferro}} [\text{Na}_2\text{SO}_4]$ [ $10^{-10} \text{ m}^2 \text{ s}^{-1}$ ]	$D_{\text{ferri}} [\text{NaOH}]$ [ $10^{-10} \text{ m}^2 \text{ s}^{-1}$ ]	$D_{\text{ferro}} [\text{NaOH}]$ [ $10^{-10} \text{ m}^2 \text{ s}^{-1}$ ]
294	5.00	4.96	5.64	5.39
298		5.60	5.93	6.06
303	5.96	6.00	6.13	7.01
308	6.35	6.57	6.31	8.41

The diffusion coefficients of ferricyanide and ferrocyanide are determined at temperatures ranging from 294 to 308 K for both NaOH and Na<sub>2</sub>SO<sub>4</sub> as supporting electrolyte. Density and viscosity data are taken from Vazquez et. al. (1996); Perry et. al. (1997); Hodgman et. al. (1962); Washburn et. al. (1926). The measured diffusion coefficients are listed in Table A6.1. The results strongly agree with correlations given by Hiraoka et al. (1981).

#### A6.4. Concluding remarks

Studies concerning the measurement of particle-liquid mass transfer coefficients in trickle-beds are frequently employed with air as the gas-phase. Using nitrogen gas may be troublesome in needing a gas recycle, especially when the experiments are conducted in large packed columns. When using air as the gas-phase, the effect of the reduction of dissolved oxygen at a cathodic working electrode leads to an overestimation of the particle-liquid mass transfer coefficient. By applying an anodic working electrode, solely the oxidation of ferrocyanide takes place at the working electrode. The measured limiting current then is a direct measure of the mass transfer rate. By substituting NaOH as supporting electrolyte by Na<sub>2</sub>SO<sub>4</sub>, oxygen evolution is shifted towards much higher electrode potentials. This gives rise to a broad limiting current plateau.

#### Notation

$C_b$	bulk concentration electrochemical active species	[ $\text{mol m}^{-3}$ ]
$D$	diffusion coefficient	[ $\text{m}^2 \text{ s}^{-1}$ ]
$i_l$	limiting current density	[ $\text{A m}^{-2}$ ]
$f_{\text{RTD}}$	disc rotation frequency	[ $\text{s}^{-1}$ ]
$F$	Faraday constant	[ $\text{C mol}^{-1}$ ]
$n$	number of electrons	[-]
$\nu$	kinematic viscosity	[ $\text{m}^2 \text{ s}^{-1}$ ]

---

## Chapter 7

---

# Dynamic Modeling of Periodically Operated Trickle-Bed Reactors

---

### Abstract

A dynamic model is developed to study the effect of periodic operation on trickle-bed reactor performance for both liquid-limited and gas-limited reactions. Internal diffusion is incorporated in the model since the rate of internal diffusion largely determines the optimal cycle periods. The objective of the present dynamic modeling study is to formulate general rules for the periodic operation of a trickle-bed reactor. The effect of periodic operation on conversion, selectivity and production capacity is investigated.

Periodic operation results in significant increases in production capacity and conversion compared to steady state operation for gas-limited reactions. For liquid-limited reactions, however, steady state operation is superior to periodic operation.

The optimal duration of the high and low (zero) liquid feed strongly interdepend. For fast reactions, a short period of low (zero) liquid feed and a high ratio of the period of high liquid feed to the period of low (zero) liquid feed are preferred compared to slow reactions since the liquid phase reactant is consumed faster.

The selectivity of consecutive reactions during periodic operation seems always less for linear kinetics than for steady state operation due to the enhanced residence time and the higher concentration levels of the product inside the catalyst.

A fast cycling of the liquid feed is most effective in terms of production capacity, conversion and selectivity. The reaction is confined near the catalyst surface. With increasing cycled liquid feed frequency, the time average concentration of the liquid phase reactant inside the catalyst increases and the time-average concentration of the product decreases. High concentrations of liquid phase reactant result in high reaction rates for the desired reaction. Low concentration levels of the product lead to low reaction rates for the undesired reaction.

This chapter is in preparation for publication as:

Boelhouwer J.G., Piepers H.W. and Drinkenburg A.A.H., Dynamic modeling of periodically operated trickle-bed reactors, to be published

## 7.1. Introduction

Most commercial trickle-bed reactors adiabatically operate at high temperatures and high pressures and often involve hydrogen and organic liquids with superficial gas and liquid velocities up to 0.3 and 0.01 m s<sup>-1</sup>, respectively. Kinetics and/or thermodynamics of reactions conducted in trickle-bed reactors often require high temperatures. Elevated pressures (up to 30 MPa) are necessary to improve the gas solubility and the mass transfer rates.

Trickle-bed reactors are usually operated at steady state conditions in the trickle flow regime. Recent studies have demonstrated reactor performance improvement over the optimal steady state under forced, time-varying liquid flow rates (Haure et al., 1989; Lange et al., 1994; Castellari and Haure, 1995; Gabarain et al., 1997). In this mode of operation, the liquid feed is cycled while the gas is continuously fed. Since in the above mentioned studies, the cycle periods during periodic operation are much larger than the liquid residence time, steady state models are used to calculate performance improvement. When cycle periods are comparable to or even smaller than the liquid phase residence time, these pseudo steady state models are probably not adequate.

Most reaction systems can be classified as being liquid reactant or gas reactant limited (Mills and Dudukovic, 1980; Khaldikar et al., 1996). For liquid-limited reactions, the highest possible particle-liquid mass transfer rate and wetting efficiency result in the fastest transport of the liquid phase reactant to the catalyst. For gas-limited reactions, partial wetting is preferred since it facilitates more effective mass transfer of the gaseous reactant to the catalyst. The main problem is how to attain partial wetting without gross liquid maldistribution, which leads to unpredictable and uncontrollable reactor performance. If large sections of the bed are completely dry, the reaction may become severely limited by mass transfer of the liquid-phase reactant (Beaudry et al., 1987). On the other hand, on dry areas well fed by reactants from the gas phase, hot spots may occur. The periodic operation of a trickle-bed reactor facilitates controlled temporal variations in wetting efficiency without the problem of gross liquid maldistribution. The danger of hot spot formation is prevented when natural pulses are induced during the period of high liquid feed. The durations of the high and low liquid flow rate are restricted to relatively high values since the induced liquid-rich shock waves are unstable. A fast mode of periodic operation is, however, possible by the induction of individual natural pulses. The pulse frequency is externally set by the cycled liquid feed frequency.

## 7.2. Scope and objective

A dynamic model is developed to study the effect of periodic operation on trickle-bed reactor performance for both liquid-limited and gas-limited reactions. Both a single step and a consecutive reaction are used as model reactions. Internal diffusion is incorporated in the model since it is believed that the rate of internal diffusion largely determines the optimal cycle periods. The objective of this dynamic modeling study is the formulation of general rules for the periodic operation of a trickle-bed reactor. This is of particular interest since the efforts to find the optimal periodic state, as reported in published experimental studies, are merely based on trial and error.

## 7.3. Model development

### 7.3.1. Qualitative model description

The catalyst is represented as a vertical slab containing pores of a length of  $10^{-4}$  m. The catalytically active material is situated only inside the pores, not on the outer surface of the catalyst. The much larger internal surface area of a catalyst compared to the external surface area justifies this assumption. The model thus represents the catalyst as a thinly washcoated shell catalyst with an impermeable core. Another simplification made is that no lateral mass transfer between the individual pores is allowed to occur. Schematic illustrations of the porous catalyst slab are presented in Figs. 7.1 and 7.2.

Since the model is developed to determine the performance of a trickle-bed reactor under time-varying liquid flow rates, a temporal variation in wetting of the catalyst prevails. The slab representing the catalyst is therefore divided into two sections. One section of the slab is continuously wetted by the liquid phase, both during the low and high part of the feed cycle. The other section of the slab is only wetted during the high part of the feed cycle. Hence, the periodically wetted section of the catalyst is alternately exposed to the gas and liquid phase. The relative areas of the continuously and periodically wetted part of the slab are determined by the wetting efficiency during the low part of the feed cycle ( $f_{lb}$ ), respectively the difference in wetting efficiency during the high and low part of the feed cycle ( $f_{lp} - f_{lb}$ ). The part of the catalyst that is never in contact with the liquid phase ( $1-f_{lp}$ ), does not contribute to the reaction at all.

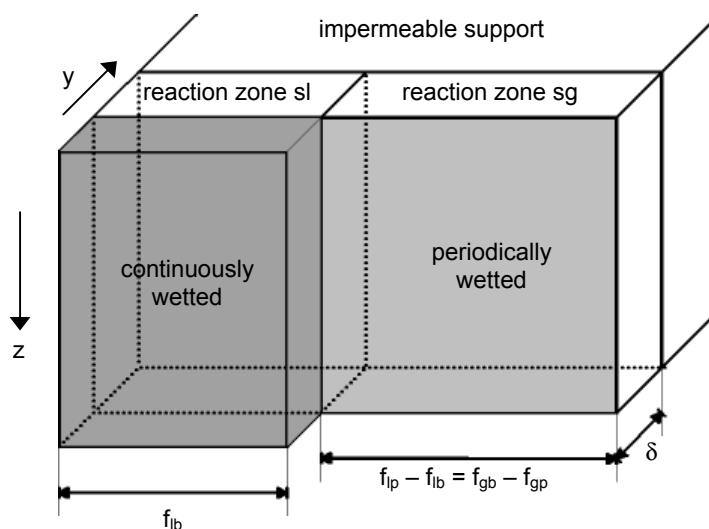
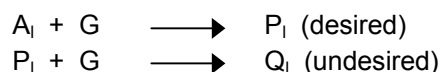


**Figure 7.1.** Schematic illustration of the model catalyst under periodic operation ( $f_{lb}$ : wetting efficiency during low liquid flow rate;  $f_{ip}$ : wetting efficiency during high liquid flow rate;  $f_{gb}$ : gas-solid contacting efficiency during low liquid flow rate;  $f_{gp}$ : gas-solid contacting efficiency during high liquid flow rate)

The following assumptions are made: a: no axial and radial dispersion; b: adiabatic operation; c: completely liquid-filled pores due to capillary effects; d: no intraparticle temperature gradients; e: non-volatile liquid phase; f: no stagnant liquid holdup; g: constant reactor pressure; h: no change in liquid physical properties due to reaction; i: negligible heat capacity of the gas phase; j: negligible gas-side mass transfer resistance.

### 7.3.2. Reaction kinetics

A simple reaction scheme is used to model trickle-bed reactor performance during unsteady state conditions:



Both the single step and the consecutive reaction are simulated.

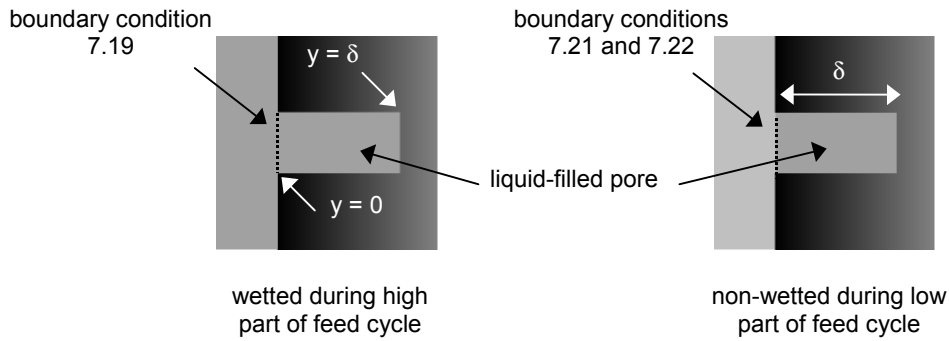


**Figure 7.2.** Schematic illustration of the periodically wetted section of the catalyst with the appropriate boundary conditions

The kinetics are described by simple first order expressions for both reaction steps:

$$r_1^{sj} = k_{r1} C_A^{sj} C_G^{sj} \quad [7.1]$$

$$r_2^{sj} = k_{r2} C_P^{sj} C_G^{sj} \quad [7.2]$$

The parameter  $sj$  denotes either the continuously wetted (sl) or the periodically wetted (sg) part of the catalyst. The reaction rate constants  $k_{r1}$  and  $k_{r2}$  depend on the temperature of the catalyst conform the Arrhenius expression:

$$k_{ri} = k_{ri}^0 e^{-\frac{E_{ai}}{RT_s}} \quad [7.3]$$

In case the single step reaction is used in the model, the second reaction rate constant  $k_{r2}$  is set to zero.

### 7.3.3. Hydrodynamics

Since periodic operation concerns waves of a relatively high liquid holdup moving over a background of much lower liquid holdup, a time-varying liquid holdup at the column inlet is used to model unsteady state hydrodynamics.



At the reactor inlet, the liquid holdup obeys:

$$\begin{aligned} \beta &= \beta_b & n_p (t_b + t_p) &\leq t < n_p (t_b + t_p) + t_b \\ \beta &= \beta_p & n_p (t_b + t_p) + t_b &\leq t < (n_p + 1) (t_b + t_p) \end{aligned} \quad [7.4]$$

The integer variable  $n_p$  stepwise increases when a liquid feed cycle is ended. The dynamic liquid holdup in the column is calculated by:

$$\frac{\partial \beta}{\partial t} = -V_p \frac{\partial \beta}{\partial z} \quad [7.5]$$

In this equation,  $V_p$  is the velocity of the waves. For a perfect square wave, the term  $d\beta/dz$  can only be zero or infinite. Since the distance between two axial gridpoints is finite, nearly square wave shaped waves of a high liquid holdup are simulated by equation 7.5. For continuity shock waves the following equation applies (chapter 4):

$$V_p = \frac{U_{lp} - U_{lb}}{\beta_p - \beta_b} \quad [7.6]$$

By representing the hydrodynamics as a differential equation, the liquid-rich shock waves take in liquid at the front and leave liquid behind at the back. The superficial liquid velocity is expressed as a function of the actual liquid holdup. Local axial wetting efficiency, heat and mass transfer rates and gas-liquid specific area are expressed as functions of the actual superficial liquid velocity (and superficial gas velocity) using literature correlations. The data on liquid holdup are taken from chapters 2 and 4. The hydrodynamics of the gas phase are modeled by using the ideal gas law.

#### 7.3.4. Mass balance equations

The mass balance equation for the gaseous reactant G in the gas phase:

$$\begin{aligned} (\varepsilon - \beta) \frac{\partial C_G^g}{\partial t} = & - \frac{\partial (U_g C_G^g)}{\partial z} - k_{l,G} a_{gl} \left( \frac{C_G^g}{m} - C_G^l \right) - \\ & k_{g,G} (f_g - f_{gp}) \varepsilon_p a_s \left( C_G^g - m C_G^{sg}|_{y=0} \right) \end{aligned} \quad [7.7]$$

The third term on the right of eq. 7.7 represents the direct mass transfer of the gaseous reactant to the surface of the periodically wetted section of the catalyst, which only occurs during the low part of the feed cycle. In this equation,  $f_g$  is the local actual gas-solid contacting efficiency, expressed as a function of the local actual liquid velocity. When  $f_g$  exceeds the fixed contacting efficiency of the gas phase with the catalyst during the high liquid flow rate,  $f_{gp}$ , gas-solid mass transfer occurs. During the period of high liquid feed,  $f_g$  equals  $f_{gp}$ , and no direct mass transfer between the gas phase and the catalyst occurs. The boundary condition at the reactor inlet for the concentration of the gaseous reactant G in the gas phase:

$$C_{G|z=0}^g = \frac{P_G}{RT_0} \quad [7.8]$$

Since a pure gaseous reactant is used in the model and the liquid phase is non-volatile, the partial pressure of the gas phase reactant G equals the total pressure in the reactor. The initial concentration of the gaseous reactant G in the gas phase over the entire reactor length is equal to:

$$C_{G|t=0}^g = \frac{P_G}{RT_0} \quad [7.9]$$

Hence, the reactor is suddenly switched on at time zero. The mass balance for the gaseous component G in the dynamic liquid phase obeys the following equation:

$$\beta \frac{\partial C_G^l}{\partial t} = -U_l \frac{\partial C_G^l}{\partial z} + k_{l,G} a_{gl} \left( \frac{C_G^g}{m} - C_G^l \right) - k_{s,G} f_{lb} \varepsilon_p a_s (C_G^l - C_{G|y=0}^{sl}) - k_{s,G} (f_l - f_{lb}) a_s \varepsilon_p (C_G^l - C_{G|y=0}^{sg}) \quad [7.10]$$

The third term on the right of eq. 7.10 indicates the liquid-solid mass transfer of the dissolved gaseous reactant to the continuously wetted section of the catalyst. The fourth term on the right denotes the liquid-solid mass transfer of the dissolved gaseous reactant to the periodically wetted section of the catalyst. The liquid-solid mass transfer to the periodically wetted section of the catalyst is turned on when the local actual wetting efficiency ( $f_l$ ) exceeds the fixed wetting efficiency ( $f_{lb}$ ) during the low liquid flow rate.

For the liquid phase components A, P and Q, the following mass balance equation in the dynamic liquid phase applies:

$$\beta \frac{\partial C_i^l}{\partial t} = -U_l \frac{\partial C_i^l}{\partial z} - k_{s,i} f_{lb} a_s \varepsilon_p (C_i^l - C_i^{sl}|_{y=0}) - k_{s,i} (f_l - f_{lb}) a_s \varepsilon_p (C_i^l - C_i^{sg}|_{y=0}) \quad [7.11]$$

At the reactor inlet, the following boundary conditions for equations 7.10 and 7.11 apply:

$$C_A^l|_{z=0} = C_{Af}^l \quad [7.12]$$

$$C_G^l|_{z=0} = C_P^l|_{z=0} = C_Q^l|_{z=0} = 0 \quad [7.13]$$

The initial concentrations for equations 7.10 and 7.11 over the entire reactor length:

$$C_A^l|_{t=0} = C_{Af}^l \quad [7.14]$$

$$C_G^l|_{t=0} = C_P^l|_{t=0} = C_Q^l|_{t=0} = 0 \quad [7.15]$$

The mass balance equation for all components inside the pores of the catalyst obeys:

$$\frac{\partial C_i^{sj}}{\partial t} = D_{e,i} \frac{\partial^2 C_i^{sj}}{\partial y^2} - R_i^j \quad [7.16]$$

$$R_i^{sj} = r_1^{sj} + r_2^{sj} \quad \text{for component G}$$

$$R_i^{sj} = r_1^{sj} \quad \text{for component A}$$

$$R_i^{sj} = -r_1^{sj} + r_2^{sj} \quad \text{for component P}$$

$$R_i^{sj} = r_2^{sj} \quad \text{for component Q}$$

In this equation,  $i$  can be either component G, A, P or Q, and  $sj$  could be either the continuously wetted part (sl) or the periodically wetted part (sg) of the catalyst.

For the continuously wetted catalyst section, the following boundary conditions apply at all times:

$$\frac{dC_i^{sl}}{dy} \Big|_{y=0} = -\frac{k_{s,i}}{D_{e,i}} (C_i^l - C_i^{sl} \Big|_{y=0}) \quad [7.17]$$

$$\frac{dC_i^{sl}}{dy} \Big|_{y=\delta} = 0 \quad [7.18]$$

The boundary conditions for all components G, A, P and Q in the periodically wetted section of the catalyst during the high part of the cycle are:

$$\frac{dC_i^{sg}}{dy} \Big|_{y=0} = -\frac{k_{s,i}}{D_{e,i}} (C_i^l - C_i^{sg} \Big|_{y=0}) \quad [7.19]$$

$$\frac{dC_i^{sg}}{dy} \Big|_{y=\delta} = 0 \quad [7.20]$$

For the gas phase reactant G during the low part of the cycle, the following boundary condition is appropriate:

$$\frac{dC_G^{sg}}{dy} \Big|_{y=0} = -\frac{k_{g,G}}{D_{e,G}} (C_G^g - m C_G^{sg} \Big|_{y=0}) \quad [7.21]$$

For the liquid components A, P and Q, during the low part of the feed cycle, the following boundary condition applies:

$$\frac{dC_i^{sg}}{dy} \Big|_{y=0} = 0 \quad [7.22]$$

For all components G, A, P and Q:

$$\frac{dC_i^{sg}}{dy} \Big|_{y=\delta} = 0 \quad [7.23]$$

During the high part of the feed cycle, boundary condition 7.19 allows for mass transfer of all components between the liquid phase and the periodically wetted section of the catalyst. During the low part of the feed cycle, the periodically wetted section of the catalyst is in contact with the gas phase only. Direct mass transfer of the gaseous component from the gas phase occurs through boundary condition 7.21. The liquid phase components remain inside the catalyst pores conform boundary condition 7.22. The alternate use of boundary conditions 7.19, 7.21 and 7.22 are depicted in Fig. 7.2. The initial concentrations for all components G, A, P and Q inside the catalyst pores are set to zero:

$$C_i^{sj} \Big|_{t=0} = 0 \quad [7.24]$$

### 7.3.5. Heat balance equations

The heat balance equation for the entire catalyst phase is given by:

$$\begin{aligned} & \left[ \varepsilon_p (1-\varepsilon) \rho_l c_{pl} + (1-\varepsilon)(1-\varepsilon_p) \rho_s c_{ps} \right] \frac{\partial T_s}{\partial t} = \\ & a_s \varepsilon_p (-\Delta H_1) \left[ f_{lb} \int_{y=0}^{y=\delta} r_1^{sl} dy + (f_{gb} - f_{gp}) \int_{y=0}^{y=\delta} r_1^{sg} dy \right] + \\ & a_s \varepsilon_p (-\Delta H_2) \left[ f_{lb} \int_{y=0}^{y=\delta} r_2^{sl} dy + (f_{gb} - f_{gp}) \int_{y=0}^{y=\delta} r_2^{sg} dy \right] - \alpha_p f_l a_s (T_s - T_l) \end{aligned} \quad [7.25]$$

It is assumed that the entire catalyst, including the impermeable core instantaneously absorbs the generated heat. Essentially, this assumption means that when the steady periodic state is achieved, no intraparticle temperature gradients exist. For the dynamic liquid phase the following heat balance equation applies:

$$\rho_l c_{pl} \beta_d \frac{\partial T_l}{\partial t} = -U_l \rho_l c_{pl} \frac{\partial T_l}{\partial z} + \alpha_p f_l a_s (T_s - T_l) \quad [7.26]$$

With the boundary condition at the reactor inlet:

$$T_l \Big|_{z=0} = T_0 \quad [7.27]$$

The initial conditions for eqs. 7.25 and 7.2 over the entire reactor length:

$$T_l|_{t=0} = T_s|_{t=0} = T_0 \quad [7.28]$$

### 7.3.6. Output parameters

The conversion, selectivity and production capacity during the periodic operation are defined as respectively:

$$X = \frac{\int_{t_p+t_b}^{t_p+t_b} U_l (C_P^l + C_Q^l) dt}{\int_{t_p+t_b}^{t_p+t_b} U_l C_{Af}^l dt} \quad [7.29]$$

$$S = \frac{\int_{t_p+t_b}^{t_p+t_b} U_l C_P^l dt}{\int_{t_p+t_b}^{t_p+t_b} U_l (C_P^l + C_Q^l) dt} \quad [7.30]$$

$$P_c = \frac{1}{t_p + t_b} \int_{t_p+t_b}^{t_p+t_b} U_l C_P^l dt \quad [7.31]$$

The conversion, selectivity and production capacity are based on the concentrations of the desired product P in the liquid phase and/or the undesired product Q at the reactor outlet.

### 7.3.7. Method of solution

Mathematically, the system consists of first order hyperbolic partial differential equations coupled to ordinary differential equations. The system was solved by the numerical method of lines (Schiesser, 1991). The PDE's were converted to ODE's by discretization of the spatial derivatives with finite differences. Backward difference formulas were used for the convective terms and central difference formulas were applied to the diffusion terms. Simultaneous integration of the ODE's was conducted by the Runge-Kutta-Fehlberg method (Schiesser, 1991).

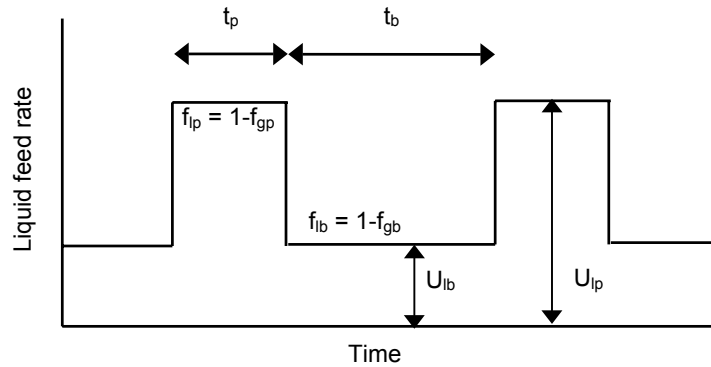


**Figure 7.3.** Schematic illustration of the characterization of the cycled liquid feed ( $U_{lb}$ : low liquid feed;  $U_{lp}$ : high liquid feed;  $t_b$ : duration of low liquid feed;  $t_p$ : duration of high liquid feed;  $f_{lb}$ : wetting efficiency during  $U_{lb}$ ;  $f_{lp}$ : wetting efficiency during  $U_{lp}$ ;  $f_{gb}$ : gas-solid contacting efficiency during  $U_{lb}$ ;  $f_{gp}$ : gas-solid contacting efficiency during  $U_{lp}$  )

#### 7.4. Simulation parameters and steady state results

The liquid holdup at the column entrance is cycled in a square wave manner, schematically shown in Fig. 7.3. The period of low liquid holdup and liquid velocity is denoted by  $t_b$ , while the period of high liquid holdup and liquid velocity is denoted by  $t_p$  throughout this chapter. Both  $t_p$  and  $t_b$  were varied between 1 and 200 s in the simulations. Shorter periods than 1 s were not applied since the number of axial gridpoints needed in this case would become that large, that simulations take more than three weeks on a Pentium III personal computer.

A summary of the correlations used in the model is presented in Table 7.1. The various parameters applied in the simulations are summarized in Table 7.2. The Thiele modulus based on the gas phase reactant G is defined by:

$$\phi = \delta \sqrt{\frac{k_r C_A^{s_i}}{D_{e,G}}} \quad [7.32]$$

In the simulations, the Thiele modulus is varied between 1.5 and 17, which means that internal diffusion barely respectively severely limits reaction. Higher Thiele moduli increase the importance of the external mass transfer. A plot of the steady state conversion versus the reaction rate constant is shown in Fig. 7.4.

**Table 7.1.** Summary of correlations used in the model

parameter		reference
volumetric gas-liquid mass transfer coefficient	$k_{l a_{lg}}$	Goto and Smith (1975)
liquid-solid mass transfer coefficient	$k_s$	Chou et. al. (1979)
gas-particle mass transfer coefficient	$k_g$	Dwivedi and Upadhyay (1977)
wetting efficiency	$f_l$	Mendizaball et. al. (1998)
particle-liquid heat transfer coefficient	$\alpha_p$	Chapter 3

**Table 7.2.** Parameters used in the model

parameter	symbol	value used
column height	$H_c$	1.0 m
specific catalyst area	$a_s$	1200 m <sup>-1</sup>
porosity packed column	$\varepsilon$	0.5
catalyst porosity	$\varepsilon_p$	0.5
pore length	$\delta$	0.0001 m
skeletal catalyst density	$\rho_s$	3500 kg m <sup>-3</sup>
liquid phase density	$\rho_l$	900 kg m <sup>-3</sup>
liquid phase viscosity	$\mu_l$	0.0006 Pa s
liquid phase heat capacity	$C_{pl}$	1800 J kg <sup>-1</sup> K <sup>-1</sup>
gas phase viscosity	$\mu_g$	0.00009 Pa s
catalyst heat capacity	$C_{ps}$	800 J kg <sup>-1</sup> K <sup>-1</sup>
molecular diffusion coefficient G	$D_G$	8.0 10 <sup>-9</sup> m <sup>2</sup> s <sup>-1</sup>
molecular diffusion coefficient A, P and Q	$D_i$	1.0 10 <sup>-9</sup> m <sup>2</sup> s <sup>-1</sup>
effective diffusion coefficient G	$D_{eff,G}$	8.0 10 <sup>-10</sup> m <sup>2</sup> s <sup>-1</sup>
effective diffusion coefficient A, P and Q	$D_{eff,i}$	8.0 10 <sup>-10</sup> m <sup>2</sup> s <sup>-1</sup>
modified Henry coefficient ( $C_G^g C_{Geq}^l^{-1}$ )	$m$	50
operating pressure	$P$	10 bar
liquid feed temperature	$T_0$	320 K
feed concentration liquid phase reactant	$C_{Af}^l$	500 mol m <sup>-3</sup>
activation energy	$E_{ai}$	80000 J mol <sup>-1</sup>
reaction enthalpy	$-\Delta H_i$	200000 J mol <sup>-1</sup>
superficial liquid velocity	$U_l$	0 – 0.02 m s <sup>-1</sup>
superficial gas velocity	$U_g$	0.1 m s <sup>-1</sup>



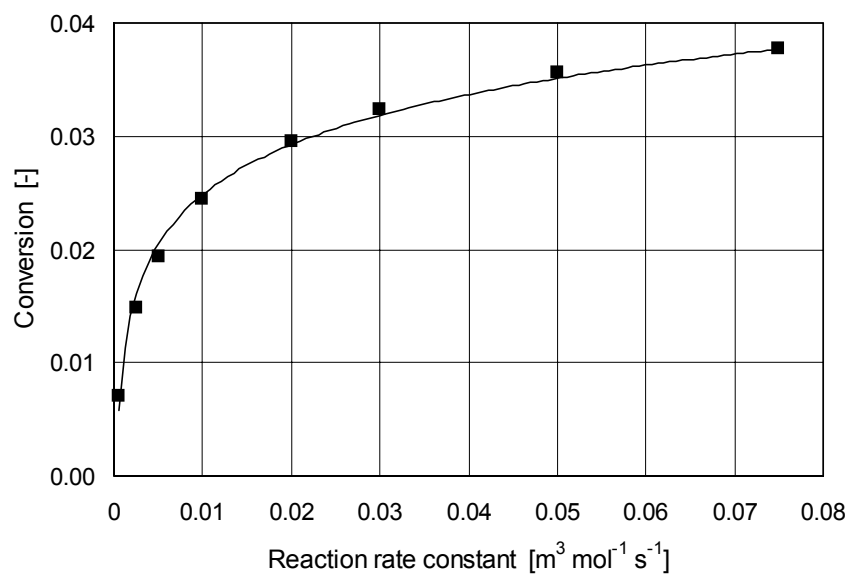


**Figure 7.4.** Conversion versus reaction rate constant ( $U_l = 0.008 \text{ m s}^{-1}$ ;  $U_g = 0.1 \text{ m s}^{-1}$ )

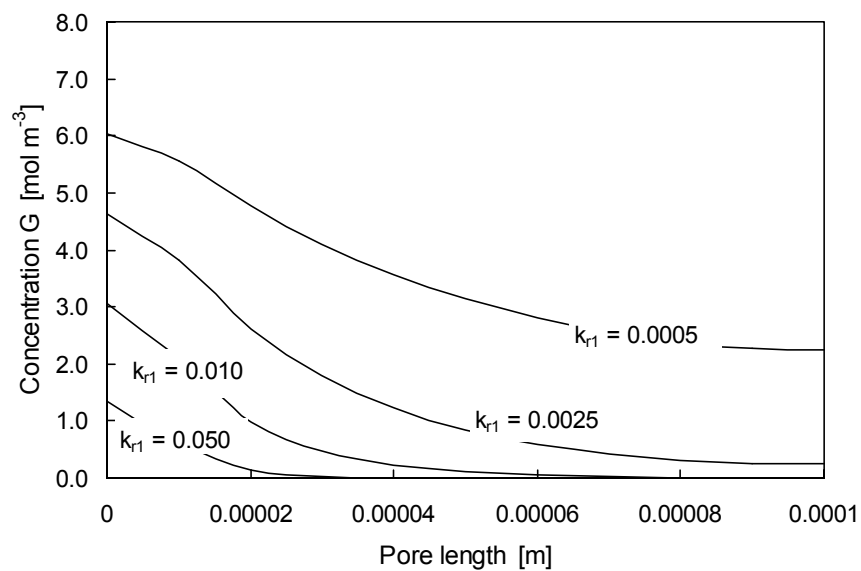


**Figure 7.5.** Steady state concentration profiles for the gas phase reactant G inside the catalyst pores for several reaction rate constants ( $U_l = 0.008 \text{ m s}^{-1}$ ;  $U_g = 0.1 \text{ m s}^{-1}$ ).

Some of the corresponding steady state concentration profiles for the gaseous reactant G inside the catalyst pores are presented in Fig. 7.5. With increasing reaction rate constant, penetration of the gaseous reactant G in the catalyst pores is less deep and the reaction is more confined near the external particle surface. The concentration level of the liquid phase reactant A (not presented) inside the catalyst pores is much higher since the gas phase reactant is only slightly soluble and conversions are low.

A sensitivity analysis is performed to quantify the important and rate determining steps for the reaction system. The conversion is most sensitive to variations in the volumetric gas-liquid mass transfer coefficient and the operating pressure. A ten-fold increase in  $k_{l,G}a_{gl}$  results in a three-fold increase in conversion, and a ten-fold decrease in  $k_{l,G}a_{gl}$  results in a seven-fold decrease in the conversion. A five-fold increase in the operating pressure results in a five-fold increase in conversion. The sensitivity analysis clearly shows the limiting effect of the overall mass transfer of the gaseous reactant on conversion.

## 7.5. Single step reaction

### 7.5.1. Production capacity

For the single step reaction, selectivity is not an issue and therefore the production capacity and the conversion are the objectives that should be optimized. The production capacity for an on-off mode and a low-high mode of periodic operation is compared to the steady state production capacity in Fig. 7.6. The average superficial liquid velocity is selected as the basis for comparison, as usually encountered in literature studies. In these simulations,  $t_p$  is fixed at 20 s and  $t_b$  is varied in a broad range between 1 and 200 s. Also presented in this figure is the production capacity for a low-high cycled liquid feed at a fixed  $t_b$  of 20 s and a  $t_p$  varying between 1 and 60 s. The production capacity during periodic operation is significantly higher compared to the steady state production capacity at equivalent (average) liquid flow rates. Two limiting cases and a maximum in production capacity are recognized. In case  $t_b$  approaches zero, the production capacity moves towards the steady state production capacity at  $U_{lp}$ . On the other hand, when  $t_b$  approaches infinity, the production capacity approaches the production capacity at  $U_{lb}$ . For an on-off cycled liquid feed, this limiting production capacity is zero.

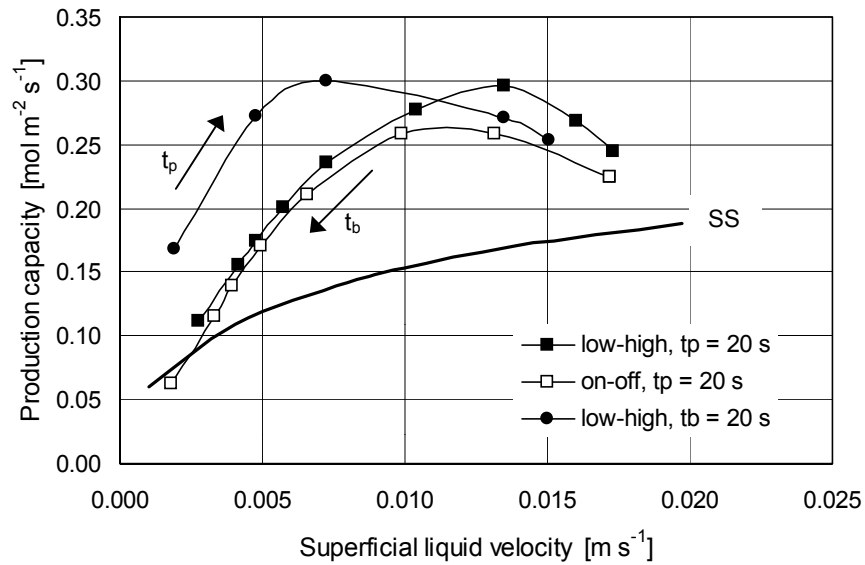


**Figure 7.6.** Comparison between production capacity during periodic operation and steady state operation ( $U_{lp} = 0.0197 \text{ m s}^{-1}$ ;  $U_{lb} = 0.001 \text{ m s}^{-1}$  (low-high) resp.  $U_{lb} = 0.0 \text{ m s}^{-1}$  (on-off);  $k_{r1} = 0.05 \text{ m}^3 \text{ mol}^{-1} \text{ s}^{-1}$ )

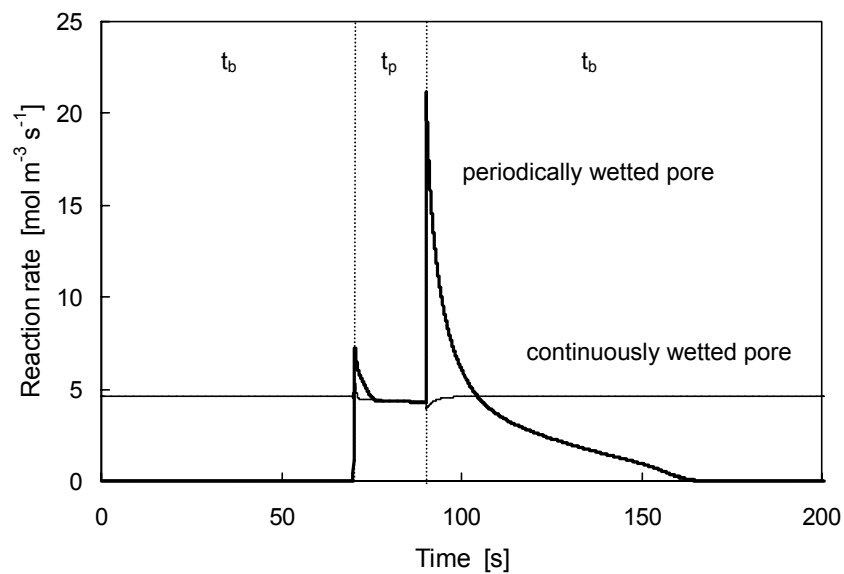


**Figure 7.7.** Volume-average reaction rate inside a periodically wetted respectively a continuously wetted catalyst pore ( $U_{lb} = 0.001 \text{ m s}^{-1}$ ;  $U_{lp} = 0.0197 \text{ m s}^{-1}$ ;  $t_p = 20$  s;  $t_b = 200$  s;  $k_{r1} = 0.05 \text{ m}^3 \text{ mol}^{-1} \text{ s}^{-1}$ )

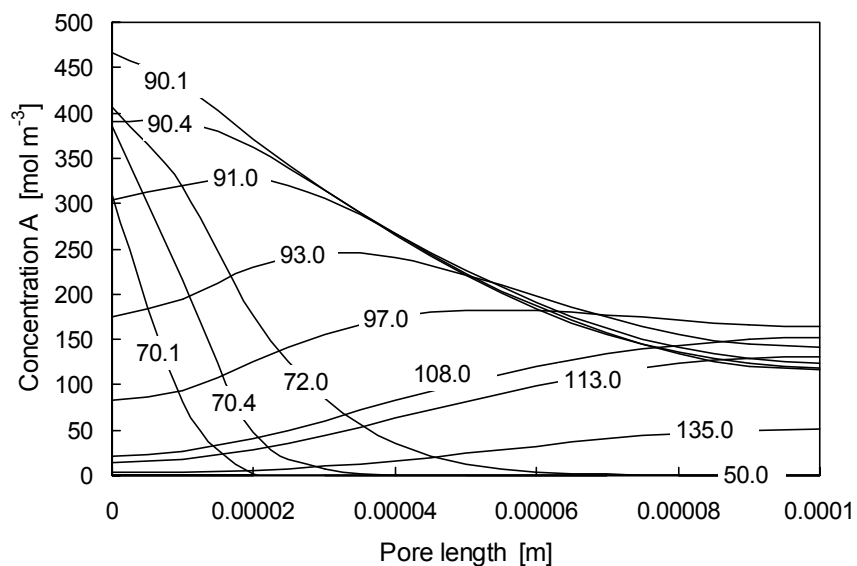


**Figure 7.8.** Concentration profiles of liquid phase reactant A inside a periodically wetted pore during an entire cycle period. The numbers denoted in the figure represent the time for which the reaction rates are given in Fig. 7.7

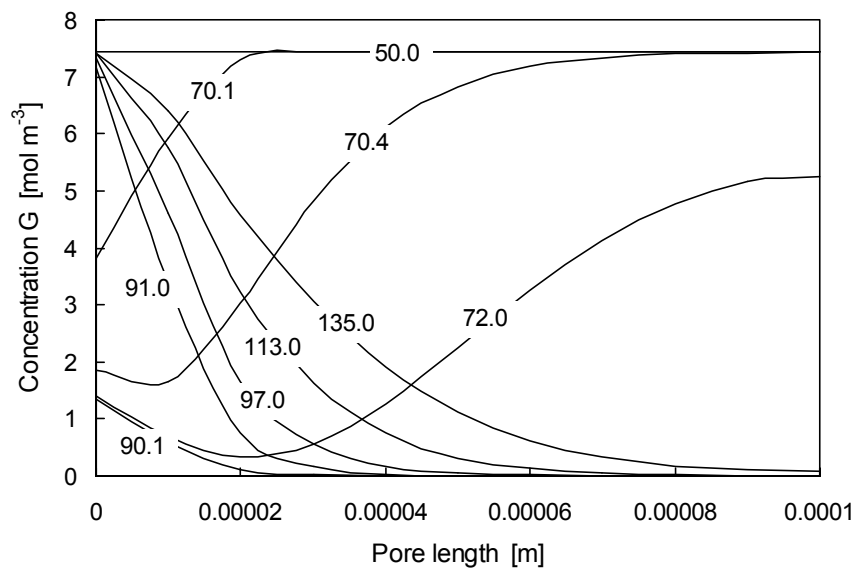


**Figure 7.9.** Concentration profiles of gas phase reactant G inside a periodically wetted pore for an entire cycle period. The numbers denoted in the figure represent the time for which the reaction rates are given in Fig. 7.7

In these three situations, a maximum in the production capacity is observed. The maximum in production capacity corresponds with the maximum in the time-average overall reaction rate. This maximum in the reaction rate inside the periodically wetted catalyst pore can be rationalized on the basis of Fig. 7.7 in which the volume-average reaction rate inside a continuously wetted and a periodically wetted catalyst pore is plotted versus time. The corresponding evolving concentration profiles of the liquid phase reactant A respectively the gas phase reactant G inside a periodically wetted catalyst pore, are plotted in Figs. 7.8 and 7.9. The durations  $t_p$  and  $t_b$  are sufficiently long to obtain steady state within both  $t_b$  and  $t_p$ . During  $t_b$ , a decrease in the concentration of liquid phase reactant A occurs since it is consumed by reaction. In case  $t_b$  is sufficiently long, liquid phase reactant A becomes entirely depleted, as shown in Fig. 7.8 ( $t = 50$  s). Therefore, the reaction rate inside the periodically wetted pore eventually becomes zero during  $t_b$ . Since liquid phase reactant A is depleted, the pore becomes saturated with the gas phase reactant G, as shown in Fig. 7.9 ( $t = 50$  s). When the liquid feed is subsequently increased, liquid phase reactant A is transferred to the catalyst. The initial reaction rate during  $t_p$  exhibits an overshoot since the periodically wetted catalyst pore is saturated with gas phase reactant G. After some time, steady state is achieved and the reaction rate inside the periodically wetted pore equals the reaction rate inside the continuously wetted pore. When the liquid flow rate is reduced, effective mass transfer of gaseous reactant G occurs at the dry catalyst surface. The concentration of the gas phase reactant G at the outer surface of the catalyst then approaches the gas-liquid equilibrium concentration, as depicted in Fig. 7.9 ( $t = 91$  s). Initially, the reaction rate is very high since the concentration of the liquid phase reactant A is at its highest value. The concentration of A decreases due to reaction and subsequently the reaction rate decreases. After about 15 s from the onset of  $t_b$ , the reaction rate inside the periodically wetted pore drops below the reaction rate in the continuously wetted pore. At a fixed  $t_p$  of 20 s, a  $t_b$  higher than approximately 15 s results in a decrease in the time-average reaction rate and hence a decrease in the time-average production capacity. For a relatively long  $t_p$ , the  $t_b$  at which the maximum time-average reaction rate is obtained closely corresponds to the  $t_b$  at which the reaction rate inside the periodically wetted pore eventually equals the reaction rate inside the continuously wetted pore.

The production capacity for simulations performed with a fixed  $t_b$  of 20 s and varying  $t_p$  exhibits a maximum for  $t_p$  of about 10 s. The concentration profiles for the liquid phase reactant A inside the periodically wetted pore at the onset of  $t_b$  are plotted in Fig. 7.10 for several applied  $t_p$ .

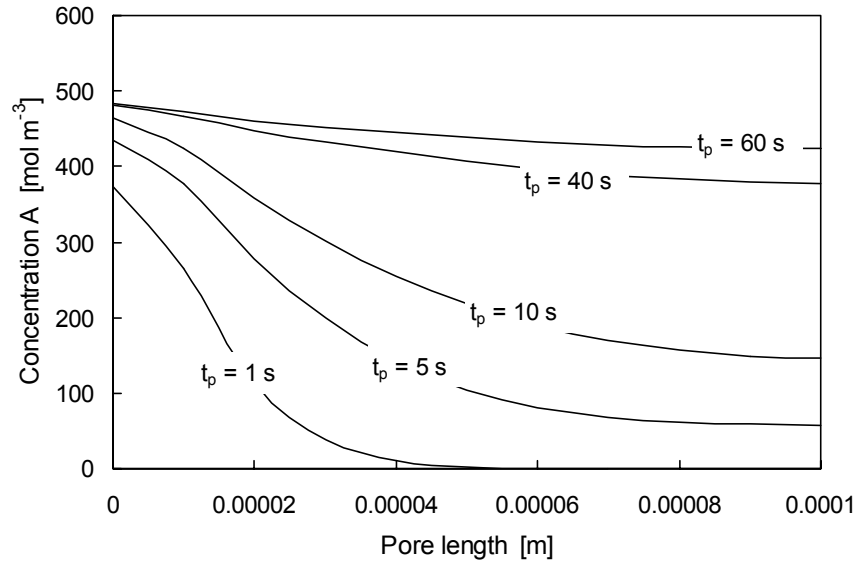


**Figure 7.10.** Concentration profiles of liquid phase reactant A inside a periodically wetted catalyst pore at the onset of  $t_b$  ( $U_{lb} = 0.001 \text{ m s}^{-1}$ ;  $U_{lp} = 0.0197 \text{ m s}^{-1}$ ;  $t_b = 20 \text{ s}$ ;  $k_{r1} = 0.05 \text{ m}^3 \text{ mol}^{-1} \text{ s}^{-1}$ )

The concentration of A at the onset of the low part of the feed cycle decreases with decreasing applied  $t_p$ , since during a shorter  $t_p$  less fresh liquid phase reactant A is supplied to the pores. Therefore, at a decreasing applied  $t_p$  (at fixed  $t_b$ ), the reaction rate during  $t_b$  drops faster below the reaction rate in the continuously wetted pore due to depletion of A. Hence, a reduction in the overall reaction rate occurs at decreasing  $t_p$  with respect to the optimal  $t_p$ . At  $t_p$  higher than the optimal  $t_p$ , a greater amount of liquid phase reactant A is supplied to the periodically wetted catalyst pore with respect to the optimal  $t_p$ . Hence, the time average concentration of A is higher than the optimal  $t_p$ . However, the reaction rate averaged over the entire cycle period is lower than for the optimal  $t_p$ , since the relative contribution of the (low) reaction rate during  $t_p$  to the time-average reaction rate increases. Hence, a maximum in the production capacity is observed.

For steady state operation, the reaction zone is confined near the catalyst surface, while during a relatively slow mode of periodic operation, the reaction zone occupies the entire pore. The concentration profiles of A and G inside the periodically wetted pore, shown in Figs. 7.8 and 7.9, clearly demonstrate this increased size of the reaction zone compared to steady state operation (Fig. 7.5). The applied  $t_p$  and  $t_b$  are strongly interdependent.

### 7.5.2. Fast mode periodic operation

The durations of the high and low liquid feed are strongly interdependent. During  $t_b$ , liquid phase reactant A is consumed by reaction. The amount of A that is consumed during  $t_b$  must be supplied during  $t_p$ . An increasing  $t_b$  must therefore be accompanied by an increase in  $t_p$ . During a relatively slow liquid feed cycling, the concentration of the gas phase reactant G inside the catalyst pores becomes relatively small in the course of  $t_p$  and the concentration of the liquid phase reactant A becomes relatively small in the course of  $t_b$ . For a relatively fast cycled liquid feed, the variations in the concentrations throughout one cycle period will be much smaller and the concentrations are higher on a time average basis.

In Fig. 7.11 and Fig. 7.12, the upper and lower limit of the concentration profiles at the onset of respectively  $t_p$  and  $t_b$  for liquid phase reactant A and gas phase reactant G inside the periodically wetted catalyst pore is plotted. These simulations are performed for equal  $t_p$  and  $t_b$  and hence for equivalent average superficial liquid velocities. Only the frequency of the cycled liquid feed varies. The time average concentration of the liquid phase reactant A inside the periodically wetted pore increases with increasing cycled liquid feed frequency. A similar effect of the cycled liquid feed frequency is obtained for the concentration profiles of gas phase reactant G. The higher time average concentration of the liquid phase reactant A and gas phase reactant G inside the periodically wetted pore leads to higher average reaction rates.

In the fast cycling case, the periodic variation in the concentration profiles for liquid phase reactant A and gas phase reactant G is confined near the external particle surface, while for relatively slow cycling of the liquid feed, this periodic variation propagates further into the catalyst pores. The reaction zone thus becomes more confined near the catalyst surface as the frequency of the cycled liquid feed increases. At much higher cycled liquid feed frequencies than applied in this modeling study, the fluctuations in mass transfer at the outer surface of the catalyst will become so rapid, that the system cannot follow them anymore and a new apparent steady state is achieved. Kouris et. al. (1998) modeled parallel reactions in a periodically wetted catalyst particle to evaluate the effectiveness factor under dynamic wetting conditions. They found that, when the fluctuation frequency tends to infinity, the catalyst particle is unable to follow the rapid changes in wetting. The particle then reaches a stationary state, which depends on the time-average wetting efficiency. The effectiveness factor for this pseudo steady state is the highest possible.

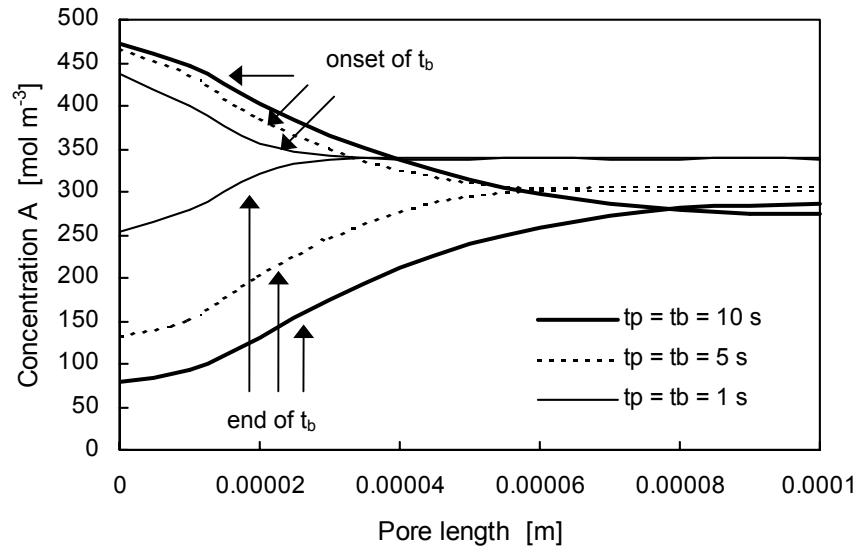


**Figure 7.11.** Concentration profiles of liquid phase reactant A inside a periodically wetted pore at the onset and ending of  $t_b$  for a relatively fast cycled liquid feed ( $U_{lp} = 0.0197 \text{ m s}^{-1}$ ;  $U_{lb} = 0.001 \text{ m s}^{-1}$ ;  $k_{r1} = 0.05 \text{ m}^3 \text{ mol}^{-1} \text{ s}^{-1}$ )

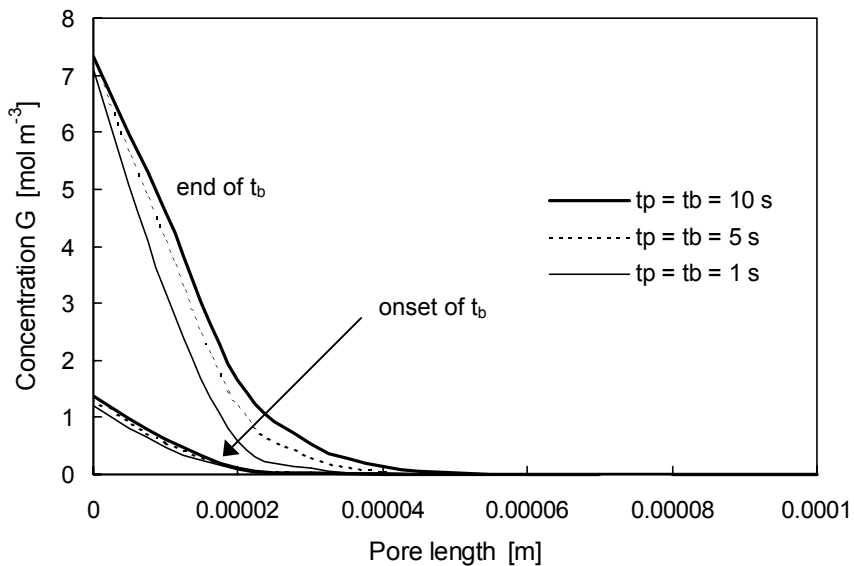


**Figure 7.12.** Concentration profiles of gas phase reactant G inside a periodically wetted pore at the onset and ending of  $t_b$  for a relatively fast cycled liquid feed ( $U_{lp} = 0.0197 \text{ m s}^{-1}$ ;  $U_{lb} = 0.001 \text{ m s}^{-1}$ ;  $k_{r1} = 0.05 \text{ m}^3 \text{ mol}^{-1} \text{ s}^{-1}$ )



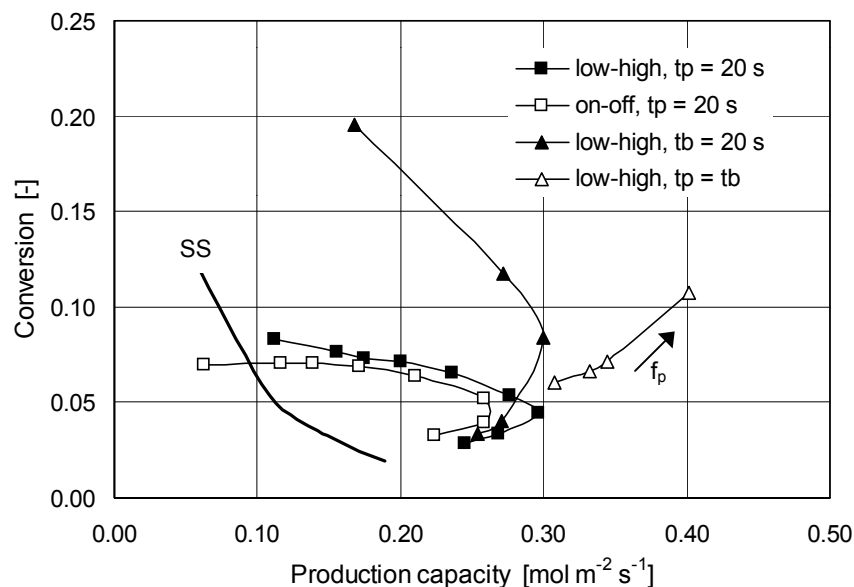


**Figure 7.13.** Conversion versus production capacity for steady state and periodic operation ( $U_{ip} = 0.0197 \text{ m s}^{-1}$ ;  $U_{lb} = 0.001 \text{ m s}^{-1}$  (low-high) resp.  $U_{lb} = 0.0 \text{ m s}^{-1}$  (on-off);  $k_{r1} = 0.05 \text{ m}^3 \text{ mol}^{-1} \text{ s}^{-1}$ )

### 7.5.3. Conversion

For optimization purposes, not only production capacity is important, but conversion as well. High production capacities at low conversions mean that large bed heights or high liquid phase recycling ratios are required to obtain large conversions. The conversion versus the production capacity for steady state operation and the various modes of periodic operation is plotted in Fig. 7.13. Clearly, a fast cycling of the liquid feed results in the highest production capacities accompanied by relatively high conversions.

It is interesting to notice the various limiting cases for the production capacity-conversion curves. For the on-off cycled liquid feed, the conversion remains constant at decreasing production capacities denoted by the arrow. This is due to the fact that for sufficiently long  $t_b$ , all the liquid phase reactant A, which is supplied to the periodically wetted catalyst pore during  $t_p$ , is converted. Therefore, increasing  $t_b$  leads to lower production capacities but conversions remain constant. For the low-high cycled liquid feed, the conversion approaches the steady state conversion at  $U_{lb}$  when the ratio  $t_b/t_p$  approaches infinity.

In case of fixed  $t_b$ , very high conversions are obtained compared to the curve for fixed  $t_p$ . Since at decreasing  $t_p$ , less liquid phase reactant A is fed to the reactor, higher conversions are achieved. The production capacity-conversion curve for the faster mode of cycling will end in a point at which the pseudo steady state is achieved at very high cycled liquid feed frequencies.

Most experimental studies concerning reactor performance improvement during periodic operation focus on the optimization of the conversion. In Fig. 7.13, it is clearly exposed that indeed very high conversions can be obtained. However, very high conversions can be accompanied by relatively low production capacities. One should aim at the optimal combination of production capacity and conversion instead of conversion alone.

#### 7.5.4. Temperature

Periodic operation results in higher bed temperatures compared to steady state operation since the time-average particle-liquid heat transfer rates and wetting efficiency are reduced and reaction rates are higher. The adiabatic temperature rise during periodic operation is compared to the adiabatic temperature rise during steady state operation in Fig. 7.14. The adiabatic temperature rise steadily increases with increasing ratio  $t_b/t_p$ . Apparently, the reduction in average particle-liquid heat transfer rates compared to steady state operation dominates this process since no maximum is observed as for the reaction rate. The highest bed temperatures are obtained when the time average particle-liquid heat transfer coefficient is lowest.

To investigate the relative contribution of a higher bed temperature to the overall rate enhancement, simulations were performed with zero reaction enthalpy. Only about 5% of the rate enhancement is due to higher operating temperatures. The higher bed temperatures are rather the effect of poor heat removal and high reaction rates than a cause for the high reaction rates.

Most of the heat is produced by reaction during  $t_b$ . During the on-off cycling of the liquid feed, this reaction heat is, however, not removed in the course of  $t_b$ . During the low-high cycling of the liquid feed, the reaction heat is poorly removed caused by the low  $U_{lb}$ . Hence, the highest catalyst temperatures are obtained at the end of  $t_b$ . During  $t_p$ , more effective heat removal occurs by the high  $U_{lp}$ . Hence the lowest bed temperature is obtained at the end of  $t_p$ . The maximum difference in the fluctuating bed temperature is plotted versus the average superficial liquid velocity in Fig. 7.15. Although for the fast cycling of the liquid feed, high average catalyst temperatures prevail, the fluctuations in the bed temperature are by far the lowest.

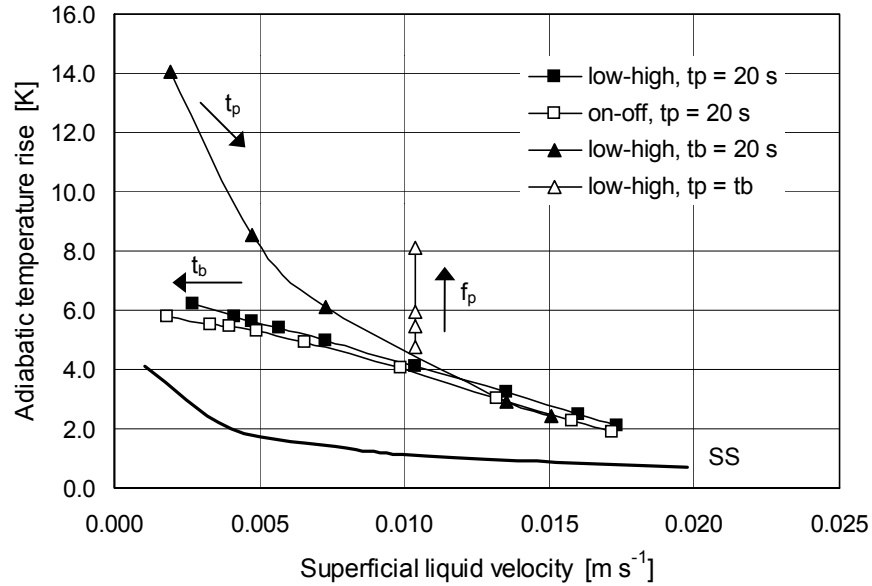


**Figure 7.14.** Comparison between adiabatic temperature rise during periodic operation with steady state (SS) operation ( $U_{lp} = 0.0197 \text{ m s}^{-1}$ ;  $U_{lb} = 0.001 \text{ m s}^{-1}$  (low-high) resp.  $U_{lb} = 0.0 \text{ m s}^{-1}$  (on-off);  $k_{r1} = 0.05 \text{ m}^3 \text{ mol}^{-1} \text{ s}^{-1}$ )

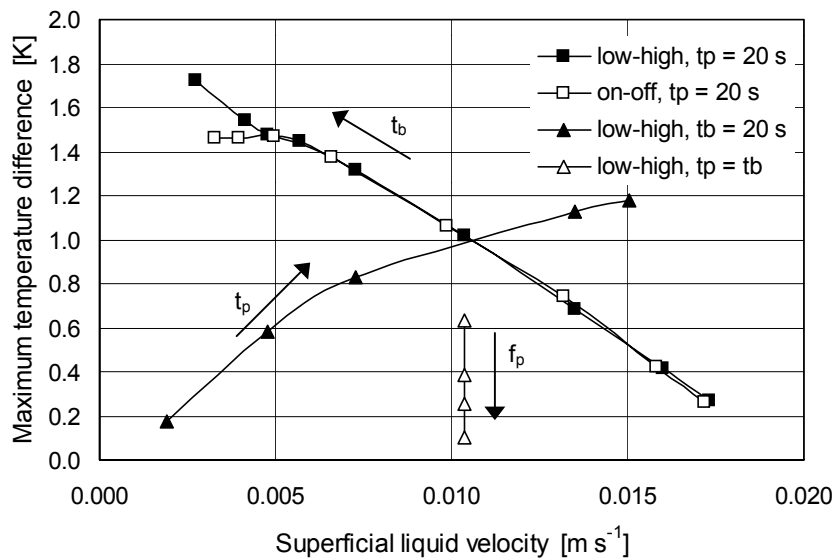


**Figure 7.15.** Maximum temperature difference obtained during one cycled liquid feed period ( $U_{lp} = 0.0197 \text{ m s}^{-1}$ ;  $U_{lb} = 0.001 \text{ m s}^{-1}$  (low-high) resp.  $U_{lb} = 0.0 \text{ m s}^{-1}$  (on-off);  $k_{r1} = 0.05 \text{ m}^3 \text{ mol}^{-1} \text{ s}^{-1}$ )

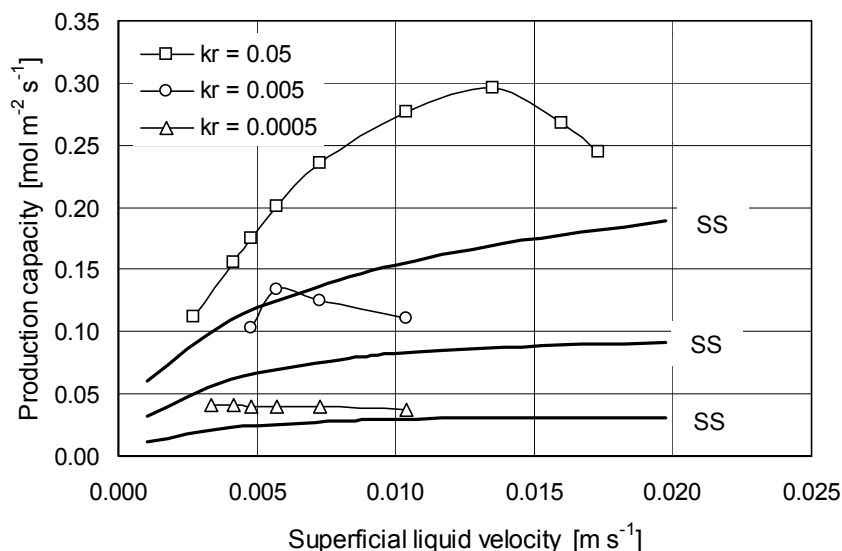


**Figure 7.16.** Production capacity for steady state and periodic operation versus the superficial liquid velocity for three different reaction rate constants ( $U_{lp} = 0.0197 \text{ m s}^{-1}$ ;  $U_{lb} = 0.001 \text{ m s}^{-1}$ ;  $t_p = 20 \text{ s}$ )

Smaller fluctuations of the catalyst temperature may reduce the chance of a thermal shock.

#### 7.5.5. Effect of kinetics

The relative improvement in production capacity by periodic operation is about equal for reaction rate constants varying between  $0.0005$  and  $0.05 \text{ m}^3 \text{ mol}^{-1} \text{ s}^{-1}$  as the results in Fig. 7.16 indicate. Apparently, in all cases, the reaction is sufficiently fast so that an increase in the overall rate of mass transfer of the gas phase reactant G during periodic operation results in large increases in reaction rates. However, for reactions that are entirely kinetically controlled, an increase in the mass transfer rate will not result in higher reaction rates.

The maximum in the production capacity during periodic operation is shifted towards lower average superficial liquid velocities when the reaction rate constant decreases. This means that a longer  $t_b$  with respect to  $t_p$  must be applied for slower reactions. For slower reactions, it takes more time for the reaction rate inside the periodically wetted pore to drop below the reaction rate inside the continuously wetted pore, since the depletion time for liquid phase reactant A is much longer.

Additionally, less liquid phase reactant A needs to be supplied during  $t_p$  compared to relatively fast reactions at constant  $t_b$ . The reaction rate constant thus affects the optimal ratio of  $t_p$  to  $t_b$ . With increasing reaction rate constant, higher  $t_p/t_b$  ratios are optimal. The optimal  $t_p/t_b$  ratio is for example 0.5 respectively 0.25 for simulations performed for  $k_{r1} = 0.05$  respectively  $0.005 \text{ m}^3 \text{ mol}^{-1} \text{ s}^{-1}$ .

#### 7.5.6. Liquid-limited reactions

To investigate the effect of periodic operation for liquid-limited reactions, simulations are performed for feed concentrations of the liquid phase reactant A of  $10 \text{ mol m}^{-3}$ . In this case, the concentration of A is approximately equal to the saturation concentration of the gas phase reactant G, while the effective diffusion coefficient of G is one order of magnitude higher than the effective diffusion coefficient of A. Hence, the reaction is liquid-limited. For liquid-limited reactions, the highest possible wetting efficiency and particle-liquid mass transfer coefficient lead to the highest possible reaction rates. Therefore, it is expected that periodic operation results in a decrease in production capacity. The production capacity for both periodic operation and steady state operation versus the average superficial liquid velocity is plotted in Fig. 7.17. Obviously, periodic operation leads to a decrease in production capacity. The on-off cycled liquid feed results in the lowest production capacity since the time-average wetting efficiency is less than the low-high periodic operation at equivalent average superficial liquid velocities.

A relatively fast cycling of the liquid feed may improve the flow distribution and wetting efficiency, since continuity shock waves are initiated by liquid feed cycling. These waves probably mix to some extent parallel flowing liquid streams and stagnant liquid holdup. A better flow distribution and wetting efficiency may persist after the lower liquid flow rate is re-introduced. Especially, at low average liquid flow rates, reactor performance for liquid-limited reactions may be improved by liquid feed cycling (Stradiotto et. al., 1999)

#### 7.6. Consecutive reaction

The selectivity obtained during periodic operation is compared with the steady state selectivity in Fig. 7.18. Selectivity during periodic operation is always (much) lower compared to steady state operation.

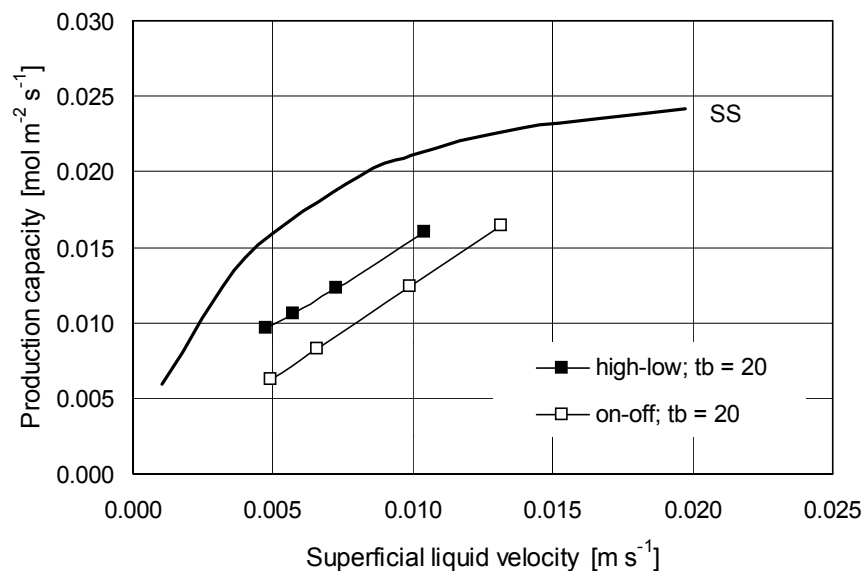


**Figure 7.17.** Production capacity versus (average) superficial liquid velocity for steady state and periodic operation for liquid-limited reactions ( $U_{lp} = 0.0197 \text{ m s}^{-1}$ ;  $U_{lb} = 0.001 \text{ m s}^{-1}$  (low-high) resp.  $U_{lb} = 0.0 \text{ m s}^{-1}$  (on-off);  $k_{r1} = 0.05 \text{ m}^3 \text{ mol}^{-1} \text{ s}^{-1}$ )

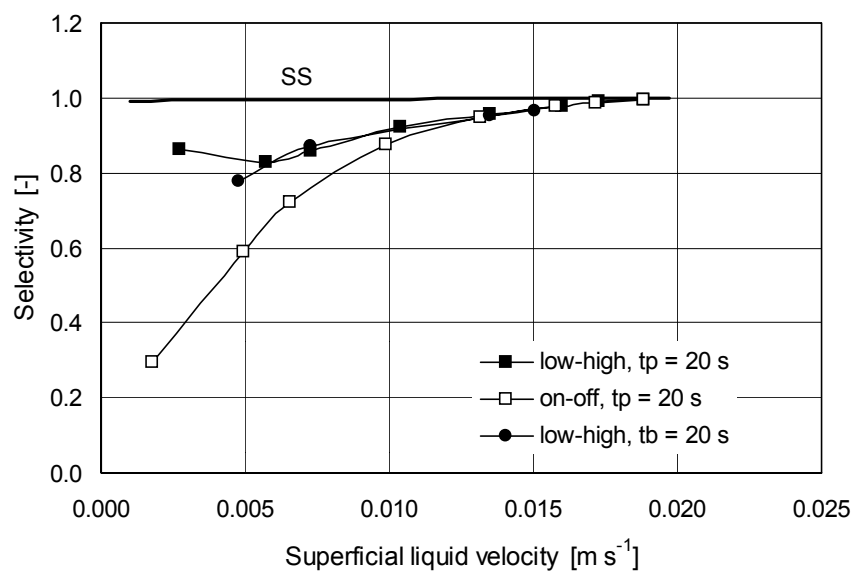


**Figure 7.18.** Selectivity versus (average) superficial liquid velocity for steady state and periodic operation ( $U_{lp} = 0.0197 \text{ m s}^{-1}$ ;  $U_{lb} = 0.001 \text{ m s}^{-1}$  (low-high) resp.  $U_{lb} = 0.0 \text{ m s}^{-1}$  (on-off);  $k_{r1} = 0.05 \text{ m}^3 \text{ mol}^{-1} \text{ s}^{-1}$ ;  $k_{r2} = 0.005 \text{ m}^3 \text{ mol}^{-1} \text{ s}^{-1}$ )

Since during  $t_b$ , the product is not removed from the periodically wetted catalyst pore, further reaction to the undesired product Q is increased. Increasing  $t_b$  leads to a reduction in selectivity due to increased residence times of the product P and due to lower concentration ratios of A to P inside the periodically wetted pores. For the low-high and on-off periodic operation, the selectivity tends towards the selectivity during steady state operation for respectively  $t_p$  and  $t_b$  approaching infinity. Most beneficial for selectivity reasons is to attain the highest possible concentration ratio of A over P inside the pore throughout the whole cycle period. As shown in the previous section, a fast cycling of the liquid feed results in the highest concentration of the liquid phase reactant A inside the pores while the highest production capacities are obtained as well. In the fast cycling case, the reaction zone is confined near the outer surface of the catalyst leading to short residence times and low concentrations of the product P. The selectivity versus the production capacity for the various modes of periodic operation are plotted in Fig. 7.19. Also plotted in this figure are the selectivities obtained during steady state operation at operating pressures of 10 and 30 bar. It is clearly shown that for the fast cycling of the liquid feed, the selectivity approaches that for the steady state at high cycled liquid feed frequencies. The production capacity is comparable to the steady state production capacity at an operating pressure of 30 bar. The concentration profiles of the liquid phase product P inside the periodically wetted catalyst pore during a relatively fast cycling of the liquid feed are plotted in Fig. 7.20. It is clearly shown that the time-average concentration of the product P inside the periodically wetted catalyst pore decreases with increasing cycled liquid feed frequency. Lower levels of the concentration of P accompanied by higher concentration levels of the liquid phase reactant A lead to higher selectivities.

Lee and Bailey (1974) modeled a complex heterogeneously catalyzed reaction under periodic variations of the reactants at the outer surface of the catalyst. Due to interacting concentration waves inside the catalyst, improved selectivity was obtained. However, such a phenomenon is not observed in the present study. This is probably due to the fact that the kinetics in this modeling study are linear, while Lee and Bailey (1974) used complex, nonlinear kinetics in their study. It might very well be, that periodic operation of a trickle-bed reactor leads to selectivity improvements in case of nonlinear kinetics.

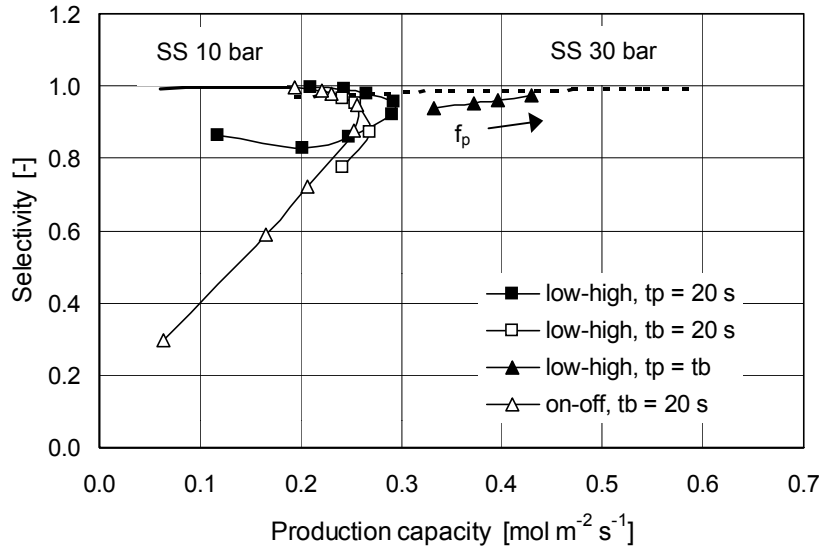


**Figure 7.19.** Selectivity versus production capacity for steady state and periodic operation ( $U_{ip} = 0.0197 \text{ m s}^{-1}$ ;  $U_{lb} = 0.001 \text{ m s}^{-1}$  (low-high) resp.  $U_{lb} = 0.0 \text{ m s}^{-1}$  (on-off);  $k_{r1} = 0.05 \text{ m}^3 \text{ mol}^{-1} \text{ s}^{-1}$ ;  $k_{r2} = 0.005 \text{ m}^3 \text{ mol}^{-1} \text{ s}^{-1}$ )

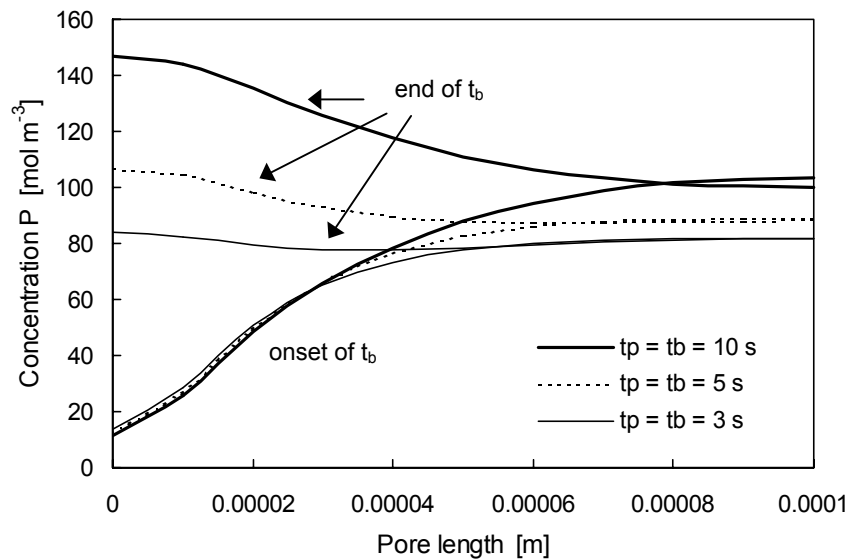


**Figure 7.20.** Concentration profiles of liquid phase product P inside a periodically wetted pore at the onset and ending of  $t_b$  for a relatively fast cycled liquid feed ( $U_{ip} = 0.0197 \text{ m s}^{-1}$ ;  $U_{lb} = 0.001 \text{ m s}^{-1}$ ;  $k_{r1} = 0.005 \text{ m}^3 \text{ mol}^{-1} \text{ s}^{-1}$ ;  $k_{r2} = 0.0005 \text{ m}^3 \text{ mol}^{-1} \text{ s}^{-1}$ )



## 7.7. Practical relevance of modeling results

### 7.7.1. Frequency of cycling

A relatively fast cycling of the liquid feed is superior to a relatively slow cycling of the liquid feed in terms of production capacity, conversion and selectivity. In a real experimental system, the frequency of the cycled liquid feed is limited to relatively low frequencies. Due to the step-change in liquid flow rate, liquid-rich continuity shock waves are initiated. These shock waves, however, decay by leaving liquid behind at the tail. This results in an increase in the tail length as the shock wave moves down the reactor. When a relatively short  $t_b$  is applied, subsequent shock waves overlap and the wetting of the catalyst in between shock waves increases. This diminishes the overall mass transfer rate of the gaseous reactant to the catalyst surface and the positive effects due to periodic operation vanish, as discussed in chapter 5. A relatively fast cycling of the liquid feed is, however, possible by the fast mode of liquid-induced pulsing flow. In this mode of operation, individual natural pulses are induced at a pre-determined frequency. All frequencies less than 1 Hz can be obtained with this mode of operation, while frequencies during natural pulsing flow vary between 1 and 10 Hz. Since pulse durations are rather short (0.3 s), the ratio of pulse ( $t_p$ ) to base ( $t_b$ ) duration cannot be adjusted at all desired values. However, with the fast mode of liquid-induced pulsing flow it is also possible to induce triple pulses in a controlled manner and externally control the period in between the cluster of pulses. This may be a method to gain more freedom in choosing the ratio of  $t_p$  to  $t_b$ .

### 7.7.2. Selectivity

The model predicts that the selectivity for consecutive reactions with linear kinetics during periodic operation is in all cases less compared to the selectivity during steady state operation, caused by the relatively high average concentration levels of the product P inside the catalyst. The model, however, idealizes trickle flow operation since the impact of stagnant liquid holdup, axial dispersion, flow maldistribution and localized hot spots is neglected. These may negatively affect selectivity in trickle flow operation. Since pulses continuously mobilize the stagnant holdup, diminish axial dispersion and prevent flow maldistribution and hot spot formation, selectivity during the fast mode of liquid-induced pulsing flow may be comparable or even higher than selectivity during trickle flow operation. Wu et. al. (1999) obtained higher selectivities for the selective hydrogenation of phenylacetylene to styrene (and ethyl benzene) during pulsing flow.

Their modeling efforts (Wu et. al., 1995) predict increased selectivity depending on the pulse frequency. However, their model neglects the impact of internal diffusion. Although, in case of linear reaction kinetics, selectivity decreases due to periodic operation, increases in selectivity may be obtained for reactions with non-linear kinetics (Lee and Bailey, 1974).

### 7.7.3. Liquid-limited reactions

Periodic operation negatively affects reactor performance in case of liquid-limited reactions. However, a relatively fast cycling of the liquid feed may improve the flow distribution and wetting efficiency, since continuity shock waves are initiated by liquid feed cycling. These waves probably mix to some extent parallel flowing liquid streams and stagnant liquid holdup. A better flow distribution may persist after the lower liquid flow rate is re-introduced. With this mode of operation, wetting efficiency may be increased while the liquid phase residence time remains comparable to trickle flow operation. Periodic operation should then increase reactor performance for liquid-limited reactions as well.

## 7.8. Concluding remarks

The model presented in this chapter is developed to gain a better insight in the effect of periodic operation on production capacity, conversion and selectivity. Although the model is a simplification of reality, some general conclusions based on the modeling results can be drawn.

The optimal duration of the high and of the low (zero) liquid feed strongly interdepend. With increasing  $t_b$ , an increasing amount of the liquid phase reactant is consumed during  $t_b$ . Hence, increasing  $t_b$  must be accompanied by increasing  $t_p$  since a greater amount of liquid phase reactant must be supplied during  $t_p$ . With decreasing reaction rate constant, the liquid phase reactant is less fast consumed by reaction during  $t_b$ , and a shorter  $t_p$  is sufficient to supply fresh liquid phase reactant to the catalyst. Therefore, the optimal  $t_b$  and ratio of  $t_p$  to  $t_b$  strongly depend on the reaction rate constant. For fast reactions, a shorter  $t_b$  and a higher ratio of  $t_p$  to  $t_b$  compared to slow reactions are preferred. The selectivity of consecutive reactions during periodic operation always seems less for linear kinetics than for steady state operation due to the enhanced residence time of the product and the higher concentration levels of the product inside the catalyst.

A fast cycling of the liquid feed is most effective in terms of production capacity, conversion and selectivity.

With increasing cycled liquid feed frequency, the time average concentration of the liquid phase reactant A inside the periodically wetted catalyst pores increases and the time-average concentration of the product P decreases. High concentrations of liquid phase reactant A result in high reaction rates for the desired reaction. Low concentration levels of the product P lead to low reaction rates for the undesired reaction. Furthermore, at fast liquid feed cycling, the reaction zone is confined near the catalyst surface. This means that the residence time of the product P in the reaction zone is decreased. To overcome selectivity problems during periodic operation, it would be beneficial to use a thinly washcoated impermeable catalyst. The use of such a catalyst will require a relative fast liquid feed cycling.

Most experimental studies concerning reactor performance improvement during periodic operation focus on the optimization of the conversion. In Fig. 7.13 it is clearly exposed that indeed very high conversions can be obtained during periodic operation. However, very high conversions are accompanied by relatively low production capacities. One should aim at the optimal combination of production capacity and conversion instead of conversion alone.

In industrial trickle-bed reactors, high operating pressures are applied to increase the solubility of the gaseous reactant in the liquid phase. By periodic operation of a trickle-bed reactor, the mass transfer rate of the gaseous reactant is enormously increased. Therefore, it is possible to operate the reactor at lower pressures under periodic operation, which reduces capital and energy costs. Since the production capacity may be increased by a factor 4 (Gabarain et. al., 1997), a four-fold reduction in pressure is possible, since the reaction rate is usually first order in the gas phase (partial) pressure. The reduction in pressure is, however, limited to the pressure needed to keep the liquid phase as liquid at the desired operating temperature.

## Notation

$a_{gl}$	specific gas-liquid interfacial area	$[m^{-1}]$
$a_s$	specific catalyst surface area	$[m^{-1}]$
$C_i^j$	concentration component i in phase j	$[mol\ m^{-3}]$
$C_{if}$	feed concentration component i	$[mol\ m^{-3}]$
$c_{pl}$	heat capacity liquid phase	$[J\ kg^{-1}\ K^{-1}]$
$c_{ps}$	heat capacity catalyst	$[J\ kg^{-1}\ K^{-1}]$
$D_{ei}$	effective diffusion coefficient	$[m^2\ s^{-1}]$

Dynamic modeling of periodically operated trickle-bed reactors

---

$E_{ai}$	activation energy reaction i	$[J\ mol^{-1}]$
$f_g$	actual gas-catalyst contacting efficiency	$[-]$
$f_{gb}$	gas-catalyst contacting efficiency during low feed	$[-]$
$f_{gp}$	gas-catalyst contacting efficiency during high feed	$[-]$
$f_i$	actual wetting efficiency	$[-]$
$f_{lb}$	wetting efficiency during low liquid feed	$[-]$
$f_{lp}$	wetting efficiency during high liquid feed	$[-]$
$f_p$	cycled liquid feed frequency	$[s^{-1}]$
$k_{g,G}$	gas-particle mass transfer coefficient	$[m\ s^{-1}]$
$k_{l,G}$	gas-liquid mass transfer coefficient	$[m\ s^{-1}]$
$k_{ri}$	reaction rate constant reaction i	$[m^3\ mol^{-1}\ s^{-1}]$
$k_{ri}^0$	frequency factor reaction i	$[m^3\ mol^{-1}\ s^{-1}]$
$k_{s,i}$	particle-liquid mass transfer coefficient	$[m\ s^{-1}]$
$m$	modified Henry coefficient	$[C_G^g\ C_{Geql}^l]$
$n_p$	integer parameter	$[-]$
$P$	pressure	$[N\ m^{-2}]$
$P_c$	production capacity defined by eq. 7.31	$[mol\ m^{-2}\ s^{-1}]$
$P_G$	partial pressure gas phase reactant G	$[N\ m^{-2}]$
$r_i^j$	reaction rate of reaction i in phase j	$[mol\ m^{-3}\ s^{-1}]$
$R$	gas constant	$[J\ mol^{-1}\ K^{-1}]$
$R_i^j$	total reaction rate component i in phase j	$[mol\ m^{-3}\ s^{-1}]$
$S$	selectivity defined by eq. 7.30	$[-]$
$t_b$	duration of base feed	$[s]$
$T_i$	temperature of phase i	$[K]$
$t_p$	duration of pulse feed	$[s]$
$U_i$	superficial velocity phase i	$[m\ s^{-1}]$
$V_s$	shock wave velocity	$[m\ s^{-1}]$
$X$	conversion defined by eq. 7.29	$[-]$
$\alpha_p$	particle-liquid heat transfer coefficient	$[W\ m^{-2}\ K^{-1}]$
$\beta$	liquid holdup (based on empty column)	$[-]$
$\beta_b$	liquid holdup during low liquid feed	$[-]$
$\beta_p$	liquid holdup during high liquid feed	$[-]$
$-\Delta H_i$	reaction enthalpy reaction i	$[J\ mol^{-1}]$
$\delta$	pore length	$[m]$
$\varepsilon$	porosity packed bed	$[-]$
$\varepsilon_p$	catalyst porosity	$[-]$

$\phi$	Thiele modulus defined by equation 7.32	[-]
$\rho_l$	density liquid phase	[kg m <sup>-3</sup> ]
$\rho_s$	skelet density catalyst	[kg m <sup>-3</sup> ]

## Literature cited

- Beaudry E.G., Dudukovic M.P. and Mills P.L., Trickle-bed reactors: liquid diffusional effects in a gas-limited reaction., *AIChE J.*, **33**, 1435-1447, 1987
- Castellari A.T. and Haure P.M., Experimental study of the periodic operation of a trickle bed reactor, *AIChE J.*, **41**, 1593-1597, 1995
- Chou T.S., Worley F.J. and Luss D., Local particle-liquid mass transfer fluctuations in mixed-phase cocurrent downflow through a fixed bed in the pulsing regime, *Ind. Eng. Chem. Fund.*, **18**, 279-283, 1979
- Dwivedi P.N. and Upadhyay S.N., Particle-fluid mass transfer in fixed and fluidized beds, *Ind. Eng. Chem. Proc. Des. Dev.*, **16**, 157-165, 1977
- Gabarain L., Castellari A.T., Cechini J., Tobolski A. and Haure P.M., Analysis of rate enhancement in a periodically operated trickle-bed reactor, *AIChE J.*, **43**, 166-172, 1997
- Goto S. and Smith J.M., Trickle-bed reactor performance. Part I: Holdup and mass transfer effects, *AIChE J.*, **21**, 698, 1975
- Haure P.M., Hudgins R.R. and Silveston P.L., Periodic operation of a trickle-bed reactor, *AIChE J.*, **35**, 1437-1444, 1989
- Lange R., Hanika J., Stradiotto D., Hudgins R.R. and Silveston P.L., Investigations of periodically operated trickle-bed reactors, *Chem. Eng. Sci.*, **49**, 5615-5621, 1994
- Lee C.K. and Bailey J.E., Diffusion waves and selectivity modifications in cyclic operation of a porous catalyst, *Chem. Eng. Sci.*, **29**, 1157-1163, 1974
- Khaldikar M.R., Wu Y.X., Al-Dahhan M.H., Dudukovic M.P. and Colakyan M., Comparison of trickle bed and upflow performance at high pressure. Model predictions and experimental observations, *Chem. Eng. Sci.*, **51**, 2139, 1996
- Kouris Ch., Neophytides St., Vayenas C.G. and Tsamopoulos J., Unsteady state operation of catalytic particles with constant and periodically changing degree of external wetting, *Chem. Eng. Sci.*, **53**, 3129-3142, 1998
- Mendizaball D.G., Aguilera M.E. and Pironti F., Solid-liquid mass transfer and wetting factors in trickle-bed reactors, *Chem. Eng. Commun.*, **169**, 37-55, 1998
- Mills P.L. and Dudukovic M.P., Analysis of catalyst effectiveness in trickle bed reactors processing volatile or nonvolatile reactants, *Chem. Eng. Sci.*, **35**, 2267, 1980
- Schiesser W.E., *The numerical method of lines*, Academic Press, London, 1991
- Stradiotto D.A., Hudgins R.R. and Silveston P.L., Hydrogenation of crotonaldehyde under periodic flow interruption in a trickle bed, *Chem. Eng. Sci.*, **54**, 2561-2568, 1999
- Wu R., McCready M.J. and Varma A., Influence of mass transfer coefficient fluctuation frequency on performance of three-phase packed bed reactors, *Chem. Eng. Sci.*, **50**, 3333-3344, 1995
- Wu R., McCready M.J. and Varma A., Effect of pulsing on reaction outcome in a gas-liquid catalytic packed-bed reactor, *Catalysis Today*, **48**, 195-198, 1999

---

## Chapter 8

---

# Nonsteady Operation State of the Art and Perspectives

---

### 8.1. Introduction

Gas-liquid downflow through fixed beds of catalyst particles is frequently selected in chemical reactor design. These trickle-bed reactors are often applied to perform strong exothermic reactions such as hydrogenations and oxidations. At present, steady state operation in the trickle flow regime is most common in industrial applications. Liquid maldistribution and the formation of hot spots are the most serious problems experienced during trickle flow operation.

Cycling the liquid flow rate results in large performance improvements compared to the optimal steady state (Haure et. al., 1989; Lange et. al., 1994; Lee et. al., 1995; Castellari et. al., 1995; Gabarain et. al., 1997; Khaldikar et. al., 1999). However, periodic operation of trickle-bed reactors is not commercially implemented because of (a) a lack of knowledge of the transport and kinetic parameters under dynamic conditions; (b) a lack of an established methodology to determine the optimal operating parameters; (c) uncertainty regarding operation and control of large-scale trickle-bed reactors under transient conditions.

This chapter summarizes the various modes of nonsteady operation of trickle-bed reactors and discusses the potential advantages gained. Moreover, future challenges are discussed.

### 8.2. Hydrodynamic description of operation modes

In this thesis, several nonsteady state operation modes of trickle-bed reactors are developed and investigated. These operation methods are nonsteady state in the sense that the column is run through with waves of liquid and hence the liquid flow rate in the column fluctuates. The several modes of nonsteady state operation in terms of liquid holdup traces are schematically shown in Fig. 8.1.

Cycling the liquid feed results in the formation of liquid-rich continuity shock waves in the column (Fig. 8.1a). This is essentially the nonsteady operation mode encountered in the literature studies mentioned earlier.

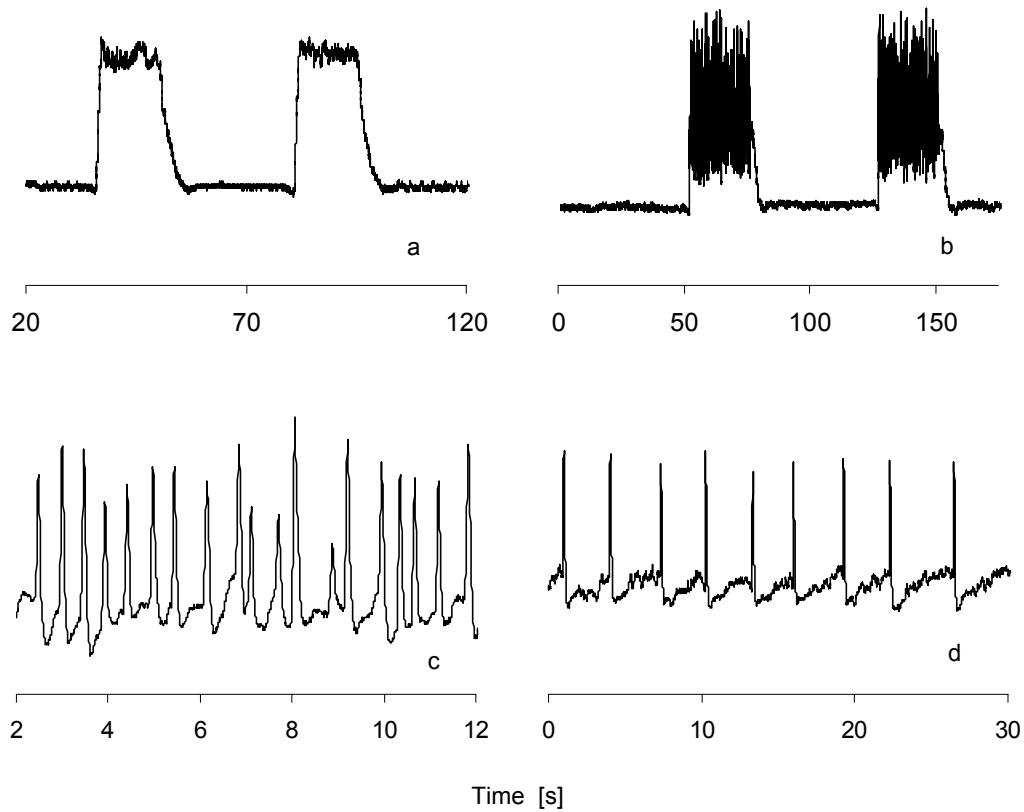


**Figure 8.1.** Liquid holdup traces of the various hydrodynamic nonsteady operation modes of a trickle-bed reactor (a: continuity shock waves; b: slow mode liquid-induced pulsing flow; c: natural pulsing flow; d: fast mode of liquid-induced pulsing flow)

The bed is alternately exposed to high and low (zero) liquid flow rates. However, the flow regime during both high and low liquid flow rates is trickle flow. At sufficiently high gas flow rates, inception of pulses occurs within the liquid-rich shock waves. This is referred to as the slow mode of liquid-induced pulsing flow (Fig. 8.1b). The pulses are characterized by high mass and heat transfer rates and complete catalyst wetting. The shock waves, whether they contain pulses or not, decay by leaving liquid behind at the tail. Relatively long periods of the high and low liquid feed must be applied to prevent total collapse of the shock waves respectively overlap between successive shock waves. Overlap between successive shock waves causes the periods of low (zero) liquid flow rate to vanish and hence the positive effects resulting from periodic operation disappear.

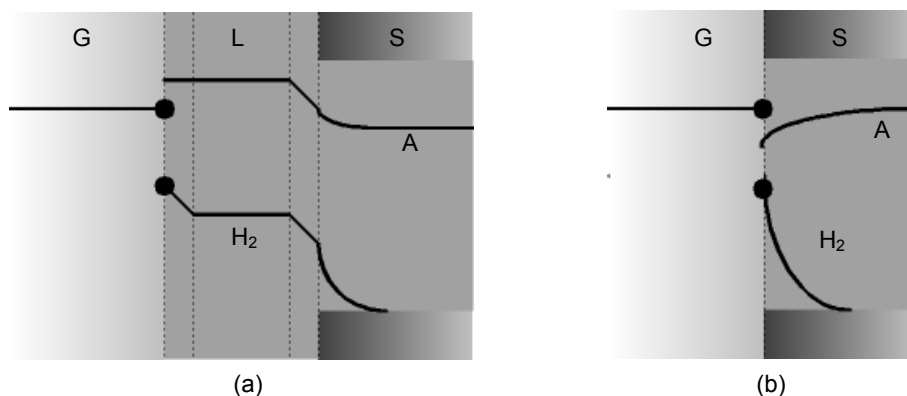


**Figure 8.2.** Concentration profiles for a liquid phase reactant A and a gas phase reactant H<sub>2</sub> inside a catalyst pore, which is in contact with respectively (a) the liquid; (b) the gas

A fast cycling of the liquid flow rate in the bed is achieved by the natural pulsing flow regime, schematically shown in Fig. 8.1c. Pulse frequencies are typically between 1 and 10 Hz. Much lower pulse frequencies are achieved by the fast mode of liquid-induced pulsing flow as is schematically shown in Fig. 8.1d. By applying short periods of a high liquid flow rate, individual natural pulses are induced at sufficiently high gas flow rates. The frequency of the pulses during the fast mode of liquid-induced pulsing flow is externally set by the cycled liquid feed frequency. All pulse frequencies less than 1 Hz can be obtained with this mode of operation.

### 8.3. Gas-limited reactions

Hydrogenations and oxidations often suffer from the low solubility of the gas phase reactant (H<sub>2</sub>, O<sub>2</sub>) in the liquid phase. Therefore, elevated pressures (up to 30 MPa) are required to improve the gas solubility and the driving force for mass transfer of the gaseous reactant. For a completely wetted catalyst particle, the gaseous reactant must overcome both the gas-liquid and liquid-solid mass transfer resistances, as schematically shown in Fig. 8.2a. Note that the drawing in Fig. 8.2 is very schematic. In fact, the two boundary layers may overlap. Partial wetting facilitates a much more effective transport of the gaseous reactant at the dry surface since the liquid film mass transfer resistance is largely eliminated.



This situation is schematically presented in Fig. 8.2b. Direct contact of the gas phase with the catalyst facilitates a high flux of the gaseous reactant at the catalyst surface. Moreover, the concentration of the gaseous reactant at the catalyst surface approaches the concentration in gas-liquid equilibrium, which results in a steeper concentration gradient inside the catalyst. The reduction of the mass transfer resistance for the rate-limiting gaseous reactant on partially wetted pellets leads to much higher observed reaction rates. Hence, for gas-limited reactions, partial wetting conditions are preferred. The main problem during steady state operation is to attain partial wetting without gross liquid maldistribution, which usually leads to unpredictable and uncontrollable reactor performance. When large parts of the bed are dry, hot spots may appear or liquid phase reactant mass transfer may limit the reaction in these parts.

Cycling the liquid feed results in temporal variations in the wetting efficiency of the catalyst particles, without the problem of gross liquid maldistribution and the danger of hot spot formation. During the non-wetted part of the feed cycle, the gaseous reactant has increased access to the catalyst. During the wetted part of the feed cycle, the heat and reaction products are removed from the catalyst and fresh liquid phase reactant is supplied. Since the higher reaction rates prevail during the non-wetted part of the feed cycle, shorter flushes increase reactor performance even more. Shorter flushes can be achieved by the slow mode of liquid-induced pulsing flow, since the pulses enhance the rate of heat removal and mass transfer of the products and reactants. Especially, the danger of hot spot formation is prevented during the slow mode of liquid-induced pulsing flow, since the pulses are characterized by complete catalyst wetting and high particle-liquid heat transfer rates. This heat elimination is of particular interest since during the low part of the feed cycle, the liquid insufficiently removes the reaction heat and a significant temperature increase of the catalyst bed prevails.

For consecutive reactions, selectivity might be a problem during periodic operation. During the non-wetted part of the feed cycle, the product remains inside the catalyst and the likelihood for further reaction to the undesired product is enhanced. Therefore, a faster mode of periodic operation is necessary. During a fast mode of periodic operation, the residence time of the product inside the reaction zone in the catalyst is reduced and the time-average concentration ratio of the liquid phase reactant to the liquid phase product inside the catalyst is enhanced. Hence, the importance of the reaction to the desired product with respect to the reaction to the undesired product increases.

Due to the decay of the shock waves, the frequency of the cycled liquid feed is limited to relatively low values. The fast mode of liquid-induced pulsing flow offers the possibility of a high frequency liquid flow rate cycling. Inside the pulses, catalyst wetting is complete. An unresolved issue at this moment concerns the wetting efficiency in between pulses. Draining needs time and therefore the wetting efficiency of the catalyst will gradually decrease when a pulse has passed. For gas-limited reactions, however, it is important to obtain the lowest possible wetting in between pulses since then the largest increase in the mass transfer rate of the gaseous reactant to the catalyst surface is obtained. It is reasonable to assume that wetting efficiency in between pulses during the fast mode of liquid-induced pulsing flow is intermediate and very thin liquid films exist. Moreover, the volumetric gas-liquid mass transfer rates are greatly enhanced, since pulses are characterized by large gas-liquid specific areas and gas-liquid surface renewal rates. To overcome selectivity problems during periodic operation it would certainly be beneficial to use a thinly washcoated impermeable catalyst. The use of such a catalyst will require a much faster liquid feed cycling.

In industrial operations, high operating pressures are applied in order to increase the solubility of the gaseous reactant in the liquid phase. By periodic operation of a trickle-bed reactor, the mass transfer rate of the gaseous reactant is tremendously increased. Therefore, it is possible to operate the reactor at lower pressures under periodic operation, which reduces capital and energy costs. Increases in reaction rate up to a factor of 4 can be achieved by periodic operation of a trickle-bed reactor (Gabarain et. al., 1997). Since the reaction rate is usually first order in the gas phase (partial) pressure, a 4-fold reduction in pressure is possible. The reduction in pressure is however limited to the pressure required to keep the liquid phase as liquid at the desired operating temperature.

#### **8.4. Liquid-limited reactions**

Liquid-limited reactions are frequently encountered in high-pressure operations in petroleum processing and in processes in which a diluted liquid phase reactant must be converted, as in hydrodesulfurization and oxidation of organic compounds in waste water treatment. For liquid-limited reactions, the highest possible wetting efficiency and the highest possible particle-liquid mass transfer rate result in the fastest transport of the liquid phase reactant to the catalyst.

The operation of a trickle-bed reactor in the natural pulsing flow regime at high pulse frequencies results in complete catalyst wetting and high particle-liquid mass transfer rates. Therefore, pulsing flow is appropriate for liquid-limited reactions. However, relatively high gas and liquid flow rates are required to achieve the natural pulsing flow regime. High flow rates of the liquid phase result in a relatively short residence time of the liquid in the reactor. Shorter liquid residence times are associated with lower conversions per unit reactor length. The enhanced volumetric particle-liquid mass transfer rates during natural pulsing flow may therefore be counterbalanced by shorter residence times of the liquid phase. By applying the fast mode of liquid-induced pulsing flow, 25% lower liquid flow rates are needed at the expense of lower pulse frequencies. As mentioned in the previous section, it is not clear at this moment by what amount the wetting efficiency is diminished at low frequency pulsing.

A relatively fast cycling of the liquid feed without pulse induction may improve the flow distribution and wetting efficiency, since continuity shock waves are initiated by liquid feed cycling. These waves probably mix to some extent parallel flowing liquid streams and stagnant liquid holdup. A better flow distribution may persist after the lower liquid flow rate is re-introduced. With this mode of operation, wetting efficiency may increase while the residence time of the liquid phase remains comparable to trickle flow operation.

### **8.5. Hot spot control by periodic operation**

The avoidance of hot spots is extremely important from its safe operation point of view. Hot spots are created due to liquid maldistribution that causes parts of the catalyst bed to be dry. In a dry region, reaction between volatile reactants proceeds, its rate being usually higher than during liquid phase conditions. Since the liquid phase is absent, the reaction heat is insufficiently removed. The higher reaction rate accelerates heat production and thus hot spot enlargement is often observed. Hot spot formation is one of the major problems experienced during steady state trickle flow operation.

Development of hot spots takes time and can be cut off by periodically flooding the trickle-bed reactor with the liquid phase. The periodic induction of natural pulses at relatively low frequencies seems most appropriate for hot spot control. Natural pulses are characterized by complete catalyst wetting and high particle-liquid heat transfer rates.

Moreover, the pulses periodically mix the stagnant liquid holdup that could act as a heat sink. The fast mode of liquid-induced pulsing flow at very low pulse frequencies could be used for hot spot control. The trickle-bed reactor is then essentially operated in the trickle flow regime while at designated times one or more pulses are induced by periodically raising the liquid feed.

## 8.6. Future challenges

### 8.6.1. Reaction study

Spectacular increases in reaction rates were obtained for the hydrogenation of  $\alpha$ -methyl styrene during the periodic operation (e.g. Castellari and Haure, 1995; Gabarain et. al., 1997). Since the strategies for liquid feed cycling are expanded to include the slow and fast mode of liquid-induced pulsing flow, it is crucial to test these feed strategies in a reaction system. Especially, selective reactions need to be tested since it seems that periodic operation may give rise to selectivity problems. Up until now, the effect of periodic operation on selectivity has not been reported in literature.

### 8.6.2. Wetting in between pulses

An unresolved issue at this moment concerns the catalyst wetting in between pulses during both natural pulsing flow and the fast mode of liquid-induced pulsing flow. Draining needs time and therefore the wetting efficiency will gradually decrease after the passage of a pulse. Wetting is thus a dynamic process. For gas-limited reactions, however, it is important to achieve the lowest possible wetting in between pulses since then the largest increase in the mass transfer rate of the gaseous reactant to the catalyst surface is obtained. It is reasonable to assume that wetting in between pulses is near complete at high pulse frequencies during natural pulsing flow and that an intermediate wetting efficiency in between pulses exists at low pulse frequencies during the fast mode of liquid-induced pulsing flow. It would, however, be desirable to quantify the wetting efficiency in between pulses as a function of the pulse frequency or to control the wetting efficiency in between pulses by modification of the wetting characteristics of the catalyst.

Instantaneous local wetting efficiency could be measured by a custom-made anemometer. The anemometer should then consist of a packing particle coated with a thin Pt film. In chapter 2, a small hot film anemometer was situated in between the packing interstices. In between pulses, the anemometer was randomly exposed to the gas respectively the liquid phase.

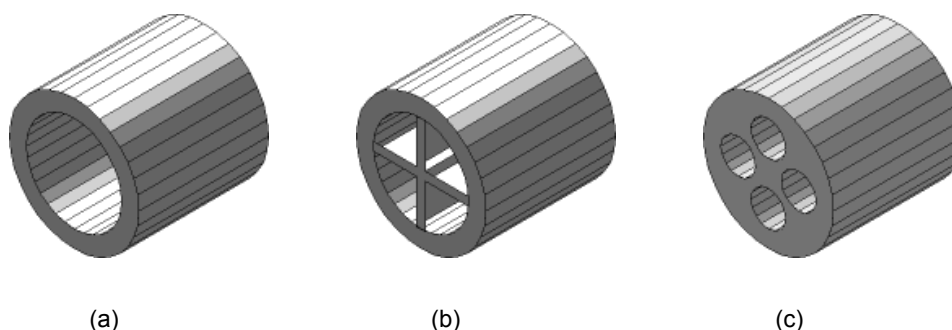


**Figure 8.3.** Different packing materials with a large specific area (a: hollow cylinder; b: wagon wheel; c: multiple-hole pellet)

In addition, the liquid holdup in between pulses is very low, so presumably some temporal segregation in wetting efficiency exists. It might be possible to determine the dynamic wetting efficiency during natural pulsing flow and the fast mode liquid-induced pulsing flow with this kind of probe.

A method to control wetting efficiency is modification of the wettability of the catalyst. Horowitz et. al. (1999) examined the effect of catalyst wettability on the oxidation of ethanol dissolved in water. The catalyst was coated with Teflon fibers to make the particle surface hydrophobic. A remarkable improvement in the reactor performance was found when a hydrophobic catalyst or mixtures of hydrophobic and hydrophilic catalyst were used. Increases in conversion up to 100% were achieved. Rangwala et. al. (1990) measured a seven-fold decrease in liquid holdup for a NaOH-solution upon a change in hydrophilic to hydrophobic packing particles. This clearly demonstrates the possibility to decrease the wetting efficiency by modification of the wettability of the catalyst.

### 8.6.3. Catalyst design

The observed rate of chemical reactions carried out in trickle-bed reactors is often diffusion-limited due to the low rate of diffusion of the reactants relative to that of chemical reaction. Increasing the external surface area of the catalyst particles by decreasing the pellet size reduces the deleterious impact of diffusion limitations. The reduced particle size, however, increases the pressure drop over the bed. An alternative method is to modify the shape of the catalyst pellets with exterior lobes or holes.

Sims et. al. (1993) measured instantaneous particle-liquid mass transfer rates for hollow pellets in the pulsing flow regime. They found that at the inner surface of the hollow pellets, mass transfer fluctuations during pulsing flow were almost comparable to the external mass transfer fluctuations. This suggests that the internal surface area of such a packing material actively participates in the dynamic process of mass transfer during periodic operation. Different shapes of hollow pellets are presented in Fig. 8.3. The ultimate shape of such particles could be a small monolith: miniliths.

As previously stated, modification of the catalyst wetting characteristics may result in large increases in reaction rates. Such a packing material facilitates forced control of the wetting efficiency. Modification of the wettability of the catalyst may also reduce the wetting in between pulses during the fast mode of liquid-induced pulsing flow thus improving the mass transfer rates of the gaseous reactant.

The use of a thinly washcoated impermeable catalyst may strongly benefit selectivity at the expense of production capacity. However, the increase in production capacity due to periodic operation of a trickle-bed reactor may result in higher selectivities at comparable or higher production capacities. The use of such a catalyst will require a much faster liquid feed cycling

#### **8.6.4. Liquid distribution during periodic operation**

As mentioned before, a relatively fast cycling of the liquid feed without pulse induction may improve the flow distribution and wetting efficiency, since continuity shock waves are initiated by liquid feed cycling. These waves to some extent mix parallel flowing liquid streams and stagnant liquid holdup. A better flow distribution may persist after the lower liquid flow rate is re-introduced. With this mode of operation, wetting efficiency may be increased. This results in performance improvement for liquid-limited reactions and may be utilized to control hot spot formation.

No studies are reported concerning the distribution of flow during cycled liquid feed conditions. Stradiotto et. al. (1999) explained the conversion enhancement for crotonaldehyde hydrogenation during liquid-limited conditions by an improved wetting efficiency due to liquid feed cycling at relatively low liquid flow rates. Possible improvements of liquid distribution by cycling the liquid feed justify experimental studies on this subject.

### 8.6.5. Operation near the boiling point of the liquid

Periodic operation may also be regarded as a method to operate the reactor for a certain period in a steady state situation that creates high reaction rates but is not feasible as steady state operation. A gas phase reaction is accompanied by large reaction rates compared to liquid phase conditions. At low liquid velocities, a pure gas phase reaction was observed by Castellari et. al. (1997) and Satterfield and Ozel (1973), although initially a gas-liquid reaction occurred. However this gas phase reaction may not be feasible as steady state operation due to the very poor heat removal and the danger of hot spot formation. By periodic operation it is possible to operate the reactor alternately in the gas-phase regime and gas-liquid phase regime. During the low part of the feed cycle, the heat of reaction must evaporate the liquid phase. The operating temperature must therefore be near the boiling point of the liquid. During the gas-phase regime, high reaction rates are encountered, while during the gas-liquid regime, the heat is removed from the catalyst. An opportunity might be found if the evaporation of the liquid in the catalyst pores is so fast, that during a dry period all liquid is removed geysierlike, while fresh liquid is drawn in during the next pulse time. Then a 'breathing catalyst', the dream of the chemical engineer, can eventually be realized. It would be worth investigating the cycling of the reactor between the gas phase regime and the gas-liquid phase regime.

### 8.6.6. Large diameter columns

An unresolved issue concerns pulse formation in columns with larger diameter than the lab-scale trickle-bed columns. Christensen et. al. (1986) performed experiments in a rectangular column with a cross-section of 0.05 x 0.4 m. Upon increasing the gas flow rate, local pulsing was initially obtained and eventually pulses spanning the entire column cross-section were observed. Krieg et. al. (1995) suggested that the pulse frequency for a given packing material depends on the column diameter. Kolb et. al. (1990) indeed observed pulse frequencies up to 80 Hz in a column of 2.5 mm in diameter. No systematic studies concerning the effect of column diameter on pulsing flow hydrodynamics are reported in literature.

In case pulses that not span the entire column cross-section are obtained in large diameter columns at feasible gas flow rates, one might consider application of a compartmentalized trickle-bed reactor. This type of reactor leads to higher investment costs. However, since reactors may be smaller in case of periodic operation and the operating pressure may be reduced, it might be attractive to apply compartmentalized trickle-bed reactors.

## 8.7. Concluding remarks

For both liquid-limited and gas-limited reactions, different nonsteady operation modes exist that increase the mass transfer of the rate-limiting reactant. Periodic operation of a trickle-bed reactor may be utilized to diminish flow maldistribution and to prevent the formation of hot spots, which are the main problems experienced during steady state trickle flow operation. Since the periodic operation rests upon the manipulation of an external variable, existing trickle-bed reactors may simply be modified to meet the demands of performance improvement. For trickle-bed reactors to be developed, a decrease in investment cost is expected, since liquid redistributers and inter-bed heat exchangers may be eliminated. Moreover, smaller reactors and reduced operating pressures may be achieved. These considerations suggest that periodic operation is a general method and should find wide application.

## Literature cited

- Castellari A.T. and Haure P.M., Experimental study of the periodic operation of a trickle bed reactor, *AIChE J.*, 41, 1593-1597, 1995
- Castellari A.T., Cechini J.O., Gabarain L.J. and Haure P.M., Gas-phase reaction in a trickle-bed reactor operated at low liquid flow rates, *AIChE J.*, 43, 813-1818, 1997
- Christensen G., McGovern J. and Sundaresan S., Cocurrent downflow of air and water in a two-dimensional packed column, *AIChE J.*, 32, 1677-1689, 1986
- Gabarain L., Castellari A.T., Cechini J., Tobolski A. and Haure P.M., Analysis of rate enhancement in a periodically operated trickle-bed reactor, *AIChE J.*, 43, 166-172, 1997
- Haure P.M., Hudgins R.R. and Silveston P.L., Periodic operation of a trickle-bed reactor, *AIChE J.*, 35, 1437-1444, 1989
- Horowitz G.I., Martinez O., Cukierman A.L. and Cassanello M.C., Effect of the catalyst wettability on the performance of a trickle-bed reactor for ethanol oxidation as case study, *Chem. Eng. Sci.*, 54, 4811-4816, 1999
- Khaldikar M.R., Al-Dahhan M.H. and Dudukovic M.P., Parametric study of unsteady-state flow modulation in trickle-bed reactors, *Chem. Eng. Sci.*, 54, 2585-2595, 1999
- Krieg D.A., Helwick J.A., Dillon P.O. and McCready M.J., Origin of disturbances in cocurrent gas-liquid packed bed flows, *AIChE J.*, 41, 1653-1666, 1995
- Kolb W.B., Melli T.R., Santos de J.M. and Scriven L.E., Cocurrent downflow in packed beds. Flow regimes and their acoustic signatures, *Ind. Eng. Chem. Res.*, 29, 2380-2389, 1990
- Lange R., Hanika J., Stradiotto D., Hudgins R.R. and Silveston P.L., Investigations of periodically operated trickle-bed reactors, *Chem. Eng. Sci.*, 49, 5615-5621, 1994
- Lee K.J., Hudgins R.R. and Silveston P.L., A cycled trickle bed reactor for SO<sub>2</sub> oxidation, *Chem. Eng. Sci.*, 50, 2523-2530, 1995



- Rangwala H.A., Otto F.D., Wanke S.E. and Chuang K.T., Mass transfer in a trickle-bed column packed with a mixture of hydrophobic and hydrophilic spheres, *Can. J. Chem. Eng.*, 68, 237-241, 1990
- Satterfield C.N. and Ozel F., Direct solid-catalyzed reaction of a vapor in an apparently completely wetted trickle bed reactor, *AIChE J.*, 19, 1259-1261, 1973
- Sims W.B., Schulz F.G. and Luss D., Solid-liquid mass transfer to hollow pellets in a trickle bed, *Ind. Eng. Chem. Res.*, 32, 1895-1903, 1993
- Stradiotto D.A., Hudgins R.R. and Silveston P.L., Hydrogenation of crotonaldehyde under periodic flow interruption in a trickle bed, *Chem. Eng. Sci.*, 54, 2561-2568, 1999

---

## Dankwoord

---

De totstandkoming van dit proefschrift is niet alleen het resultaat van de inspanningen van de auteur zelf. Op de eerste plaats gaat mijn dank uit naar mijn promotor Bart Drinkenburg en mijn coach Hub Piepers, die naast serieuze begeleiders gelukkig ook zeer niet-serieuze mensen blijken te zijn. Bart, bedankt voor alle vrijheid die je me hebt gegeven om het onderzoek in belangrijke mate zelf in te vullen en alle kansen die je me hebt geboden om met belangstellenden van buiten de TUE te discussiëren over het onderzoek. Hub, naast de dagelijkse begeleiding, bedankt voor alle gezelligheid op de TUE en tijdens onze congresbezoeken.

Dit proefschrift berust voor een groot deel op experimenteel werk waarbij een aantal experimentele opstellingen en meettechnieken onontbeerlijk waren. Ofschoon ik toch enkele technische vaardigheden onder de knie gekregen heb, vrees ik dat het proefschrift puur theoretisch geworden zou zijn indien ik niet de hulp van de volgende mensen zou hebben gehad: Paul Aendenroomer, Anton Bombeeck, Henk Hermans, Rinus Janssen, Jan Ketelaars, Chris Luyk, Theo Maas, Jovita Moerel, Jan den Otter en Hans Wijtvliet. Mijn speciale dank gaat uit naar Vincent Arts die overal verstand van heeft.

De bijdrage van de volgende afstudeerders en researchstagiaires is zeer hulpvol geweest bij de totstandkoming van dit proefschrift: Ruben Bayens, Bauke Hoogenstrijd, Ralph van Lankveld, Hatim Machrafi en Sanne Severins.

Sonja Boelhouwer, bedankt dat je een betere spellingscontrole bent dan die in MS Word opgenomen is. Joop Boonstra, door jou kunnen computers en ik beter met elkaar overweg. Wil Heugen, bedankt voor alles dat niet in je officiële functiebeschrijving staat. Joost Heijnen, die inmiddels ook het een en ander over trickle-bed reactoren afweet, bedankt voor je kritische commentaar. Jos Janssen en mevrouw Blijlevens, dat elektrochemie ook een vak is, heb ik van jullie geleerd.

Naast de inspanningen hebben ook de ontspanningen geleid tot dit proefschrift. Vincent Arts, Joop Boonstra, Joost Heijnen, Wil Heugen, Martijn Kuijpers, Chris Luyk, Rob Receveur, Toon Rooijackers, Stefan van der Sanden, Gerard Schepens, Chris Scholtens en Xiao jun Zhu, bedankt voor de vele gezellige momenten en al het geld dat ik met rikken verdiend heb. De gehele vakgroep SPD wordt bedankt voor de prettige werksfeer waarin ik 4 jaar heb mogen vertoeven.



---

## Publications

---

- [1] Boelhouwer, J.G., Piepers H.W. and Drinkenburg A.A.H., Enlargement of the pulsing flow regime by periodic operation of a trickle-bed reactor, *Chem. Eng. Sci.*, 54, 4661-4667, 1999
- [2] Boelhouwer J.G., Piepers H.W. and Drinkenburg A.A.H., Liquid-induced pulsing flow in trickle-bed reactors, proceedings AIChE Annual Meeting, paper 304b, Dallas, TX, U.S.A, 2000
- [3] Boelhouwer J.G., Piepers H.W. and Drinkenburg A.A.H., The induction of pulses in trickle-bed reactors by cycling the liquid-feed, *Chem. Eng. Sci.*, 56, 2605-2614, 2001
- [4] Boelhouwer J.G., Piepers H.W. and Drinkenburg A.A.H., Particle-liquid heat transfer in trickle-bed reactors, *Chem. Eng. Sci.*, 56, 1181-1187, 2001
- [5] Boelhouwer J.G., Piepers H.W. and Drinkenburg A.A.H., Nature and characteristics of pulsing flow in trickle-bed reactors, proceedings AIChE Annual Meeting, paper337g, Los Angeles, CA, U.S.A., 2001
- [6] Boelhouwer J.G., Piepers H.W. and Drinkenburg A.A.H., Particle-liquid heat transfer in trickle-bed reactors, proceedings AIChE Annual Meeting, paper 333f, Los Angeles, CA, U.S.A., 2001
- [7] Boelhouwer J.G., Piepers H.W., and Drinkenburg A.A.H., Non-steady state operation of trickle-bed reactors, proceedings of "3rd international symposium of reaction kinetics and the development and operation of catalytic processes", Oostende, Belgium, 2001
- [8] Boelhouwer J.G., Periodieke bedrijfsvoering van trickle-bed reactoren, *Chemisch 2 Weekblad*, 97, no 15, 14, 2001
- [9] Boelhouwer J.G., Hoogenstrijd B.W.J.L., Piepers H.W., Janssen L.J.J. and Drinkenburg A.A.H., Comments on the electrochemical method to determine mass transfer coefficients in trickle-bed reactors, *Chem. Eng. Sci.*, submitted for publication
- [10] Boelhouwer J.G., Piepers H.W. and Drinkenburg A.A.H., Nature and characteristics of pulsing flow in trickle-bed reactors, *Chem. Eng. Sci.*, submitted on invitation
- [11] Boelhouwer J.G., Piepers H.W. and Drinkenburg A.A.H., Liquid-induced pulsing flow in trickle-bed reactors, *Chem. Eng. Sci.*, submitted on invitation
- [12] Boelhouwer J.G., Piepers H.W. and Drinkenburg A.A.H., Advantages of forced nonsteady operated trickle-bed reactors, *Chem. Eng. Tech.*, submitted on invitation
- [13] Boelhouwer J.G., Piepers H.W. and Drinkenburg A.A.H., Particle-liquid mass transfer in trickle-bed reactors, in preparation
- [14] Boelhouwer J.G., Piepers H.W. and Drinkenburg A.A.H., Pulse induction in trickle-bed reactors by cycling the gas feed, in preparation
- [15] Boelhouwer J.G., Piepers H.W. and Drinkenburg A.A.H., Dynamic modeling of periodically operated trickle-bed reactors, in preparation

---

## Presentations

---

- [1] *Enlargement of the pulsing flow regimes by periodic operation of a trickle-bed reactor*, OSPT meeting Lunteren, January 1998
- [2] *Enlargement of the pulsing flow regimes by periodic operation of a trickle-bed reactor*, USPC-3 conference, St Petersburg, Russia, June 1998
- [3] *Liquid-induced pulsing flow in trickle-bed reactors* (poster presentation), OSPT-meeting Lunteren, January 1999
- [4] *Liquid-induced pulsing flow in trickle-bed reactors*, Washington University, Saint Louis, U.S.A. (Visit Prof. M.P. Dudukovic), February 1999
- [5] *Liquid-induced pulsing flow in trickle-bed reactors*, Notre Dame University, South Bend, U.S.A. (Visit Prof. A. Varma), Februari 1999
- [6] *The induction of pulses in trickle-bed reactors by cycling the liquid feed*, AIChE Annual Meeting, Dallas, U.S.A., November 1999
- [7] *Particle-liquid heat transfer in trickle-bed reactors* (poster presentation), OSPT-meeting Lunteren, January 2000
- [8] *Liquid-induced pulsing flow in trickle-bed reactors and Particle-liquid heat transfer in trickle-bed reactors*, Visit Prof. G. Wild (Université de Nancy), Eindhoven, March 2000
- [9] *Liquid-induced pulsing flow in trickle-bed reactors and Particle-liquid heat transfer in trickle-bed reactors*, Aristoteles University of Thessaloniki, Greece (Visit Prof. A.J. Karabelas), April 2000
- [10] *Particle-liquid heat transfer in trickle-bed reactors*, AIChE Annual meeting, Los Angeles, U.S.A., November 2000
- [11] *Nature and characteristics of pulsing flow in trickle-bed reactors*, AIChE Annual meeting, Los Angeles, U.S.A., November 2000
- [12] *Particle-liquid heat transfer in trickle-bed reactors* (poster presentation), ISCRE, Krakow, Poland, September 2000
- [13] *Hydrodynamics, heat and mass transfer in periodically operated trickle-bed reactors*, Meeting EU-project CYCLOP (Cyclic operation of trickle-bed reactors), Thessaloniki, Greece, March 2001
- [14] *Non-steady state operation of trickle-bed reactors*, International symposium on reaction kinetics and the development and operation of catalytic processes, Oostende, Belgium, May 2001
- [15] *Hydrodynamics, heat and mass transfer in periodically operated trickle-bed reactors*, DSM price for chemistry and Technology, May 2001
- [16] *Dynamic modeling of periodically operated trickle-bed reactors*, Meeting EU-project CYCLOP (Cyclic operation of trickle-bed reactors), Dortmund, Germany, June 2001
- [17] *Hydrodynamics, heat and mass transfer in periodically operated trickle-bed reactors*, Invited lecture at Shell, Amsterdam, October 2001

---

## Curriculum Vitae

---

Jaco Boelhouver werd op 16 augustus 1973 geboren te Linschoten. Na afronding van Atheneum B aan de Stedelijke Scholengemeenschap te Roermond besloot hij Scheikundige Technologie te gaan studeren aan de Technische Universiteit Eindhoven. In 1997 behaalde hij het diploma. Het afstudeerwerk werd verricht op het gebied van emulsiocopolymerisatie. In oktober van hetzelfde jaar begon hij aan zijn promotieonderzoek in de capaciteitsgroep Procesontwikkeling aan de TU Eindhoven onder supervisie van Prof. Dr. Ir. A.A.H. Drinkenburg. Dit promotieonderzoek werd in mei 2001 beloond met één van de DSM prijzen voor Chemie en Technologie.